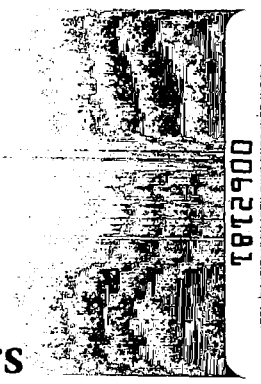

NASA Contractor Report 3639

The Receptivity of Boundary Layers on Blunt Bodies to Oscillations in the Free Stream

C. E. Grosch

GRANT NAG1-96
NOVEMBER 1982

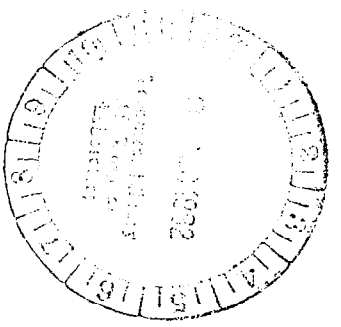

NASA

NASA Contractor Report 3639

The Receptivity of Boundary Layers on Blunt Bodies to Oscillations in the Free Stream

C. E. Grosch
Old Dominion University
Norfolk, Virginia

Prepared for
Langley Research Center
under Grant NAG1-96

National Aeronautics
and Space Administration

**Scientific and Technical
Information Branch**

1982

TABLE OF CONTENTS

LIST OF TABLES

LIST OF FIGURES

Figure

Figure

Figure

Figure

Figure

Figure

Figure

THE RECEPTIVITY OF BOUNDARY LAYERS ON BLUNT BODIES TO OSCILLATIONS IN THE FREE STREAM

By

Chester E. Grosch*

INTRODUCTION

The prediction of the position of transition on a body is one of the most difficult problems in fluid dynamics. Linear stability theory with the "e^n" criterion (see Mack, 1977, for an extended discussion) is probably the most widely used method of predicting transition. The major weakness of this method is that it employes a relative measure of flow instability; the growth of some measure of the disturbance size, whether amplitude, energy, or whatever, relative to an unknown initial size of the disturbance.

It is clear, as pointed out by Mack (1977), that the position of transition must depend on the absolute size of the disturbance, and thus on the initial size of the disturbance as well as the growth rate of the unstable disturbance. If there were no disturbance at all, that is the initial size were zero, the stability or instability of the flow would be irrelevant. The flow would remain laminar, and transition would not occur anywhere on the body unless, of course, the flow separated. On the other hand, if the initial disturbance were very large, say of the order of the mean flow speed, then transition would, presumably, occur very near the front of the body, perhaps in the immediate vicinity of the stagnation point or line.

A rough estimate of the magnitude of the initial amplitude of the Tollmien-Schlichting waves at the beginning of the region of instability can be made if it is assumed that the "e^n" criterion is an approximately valid transition method and if one accepts the estimate of Klebanoff, Tidstron, and Sargent (1962) that, at the beginning of transition, the rms value of the perturbation velocity is about 1.5% of the free stream speed. Since the

*Professor, Department of Oceanography, Old Dominion University, Norfolk, Virginia 23508.

initial proposal of the "e^n" criterion by Smith (1956) and Van Ingen (1956), extensive studies of transition data have shown that n varies from about 2.5 to 10.0, depending on the test facility. Taking the disturbance amplitude at transition to be 0.015 of the free stream speed, and n to vary from 2.5 to 10.0, it follows that the amplitude of the disturbance at the beginning of the region of flow instability is in the range 10^{-3} to 10^{-6} of the free stream speed. This suggests that a very weak coupling of free stream disturbances to Tollmien-Schlichting waves in the boundary layer may be extremely important in the initiation of the transition process. If the free stream disturbances have amplitudes of $O(\varepsilon)$, even disturbances in the boundary layer of $O(\varepsilon^2)$ may play a role in initiating transition.

In order to incorporate the influence of the flow environment in stability prediction methods, and thereby provide a rational basis for these methods, it is necessary to be able to calculate the initial size of the disburbance caused by external, i.e. free stream, disturbances. There are four classes of free stream disturbances which may be responsible for the generation of the Tollmien-Schlichting waves which lead to transition (Obremski, Morkovin, and Landhal, 1969). They are: mean flow unsteadiness, free stream vorticity, sound, and entropy fluctuations. If the fluid were truly incompressible, only the unsteadiness of the mean flow and free stream vorticity could exist and initiate the transition process. In reality, sound waves are always present. Entropy fluctuations appear to occur only at high supersonic speeds. In a recent study, Harvey and Bobbitt (1981) have examined the anomolies between wind tunnel and flight transition measurements. They state that the experimental results show"... the dominance of free-stream disturbance level on the transition process from beginning to end." Further, they conclude that there is a question of"... whether sound, unsteadiness, or spectral peaks is the most influential on boundary layer receptivity,..." Morkovin (1978) has argued that, in medium to low subsonic flows, sound waves can be modeled quite accurately by a time varying oscillation superimposed upon a steady mean flow, provided that the wavelength of the sound wave is much larger than the characteristic length scale of the body. For a sound wave impinging on the nose of a body this characteristic scale length would appear to be the radius of curvature of the body at the forward stagnation point.

Recent studies, (Salwen, Kelly, and Grosch, 1980; Grosch and Salwen, 1980; Salwen and Grosch, 1981) have been addressed to the problem of calculating the amplitudes of the discrete and continuum eigenfunctions of the linearized, parallel flow stability problem. The results of these studies can be summarized as follows: first, the proper inner products for orthogonality of these eigenfunctions were found; second, it was shown that the set of discrete and continuum eigenfunctions for both the temporal and spatial problems is complete; and third, a procedure for calculating the amplitudes of the discrete and continuum eigenfunctions was found. In order to calculate these amplitudes, the disturbance must be known, as a function of time, on a plane perpendicular to the boundary.

In order for this procedure to be applied it is necessary for the disturbance to be small so that linearization is valid; that the parallel flow approximation be valid, at least approximately; and that the form of the disturbance be known throughout the boundary layer and free stream at one location on a two-dimensional body. Even if the disturbances are small, this theory cannot be applied in the immediate vicinity of the leading edge of a body because the flow in that region is not even approximately parallel. A basic problem is to determine the flow within the boundary layer caused by disturbances propagating and being advected by the mean flow toward the front of a blunt body.

The response of the boundary layer on a body to oscillations in the free stream has been the subject of a number of studies beginning in the early 1950's. Some representative examples are the work of Moore (1951), Lighthill (1954), Stuart (1955), Rott (1956), Lin (1956), Glauert (1956), Carrier and Di Prima (1957), Gibson (1957), Watson (1959), Lam and Rott (1960), Rott and Rosenzweig (1960), Sarma (1964), Stuart (1966), and Ackerberg and Phillips (1972). Riley (1975) and Schlichting (1979, Chapter 15) give comprehensive reviews of recent work in unsteady boundary layer theory. None of these authors have considered the application of their results to the boundary layer receptivity problem.

These studies have considered either the unsteady flow in the vicinity of a stagnation point or on a flat plate. The flat plate problem presents

great difficulties because of the singularity of the boundary layer equations at the leading edge of the plate. Carrier and Di Prima (1957) studied this problem within the framework of a linearized, Oseen approximation, to first order in the amplitude of the oscillation. They found that, far from the leading edge of the plate, the time dependent part of the flow is a Stokes shear wave. Ackerberg and Phillips (1972) studied the same problem using asymptotic, again to first order in the amplitude of the oscillation, and numerical techniques. They also found that, far downstream of the leading edge, the flow develops into a nearly Blasius steady flow and a Stokes shear layer imbedded within the steady boundary layer. The most surprising, and unexpected, result of Ackerberg and Phillips is that "... most flow quantities approach their asymptotic values far downstream through damped oscillations."

Grosch and Salwen have found a solution of the Navier-Stokes equations for an incompressible stagnation point flow whose magnitude oscillates in time about a constant, nonzero, value. (See Appendix B.) The analytic solutions, to third order in the amplitude, obtained using inner and outer expansions, are in complete agreement with the results of numerical integrations. The mean flow is the steady stagnation point flow plus second, and higher, order flows driven by the Reynolds stress of the oscillatory components. The oscillatory flow is that of the fundamental and all of the higher harmonics of the fundamental.

The mean flow is, to lowest order, independent of the oscillating flow. The structure of the oscillatory components of the flow depends on the frequency of oscillation, not on the distance from the stagnation point. As was expected, the oscillatory flow develops into a Stokes shear layer at high frequencies. The results of Carrier and Di Prima and Ackerberg and Phillips that the Stokes shear layer develops far downstream may be due to the use of the boundary layer equations in a region in which they are invalid.

In any case, the flat plate with zero thickness and a "sharp" leading edge is a nonphysical model; all physical bodies have a blunt leading edge, at least if a continuum approximation can be applied to the flow past the body.

In this paper we examine one aspect of the boundary layer receptivity problem; that of the flow induced in the boundary layer on the forward portion of a blunt body by unsteadiness in the mean flow. As was mentioned above, this is also an approximate solution for the disturbances generated in the boundary layer by a long wavelength sound wave impinging normally on the front of a body in steady motion. This work is an extension of our previous study of the flow in the neighborhood of a stagnation point (Grosch and Salwen, Appendix B).

FORMULATION

Consider the flow past a blunt, two-dimensional body. The usual boundary layer coordinates are used: $\tilde{x}$ is the distance along the surface of the body from the forward stagnation point and $\tilde{y}$ is the distance from the body along the normal to the body. A solution is to be found for $\tilde{x} \geq 0$ of the time-dependent, two-dimensional boundary layer equations

$$\frac{\partial u}{\partial \tilde{x}} + \frac{\partial v}{\partial \tilde{y}} = 0, \tag{1}$$

$$\frac{\partial u}{\partial t} + u \frac{\partial u}{\partial \tilde{x}} + v \frac{\partial u}{\partial \tilde{y}} = \frac{\partial U}{\partial t} + U \frac{\partial U}{\partial \tilde{x}} + \nu \frac{\partial^2 u}{\partial \tilde{y}^2}, \tag{2}$$

with the boundary conditions

$$u(\tilde{x},o,t) = v(\tilde{x},o,t) = 0, \tag{3}$$

$$u(\tilde{x},\tilde{y},t) \to U(\tilde{x},t) \text{ as } \tilde{y} \to \infty. \tag{4}$$

Here, (u,v) are the components of the velocity in the $\tilde{x}$ and $\tilde{y}$ directions, $U(\tilde{x},t)$ is the component of the potential flow which is tangential to the body surface, and ν is the kinematic viscosity. It will be

assumed that the potential flow is a temporally oscillating flow, superimposed on a steady mean flow; specifically it is assumed that,

$$U(\tilde{x},t) = U_o H(\tilde{x}/\ell)\left[1 + \varepsilon \cos \omega t\right], \tag{5}$$

where U_o is the magnitude of the mean potential flow,

ℓ is an appropriate length scale of the body,

ε is the dimensionless amplitude of the oscillating component, and,

H is a dimensionless function, giving the variation along the body of the tangential component of the potential flow.

It will be assumed that the body is symmetric and is at a zero angle of attack, so that H is of the form

$$H(\tilde{x}/\ell) = \sum_{n=0}^{\infty} a_{2n+1} (\tilde{x}/\ell)^{2n+1}, \tag{6}$$

with the $\{a_j\}$ dimensionless constants. Specific examples will be considered below.

METHOD OF SOLUTION

Define dimensionless variables

$$\xi = \tilde{x}/\ell, \tag{7}$$

$$\eta = (a_1 \mathrm{Re})^{1/2}(\tilde{y}/\ell) \tag{8}$$

$$\tau = a_1 U_o t/\ell, \tag{9}$$

and parameters, a Reynolds number

$$\mathrm{Re} = U_o \ell/\nu \tag{10}$$

and a Strouhal number, a dimensionless frequency,

$$\sigma = \omega \ell / (a_1 U_o). \tag{11}$$

Defining a stream function such that

$$u = \partial\psi/\partial\tilde{y}, \quad v = -\partial\psi/\partial\tilde{x}, \tag{12a,b}$$

by

$$\psi = \left[(U_o \ell)/(a_1 \mathrm{Re})^{1/2} \right] \phi(\xi, \eta, \tau), \tag{13}$$

equation (1) is satisfied identically and (2) is

$$\frac{\partial^3\phi}{\partial\eta^3} + a_1^{-1}\left[\frac{\partial\phi}{\partial\xi}\frac{\partial^2\phi}{\partial\eta^2} - \frac{\partial\phi}{\partial\eta}\frac{\partial^2\phi}{\partial\xi\partial\eta}\right] - \frac{\partial^2\phi}{\partial\tau\partial\eta} = \varepsilon\sigma H(\xi)\sin\sigma\tau$$
$$- a_1^{-1} H(\xi)H'(\xi)\left[1 + \varepsilon\cos\sigma\tau\right]^2. \tag{14}$$

The boundary conditions, (3) and (4) are

$$\frac{\partial\phi}{\partial\eta} = \frac{\partial\phi}{\partial\xi} = 0 \qquad \text{at } \eta = 0, \tag{15}$$

and

$$\frac{\partial\phi}{\partial\eta} \to H(\xi)\left[1 + \varepsilon\cos\sigma\tau\right] \quad \text{as } \eta \to \infty. \tag{16}$$

The tangential component of potential velocity, $H(\xi)$, is a power series in ξ. It is clear, from (14), that ϕ must also be a power series in ξ, with each coefficient a function of η, τ, and the parameter ε. Each of these coefficients will be expanded in a Fourier series in τ, with each Fourier amplitude a function of η and the parameter ε. Finally, each Fourier amplitude will be expanded in a power series in ε, with each coefficient of the power series a function of η. These functions of η are then found to be solutions of ordinary differential equations.

First, assume that

$$\phi(\xi,\eta,\tau) = \sum_{n=0}^{\infty} \left[2(n+1) - \delta_{on}\right] a_{2n+1}\, \xi^{2n+1}\, F_{2n+1}(\eta,\tau). \tag{17}$$

Substituting (6) and (17) into (14) and equating the coefficients of successive powers of ξ on the left and right sides of equation (14), the partial differential equations for the $\{F_j(\eta,\tau)\}$ are found. F_1 satisfies

$$\frac{\partial^3 F_1}{\partial\eta^3} + F_1\frac{\partial^2 F_1}{\partial\eta^2} - \left(\frac{\partial F_1}{\partial\eta}\right)^2 - \frac{\partial^2 F_1}{\partial\tau\partial\eta} = P(\tau;\varepsilon,\sigma) - Q(\tau;\varepsilon,\sigma), \tag{18}$$

where

$$P(\tau;\varepsilon,\sigma) = \varepsilon\sigma \sin\sigma\tau, \tag{19a}$$

and

$$Q(\tau;\varepsilon,\sigma) = 1 + \frac{1}{2}\varepsilon^2 + 2\varepsilon\cos\sigma\tau + \frac{1}{2}\varepsilon^2\cos 2\sigma\tau. \tag{19b}$$

Next, define the operators

$$D(F_j,F_1;j) \equiv \frac{\partial^3 F_j}{\partial\eta^3} + F_1\frac{\partial^2 F_j}{\partial\eta^2} - (j+1)\frac{\partial F_1}{\partial\eta}\frac{\partial F_j}{\partial\eta} + j\frac{\partial^2 F_1}{\partial\eta^2}F_j - \frac{\partial^2 F_j}{\partial\tau\partial\eta} \tag{20}$$

and

$$G(F_i,F_j) \equiv \frac{\partial F_i}{\partial\eta}\frac{\partial F_j}{\partial\eta} - \frac{\partial^2 F_i}{\partial\eta^2}F_j. \tag{21}$$

Then,

$$D(F_3,F_1;3) = \frac{1}{4} P - Q, \tag{22}$$

$$D(F_5,F_1;5) = \frac{1}{6} P - (1 + \frac{1}{2} C_5)\, Q + 8C_5 G(F_3,F_3), \tag{23}$$

$$D(F_7,F_1;7) = \frac{1}{8} P - (1 + C_7)\, Q + 9C_7 G(F_5,F_3) + 15\, C_7 G(F_3,F_5), \tag{24}$$

$$D(F_9,F_1;9) = \frac{1}{10} P - (1 + C_{9,1} + \frac{1}{2} C_{9,2})\, Q + \frac{1}{5} C_{9,1}\left[48\, G(F_7,F_3) + 112 G(F_3,F_7)\right] + 18\, C_{9,2} G(F_5,F_5), \tag{25}$$

$$D(F_{11},F_1;11) = \frac{1}{12} P - (1 + C_{11,1} + C_{11,2})\, Q + C_{11,1}\left[30 G(F_3,F_9) + 10 G(F_9,F_3)\right] + C_{11,2}\left[28 G(F_5,F_7) + 20 G(F_7,F_5)\right], \tag{26}$$

with

$$C_5 = a_3^2/(a_1 a_5), \tag{27a}$$

$$C_7 = a_3 a_5/(a_1 a_7), \tag{27b}$$

$$C_{9,1} = a_3 a_7/(a_1 a_9),\quad C_{9,2} = a_5^2/(a_1 a_9), \tag{27c,d}$$

$$C_{11,1} = a_3 a_9/(a_1 a_{11}),\quad C_{11,2} = a_5 a_7/(a_1 a_{11}). \tag{27e,f}$$

The boundary conditions for the $\{F_{2n+1}\}$ are

$$F_{2n+1}(0,\tau) = (\partial F_{2n+1}/\partial\eta)_{\eta=0} = 0 \tag{28}$$

and

$$[2(n+1) - \delta_{on}](\partial F_{2n+1}/\partial\eta) \to 1 + \varepsilon \cos\sigma\tau, \tag{29}$$

as $\eta \to \infty$.

We have previously found the solution for F_1 up to, and including, terms in ε^3 (Grosch and Salwen, Appendix B). Although the boundary layer equations are being used in this study, it should be noted that $\xi F_1(\eta,\tau)$ is a solution of the Navier-Stokes equations for oscillating stagnation point flow. It is easily seen that the form of the solution for each of the F_{2n+1} is the same as that for F_1. Therefore, we have for $j = 1,3,\ldots,11$

$$F_j(\eta,\tau) = \sum_{n=0}^{\infty}\left\{\varepsilon^{2m} f_{j,2m,0}(\eta) + \sum_{k=1}^{\infty}\varepsilon^{2m+k}\left[f_{j,2m,k}(\eta)\cos(k\sigma\tau) + g_{j,2m,k}(\eta)\sin(k\sigma\tau)\right]\right\}. \tag{30}$$

It is quite straightforward, but somewhat tedious, to obtain the ordinary differential equations and boundary conditions for the f's and g's. These differential equations are given in Appendix A.

One of the major problems associated with series solutions of this type is that of determining the radius of convergence. On the basis of the results from the study of oscillating stagnation point flow (Appendix B), it can be concluded that the power series in ε is rapidly convergent for $\varepsilon < 1$, except perhaps at very low frequencies. If the frequency of oscillation is low, then a quasisteady approximation is quite accurate. Because of the rapid convergence of the series in ε, for ε small, only the terms through ε^2 have been calculated.

A much more difficult problem is estimating the radius of convergence of the power series in ξ. It appears that there are no general results for determining the radius of convergence of the steady Blasius series. Van Dyke (1957) has shown that the steady Blasius series for a parabolic cylinder diverges for $\tilde{x}/r_o > 0.62$, where r_o is the radius of curvature of the parabola at the nose. The results given by Schlichting (1979) for the steady Blasius series for a sphere of radius r_o suggest that this series is convergent up to at least $\tilde{x}/r_o \approx \pi/2$. It seems reasonable to assume that the time dependent series solution given here is convergent for $\xi = \tilde{x}/\ell \lesssim 1$.

RESULTS

Numerical integration of the equations given in Appendix A yield the $\{f_{j,2n,k}, g_{j,2nk}\}$. Substituting (30) and (17) into (13) and using (12) gives, for the velocity components (u,v),

$$u/U_o = \sum_{n=0}^{\infty} \left\{ [2(n+1) - \delta_{on}]\, a_{2n+1} \xi^{2n+1} \sum_{m=0}^{\infty} [\varepsilon^{2m} f'_{2n+1,2m,0} + \sum_{k=1}^{\infty} \varepsilon^{2m+k} \{ f'_{2n+1,2m,k} \cos(k\sigma\tau) + g'_{2n+1,2m,k} \sin(k\sigma\tau)\}] \right\}, \quad (31)$$

$$v/U_o = -(a_1 \mathrm{Re})^{-1/2} \sum_{n=0}^{\infty} \left\{ [2(n+1) - \delta_{on}](2n+1)\, a_{2n+1} \xi^{2n} \sum_{n=0}^{\infty} [\varepsilon^{2m} f_{2n+1,2m,0} + \sum_{k=1}^{\infty} \varepsilon^{2m+k} \{ f_{2n+1,2m,k} \cos(k\sigma\tau) + g_{2n+1,2m,k} \sin(k\sigma\tau)\}] \right\}. \quad (32)$$

The velocity field depends on the body shape, the $\{a_j\}$, the Reynolds number, Re, and the dimensionless frequency, σ. It should be

noted that the effective Reynolds number and frequency depend, to some extent, on the body shape because the velocity scale is $a_1 U_o$, see equations (8), (10), (11), and (13). It is clear from (31) that, as usual, the tangential component of the velocity, u, has no explicit dependence on the Reynolds number which only affects the scaling in the normal (η) direction. Again, as usual, the normal component, v, is proportional to $Re^{-1/2}$ in addition to the scaled dependence of the normal coordinate.

Through the terms in ε^2,

$$u/U_o = u_{o,o}(\xi,\eta) + \varepsilon^2 u_{2,o}(\xi,\eta) + \varepsilon\left[u^{(1)}_{o,1}(\xi,\eta)\cos\sigma\tau + u^{(2)}_{o,1}(\xi,\eta)\right.$$

$$\left. \times \sin\sigma\tau\right] + \varepsilon^2\left[u^{(1)}_{o,2}\cos 2\sigma\tau + u^{(2)}_{o,2}\sin 2\sigma\tau\right], \tag{33}$$

$$v/U_o = -(a_1 Re)^{-1/2}\{v_{o,o}(\xi,\eta) + \varepsilon^2 v_{2,o}(\varepsilon,\eta) + \varepsilon\left[v^{(1)}_{o,1}(\xi,\eta)\cos\sigma\tau\right.$$

$$\left. + v^{(2)}_{o,1}\sin\sigma\tau\right] + \varepsilon^2\left[v^{(1)}_{o,2}(\xi,\eta)\cos 2\sigma\tau + v^{(2)}_{o,2}(\xi,\eta)\right. \tag{34}$$

$$\left.\sin 2\sigma\tau\right]\}$$

with,

$$u_{j,o} \approx \sum_{n=0}^{5}\left[2(n+1) - \delta_{on}\right] a_{2n+1}\,\xi^{2n+1} f'_{2n+1,j,o}(\eta), \tag{35a}$$

$$u^{(1)}_{o,j} \approx \sum_{n=0}^{5}\left[2(n+1) - \delta_{on}\right] a_{2n+1}\,\xi^{2n+1} f'_{2n+1,o,j}(\eta), \tag{35b}$$

$$u^{(2)}_{o,j} \approx \sum_{n=0}^{5}\left[2(n+1) - \delta_{on}\right] a_{2n+1}\,\xi^{2n+1} g'_{2n+1,o,j}(\eta), \tag{35c}$$

$$v_{j,o} \approx \sum_{n=0}^{5} \left[2(n+1) - \delta_{on}\right] (2n+1)\, a_{2n+1}\, \xi^{2n} f_{2n+1,j,o}(\eta), \qquad (35d)$$

$$v^{(1)}_{o,j} \approx \sum_{n=0}^{5} \left[2(n+1) - \delta_{on}\right] (2n+1)\, a_{2n+1}\, \xi^{2n} f_{2n+1,o,j}(\eta). \qquad (35e)$$

$$v^{(2)}_{o,j} \approx \sum_{n=0}^{5} \left[2(n+1) - \delta_{on}\right] (2n+1)\, a_{2n+1}\, \xi^{2n} g_{2n+1,o,j}(\eta). \qquad (35f)$$

The superscript (1) indicates the component of the velocity in the boundary layer which is in phase with the free stream oscillation, and the superscript (2) denotes the out of phase component.

Figure 1 is a sketch of a typical blunt body and the coordinate system. The tangential and normal velocity components are u and v. The Cartesian coordinate system (x,y) is also shown in figure 1. The velocity components $(\hat{u},\hat{v})$, parallel and perpendicular to the body axis are related to (u,v) by

$$\hat{u} = u \cos\theta - v \sin\theta, \qquad (36a)$$

$$\hat{v} = u \sin\theta + v \cos\theta. \qquad (36b)$$

There is an inherent difficulty in presenting the results of the calculations in such a way as to make them intelligible. The reason for this difficulty is that the character of the flow, in the boundary layer variables, changes drastically with position. In front of the body the flow is primarily directed towards the body, so u is very small and v dominates, in fact for η large, $v \approx -U_o$. As the flow moves around the body v decreases and u increases so that near the midpoint u dominates. For this reason it seems most reasonable to present the results in the (x,y) coordinate system. In particular, in terms of $\hat{u}$, the component of the velocity is parallel to the axis of the body. Note, however, that as y is varied at fixed x <u>both</u> ξ and η vary. Presentation of the results in terms of $\hat{u}$ also facilitates comparison of the results of these calculations with the experimental results of Kachanov, Kozlov, and Levchenko

(1978) although, as will be discussed below, the correspondence between the conditions of the experiment and of this calculation is not exact.

Detailed calculations have been carried out for the flow past two types of bodies; elliptic and parabolic cylinders.

3.1 Elliptic Cylinders

On the surface of an elliptic cylinder the tangential component of the potential flow is

$$H(\xi) = \left[1 + (b/a)\right] \, sn(\xi;k), \tag{37}$$

with a the semi-major axis, b the semi-minor axis,
sn the Jacobian elliptic function, and
$k^2 = 1 - (b/a)^2$ (38)

The length scale is the semi-major axis, a. The coefficients in the power series expansion for $H(\xi)$, the $\{a_{2n+1}\}$ are given in Table 1, (Cayley, 1895). The radius of convergence of the Blasius series for an elliptic cylinder is, apparently, not known. However, the calculations appear to converge up to at least the midpoint on the body, that is to

$$\xi = E(k), \tag{39}$$

where E is the complete elliptic integral of the second kind. The calculations were ended at this value of ξ because we are primarily interested in the flow on the nose.

Calculations of the velocity field have been carried out for a number of bodies with different slenderness ratios (a/b) and frequencies, σ. Results are given for three bodies; a moderately thick ellipse with $a/b = 5$; a thin ellipse, $a/b = 10$; and a very thin ellipse, $a/b = 25$, see Table 2. For each of these values of a/b calculations were carried out for a low frequency $\sigma = \pi/4$, two intermediate frequencies, $\sigma = \pi$ and 3π, and a high frequency, $\sigma = 6\pi$. In all cases the Reynolds number was

taken to be 100.0. The results at other, particularly higher, Reynolds numbers appear to have the same form when distances are rescaled to the appropriate boundary layer thickness.

Contours of the zero order steady flow, $\hat{u}_{o,o}$, are shown in Figures 2, 3, and 4. The format of these figures, and all of the others is the same. The body shape is plotted in the lower right hand corner of the figure and the flow is from left to right. For each body the semi-major axis is the same length. The body shape has not been distorted, however the region outside of the body has been stretched in order to show the details of the flow in the boundary layer. The coordinate system outside the body is the (ξ, η) system which is shown in Figure 1. The distance $\xi = 1$ corresponds to four of the major units of the scale shown on the edges of Figure 2 and all others. The distance $\eta = 1$, on the other hand, corresponds to one of these major units. Thus, for example, the coordinates of the point in the lower left hand corner of Figure 2 are $\xi = 0$ and $\eta = 4$, and those of the upper right hand corner of Figure 2 are $\xi = E(\sqrt{0.96}) = 1.05050$, and $\eta = 4.2$. Note, however, that although the (ξ, η) coordinate system is used, these are contour plots of $\hat{u}$, the velocity component parallel to axis of the ellipse.

The results shown in Figures 2, 3, and 4 show that the zero order in ε, mean flow has the same general features for bodies of different slenderness. Ahead of the body there is a boundary layer merging into the decelarating potential flow. Near the midpoint of the body the flow is nearly parallel to the body and the boundary layer flow merges into the tangential potential flow. In between there is a kind of "bubble" where $\hat{u}_{o,o}$ is small. This extends somewhat in front of and above the forward portion of the body. This region of small $\hat{u}_{o,o}$ occurs because <u>both</u> $u_{o,o}$ and $v_{o,o}$ are small and are at a substantial angle to the x axis. As the fluid flows around the nose of the body u increases but v decreases until near the middle of the body where it is $O(Re^{-1/2})$. Therefore, on the forward portion of the body, but away from the axis, u is increasing with ξ but is still not large and v is decreasing. Finally, as the body becomes more slender, the steady boundary layer tends to become thinner.

Figures 5 through 16 are contour plots of the second order steady flow, $\hat{u}_{2,o}$. Figures 5 to 8 show the results for an elliptic cylinder with $a/b = 5$ for a sequence of frequencies, $\sigma = \pi/4$, π, 3π, and 6π. Figures 9 to 12 show similar results for $a/b = 10$, while the results for $a/b = 25$ are given in Figures 13 to 16. Examination of these figures reveals some general patterns in the flow.

In all cases $\hat{u}_{2,o}$ is positive in the lower portion of the boundary layer and negative in the upper portion. At low frequencies the maximum and minimum values of $\hat{u}_{2,o}$ occur at the midpoint of the ellipse. As the frequency increases the maximum tends to shift towards the front of the body and the thickness of the regions of both positive and negative secondary mean flow tend to decrease. However, as the ellipse becomes more slender i.e., a/b increases, the region of appreciable $\hat{u}_{2,o}$ tends to be confined to the near midsection of the body. The absolute magnitude of this secondary flow also tends to decrease with increasing σ. Finally, at low frequencies the max $(\hat{u}_{2,o})$ is greater than $|\min(u_{2,o})|$, but at high frequencies this is reversed. These results show that the Reynolds stress generated by the nonlinear interaction of the fundamental oscillatory flow with itself cause the formation of a weak, secondary, shear within the main steady boundary layer. At low frequency the maximum shear occurs near the middle of the boundary layer. As the frequency increases, the position of maximum secondary shear shifts towards the boundary.

Contour plots of the amplitude and phase of $\hat{u}_{o,1}$, the fundamental oscillation at frequency σ, are given in Figures 17 through 28. As above, these show results for $a/b = 5$, 10, and 25 and $\sigma = \pi/4$, π, 3π, and 6π. The phase is, of course, arbitrary to within an additive constant. It has been assumed that for both the fundamental and the first harmonic, the phase is zero at $\xi = 0$, $\eta = 4$.

In all cases the contour maps of the amplitude of $\hat{u}_{o,1}$, Figures 17a to 28a, bear an obvious generic relationship to the corresponding contour plots of $\hat{u}_{o,o}$ for the same values of a/b. Of course, the structure of the flow does change with the frequency of oscillation. The amplitude of the oscillation decreases in front of the body and a region of reduced flow

is present above and, generally, in front of the nose of the body. As the oscillations move up onto the body, the amplitude grows. In all cases a peak in the amplitude distribution appears in the middle to lower part of the boundary layer at the midpoint of the ellipse. For a fixed value of a/b the location of this maximum of $\hat{u}_{1,o}$ moves towards the boundary as the frequency increases, reflecting the development of a Stokes shear layer at high frequencies. If the frequency, σ, is held fixed, the location of the maximum of $\hat{u}_{1,o}$ also moves deeper into the boundary layer as a/b increases, i.e. as the body becomes more slender. This is shown in Table 3, in which the location of the maximum of $\hat{u}_{o,1}$ is tabulated as a function σ and a/b.

The contour plots of the phase of $\hat{u}_{o,1}$ Figures 17b to 28b, are all quite similar. The region of deceleration of the potential flow and the development of the boundary layer are obvious, as is the thinning of the boundary layer as it develops into a Stokes layer at high frequencies. Just back of the nose, the lines of constant phase tend to be parallel to the body with a noticeable thickening at low frequency near the midpoint of the ellipse. As σ increases the region over which the phase shift occurs tends to thin. In all cases this region lies deeper in the boundary layer than the position of maximum $\hat{u}_{o,1}$. Independently of the value of a/b, the total phase shift appears, from the results given in Table 4, to be tending to $\pi/4$ as $\sigma \to \infty$.

Finally, Figures 29 through 40 are contour plots of the amplitude and phase of $\hat{u}_{o,2}$, the first harmonic of the free stream oscillation. Again these results show very substantial internal consistency.

The boundary layer in front of the body is readily apparent. The region of nonzero $|\hat{u}_{o,2}|$ decreases as the frequency increases at constant a/b and as the slenderness, a/b, increases at constant frequency. The amplitude of $\hat{u}_{o,2}$ has a maximum in the lower part of the boundary layer. For fixed a/b the position of this maximum moves lower in the boundary layer and forward on the body as σ increases. At constant frequency the height of the maximum remains nearly fixed while moving back toward the midpoint of the ellipse as a/b increases.

The phase shift of $\hat{u}_{o,2}$ is generally nearly constant over the region containing the maximum of $|\hat{u}_{o,2}|$ and then goes negative in the outer portion of the boundary layer. In this outer region the phase then increases towards zero. At low frequencies this outer phase shift occurs over a thin layer, but at higher frequencies it is fairly broad.

The first harmonic of the free stream oscillation is always confined to the steady boundary layer and, as σ increases, is confined to a thin Stokes layer adjacent to the body. As the fluid moves up onto the body, away from the nose, the amplitude increases but never becomes large. In fact, $|\hat{u}_{o,2}|$ is never greater than about 5×10^{-2}. The velocity fluctuations due to harmonics of the free stream oscillation thus never exceed $5 \times 10^{-2}\ \varepsilon^2$.

3.2 Parabolic Cylinders

We next consider the flow past a parabolic cylinder

$$y^2 = 4ax, \tag{40}$$

where a is the distance from the nose to the vertex. Choosing the length scale to be a, the tangential component of the potential flow is a power series in odd powers of $\xi = x/a$. The coefficients of this series are given in Table 5. The solution does not contain any geometric parameters, that is, apart from the scaling, is independent of a and is, therefore, a similarity solution for all parabolas.

The radius of curvature at the nose of a parabola is

$$r_o = 2a. \tag{41}$$

Using Van Dyke's (1957) result that the Blasius series diverges for $x/r_o > 0.62$, the solution given here is expected to converge only for $\xi < 1.24$.

The coefficient $a_1 = 1/4$ for a parabolic cylinder, so that $\sigma = 4(\omega \ell / v_o)$. Thus the "effective" frequency in the differential equations for the f's and g's is four times the true frequency of oscillation. Of course, a similar scaling applies to elliptic cylinders, but for

an ellipse $a_1 = (1 + b/a)^{-1}$, which is nearly unity for slender ellipses. Because of the factor of four in the value of σ for a parabola, calculations were carried out for $\sigma = \pi/16$, $\pi/4$, $3\pi/4$, and $3\pi/2$, so that results would be readily comparable to those obtained for the ellipses.

Contours of $\hat{u}_{o,o}$, the 0(1) mean flow past a parabolic cylinder are given in Figure 41. The format of this, and all of the other figures showing the results of the calculations for a parabolic cylinder, is similar to those figures showing the results for elliptic cylinders. The body is shown in the lower right hand corner. Distances normal to the boundary are scaled so that one major unit of the scale on the border of the figure corresponds to one unit of η, the boundary layer coordinate. Thus the point in the lower left hand corner of the figures has the coordinates $\xi = 0.0$, $\eta = 6.0$, and the top of the parabola at the right hand side of the figures has the coordinates $\xi = 0.90$, $\eta = 0.0$.

A parabola is, in some ways, a rather peculiar blunt body in that it is not a closed body, so that there is no trailing edge, and that the thickness of the body is a monotonically increasing function of the distance from the stagnation point. Therefore, the farther back from the nose, the thicker is the region of <u>potential</u> flow which is substantially influenced by the body. This effect is apparent in Figure 41. There is a region of reduced flow in front of the parabola due to the deceleration of the potential flow and the formation of the boundary layer. This region extends far above the axis of the body because of the blocking effect of the parabola on the potential flow ahead of the body. In the region in front of the nose the contours of $u_{o,o}$ are nearly equally spaced. Just above the parabola, these contours tend to line up with the body and the distance between them becomes increasingly smaller as the flow moves onto the parabola and the quasi-parallel boundary layer flow develops.

Contours of the steady, second order, streaming flow, $\hat{u}_{2,o}$, for $4\sigma = \pi/4$, π, 3π, and 6π, are shown in Figures 42 through 45. These plots show features which are similar to those seen in the contour plots of $\hat{u}_{2,o}$ for the flow past an ellipse, Figures 5 through 16. In both sets,

$\hat{u}_{2,o}$ is positive in the lower portion of the boundary layer and negative in the upper part. The thickness of the secondary boundary layer decreases as the frequency increases and there is a slight tendency for the position of the relative maximum and minimum of $\hat{u}_{2,o}$ to shift forward towards the stagnation point as σ increases. However, as σ increases the $\max|\hat{u}_{2,o}|$ decreases significantly.

Figures 46 to 49 are contour plots of the amplitude and phase of $\hat{u}_{o,1}$, the fundamental oscillation in the free stream flow past the parabola. The contours of the amplitude of $\hat{u}_{o,1}$, show a general similarity to those of steady flow, $\hat{u}_{o,o}$. However, as σ increases a Stokes layer develops on the parabolic cylinder and moves forward towards the stagnation point. Away from the stagnation point, the contours of $\hat{u}_{o,1}$ are similar to those of $\hat{u}_{o,1}$, for an ellipse if the surfaces are rotated so as to be locally parallel. The local maximum of $\hat{u}_{o,1}$, seen in the flow past an ellipse is not, however, seen for the flow past the parabola. The contour plots of the phase of $\hat{u}_{o,1}$, also show the development of a Stokes shear layer. The total magnitudes of the phase shift for $\hat{u}_{o,1}$, in Figures 46b through 49b are quite close to those for the corresponding cases for the elliptic cylinders.

Contour plots of the amplitude and phase of $\hat{u}_{o,2}$, the first harmonic of the oscillation in the free stream speed, are shown in Figures 50 to 53. The results shown in these figures illustrate the development of a second order Stokes shear layer within the steady boundary layer as the frequency increases. The $\max|\hat{u}_{o,2}|$ increases with ξ, at all σ, at least up to the point $\xi = 0.9$. It cannot be determined whether or not there is a localized maximum in the amplitude, as was found for the elliptic cylinders, or whether the amplitude reaches a plateau. The problem is that, in order to decide this question, the calculations would have to be extended substantially beyond $\xi = 0.9$, but, as mentioned above, the series expansion probably is divergent for $\xi > 1.24$, and probably converges very slowly for ξ close to 1.24.

DISCUSSION AND CONCLUSIONS

Perhaps the most general conclusion which can be drawn from the results of this study is that in the region of the nose of a symmetric, two dimensional blunt body at zero angle of attack, the steady plus oscillating flow is very similar for a wide class of body shapes. This conclusioon has been shown to be true for elliptic cylinders with $a/b \leq 25$, and for the parabolic cylinder. Additional calculations, not reported here, were carried out for elliptic cylinders with values of a/b up to 100, with results which are very similar to those reported here. In all cases, the flow field in the nose region of a two-dimensional blunt body is generic to that of the flow in the neighborhood of the stagnation point on a plane wall.

A general picture of the flow on the forward portion of a blunt body, due to a steady plus oscillating free stream, can be sketched. Forward of the body there is a region of decelerating potential flow which merges into the viscous stagnation point boundary layer. On the stagnation stream line the boundary layer thickness is $2.38\ell(\mathrm{Re})^{-1/2}$, with ℓ the scale length of the body. If one considers $\hat{u}$, the velocity component parallel to the body axis, there is a region of small $\hat{u}$, above and ahead of the nose, where the velocity is reduced and is at a significant angle to the body axis. On the body itself, the boundary layer changes slowly with distance from the leading edge. The description, so far, applies to $\hat{u}_{o,o}$, the $0(1)$ steady flow.

If one next turns to $\hat{u}_{o,1}$ the fundamental oscillating component of the flow, the above description is, with some additions and amendations, valid. These are due to the changes with frequency in the oscillating flow. At low frequencies, $\omega\ell/a_1 U_o \leq \frac{\pi}{4}$, the flow is essentially quasi-steady; that is, it is the steady flow scaled by the instantaneous free stream speed. As the frequency increases, the oscillating boundary layer develops into a Stokes shear layer. This change occurs along, at least, the entire forward portion of the body, independent of the position on the body. This is not completely obvious when $\hat{u}_{o,1}$ is examined, but it is obvious if $u_{o,1}$, the component of the velocity locally parallel to the body is

studied. As shown in Appendix B, the development of a Stokes layer at high frequency occurs at, and in the neighborhood of, a stagnation point.

This is in marked contrast to the results of Ackerberg and Phillips (1972), who concluded that the Stokes layer only develops far downstream of the leading edge of a flat plate. This may be due to the fact that there is a singularity at the leading edge of the (nonphysical) infinitely thin flat plate, or it may be due to the scaling assumptions of Ackerberg and Phillips, which, in effect, equate low frequencies with small distance from the leading edge and large distance from the leading edge with high frequencies. In the calculations reported here, the distance from the stagnation point and the frequency are independent.

The oscillations in the boundary layer, which exist at all frequencies and at all positions on a blunt body, could be interpreted as an oscillation in the steady boundary layer thickness. In the free stream, the mean (time averaged) speed is U_o, and the boundary layer thickness is conventionally defined as the height in the boundary layer, δ, where $u(\delta) = 0.99\ U_o$. As u increases and decreases at fixed η, because of the oscillation, the instantaneous value of δ would appear to increase and decrease. It is quite easy to estimate the amplitude of the apparent oscillation in δ, if the velocity oscillations in the free stream are small. Let

$$\delta = \delta_o + \delta_1(t), \tag{42}$$

with δ_o the time averaged boundary layer thickness, and δ_1 the oscillating component of the boundary layer thickness. By definition,

$$\langle u(\delta) \rangle = 0.09 \langle U \rangle = 0.99\ U_o, \tag{43}$$

where $\langle\rangle$ is a time average. Then, if $\varepsilon \ll 1$, it is easy to see that, to lowest order in ε,

$$\delta_1 = \left[\varepsilon / \left(\frac{\partial u_{o,o}}{\partial \tilde{y}} \right)_{\tilde{y} = \delta_o} \right] \cos(\omega t + \theta), \tag{44}$$

where, as above, $u_{o,o}$ is the $0(1)$ steady boundary layer flow component parallel to the boundary, and θ is the phase of $u_{o,1}$, evaluated at $\tilde{y} = \delta_o$.

In the neighborhood of the stagnation point on any blunt, two dimensional body, δ, scaled by ℓ, is

$$\delta_o = 2.38\ (Re)^{-1/2}, \tag{45}$$

and

$$\left(\frac{\delta u_{o,o}}{\delta \tilde{y}}\right)_{\tilde{y} = \delta_o} \approx 2.6 \times 10^{-2}. \tag{46}$$

So that, in the vicinity of the stagnation point, $|\delta_1|$, scaled by ℓ, is

$$|\delta_1| \approx 38.5\ \varepsilon (a_1 Re)^{-1/2} \tag{47}$$

and

$$|\delta_1|/\delta_o \approx 16.2\ \varepsilon (a_1)^{-1/2}. \tag{48}$$

At low frequencies the flow is very nearly quasi-steady, but at high frequencies, there can be some distortion of the velocity profile. If σ is large, $u_{o,1}$ is essentially constant outside of the Stokes layer which has a thickness of $0(\delta_o \sigma^{-1/2})$. Inside the layer, $u_{o,1}$ can cause some distortion of $u_{o,o}$, while outside the Stokes layer $u_{o,1}$, only adds a constant, in η, time varying increment to $u_{o,o}$.

It may be useful, at this point, to give an idea of what is a low frequency and what is a high frequency. From equation (11),

$$\sigma = \omega \ell / (a_1 U_o).$$

If, by way of illustration, $\ell = 1m$, $a_1 = 1$, and $Uo = 10$ m /sec, then

$$\sigma = \pi f/5 \tag{49}$$

where f is the frequency in Hertz. Thus for

$$\sigma \lesssim \pi/4,$$

the low frequency region,

$$f \lesssim 5/4 \text{ Hertz}.$$

While, for high frequencies,

$$\sigma \gtrsim 6\pi, \quad f \gtrsim 30 \text{ Hertz}.$$

In summary, for this example, frequencies below 1 Hz are low frequencies, those greater than 30 Hz are high frequencies, and the range of 1 to 30 Hz is the intermediate range of frequencies.

Considering next the terms of $O(\varepsilon^2)$, there is both a second order steady streaming flow, $u_{2,o}$, and $u_{o,2}$, the first harmonic of the free stream oscillation. The steady streaming flow extends throughout the $O(1)$ boundary layer at low frequencies, but at high frequencies, it is largely, but not completely, confined to a Stokes layer. However, at high frequencies, there is a small portion of $u_{2,o}$ which decays to zero in an outer layer, with a thickness of the same order as that of the $O(1)$ mean boundary layer.

The magnitude of this flow, $|u_{2,o}|$, increases with ξ, and for an elliptic cylinder has a maximum just in front of the midpoint of the ellipse. Such a maximum may, or may not, occur on a parabolic cylinder. Because of the limited range of convergence of the series expansion, the calculation cannot be reliably extended far enough to decide.

The first harmonic, $u_{o,2}$, has a structure which is partially similar to that of the secondary streaming flow, $u_{2,o}$, and partially, to the

fundamental, $u_{o,1}$. At low frequencies it extends throughout the steady boundary layer and at high frequencies is confined to a Stokes layer. It also develops a maximum amplitude some distance from the stagnation point.

Both the first harmonic and the secondary streaming flow are present at all ξ, even at the stagnation point. Away from the stagnation point they are somewhat modified, but have the same character as in the neighborhood of the stagnation point. In particular, the estimate (see Appendix B) that they are bounded by $(\varepsilon/\sigma)^2$ seems to be valid over an appreciable range of ξ, in fact, up to the midpoint on elliptic cylinders and over the range of a convergence of the series for flow past a parabolic cylinder.

The only experiment with which the results of these calculations can, apparently, be compared is that of Kachanov, Kozlov, and Levchenko (1978). They studied the flow past a flat plate with a nose consisting of two conjugate ellipses with a semi-major axis, a = 50 mm and semi-minor axis, b = 2 mm on the working side and a = 128 mm and b = 8 mm on the other side. Figure 54 shows the cross section of this body from the nose to a distance of 20 mm back from the nose.

In Figure 2 of their paper, Kachanov et al. give contours of (in the notation used here) $\hat{u}_{o,o}$ in the region from about 10 mm in front of the nose to about 15 mm behind it, and from the axis of the body to 6 mm above. Figure 55 is an enlarged copy, supplied by Dr. Levchenko, of Figure 2 of their paper. In this figure the contours are labeled with the speed in units of meters/second.

It is obvious that there is a general, qualitative agreement between the theoretical results shown in Figures 2, 3, and 4 for the mean flow and the experimental results of Kachanov et al. shown in Figure 55. The major difference between the theoretical and experimental results is the closed contour labeled 6.0 in Figure 55; nothing like this is seen in the results of the calculations. The experimental result is rather curious. Either there is an absolute maximum within this contour, a "peak", or a local minimum lies within the contour, so that the contour is the "lip of a volcano." In either case the flow speed, as shown in Figure 55, is a maximum <u>outside of</u> the boundary layer.

It is well known that, for a potential flow, the maximum velocity occurs on the boundary. The potential flow past an ellipse is a classic problem (Milne-Thomson, 1955). Calculations of the potential flow for an ellipse with a/b = 25 confirm that the maximum of $\hat{u}_{o,o}$ occurs on the boundary at the midpoint of the ellipse. Taking into account the existence of the viscous boundary layer, the maximum speed should occur at the top of the boundary layer. How is it then possible to account for the existence of a maximum in the speed in what is, apparently, a region of potential flow?

There seems to be three possibilities. The first, and most obvious, is experimental error. This does not appear to be likely because it would require systematic errors of the order of 10% to 15%. A second possibility is that the stagnation point is not on the axis of the body (see Figure 54). If, as seems likely, the stagnation point lies below the axis, then the flow must first move through a region of adverse pressure gradient until it gets around the nose. Then, for a short distance, the pressure gradient is favorable, and then falls rapidly to almost zero just behind the nose. It is possible that there is a local flow separation and reattachment, a separation bubble, just behind the nose of the upper ellipse. This would lift the boundary layer in this region and might account for the closed contour of $\hat{u}_{o,o}$ in the results of Kachanov, Kozlov, and Levchenko. The third possibility is that the free stream vorticity is not zero. If the free stream vorticity is non-zero, perhaps there is a shear in the free stream, then, depending on the distribution of free stream vorticity, a maximum of the speed could occur virtually anywhere outside of the boundary layer.

There is, of course, a final possibility. These theoretical arguments and calculations may be wrong. It may be possible, for some reason, that a non-rotational potential flow has a maximum away from the boundaries. Or, it may be that there is a viscous effect, not included in these calculations, which causes a maximum in the speed outside of the viscous boundary layer.

Kachanov et al. also give experimental results for an oscillatory past this body. The oscillatory flow is caused by a vibrating ribbon above the axis of the plate and in front of it. As Kachanov et al. indicate,

the periodic vortices shed by this ribbon passed above the plate and only the tails of the vortices impinged on the nose of the plate. The results of the calculations given here are, at best, in rough qualitative agreement with the experimental results of Kachanov, Kozlov, and Levchenko. In part, their results show an absolute maximum in the amplitude of the oscillatory velocity in a small region just above the axis of the plate and just beyond the top of the steady boundary layer. They also show a rapid change in the oscillatory flow immediately below the region of maximum which was discussed above. As was discussed above, either the calculations reported here are in error or the experimental results reflect unnoticed effects. In fact, from the results given in Figure 1 of Kachanov et al. it appears that the oscillation has a nonzero shear in the free stream. In any event, this issue requires clarification and would seem to require further work, both on the experimental and theoretical aspects of this problem.

Finally, if the theoretical approach used here and the results are correct, it would seem to have value beyond this particular study. The general character of the flow, in the nose region of the blunt bodies considered here, is very similar to that of the flow in the immediate neighborhood of the stagnation point. As the flow moves around the nose of the body, no essentially new features appear. This suggests that the structure of the flow on the forward part of a blunt body due to more general classes of disturbances, such as vorticity waves, can be found by studying the flow due to these disturbances in the neighborhood of a stagnation point. It seems clear, at least for two dimensional flows, that a linearized, in ε, theory is sufficiently accurate. The results given here show that, for any ellipse and for any parabola, the second order terms are bounded by $(\varepsilon/\sigma)^2$ for $\sigma \gtrsim 1$. It also should be noted that the steady flow in the neighborhood of a general three-dimensional stagnation point is known. This should facilitate the theoretical study of disturbances impinging on a body in the region of a stagnation point. These approximations, flow near a stagnation point, and linearization in ε, should be a considerable simplification for both analytical and numerical studies of boundary layer receptivity.

APPENDIX A

DIFFERENTIAL EQUATIONS AND BOUNDARY CONDITIONS FOR THE F'S AND G'S

The function $F_1(\eta,\tau)$ is the solution of the oscillating stagnation point flow problem (Grosch & Salwen, Appendix B). The differential equations and boundary conditions for the f's and g's are given there through terms ε^3 and will not be repeated here.

The differential equations and boundary conditions for the f's and g's given here are those in the expansion of the $\{F_j(\eta,\tau)\}$ for $J = 3,5,\ldots,11$ and ε^n, with $n \leq 2$. First, we define an operator L by

$$L\begin{pmatrix} f_{j,k,\ell} \\ g_{j,k,\ell} \end{pmatrix} \equiv \left[\frac{d^3}{d\eta^3} + f_{1,o,o}\frac{d^2}{d\eta^2} - (j+1) f'_{1,o,o}\frac{d}{d\eta}\right.$$

$$\left. + (j) f''_{1,o,o}\right] \begin{pmatrix} f_{j,k,\ell} \\ g_{j,k,\ell} \end{pmatrix}, \tag{A1}$$

where $f_{1,o,o}(\eta)$ is the O(1) function in F_1, and is the Hiemenz function, and primes denote differentiation with respect to η. Note that in (A1) the coefficients are j and $j+1$ and that j is the first index of the f or g upon which L operates. Next we define a second operator S by

$$S(f(\eta),\ g(\eta);\alpha,\beta,\gamma) \equiv \alpha fg'' - \beta f'g' + \gamma f''g, \tag{A2}$$

where f and g are any functions of η, primes, again, denote differentiation and α, β, and γ are arbitrary constants.

Then for the terms proportional to ξ^3 we have, at O(1)

$$Lf_{3,o,o} = -1 \tag{A3a}$$

$$f_{3,o,o}(0) = f'_{3,o,o}(0) = 0, \tag{A3b}$$

$$f'_{3,o,o} \to \frac{1}{4} \quad \text{as} \quad \eta \to \infty \tag{A3c}$$

At $0(\varepsilon)$ we have

$$Lf_{3,o,1} - \sigma g'_{3,o,1} = -2 - S(f_{1,o,1}, f_{3,o,o}; 1,4,3), \tag{A4a}$$

$$Lg_{3,o,1} + \sigma f'_{3,o,1} = \frac{1}{4}\sigma - S(g_{1,o,1}, f_{3,o,o}; 1,4,3), \tag{A4b}$$

$$f_{3,o,1}(0) = f'_{3,o,1}(0) = g_{3,0,1}(0) = g'_{3,0,1}(0) = 0, \tag{A4c}$$

$$f'_{3,0,1} \to \frac{1}{4}, \; g'_{3,o,1} \to 0 \quad \text{as} \quad \eta \to \infty \tag{A4d}$$

And at $0(\varepsilon^2)$

$$Lf_{3,2,o} = -\frac{1}{2} - S(f_{1,2,o}, f_{3,o,o}; 1,4,3) \tag{A5a}$$

$$- \frac{1}{2}\left[S(f_{1,o,1}, f_{3,o,1}; 1,4,3) + S(g_{1,o,1}, g_{3,o,1}; 1,4,3)\right],$$

$$f_{3,2,o}(0) = f'_{3,2,o}(0) = 0 \tag{A5b}$$

$$f'_{3,2,o} \to 0 \quad \text{as} \quad \eta \to \infty. \tag{A5c}$$

and

$$Lf_{3,o,2} - 2\sigma\, g'_{3,o,2} = -\frac{1}{2} - S(f_{1,o,2}, f_{3,o,o}; 1,4,3)$$

$$- \frac{1}{2}\left[S(f_{1,o,1}, f_{3,o,1}; 1,4,3) - S(g_{1,o,1}, g_{3,o,1}; 1,4,3)\right], \tag{A6a}$$

$$Lg_{3,o,2} + 2\sigma f'_{3,o,2} = - S(g_{1,o,2}, f_{3,o,o}; 1,4,3)$$

$$- \frac{1}{2}\left[S(f_{1,o,1}, g_{3,o,1}; 1,4,3) + S(g_{1,o,1}, f_{3,o,1}; 1,4,3)\right], \quad \text{(A6b)}$$

$$f_{3,o,2}(0) = f'_{3,o,2}(0) = g_{3,o,2}(0) = g'_{3,o,2}(0) = 0, \quad \text{(A6c)}$$

$$f'_{3,o,2} \to g'_{3,o,2} \to 0 \quad \text{as} \quad \eta \to \infty. \quad \text{(A6d)}$$

Next the f's and g's proportional to ξ^5 satisfy, first to $0(1)$

$$Lf_{5,o,o} = - (1 + \frac{1}{2} C_5) - 8C_5 \, S(f_{3,o,o}, \frac{1}{2}, 1, \frac{1}{2}) \quad \text{(A7a)}$$

$$f_{5,o,o}(0) = f'_{5,o,o}(0) = 0 \quad \text{(A7b)}$$

$$f'_{5,o,o} \to \frac{1}{6} \quad \text{as} \quad \eta \to \infty. \quad \text{(A7c)}$$

Then at $0(\varepsilon)$

$$Lf_{5,o,1} - \sigma g'_{5,o,1} = -2(1 + \frac{1}{2} C_5) - S(f_{1,o,1}, f_{5,o,o}; 1,6,5)$$

$$- 4C_5 \, S(f_{3,o,o}, f_{3,o,1}; 1,2,1) \quad \text{(A8a)}$$

$$Lg_{5,o,1} + \sigma f'_{5,o,1} = \frac{1}{6}\sigma - S(g_{1,o,1}, f_{5,o,o}; 1,6,5)$$

$$-4C_5 \, S(f_{3,o,o}, g_{3,o,1}; 1,2,1), \quad \text{(A8b)}$$

$$f_{5,o,1}(0) = f'_{5,o,1}(0) = g_{5,o,1}(0) = g'_{5,o,1}(0) = 0, \quad \text{(A8c)}$$

$$f'_{5,0,1} \to \frac{1}{6}, \; g'_{5,o,1} \to 0 \quad \text{as} \quad \eta \to \infty. \quad \text{(A8d)}$$

The equations and boundary conditions at $0(\varepsilon^2)$ are:

$$Lf_{5,2,o} = - \frac{1}{2}(1 + \frac{1}{2} C_5) - S(f_{1,2,o}, f_{5,o,o}; 1,6,5) - \frac{1}{2}$$

$$\times \left[S(f_{1,o,1}, f_{5,o,1}; 1,6,5) + S(g_{1,o,1}, g_{5,o,1}; 1,6,5)\right]$$

$$- 8 \, C_5 \left\{S(f_{3,2,o} f_{3,o,o}; 1,2,1)\right.$$

$$+ \frac{1}{2}\left[S(f_{3,o,1}, f_{3,o,1}; \frac{1}{2}, 1, \frac{1}{2}) + S(g_{3,o,1}, g_{3,o,1}; \right.$$

$$\left. \times \frac{1}{2}, 1, \frac{1}{2}]\right\} \qquad \text{(A9a)}$$

$$f_{5,2,o}(0) = f'_{5,2,o}(0) = 0; \quad f'_{5,2,o} \to 0 \quad \text{as} \quad \eta \to \infty; \qquad \text{(A9b,c)}$$

$$Lf_{5,o,2} - 2\sigma g_{5,o,2} = -\frac{1}{2}\left(1 + \frac{1}{2} C_5\right) - S(f_{1,o,2}, f_{5,o,o}; 1,6,5)$$

$$- \frac{1}{2}\left[S(f_{1,o,1}, f_{5,o,1}; 1,6,5) - S(g_{1,o,1}, g_{5,o,1}; 1,6,5)\right]$$

$$- 8C_5\left\{S(f_{3,o,o}, f_{3,o,2}; 1,2,1) + \frac{1}{2}\left[S(f_{3,o,1}, f_{3,o,1}; \frac{1}{2}, 1, \frac{1}{2})\right.\right.$$

$$\left.\left. - S(g_{3,o,1}, g_{3,o,1}; \frac{1}{2}, 1, \frac{1}{2})\right]\right\} \qquad \text{(A10a)}$$

$$Lg_{5,o,2} + 2\sigma f'_{5,o,2} = - S(g_{1,o,2}, f_{5,o,o}; 1,6,5) - \frac{1}{2}\left[S(f_{1,o,1}, g_{5,0,1}; \right.$$

$$\left. \times 1,6,5) + S(g_{1,o,1} f_{5,o,1}; 1,6,5)\right] - 8C_5\left\{S(f_{3,o,o}, g_{3,o,2}; \right.$$

$$\times 1,2,1) + \frac{1}{2}\left[S(f_{3,o,1}, g_{3,o,1}; \frac{1}{2}, 1, \frac{1}{2}) + \left\{S(g_{3,o,1}, f_{3,o,1}; \right.\right.$$

$$\left.\left. \times \frac{1}{2}, 1, \frac{1}{2})\right]\right\}, \qquad \text{(A10b)}$$

$$f_{5,o,2}(0) = f'_{5,o,2}(0) = g_{5,o,2}(0) = g'_{5,o,2}(0) = 0;$$

$$\times f'_{5,o,2} \to g'_{5,o,2} \to 0 \quad \text{as} \quad \eta \to \infty. \qquad \text{(A10c,d)}$$

The f's and g's which are proportional to ξ^7 satisfy the equations and boundary conditions, at $O(1)$

$$Lf_{7,o,o} = 1\ (1 + C_7) - C_7 S(f_{3,o,o}, f_{5,o,o}; 9,24,15), \tag{A11a}$$

$$f_{7,o,o}(0) = f'_{7,o,o}(0) = 0,\ f'_{7,o,o} \to \frac{1}{8} \quad \text{as} \quad \eta \to \infty \tag{A11b,c}$$

At $O(\varepsilon)$ the equations and boundary conditions are:

$$Lf_{7,o,1} - \sigma g'_{7,o,1} = -\ 2(1 + C_7) - S(f_{1,o,1}, f_{7,o,1}; 1,8,7)$$

$$-C_7[S(f_{3,o,o}, f_{5,o,1}; 9,24,15) + S(f_{3,o,1}, f_{5,o,o};$$

$$\times\ 9,24,15)], \tag{A12a}$$

$$Lg_{7,o,1} + \sigma f'_{7,o,1} = \frac{1}{8}\sigma - S(g_{1,o,1}, f_{7,o,o}; 1,8,7) -$$

$$\times\ C_7[S(f_{3,o,o}, g_{5,o,1}; 9,24,15) + S(g_{3,o,1}, f_{5,o,o};$$

$$\times\ 9,24,15)], \tag{A12b}$$

$$f_{7,o,1}(0) = f'_{7,o,1}(0) = g_{7,o,1}(0) = g'_{7,o,1}(0) = 0, \tag{A12c}$$

$$f'_{7,o,1} \to \frac{1}{8},\ g'_{7,o,1} \to 0 \quad \text{as} \quad \eta \to \infty. \tag{A12d,e}$$

While at $O(\varepsilon^2)$ we find

$$Lf_{7,2,o} = -\frac{1}{2}(1 + C_5) - S(f_{1,2,o}, f_{7,o,o}; 1,8,7) - \frac{1}{2}[S(f_{1,o,1},$$

$$\times\ f_{7,o,1}; 1,8,7) + S(g_{1,o.1}, g_{7,o,1}; 1,8,7)]$$

$$- C_7\{S(f_{3,2,o}, f_{5,o,o};9,24,15) + S(f_{3,o,o}, f_{5,2,o};9,24,15)$$

$$+ \frac{1}{2}[S(f_{3,o,1}, f_{5,o,1};9,24,15) + S(g_{3,o,1}, g_{5,o,1};$$

$$\times 9,24,15)]\}, \qquad \text{(A13a)}$$

$$f_{7,2,o}(0) = f'_{7,2,o}(0) = 0, \quad f'_{7,2,o} \to 0 \quad \text{as} \quad \eta \to \infty. \qquad \text{(A13b,c)}$$

$$Lf_{7,o,2} - 2\sigma g'_{7,o,2} = -\frac{1}{2}(1 + C_7) - S(f_{1,o,2}, f_{7,o,o};1,8,7)$$

$$- \frac{1}{2}[S(f_{1,o,1}, f_{7,o,1}, ;1,8,7) + S(g_{1,o,1}, g_{7,o,1};$$

$$\times 1,8,7)] - C_7\{S(f_{3,o,o}, f_{5,o,2};9,24,15) + S(f_{3,o,2} f_{5,o,o};$$

$$\times 9,24,15) + \frac{1}{2}[S(f_{3,o,1}, f_{5,o,1};9,24,15) - S(g_{3,o,1}, g_{5,o,1};$$

$$\times 9,24,15)]\}, \qquad \text{(A14a)}$$

$$Lg_{7,o,2} + 2\sigma f'_{7,o,1} = -S(g_{1,o,2} f_{7,o,o};1,8,7) - \frac{1}{2}[S(f_{1,o,1}, g_{7,o,1};$$

$$\times 1,8,7) + S(g_{1,o,1}, f_{7,o,1};1,8,7) - C_7\{S(f_{3,o,o}, g_{5,o,2};$$

$$\times 9,24,15) + S(g_{3,o,2}, f_{5,o,o};9,24,15) + \frac{1}{2}[S(f_{3,o,1}, g_{5,o,1};$$

$$\times 9,24,15) + S(g_{3,o,1}, f_{5,o,1};9,24,15)]\}, \qquad \text{(A14b)}$$

$$f_{7,o,2}(0) = f'_{7,o,2}(0) = g_{7,o,2}(0) = g'_{7,o,2}(0) = 0, \qquad \text{(A14c)}$$

$$f'_{7,o,2} \to g'_{7,o,2} \to 0 \quad \text{as} \quad \eta \to \infty. \qquad \text{(A14d)}$$

For the terms proportional to ξ^9 the $O(1)$ equations and boundary conditions are:

$$Lf_{9,o,o} = -\left(1 + C_{9,1} + \frac{1}{2} C_{9,2}\right) - \frac{1}{10} C_{9,1}\, S(f_{3,o,o}, f_{7,o,o};$$

$$96,320,224) - 18C_{9,2} S(f_{5,o,o}; f_{5,o,o}; \tfrac{1}{2}, 1, \tfrac{1}{2}), \qquad \text{(A15a)}$$

$$f_{9,o,o}(0) = f'_{9,o,o}(0) = 0, \quad f'_{9,o,o} \to 1/10 \quad \text{as} \quad \eta \to \infty. \qquad \text{(A15b,c)}$$

The $O(\varepsilon)$ equations and boundary conditions are:

$$Lf_{9,o,1} - \sigma g'_{9,o,1} = -2(1 + C_{9,1} + C_{9,2}) - S(f_{1,o,1}, f_{9,o,o}; 1,10,9)$$

$$- \frac{1}{10} C_{9,1}\left[S(f_{3,o,o}, f_{7,o,1}; 96,320,224) + S(f_{3,0,1}, f_{7,o,o};\right.$$

$$\left. \times\ 96,320,224)\right] - 18C_{9,2} S(f_{5,o,o}, f_{5,o,1}; 1,2,1) \qquad \text{(A16a)}$$

$$Lg_{9,o,1} + \sigma f'_{9,o,1} = \frac{1}{10}\sigma - S(g_{1,o,1}, f_{9,o,o}; 1,10,9) - \frac{1}{10} C_{9,1}$$

$$\times \left[S(f_{3,o,o}, g_{7,o,1}; 96,320,224) + S(g_{3,o,1} f_{7,o,o}; 96,320,224)\right]$$

$$- 18C_{9,2} S(f_{5,o,o}, g_{5,o,1}; 1,2,1), \qquad \text{(A16b)}$$

$$f_{9,o,1}(0) = f'_{9,o,1}(0) = g_{9,o,1}(0) = g'_{9,o,1}(0) = 0, \qquad \text{(A16c)}$$

$$f'_{9,o,1} \to \frac{1}{10}, \quad g'_{9,o,1} \to 0 \quad \text{as} \quad \eta \to \infty. \qquad \text{(A16d,e)}$$

The $O(\varepsilon^2)$ equations and boundary conditions are:

$$Lf_{9,2,o} = -\frac{1}{2}\left(1 + C_{9,1} + \frac{1}{2} C_{9,2}\right) - S(f_{1,2,o} f_{9,o,o};$$

$$\times 1,10,9)] - \frac{1}{2}\,[S(f_{1,o,1},f_{9,o,1};1,10,9) + S(g_{1,o,1},g_{9,o,1};$$

$$\times 1,10,9)] - \frac{1}{10}\,C_{9,1}\{S(f_{3,2,o}f_{7,o,o};96,320,224) + S(f_{3,o,o},$$

$$\times f_{7,2,o};96,320,224) + \frac{1}{2}[S(f_{3,o,1},f_{7,o,1};96,320,224)$$

$$+ S(g_{3,o,1},g_{7,o,1};96,320,224)]\} - 18C_{9,2}\{S(f_{5,2,o},f_{5,o,o};$$

$$\times 1,2,1) + \frac{1}{2}[S(f_{5,o,1}f_{5,o,1};\tfrac{1}{2},1,\tfrac{1}{2}) + S(g_{5,o,1},g_{5,o,1};$$

$$\times \tfrac{1}{2},1,\tfrac{1}{2})]\} \qquad \text{(A17a)}$$

$$f_{9,2,o}(0) = f'_{9,2,o}(0) = 0,\ f'_{9,2,o} \to 0 \quad \text{as} \quad \eta \to \infty, \qquad \text{(A17b,c)}$$

$$Lf_{9,o,2} - 2\sigma g'_{9,o,2} = -\frac{1}{2}(1 + C_{9,1} + \frac{1}{2}\,C_{9,2}) - S(f_{1,o,2},f_{9,o,o};1,10,9)$$

$$- \frac{1}{2}\,[S(f_{1,o,1},f_{9,o,1};1,10,9) - S(g_{1,o,1},g_{9,o,1};1,10,9)]$$

$$- \frac{1}{10}\,C_{9,1}\{S(f_{3,o,o}f_{7,o,2};96,320,224) + S(f_{3,o,2},$$

$$\times f_{7,o,o};96,320,224) + \frac{1}{2}[S(f_{3,o,1},f_{7,o,1};96,320,224)$$

$$- S(g_{3,o,1},g_{7,o,1};96,320,224)]\} - 18C_{9,2}\{S(f_{5,o,o},f_{5,o,2};$$

$$\times 1,2,1) + \frac{1}{2}[S(f_{5,o,1}f_{5,o,1};\tfrac{1}{2},1,\tfrac{1}{2}) - S(g_{5,o,1},g_{5,o,1};$$

$$\times \tfrac{1}{2},1,\tfrac{1}{2})]\}, \qquad \text{(A18a)}$$

$$Lg_{9,o,2} + 2\sigma f'_{9,o,2} = -S(g_{1,o,2},f_{9,o,o};1,10,9) - \frac{1}{2}\,[S(f_{1,o,1},g_{9,o,1};$$

$$\times 1,10,9) + S(g_{1,o,1},f_{9,o,1};1,10,9)] - \frac{1}{10} C_{9,1} S(f_{3,o,o},$$

$$\times g_{7,o,2};96,320,224) + S(g_{3,o,2},f_{7,o,o};96,320,224) + \frac{1}{2}$$

$$\times [S(f_{3,o,1},g_{7,o,1};96,320,224) + S(g_{3,o,1},f_{7,o,1};96,320,$$

$$\times 224)]\} - 18C_{9,2}\{S(f_{5,o,o},g_{5,o,2};1,2,1) + S(f_{5,o,1},g_{5,o,1};$$

$$\times 1,2,1)\}, \tag{A18b}$$

$$f_{9,o,2}(0) = f'_{9,o,2}(0) = g_{9,0,2}(0) = g'_{9,o,2}(0) = 0, \tag{A18c}$$

$$f'_{9,o,2} \to g'_{9,o,2} \to 0 \quad \text{as} \quad \eta \to \infty. \tag{A18d}$$

Finally, for the terms proportional to ξ^{11} the differential equations and boundary conditions are, at $O(1)$:

$$Lf_{11,o,o} = -(1 + C_{11,1} + C_{11,2}) - C_{11,1}S(f_{3,o,o},f_{9,o,o};10,40,30)$$

$$- C_{11,2}S(f_{5,o,o},f_{7,o,o};20,48,28) \tag{A19a}$$

$$f_{11,o,o}(0) = f'_{11,o,o}(0) = 0, \tag{A19b}$$

$$f'_{11,o,o} \to \frac{1}{12} \quad \text{as} \quad \eta \to \infty. \tag{A19c}$$

The $O(\varepsilon)$ differential equations and boundary conditions are:

$$Lf_{11,o,1} - \sigma g'_{11,o,1} = -2(1 + C_{11,1} + C_{11,2}) - S(f_{1,o,1},f_{11,o,o};$$

$$\times 1,12,11) - C_{11,1}[S(f_{3,o,o},f_{9,o,1};10,40,30)$$

$$+ S(f_{3,o,1},f_{9,o,1};10,40,30)] - C_{11,2}[S(f_{5,o,o},f_{7,o,1};$$

$$\times\ 20,48,28)] + S(f_{5,o,1}, f_{7,o.o}; 20,48,28)], \qquad \text{(A20a)}$$

$$Lg_{11,o,1} + \sigma f'_{11,o,1} = \frac{1}{12}\sigma - S(g_{1,o,1}, f_{11,o,o}; 1,12,11)$$

$$-C_{11,1}[S(f_{3,o,o}, g_{9,o,1}; 10,40,30) + S(g_{3,o,1}, f_{9,o,o};$$

$$\times\ 10,40,30)] - C_{11,2}[S(f_{5,o,o}, g_{7,o,1}; 20,48,28)$$

$$+ S(g_{5,o,1}, f_{7,o,o}; 20,48,28)], \qquad \text{(A20b)}$$

$$f_{11,o,1}(0) = f'_{11,o,1}(0) = g_{11,o,1}(0) = g'_{11,o,1}(0) = 0, \qquad \text{(A20c)}$$

$$f'_{11,o,1} \to \frac{1}{12},\ g'_{11,o,1} \to 0 \quad \text{as} \quad \eta \to \infty. \qquad \text{(A20d,e)}$$

And, lastly, the $O(\varepsilon^2)$ equations and boundary conditions are:

$$Lf_{11,2,o} = -\frac{1}{2}(1 + C_{11,1} + C_{11,2}) - S(f_{1,o,2}, f_{11,o,o}; 1,12,11)$$

$$-\frac{1}{2}[S(f_{1,o,1}, f_{11,o,1}; 1,12,11) + S(g_{1,o,1}, g_{11,o,1};$$

$$\times\ 1,12,11)] - C_{11,1}\{S(f_{3,2,o}, f_{9,o,o}; 10,40,30) + S(f_{3,o,o},$$

$$\times\ f_{9,2,0}; 10,40,30) + \frac{1}{2}[S(f_{3,o,1}, f_{9,o,1}; 10,40,30)$$

$$+ S(g_{3,o,1}, g_{9,o,1}; 10,40,30)]\} - C_{11,2}\{S(f_{5,2,o}, f_{7,o,o};$$

$$\times\ 20,48,28) + S(f_{5,o,o}, f_{7,2,o}; 20,48,28) + \frac{1}{2}[S(f_{5,o,1},$$

$$\times\ f_{7,o,1}; 20,48,28) + S(g_{5,o,1}, g_{7,o,1}; 20,48,28)]\}, \qquad \text{(A21a)}$$

$$f_{11,2,o}(0) = f'_{11,2,o}(0) = 0, \qquad \text{(A21b)}$$

$$f'_{11,2,o} \to 0 \quad as \quad \eta \to \infty. \tag{A21c}$$

$$Lf_{11,o,2} - 2\sigma g'_{11,o,2} = -\frac{1}{2}(1 + C_{11,1} + C_{11,2}) - S(f_{1,o,2}, f_{11,o,o};$$
$$\times 1,12,11) - \frac{1}{2}\left[S(f_{1,o,1}, f_{11,o,1};1,12,11) - S(g_{1,o,1},\right.$$
$$\left.\times g_{11,o,1};1,12,11)\right] - C_{11,1}\, S(f_{3,o,o}, f_{9,o,2};10,40,30)$$
$$+ S(f_{3,o,2}, f_{9,o,o};10,40,30) + \frac{1}{2}\left[S(f_{3,o,1}, f_{9,o,1};10,40,30)\right.$$
$$\left. - S(g_{3,o,1}, g_{9,o,1};10,40,30)\right] - C_{11,2}\, S(f_{5,o,o}, f_{7,o,2};$$
$$\times 20,48,28) + S(f_{5,o,2}, f_{7,o,o};20,48,28) + \frac{1}{2}\left[S(f_{5,o,1},\right.$$
$$\left.\times f_{7,o,1};20,48,28) - S(g_{5,o,1}, g_{7,o,1};20,48,28)\right], \tag{A22a}$$

$$Lg_{11,o,2} + 2\sigma f'_{11,o,2} = -S(g_{1,o,2}, f_{11,o,o};1,12,11)$$
$$- \frac{1}{2}\left[S(f_{1,o,1}, g_{11,o,1};1,12,11) + S(g_{1,o,1},\right.$$
$$\left.\times f_{11,o,1};1,12,11)\right] - C_{11,1}\left\{S(f_{3,o,o}, g_{9,o,2};10,40,30)\right.$$
$$+ S(g_{3,o,2}, f_{9,o,o};10,40,30) + \frac{1}{2}\left[S(f_{3,o,1}, g_{9,o,1};10,40,30)\right.$$
$$\left.\left. + S(g_{3,o,1}, f_{9,o,1};10,40,30)\right]\right\} - C_{11,2}\left\{S(f_{5,o,o}, g_{7,o,2};\right.$$
$$\times 20,48,28) + S(g_{5,o,2}, f_{7,o,o};20,48,28) + \frac{1}{2}\left[S(f_{5,o,1},\right.$$
$$\left.\left.\times g_{7,o,1};20,48,28) + S(g_{5,o,1}, f_{7,o,1};20,48,28)\right]\right\}, \tag{A22b}$$

$$f_{11,o,2}(0) = f'_{11,o,2}(0) = g_{11,o,2}(0) = g'_{11,o,2}(0) = 0, \qquad \text{(A22c)}$$

$$f'_{11,o,2} \to g'_{11,o,2} \to 0 \quad \text{as} \quad \eta \to \infty. \qquad \text{(A22d)}$$

REFERENCES

Ackerberg, R.C. & Phillips, J.H. 1972, J. Fluid Mech. 51, 137.

Cayley, A. 1895, "Elliptic Functions" Second Ed. Reprinted Dover Pub., New York, 1955.

Carrier, G.F. & DiPrima, R.C. 1957, J. Math. & Phys. 35, 359.

Gibson, W.E. 1957, Ph.D. Math. Thesis, Mass. Inst. Tech.

Glauert, M.B. 1956, J. Fluid Mech. 1, 97.

Grosch, C.E. & Salwen, H. 1980, Proc. 15th Int. Cong. Theor. Appl. Mech., 155, Springer-Verlag, Berlin.

Harvey, W.D. & Bobbitt, P.J. 1981, AIAA-81-1225.

Kachanov, Yu. S., Kozlov, V.V. & Levchenko, V. Ya. 1978, Isv. Akad. Nauk SSSR, Mekh. Zhid. Gaza 5, 85.

Klebanoff, P.S., Tidstrom, K.D., & Sargent, L.M. 1962, J. Fluid Mech. 12, 1.

Lam, S.H. & Rott, N. 1960, Cornell Univ. GSAE Rep. AFOSR TN-60-1100.

Lighthill, M.J. 1954, Proc. Roy. Soc., A, 224, 1.

Lighthill, M.J. 1978, J. Sound & Vib. 61, 391.

Lin, C.C. 1956, Proc. 9th Int. Cong. Theor. Appl. Mech., 136, Springer-Verlag, Berlin.

Mack, L.M. 1977, JPL Pub. 77-15, Jet Prop. Lab., Cal. Inst. Tech.

Milne-Thomson, L.M. 1955, "Theoretical Hydrodynamics", 3rd Ed. MacMillan Comp., New York.

Moore, F.K. 1951, NACA TN 2471.

Morkovin, M.V. 1978, AGARDograph No. 236, NATO, Paris.

Obremski, H. J., Morokovin, M.V., & Landahl, M. 1969, AGARDogroph No. 134, NATO, Paris.

Riley, N. 1975, SIAM Rev. 17, 274.

Rott, N. 1956, Quart. Appl. Math. 13, 444.

Rott, N. & Rosenzweig, M.L. 1960, J. Aerospace Sci. 27, 74.

Salwen, H., Kelly, K.A. & Grosch, C.E. 1980, Bull. Am. Phys. Soc. 25, 1085.

Salwen, H. & Grosch, C.E. 1981, J. Fluid Mech. 104, 445.

Sarma, G.N. 1964, Proc. Camb. Phil. Soc. 60, 137.

Schlichting, H. 1979, "Boundary Layer Theory" McGraw-Hill Comp. New York.

Smith, A.M.O. 1956, Proc. 9th Intl. Cong. Theor. Appl. Mech. Springer-Verlag, Berlin.

Stuart, J.T. 1966, J. Fluid Mech. 24, 673.

Van Dyke, M. 1956, Proc. 9th Intl. Cong. Theor. Appl. Mech. 318, Springer-Verlag, Berlin.

Van Ingen, J.L. 1956, Rept. UTH-74, Dept. Aero. Eng. Univ. of Tech. Delft.

Watson, J. 1959, Quart. J. Mech. Appl. Math. 12, 175.

Table 1. Coefficients in the power series expansion of the potential velocity function, $H(\xi)$, for flow past an elliptic cylinder.

$2n + 1$	$[1 + (b/a)]^{-1} a_{2n+1}$
1	1
3	$-(1 + k^2)/3!$
5	$(1 + 14k^2 + k^4)/5!$
7	$-(1 + 135k^2 + 135k^4 + k^6)/7!$
9	$(1 + 1228k^2 + 5478k^4 + 1228k^6 + k^8)/9!$
11	$(1 + 11069k^2 + 165826k^4 + 165826k^6 + 11069k^8 + k^{10})/11!$

Table 2. Parameters of the elliptic cylinders for which results are given.

a/b	k^2	$E(k)$
5	0.96	1.05050
10	0.99	1.01599
25	0.9984	1.00329

Table 3. The position in the boundary layer of the maximum of $\hat{u}_{1,o}$.

σ	a/b =	5.0	10.0	25.0
$\pi/4$		2.2	2.1	2.0
π		1.9	1.8	1.7
3π		1.2	1.1	1.05
6π		0.9	0.8	0.75

Table 4. Total phase shift, in degrees, of $\hat{u}_{1,o}$.

σ	a/b =	5.0	10.0	25.0
$\pi/4$		11.2	11.9	12.0
π		30.0	30.0	30.0
3π		42.0	40.0	40.0
6π		42.0	42.0	40.0

Table. 5. Coefficients in the power series expansion of the potential velocity function, $H(\xi)$, for flow past a parabolic cylinder.

$2n + 1$	$a_{2n\ 1}$
1	$1/4$
3	$-\ 1/2^2.3!$
5	$22/2^4.5!$
7	$-1168/2^6.7!$
9	$113536/2^8.9!$
11	$-17521024/2^{10}.11!$

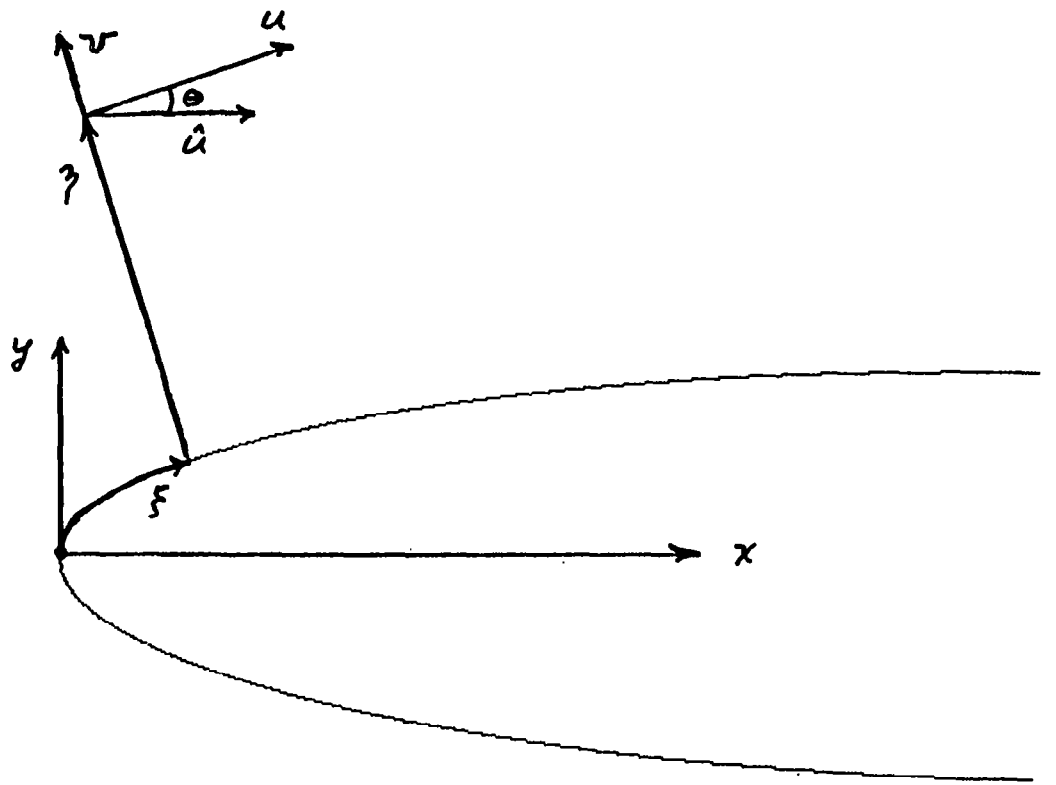

Figure 1. Coordinate system.

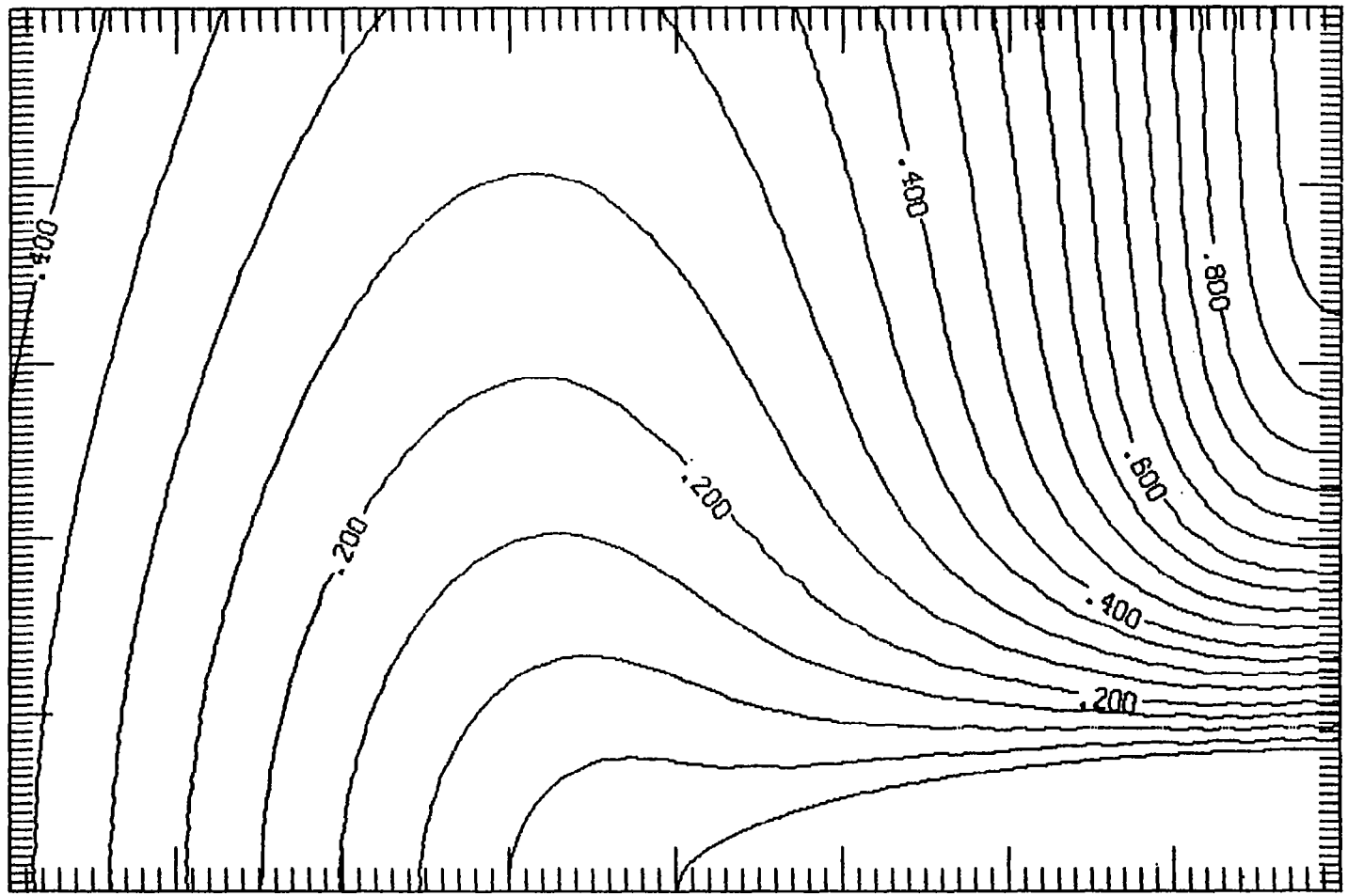

Figure 2. Contours of the zero order steady flow, $\hat{u}_{o,o}$. Contours from 0.0 to 0.90 with an interval of 0.05. The body is an ellipse with a/b = 5.

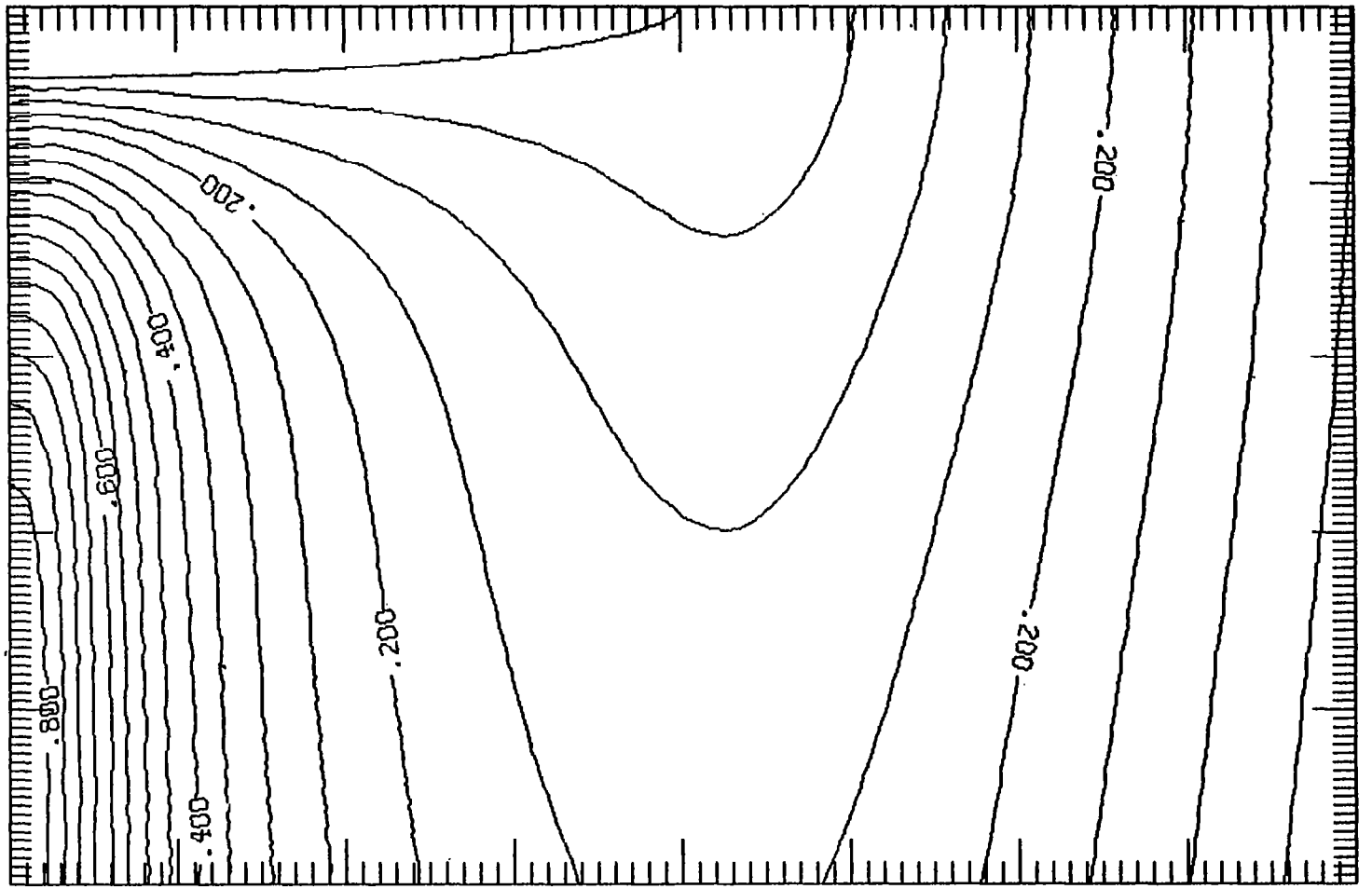

Figure 3. Contours of the zero order steady flow, $\hat{u}_{0,0}$. Contours from 0.0 to 0.80 with an interval of 0.05. The body is an ellipse with a/b = 10.

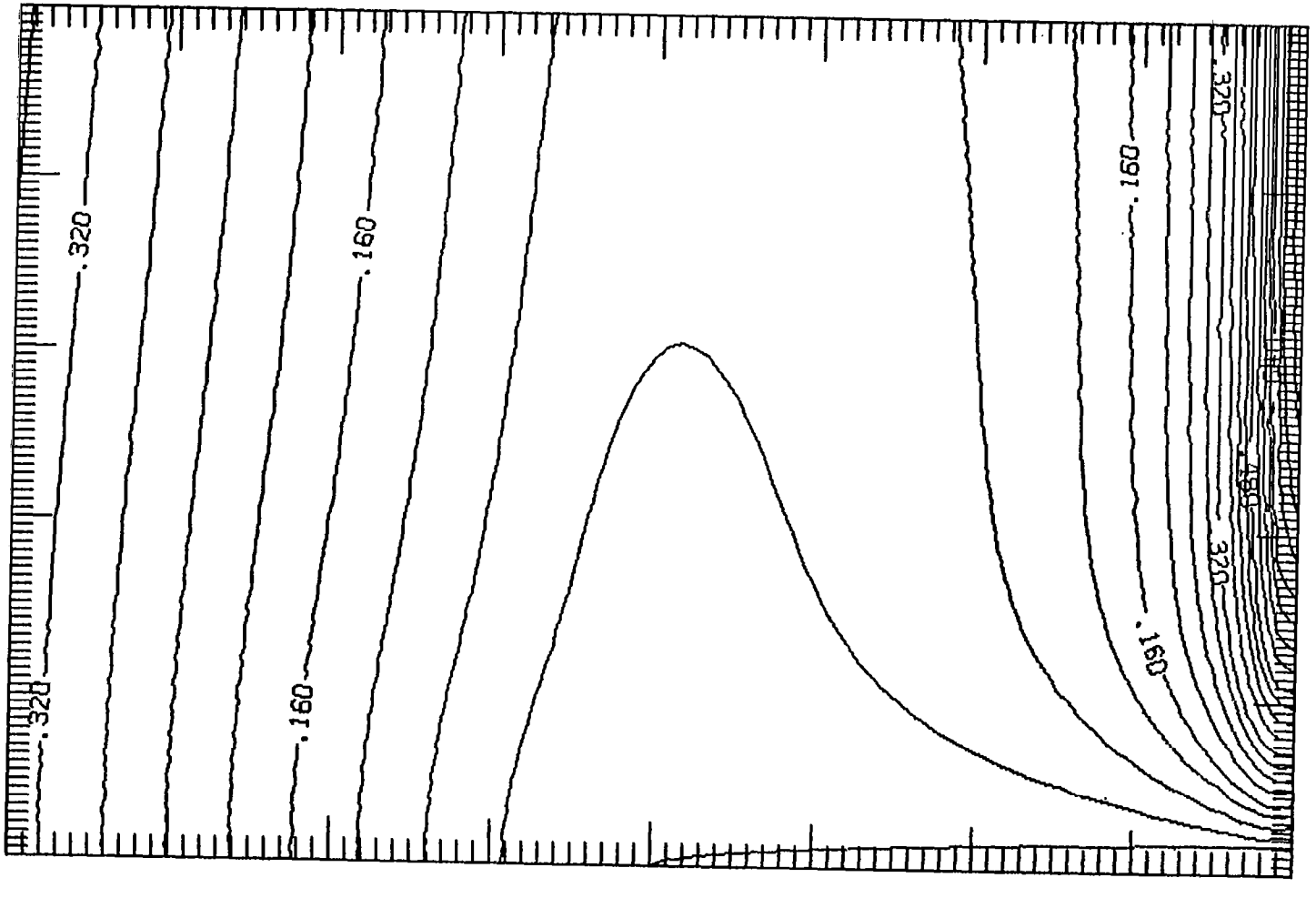

Figure 4. Contours of the zero order steady flow, $\hat{u}_{o,o}$. Contours from 0.0 to 0.74 with an interval of 0.04. The body is an ellipse with a/b = 25.

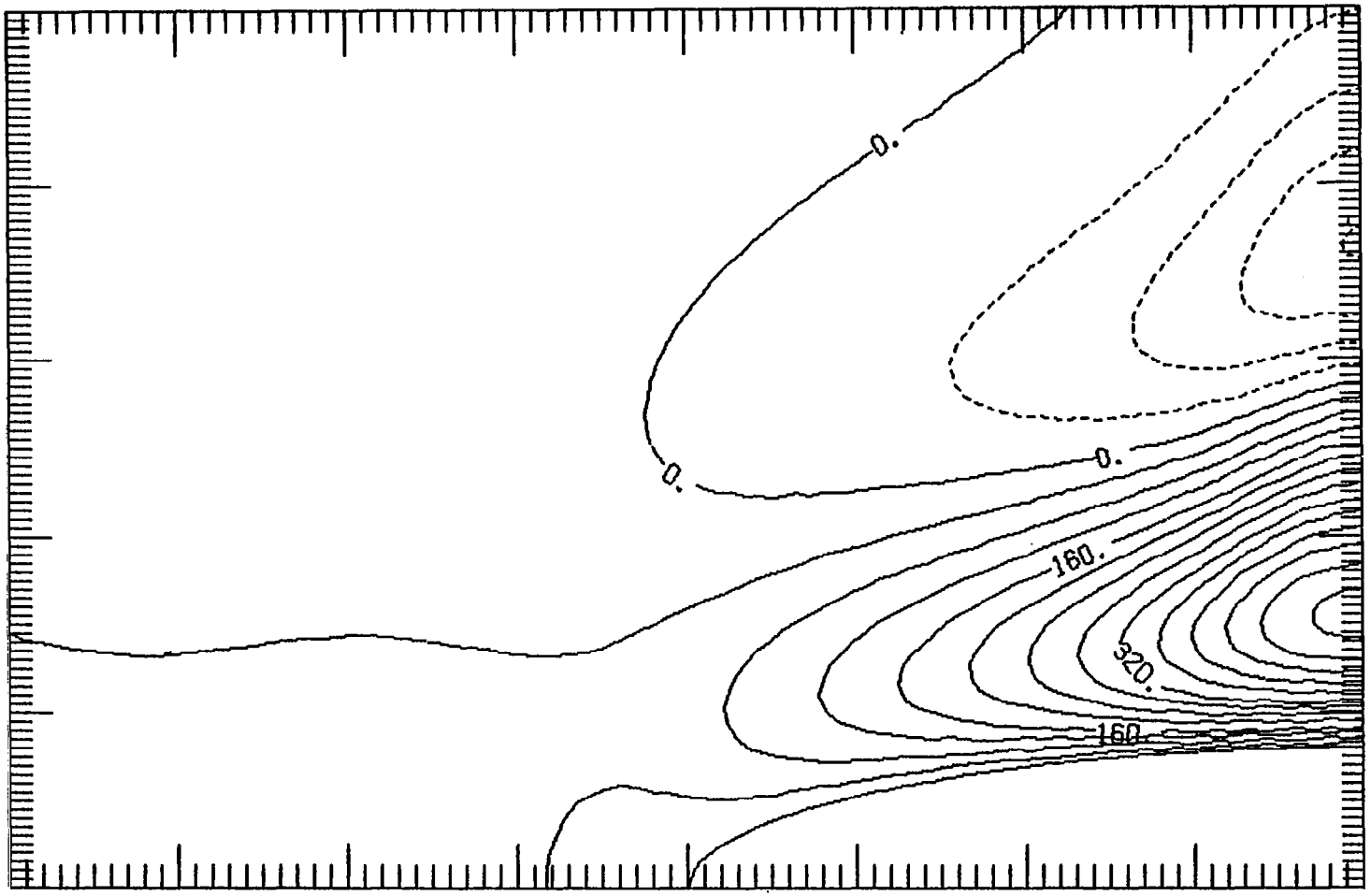

Figure 5. Contours of the second order steady flow, $\hat{u}_{2,o}$. Contours from -1.6×10^{-2} to 5.2×10^{-2} with an interval of 4.0×10^{-3}. The labels are scaled by 10^4. The body is an ellipse with a/b = 5 and $\sigma = \pi/4$.

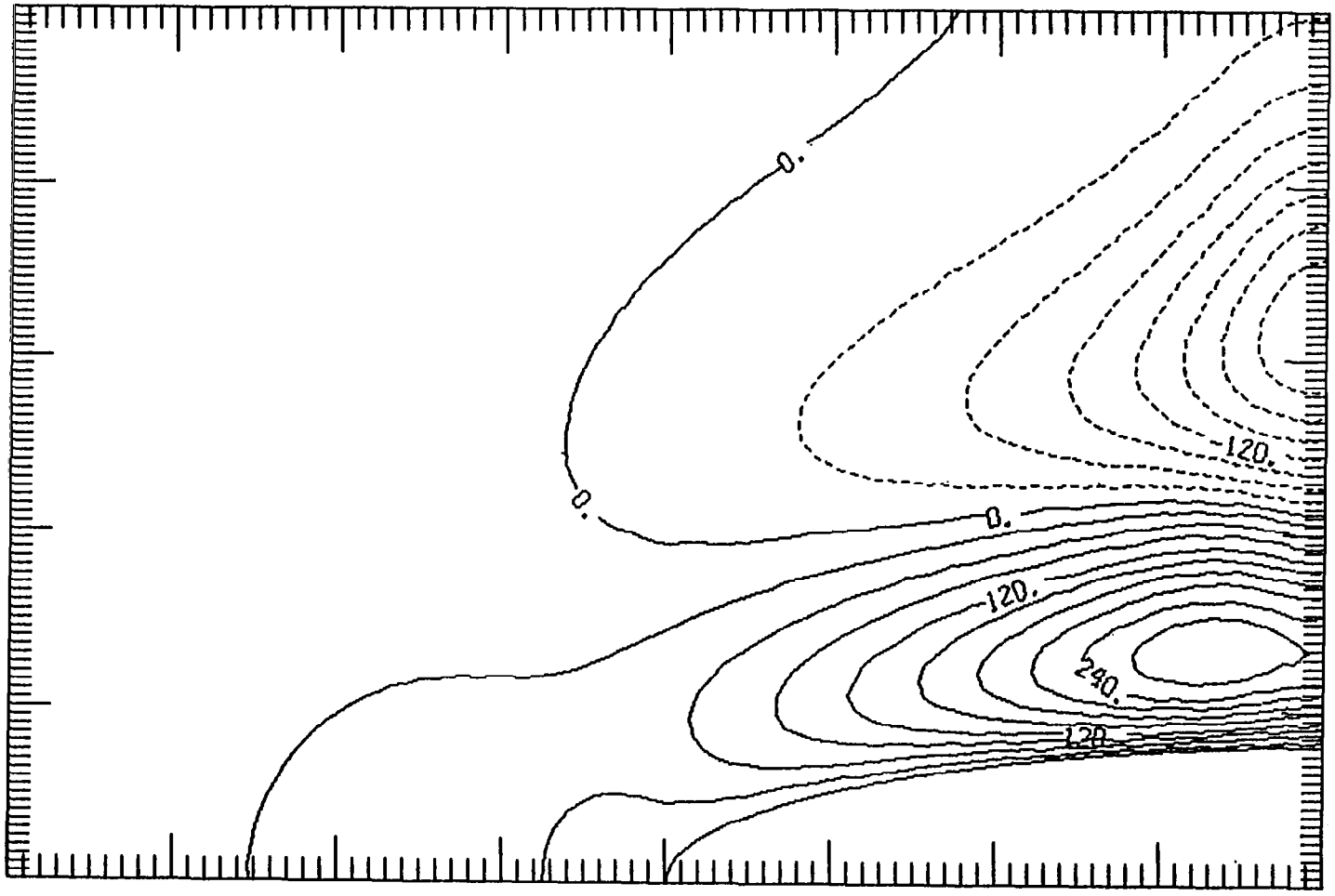

Figure 6. Contours of the second order steady flow, $\hat{u}_{2,o}$. Contours from -2.1×10^{-2} to 2.7×10^{2} with an interval of 3.0×10^{-3}. The labels are scaled by 10^{4}. The body is an ellipse with a/b = 5 and $\sigma = \pi$.

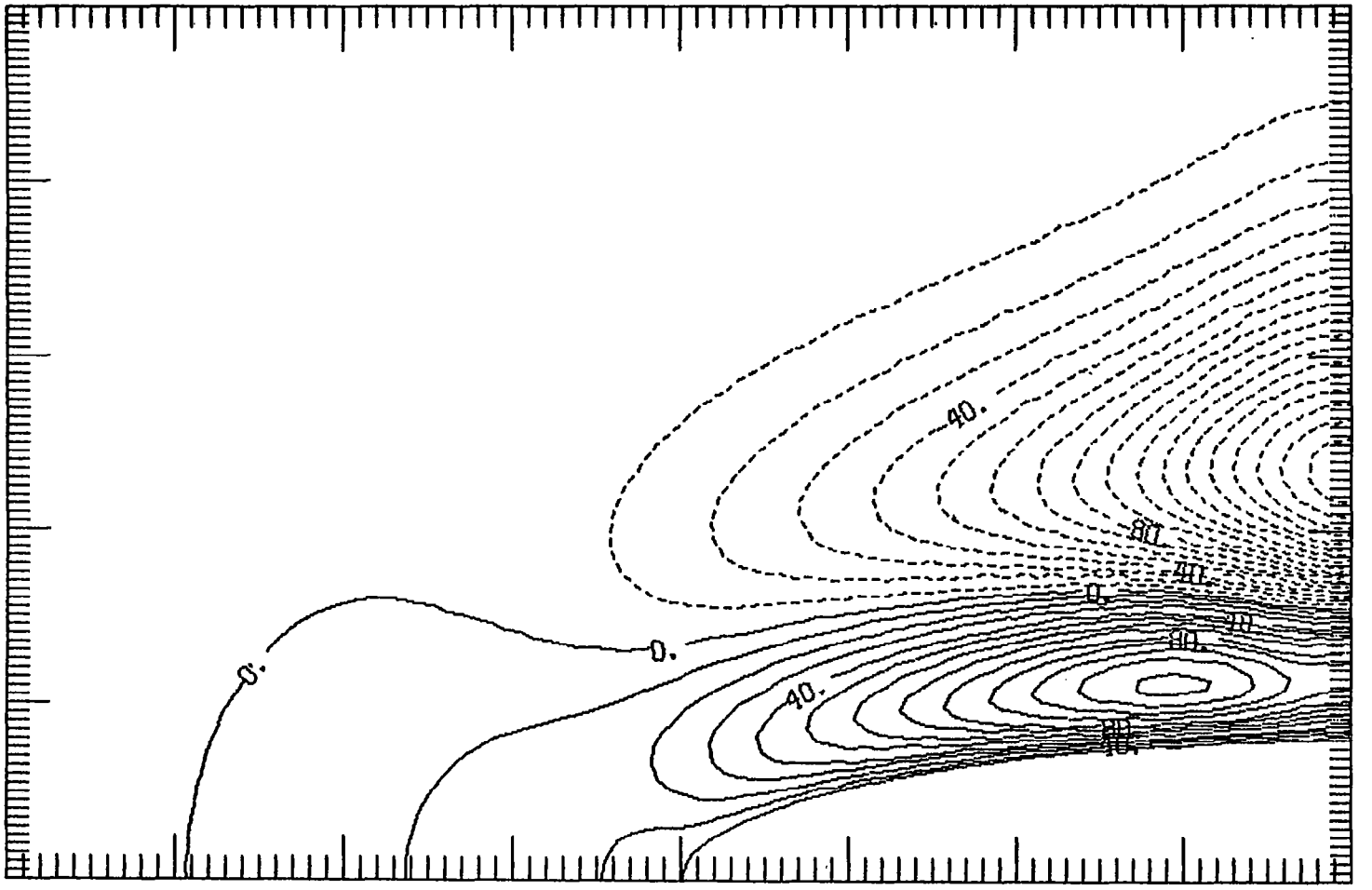

Figure 7. Contours of the second order steady flow, $\hat{u}_{2,o}$. Contours from -1.7×10^{-2} to 1.2×10^{-2} with an interval of 1.0×10^{-3}. The labels are scaled by 10^4. The body is an ellipse with a/b = 5 and $\sigma = 3\pi$.

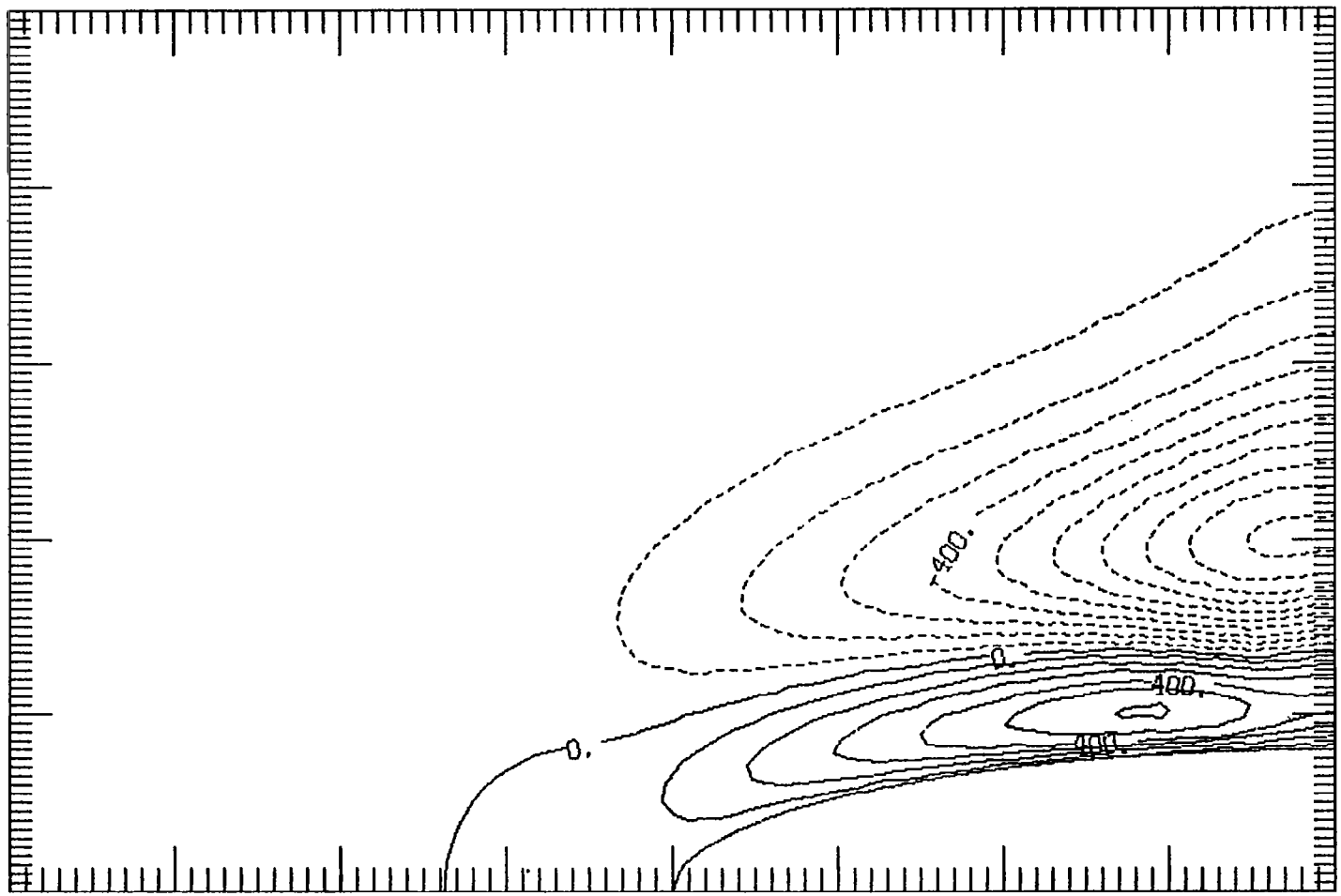

Figure 8. Contours of the second order steady flow, $\hat{u}_{2,o}$. Contours from -1.0×10^{-2} to 6.0×10^{-3} with an interval of 1.0×10^{-3}. The labels are scaled by 10^5. The body is an ellipse with a/b = 5 and $\sigma = 6\pi$.

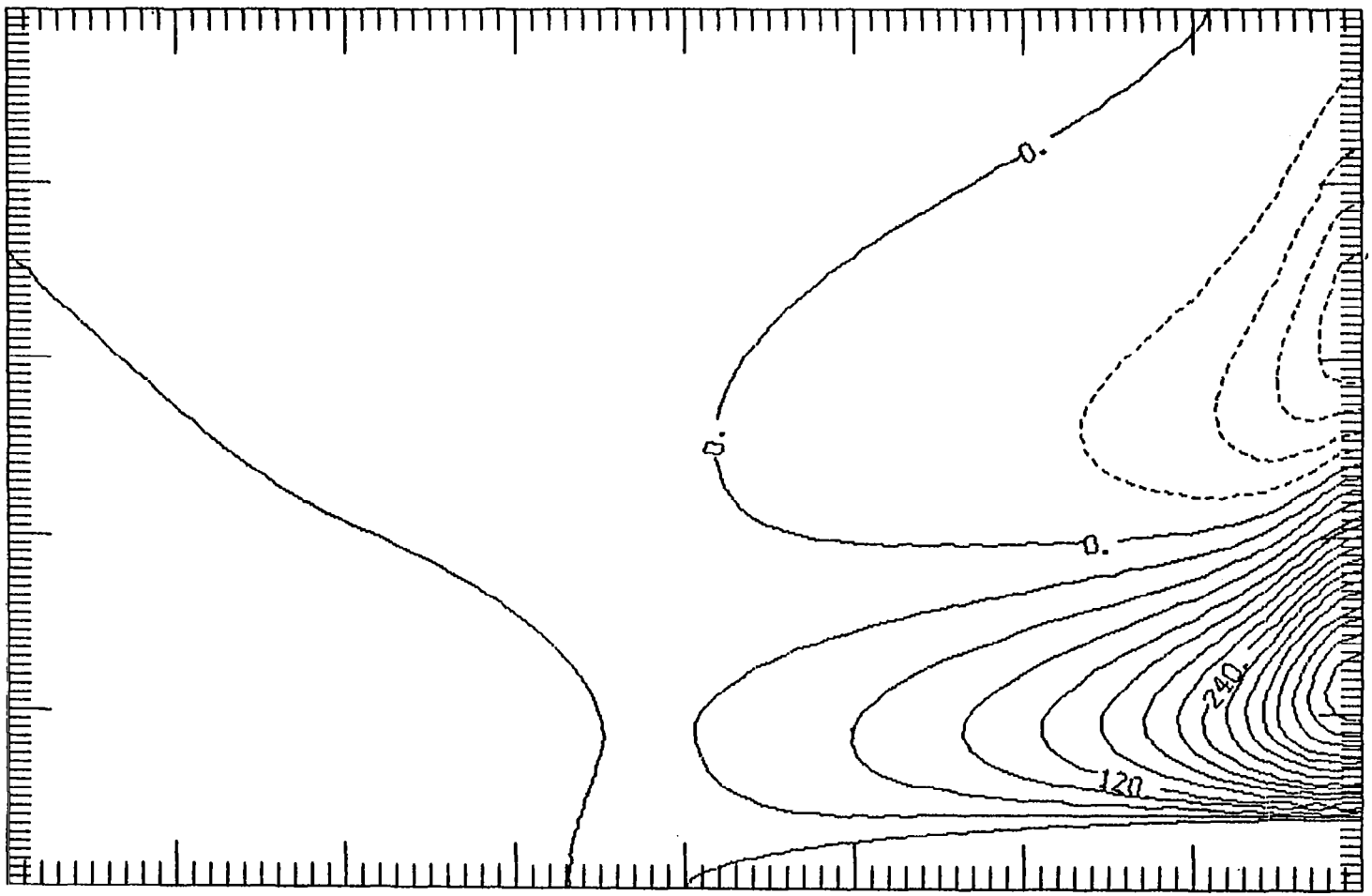

Figure 9. Contours of the second order steady flow, $\hat{u}_{2,o}$. Contours from -1.2×10^{-2} to 4.5×10^{-2} with an interval of 3.0×10^{-3}. The labels are scaled by 10^4. The body is an ellipse with a/b = 10 and $\sigma = \pi/4$.

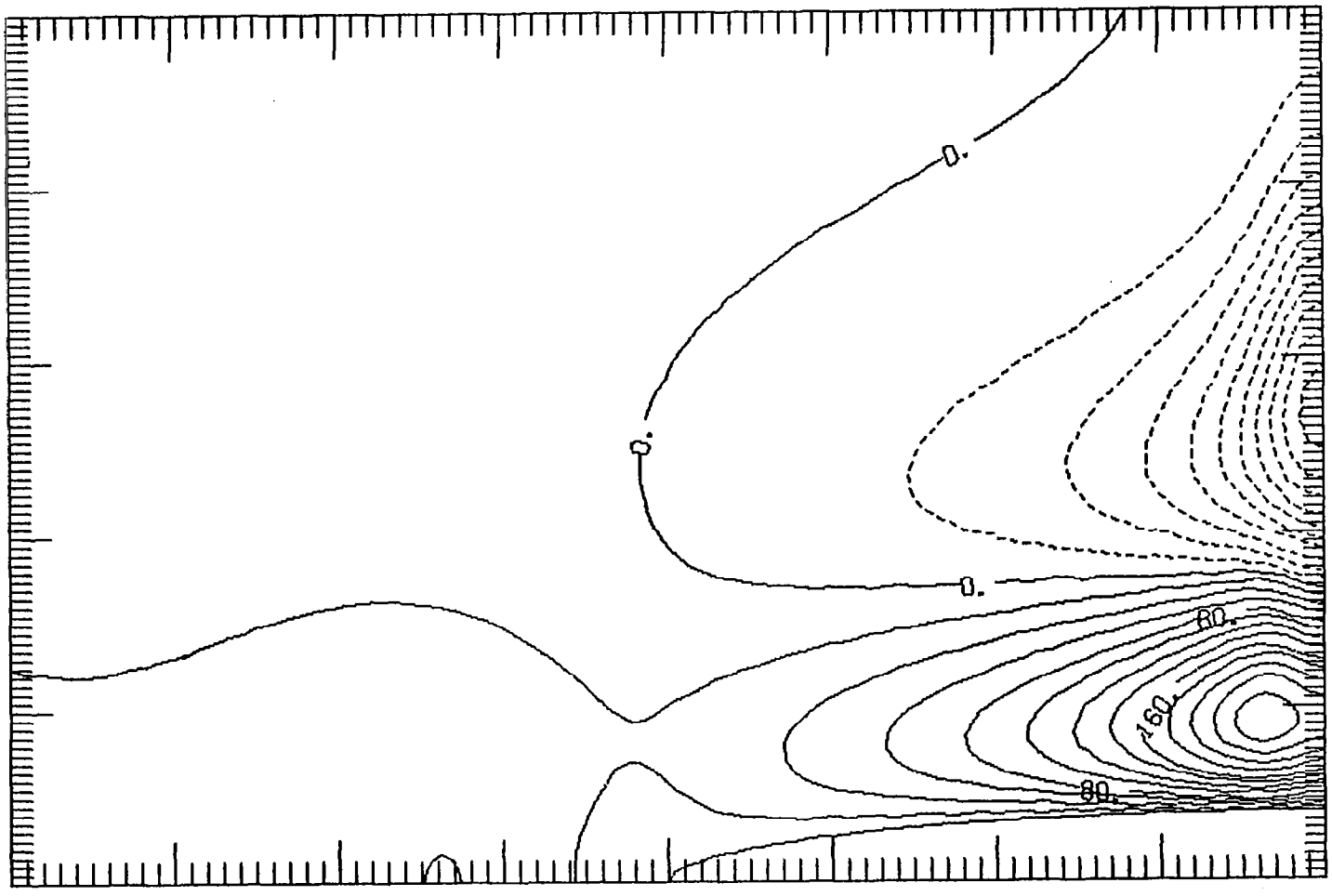

Figure 10. Contours of the second order steady flow, $\hat{u}_{2,o}$. Contours from -2.0×10^{-2} to 2.4×10^{-2} with an interval of 2.0×10^{-3}. The labels are scaled by 10^4. The body is an ellipse with a/b = 10 and $\sigma = \pi$.

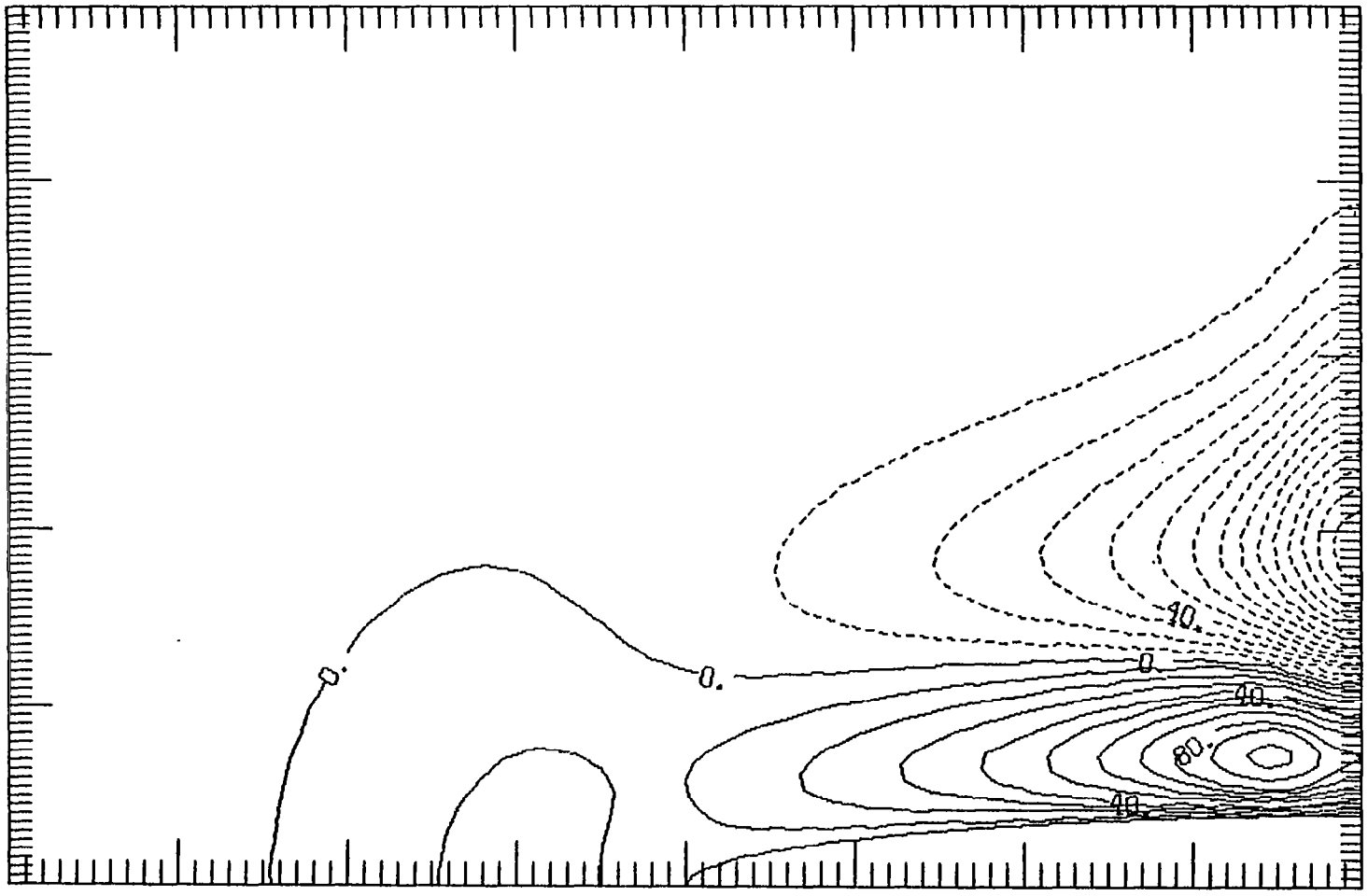

Figure 11. Contours of the second order steady flow, $\hat{u}_{2,o}$. Contours from -1.4×10^{-2} to 1.0×10^{-2} with an interval of 1.0×10^{-3}. The labels are scaled by 10^4. The body is an ellipse with a/b = 10 and $\sigma = 3\pi$.

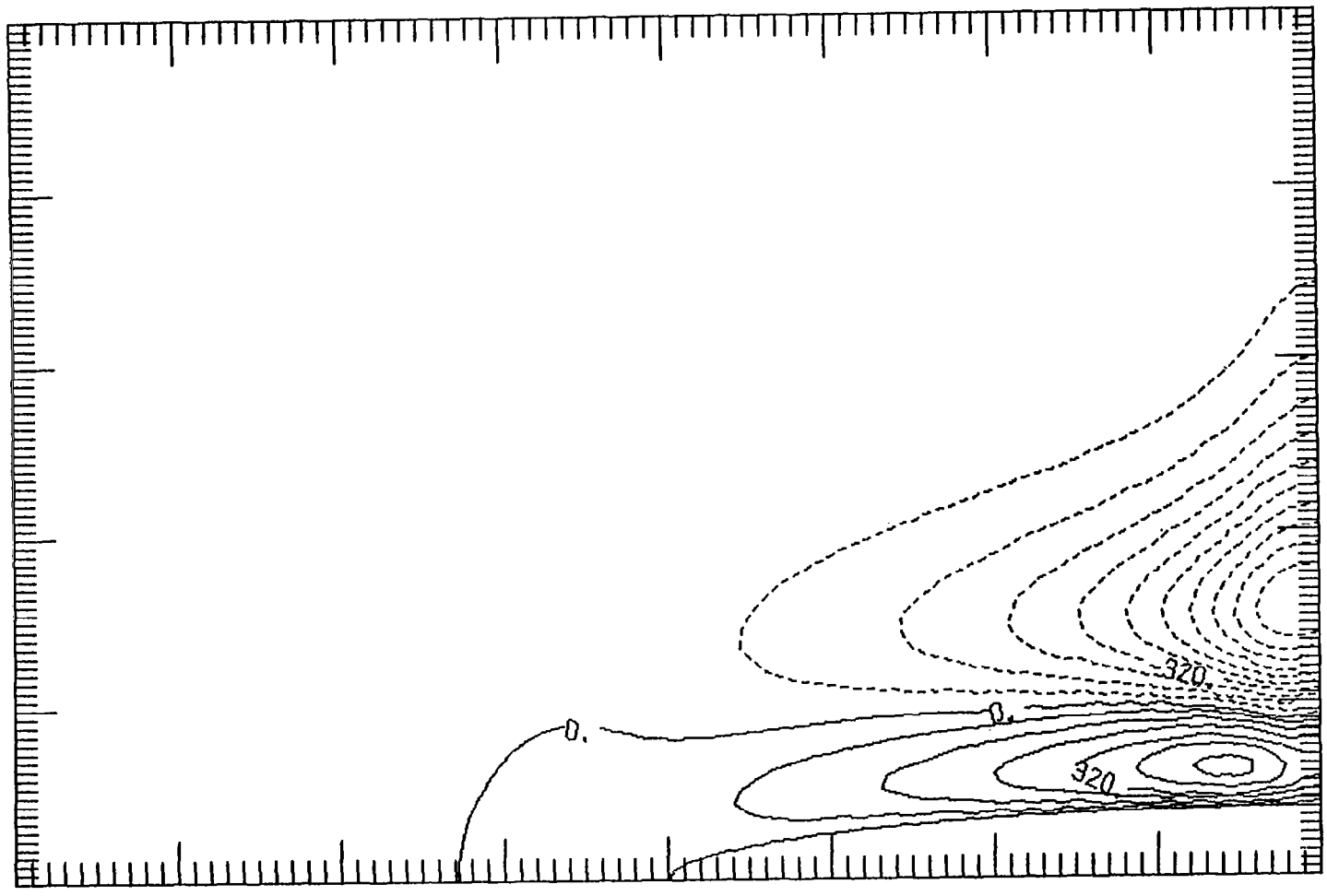

Figure 12. Contours of the second order steady flow, $\hat{u}_{2,o}$. Contours from -8.0×10^{-3} to 4.8×10^{-3} with an interval of 8.0×10^{-4}. The labels are scaled by 10^5. The body is an ellipse with a/b = 10 and $\sigma = 6\pi$.

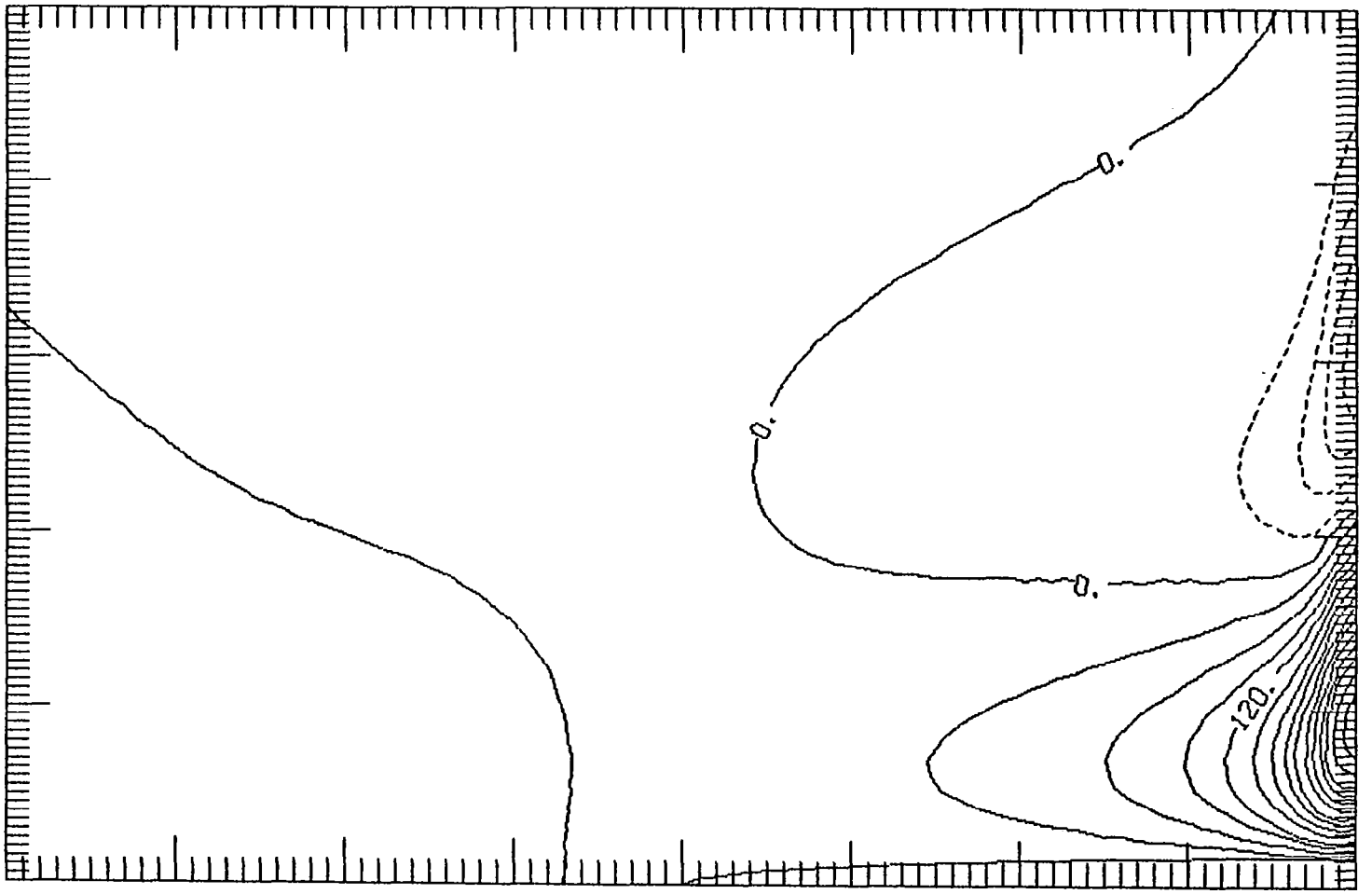

Figure 13. Contours of the second order steady flow, $\hat{u}_{2,o}$. Contours from -1.2×10^{-2} to 4.2×10^{-2} with an interval of 3.0×10^{-3}. The labels are scaled by 10^{4}. The body is an ellipse with a/b = 25 and $\sigma = \pi/4$.

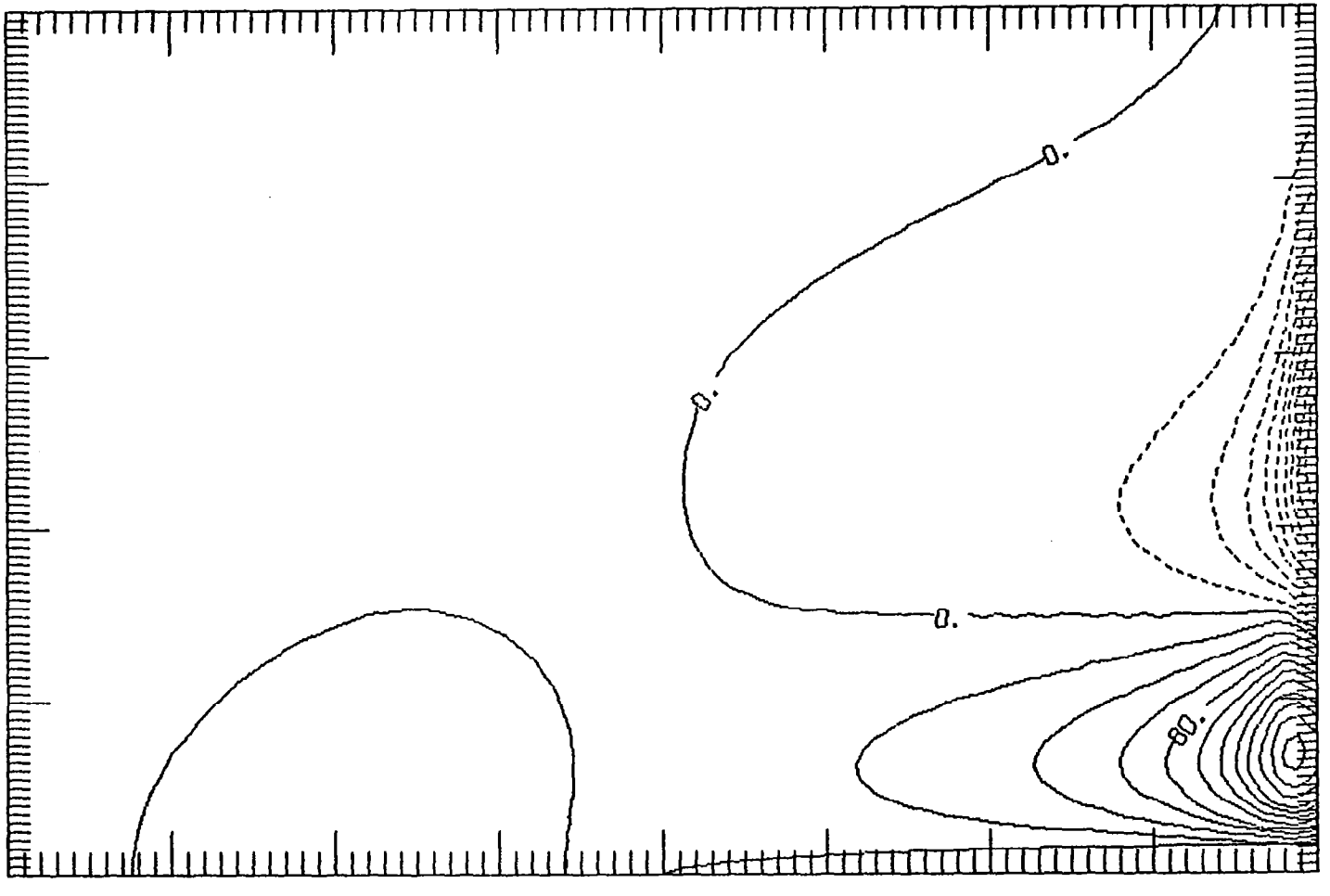

Figure 14. Contours of the second order steady flow, $\hat{u}_{2,o}$. Contours from -1.8×10^{-2} to 2.2×10^{-2} with an interval of 2.0×10^{-2}. The labels are scaled by 10^4. The body is an ellipse with a/b = 25 and $\sigma = \pi$.

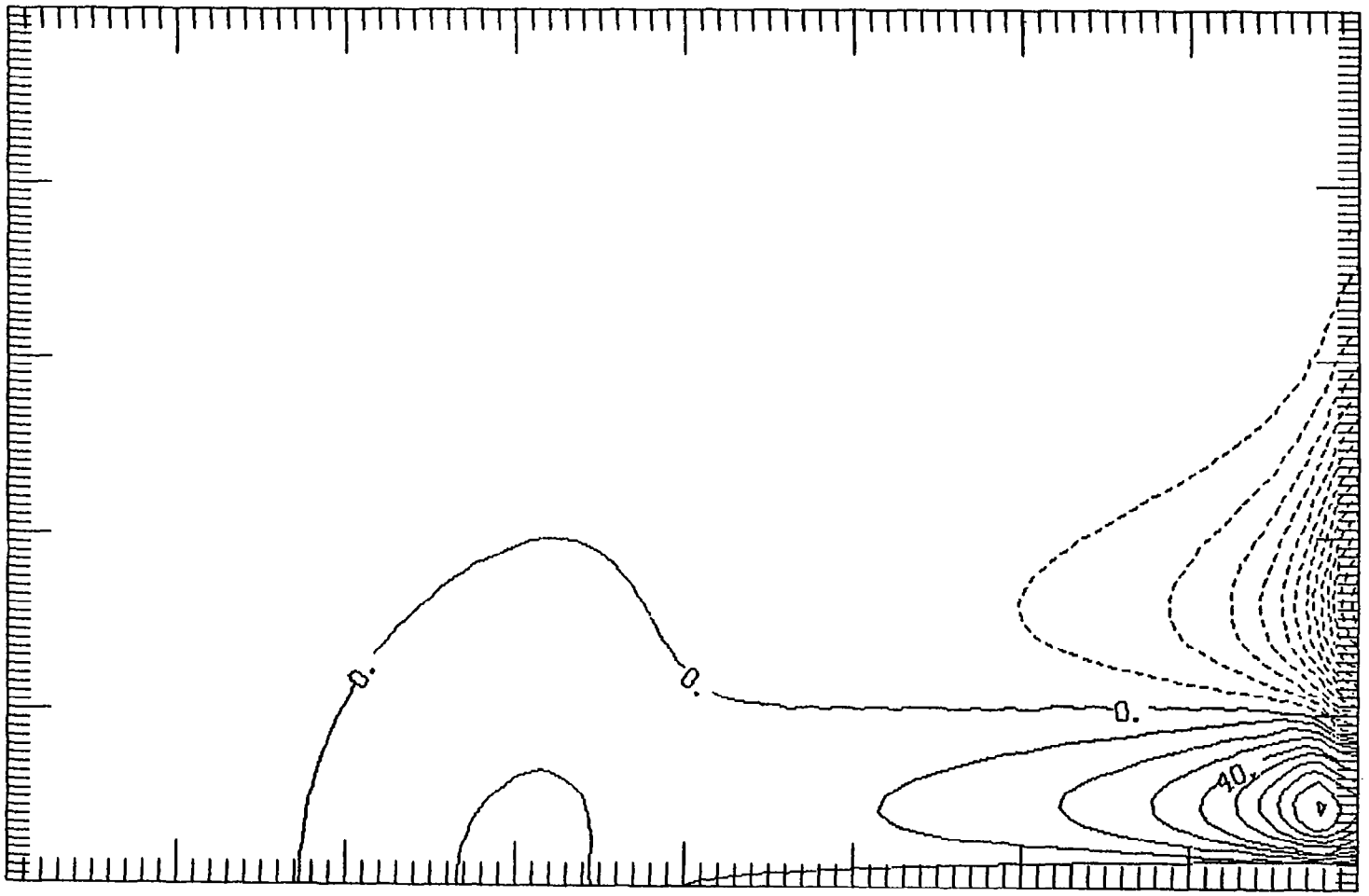

Figure 15. Contours of the second order steady flow, $\hat{u}_{2,o}$. Contours from -1.3×10^{-2} to 8.0×10^{-3} with an interval of 1.0×10^{-3}. The labels are scaled by 10^4. The body is an ellipse with a/b = 25 and $\sigma = 3\pi$.

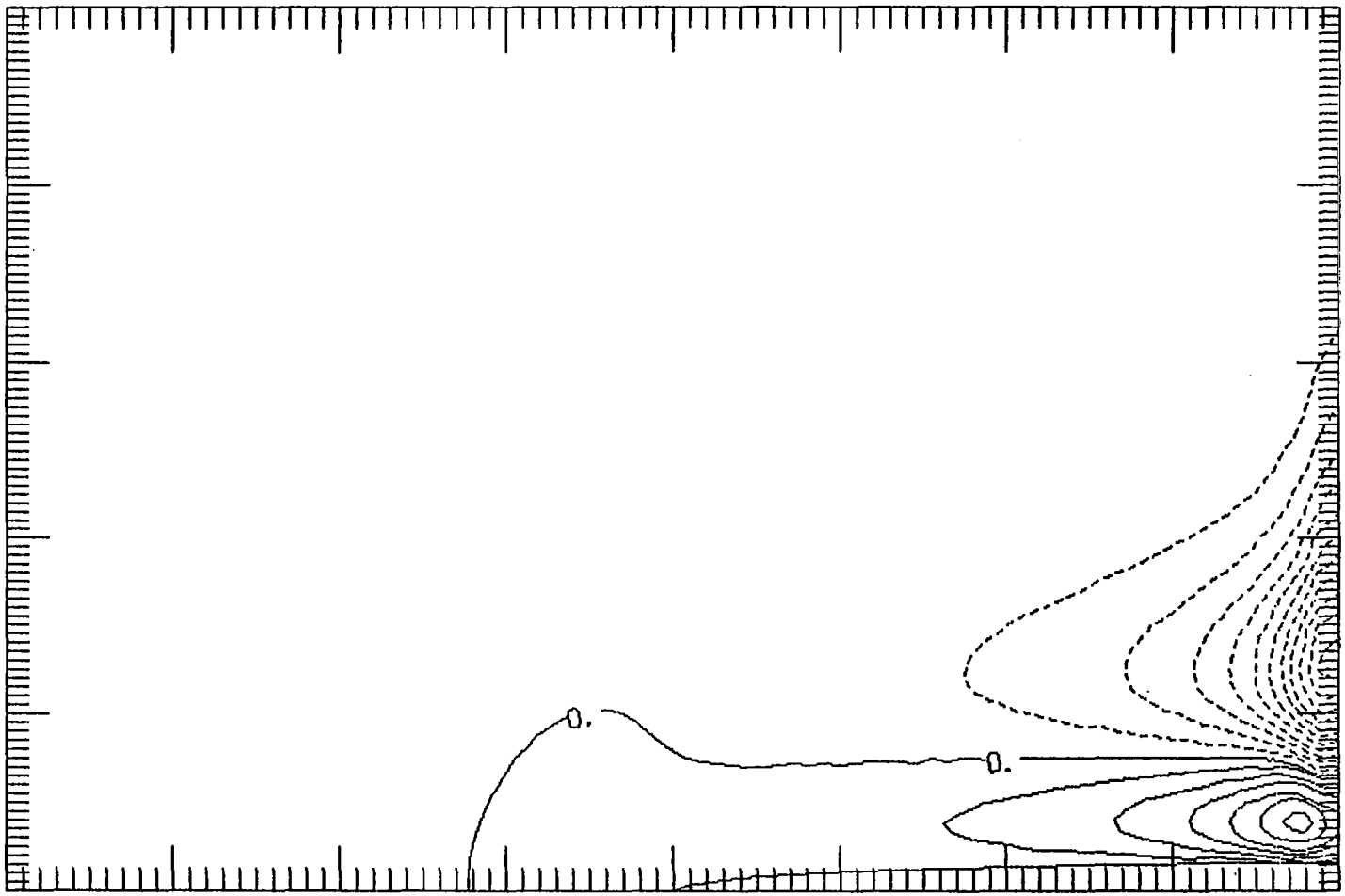

Figure 16. Contours of the second order steady flow, $\hat{u}_{2,o}$. Contours from -7.7×10^{-3} to 4.2×10^{-3} with an interval of 7.0×10^{-4}. The labels are scaled by 10^5. The body is an ellipse with a/b = 25 and $\sigma = 6\pi$.

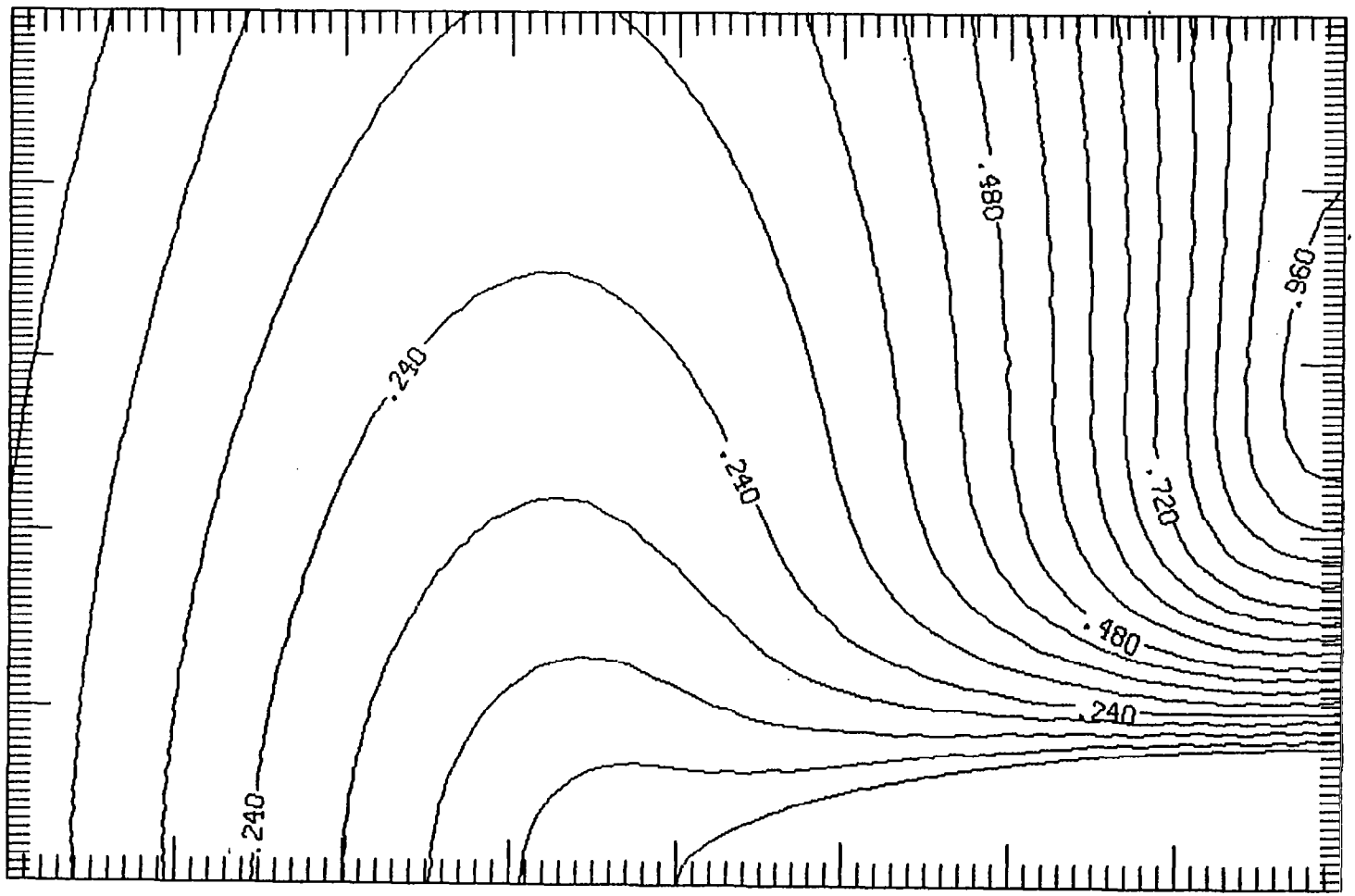

Figure 17a. Contours of the amplitude of $\hat{u}_{o,1}$, the fundamental oscillation. Contours from 0.0 to 0.96 with an interval of 0.06. The body is an ellipse with a/b = 5, and $\sigma = \pi/4$.

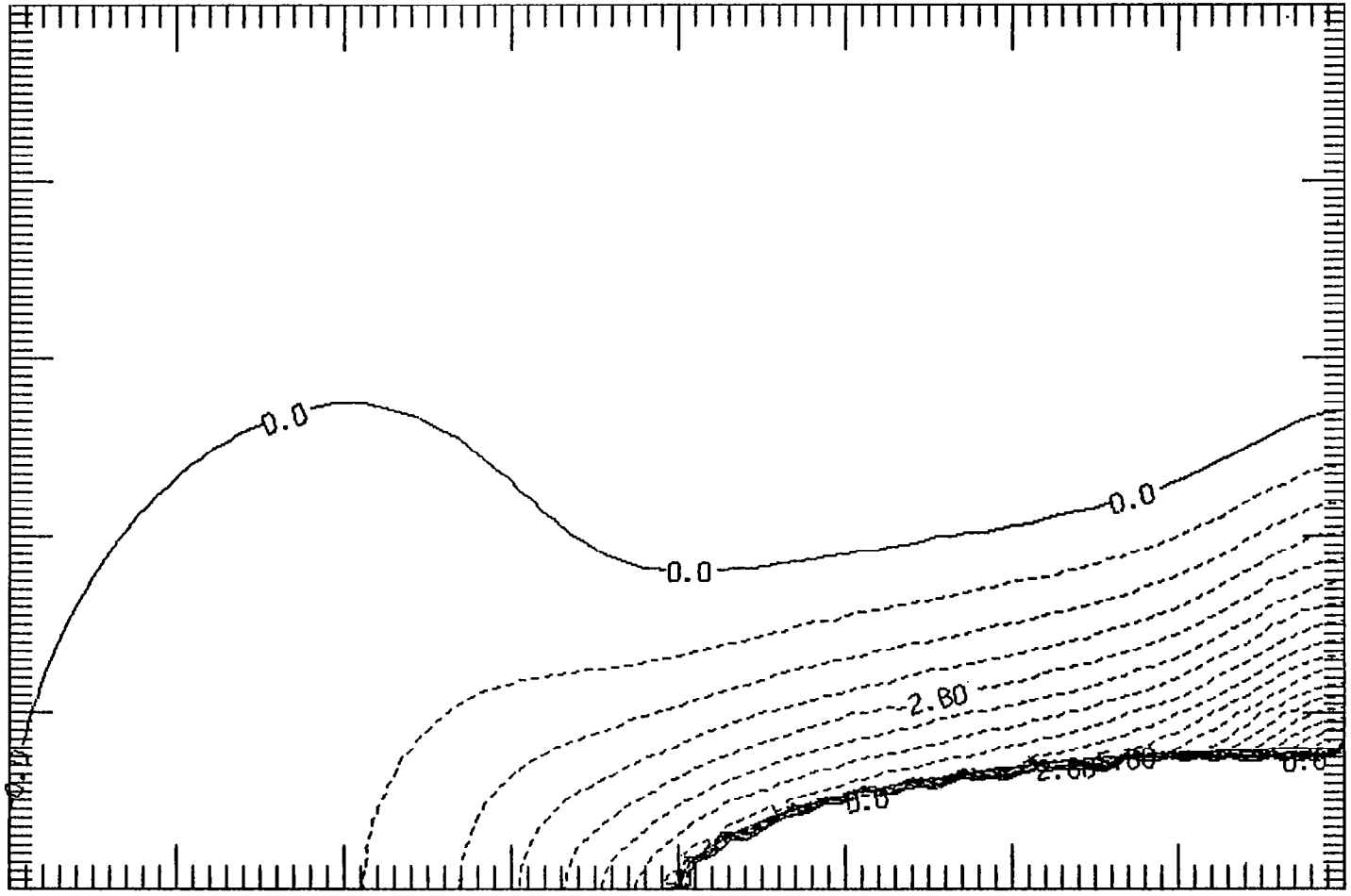

Figure 17b. Contours of the phase, in degrees, of $\hat{u}_{o,1}$, the fundamental oscillation. Contours from -11.2° to 0° with an interval of 0.7°. The body is an ellipse with a/b = 5, and $\sigma = \pi/4$.

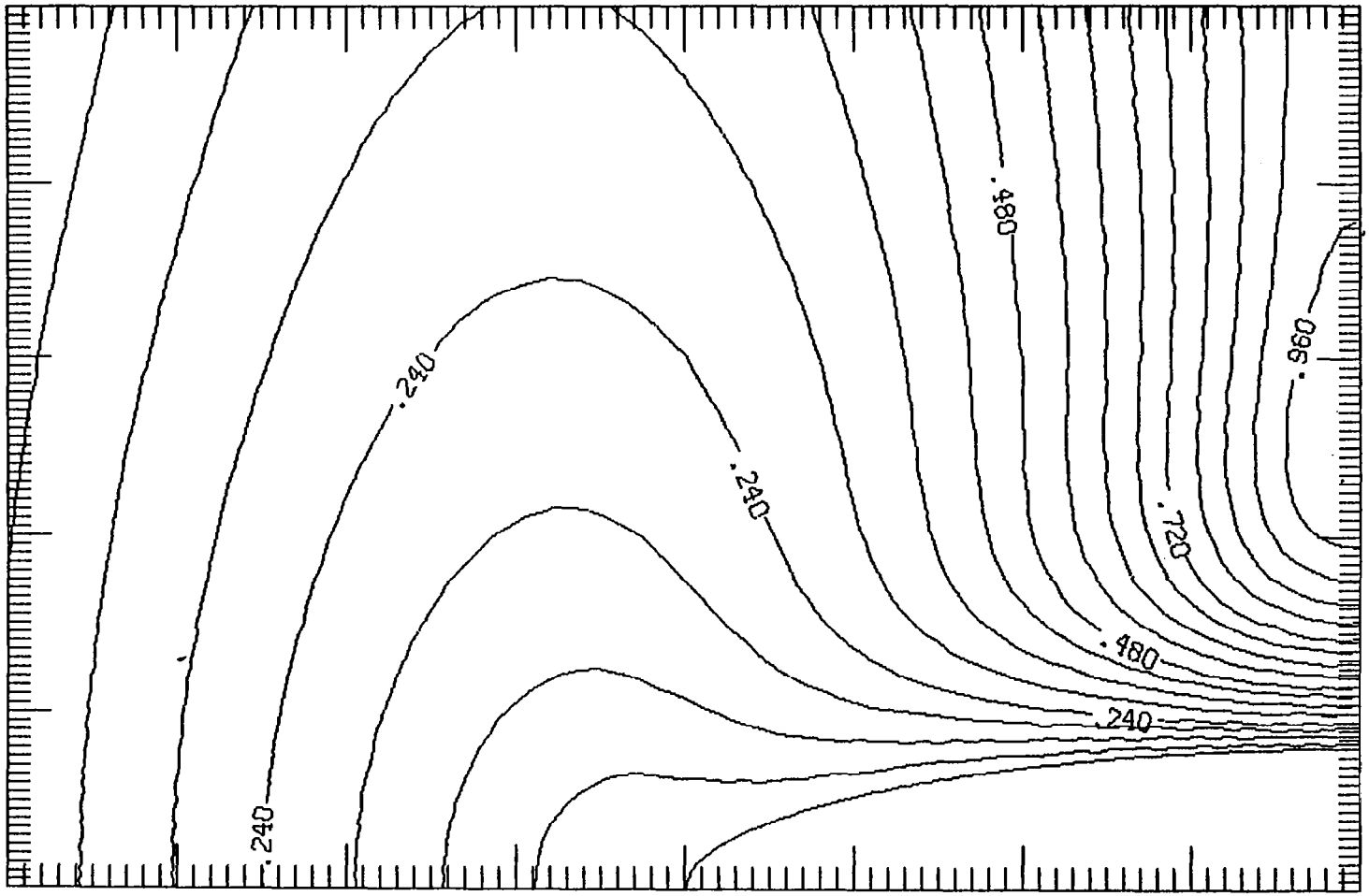

Figure 18a. Contours of the amplitude of $\hat{u}_{0,1}$, the fundamental oscillation. Contours from 0.0 to 0.96 with an interval of 0.06. The body is an ellipse with a/b = 5, and $\sigma = \pi$.

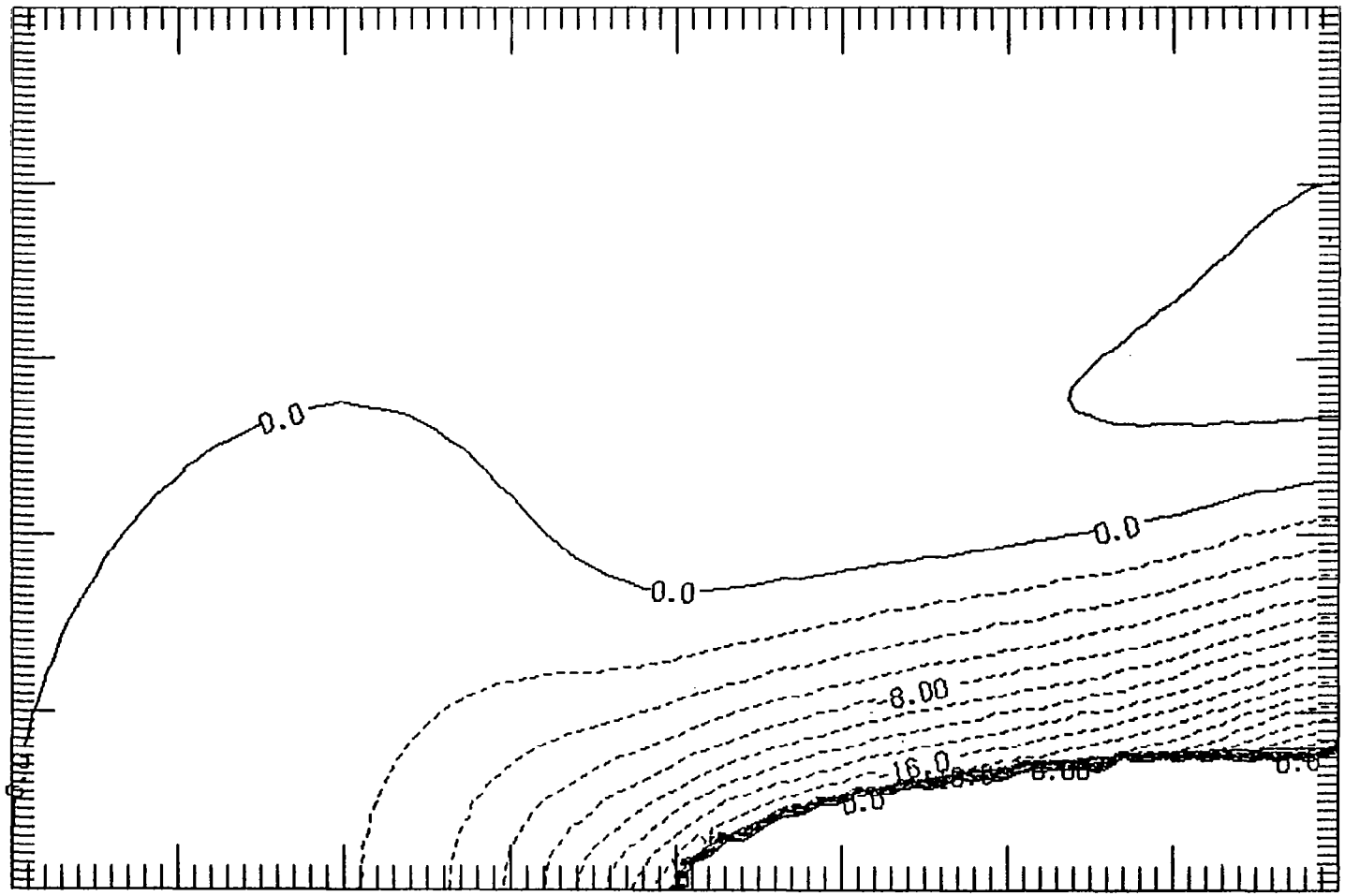

Figure 18b. Contours of the phase, in degrees, of $\hat{u}_{o,1}$, the fundamental oscillation. Contours from -28.0° to 2.0° with an interval of 2.0°. The body is an ellipse with a/b = 5, and σ = 5.

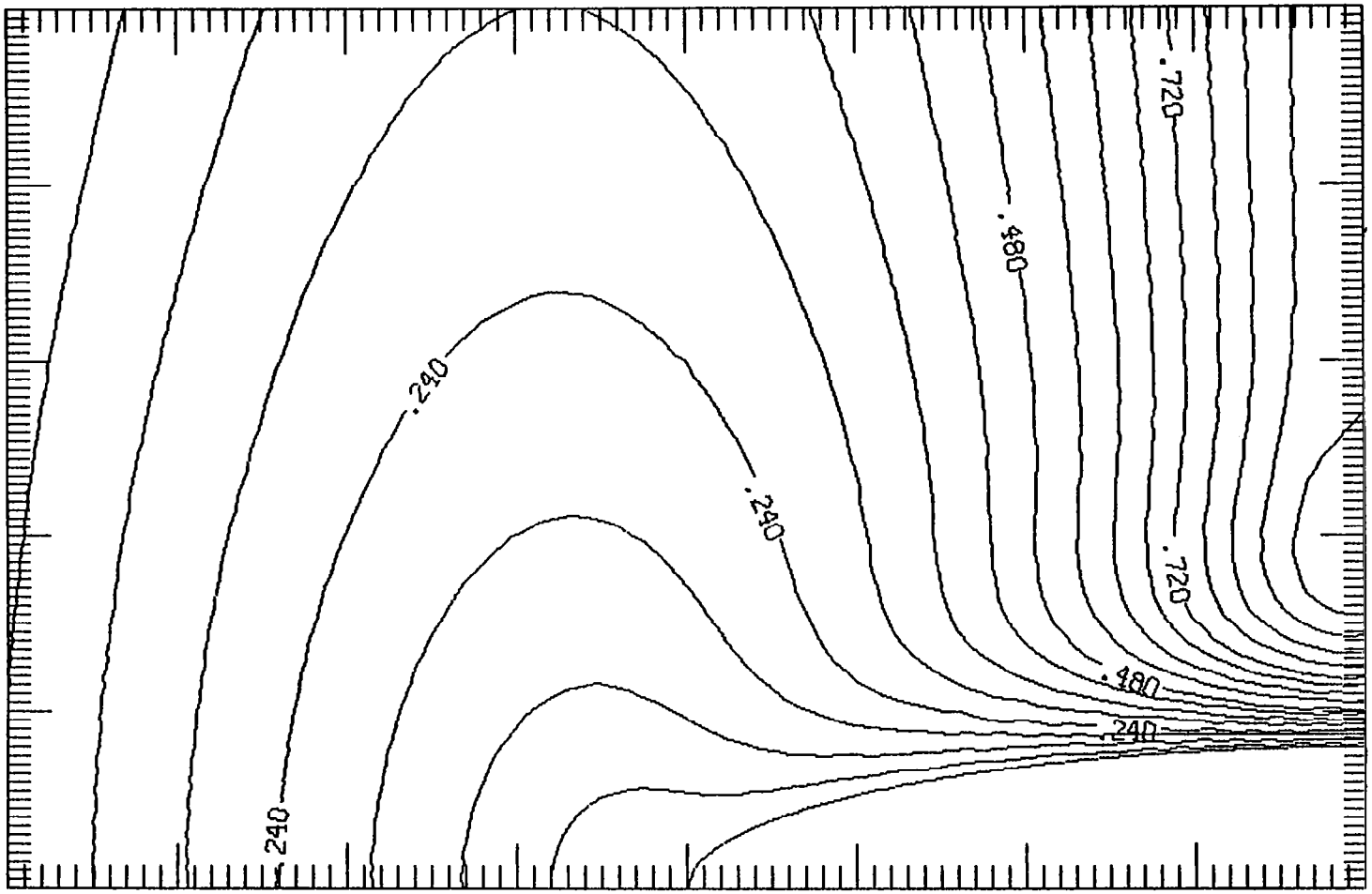

Figure 19a. Contours of the amplitude of $\hat{u}_{o,1}$, the fundamental oscillation. Contours from 0.0 to 0.96 with an interval of 0.06. The body is an ellipse with a/b = 5, and $\sigma = 3\pi$.

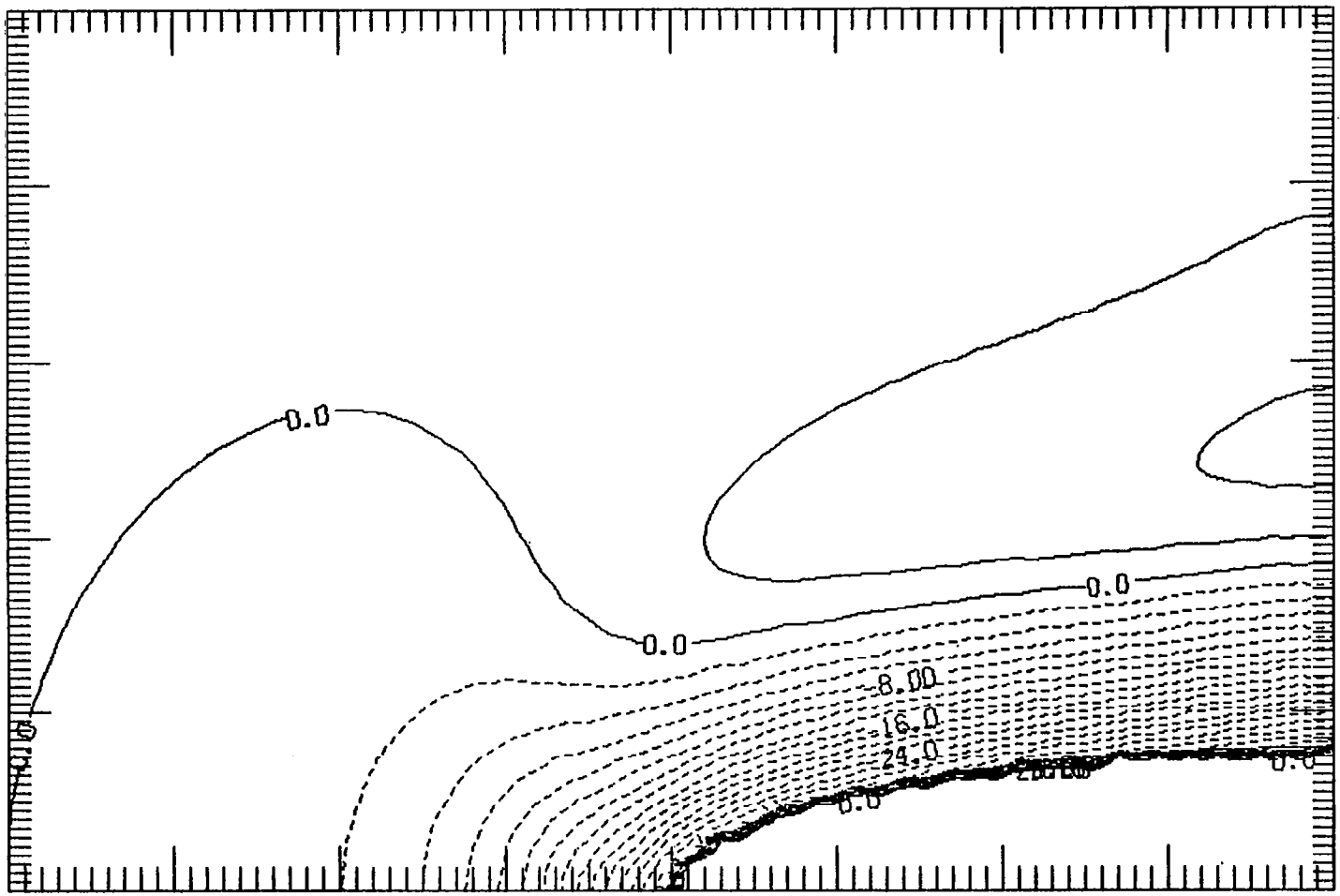

Figure 19b. Contours of the phase, in degrees, of $\hat{u}_{0,1}$, the fundamental oscillation. Contours from $-38.0°$ to $4.0°$ with an interval of $2.0°$. The body is an ellipse with a/b = 5, and $\sigma = 3\pi$.

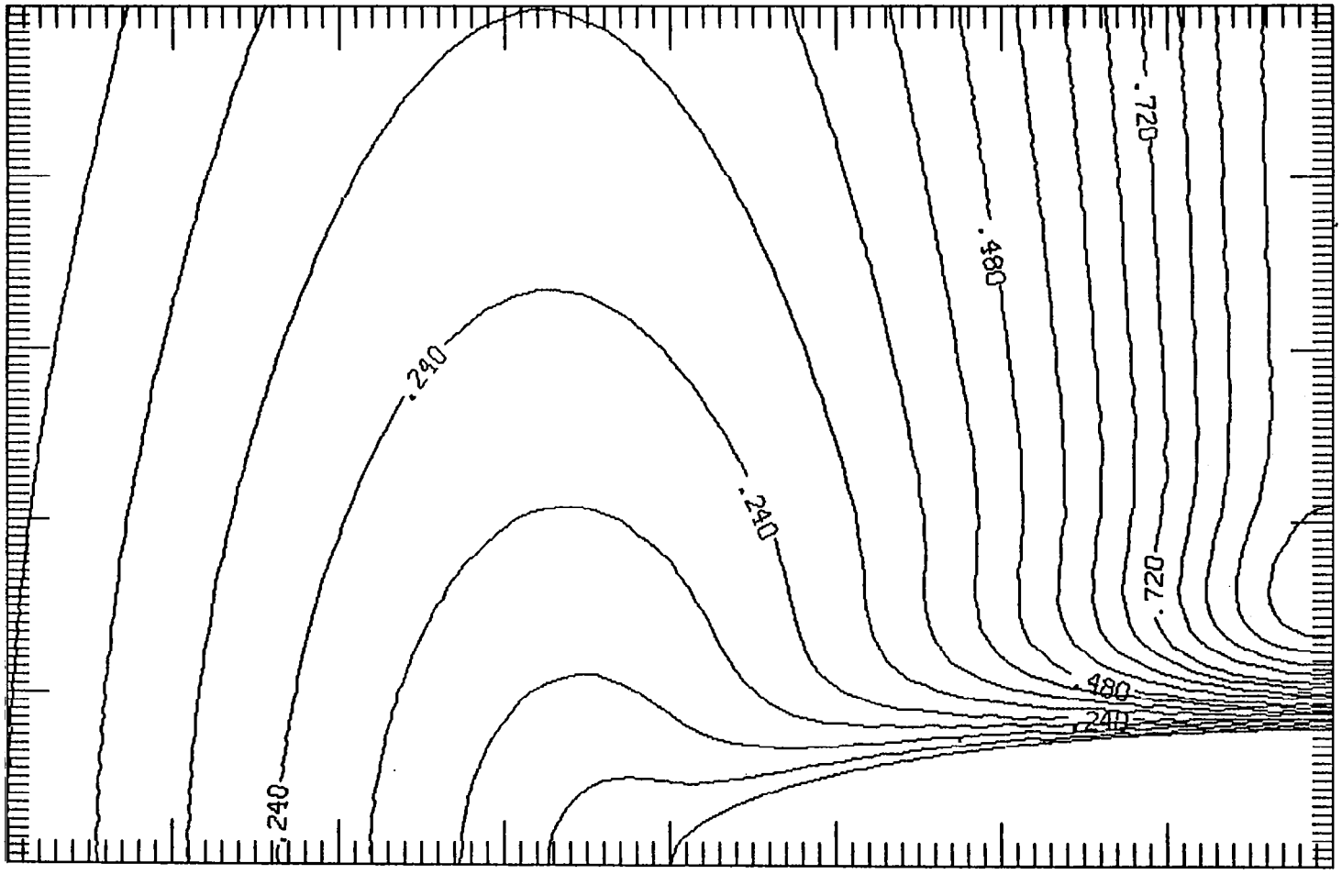

Figure 20a. Contours of the amplitude of $\hat{u}_{0,1}$, the fundamental oscillation. Contours from 0.0 to 0.96 with an interval of 0.06. The body is an ellipse with a/b = 5, and $\sigma = 6\pi$.

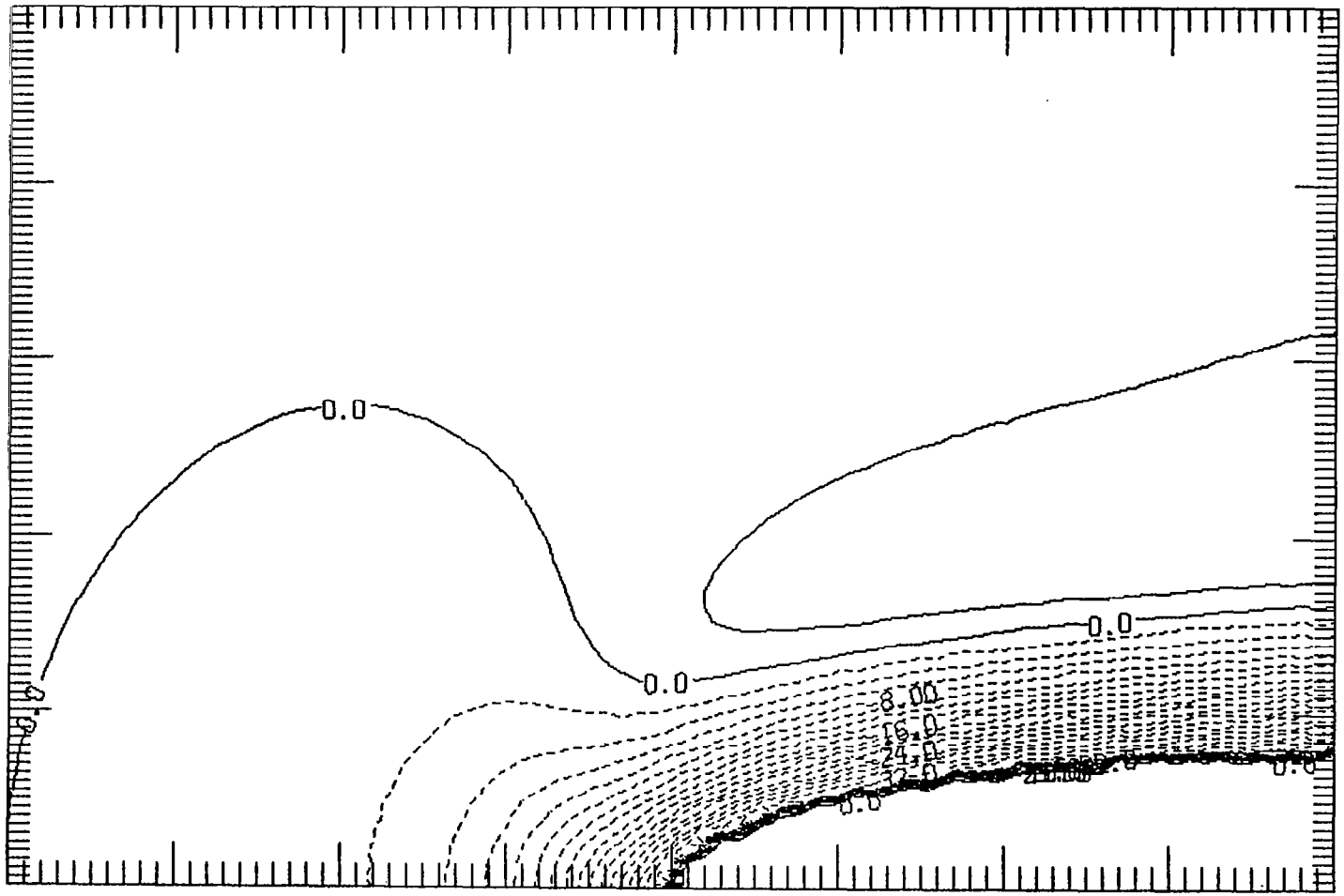

Figure 20b. Contours of the phase, in degrees, of $\hat{u}_{o,1}$, the fundamental oscillation. Contours from -40.0° to 2.0° with an interval of 2.0°. The body is an ellipse with a/b = 5, and $\sigma = 6\pi$.

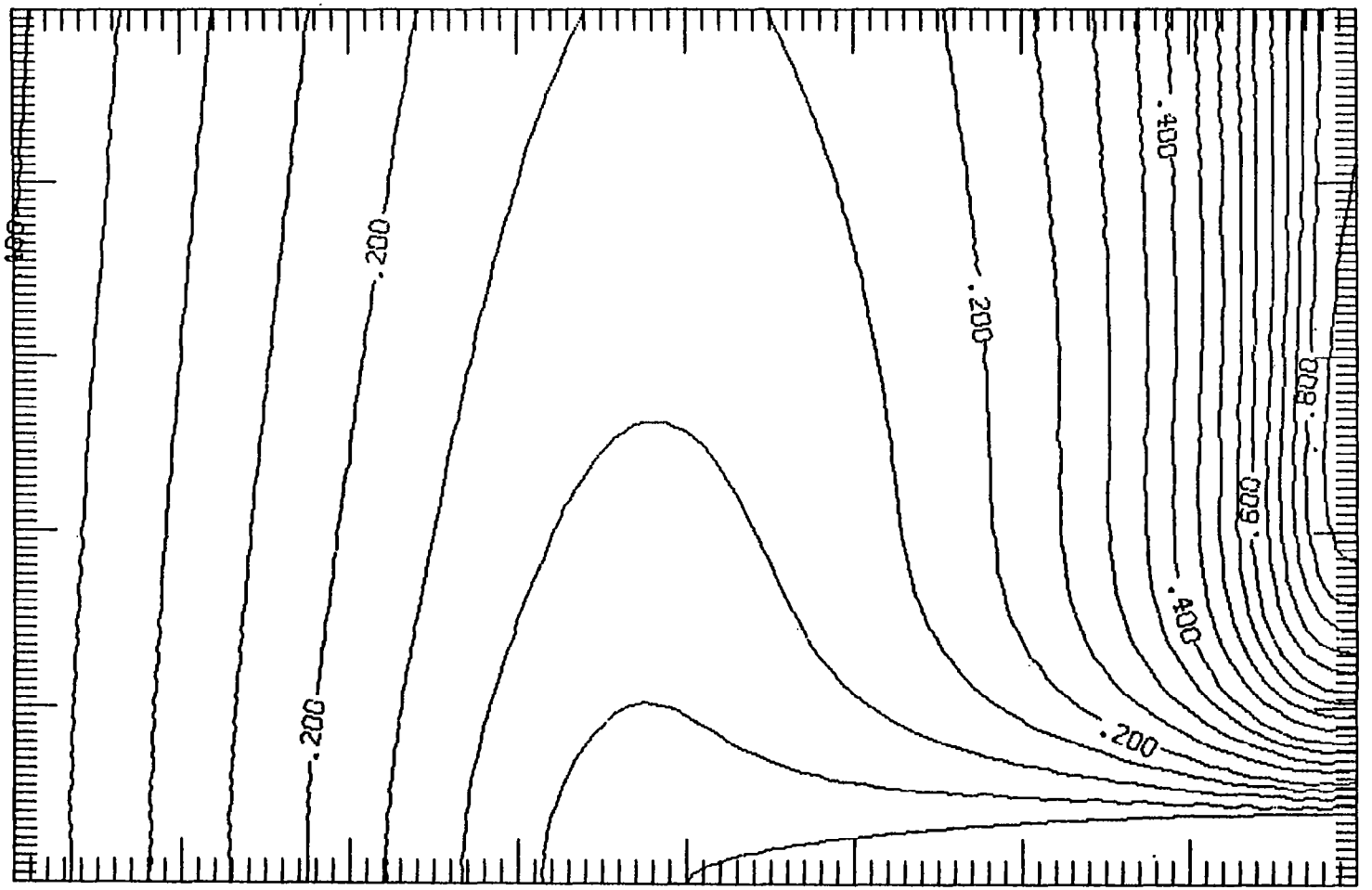

Figure 21a. Contours of the amplitude of $\hat{u}_{o,1}$, the fundamental oscillation. Contours from 0.0 to 0.85 with an interval of 0.05. The body is an ellipse with a/b = 10, and $\sigma = \pi/4$.

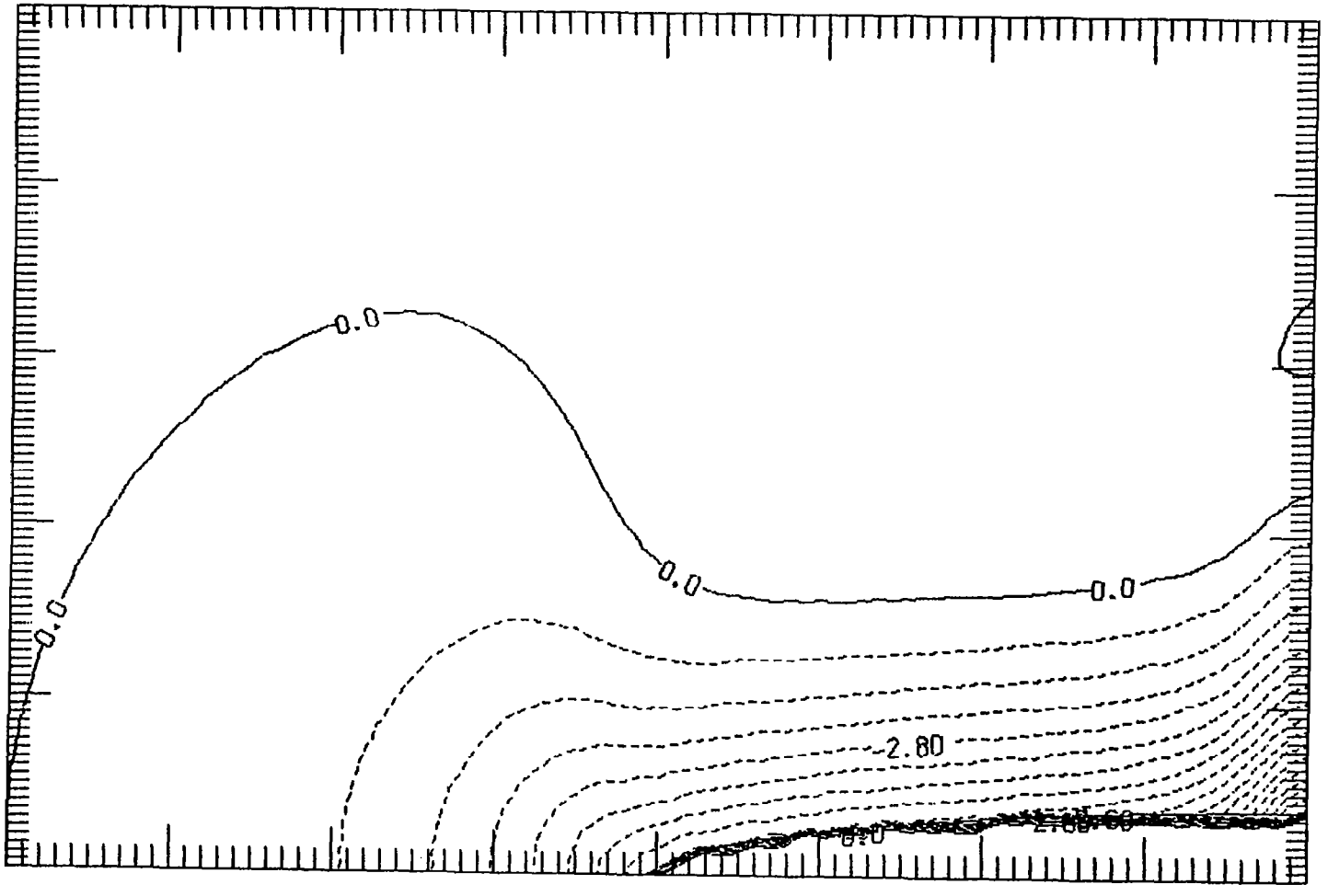

Figure 21b. Contours of the phase, in degrees, of $\hat{u}_{o,1}$, the fundamental oscillation. Contours from -11.2° to 0.7° with an interval of 0.7°. The body is an ellipse with a/b = 10, and $\sigma = \pi/4$.

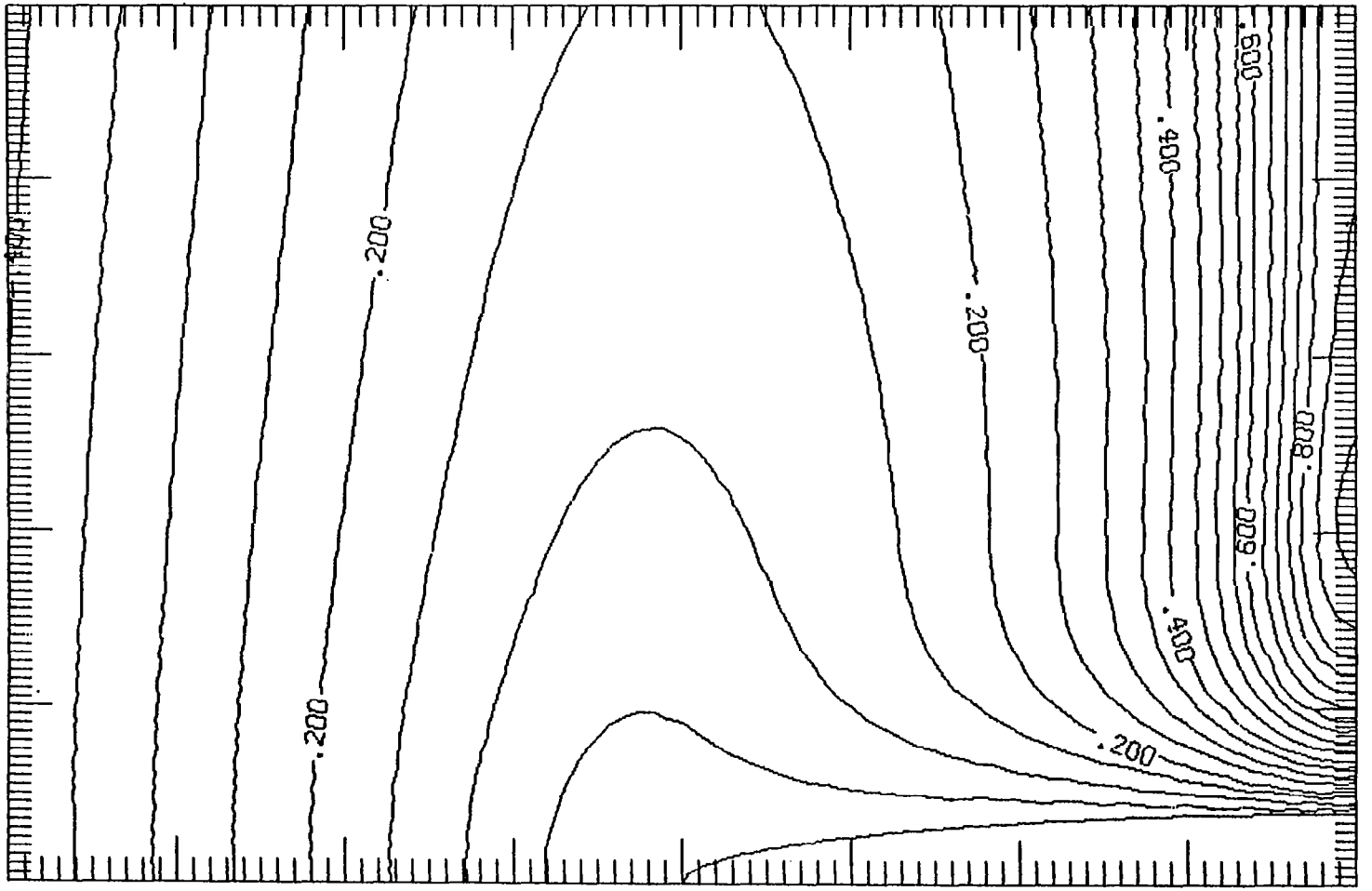

Figure 22a. Contours of the amplitude of $\hat{u}_{o,1}$, the fundamental oscillation. Contours from 0.0 to 0.90 with an interval of 0.05. The body is an ellipse with a/b = 10, and $\sigma = \pi$.

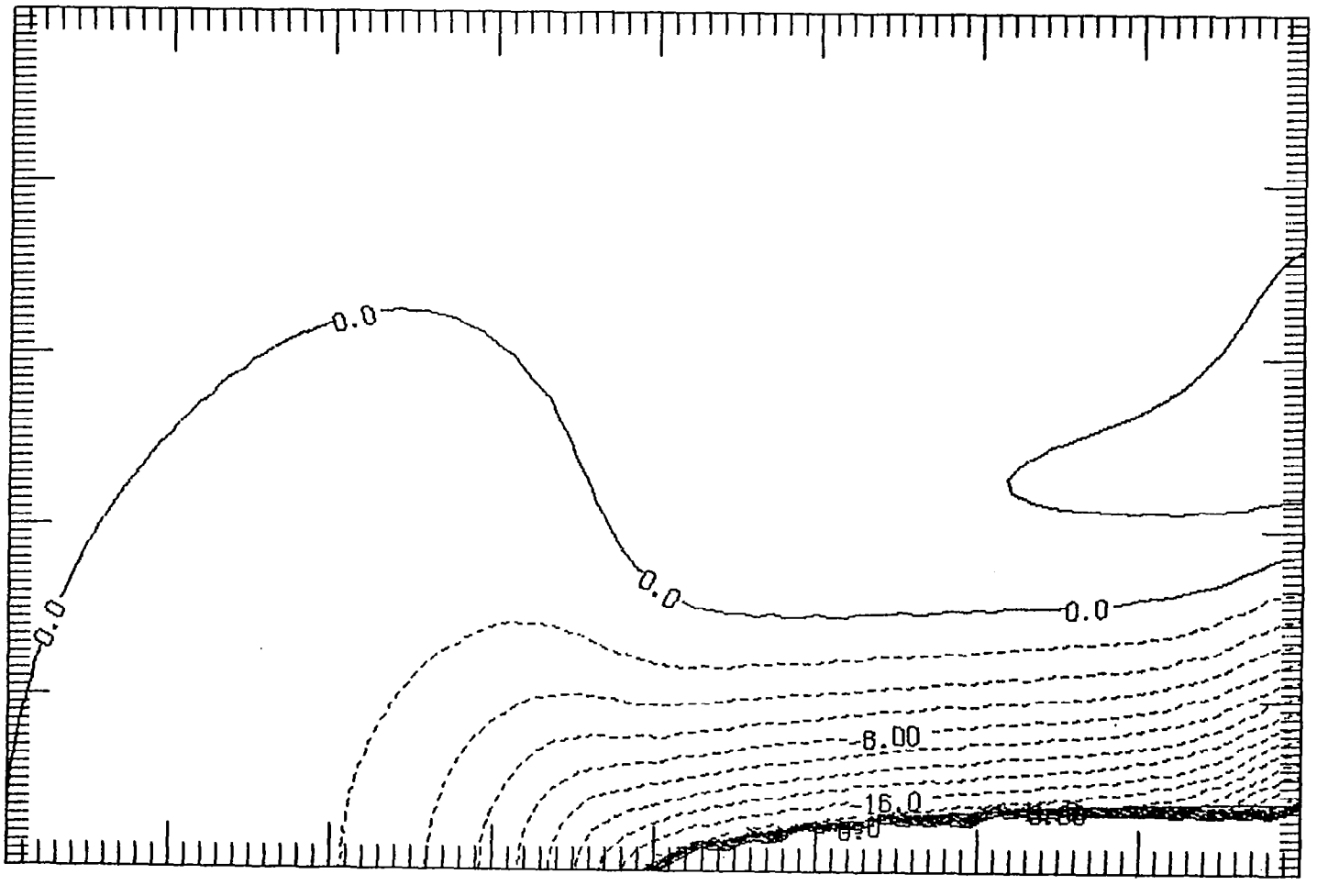

Figure 22b. Contours of the phase, in degrees, of $\hat{u}_{o,1}$, the fundamental oscillation. Contours from -28.0° to 2.0° with an interval of 2.0°. The body is an ellipse with a/b = 10, and $\sigma = \pi$.

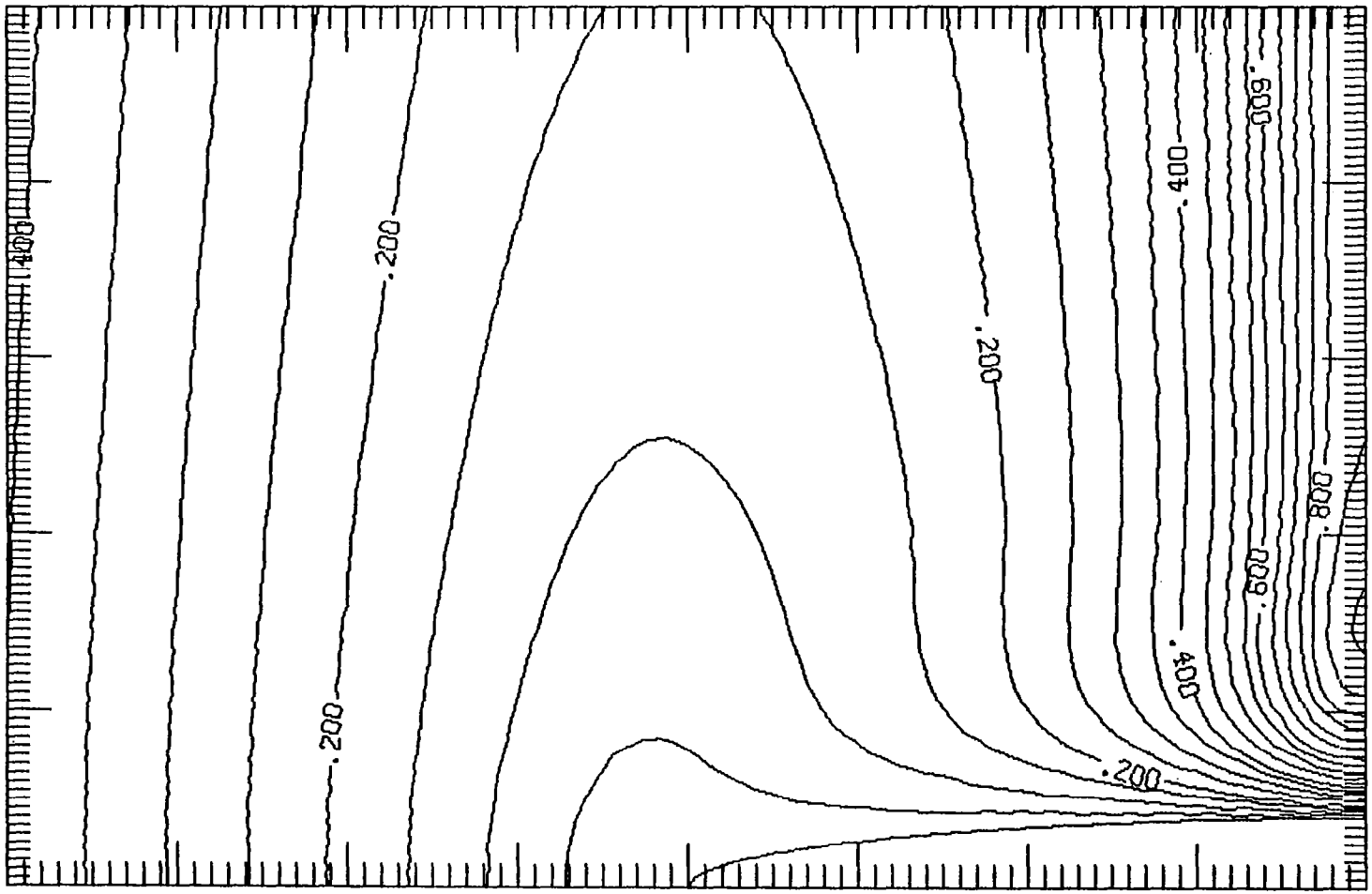

Figure 23a. Contours of the amplitude of $\hat{u}_{o,1}$, the fundamental oscillation. Contours from 0.0 to 0.90 with an interval of 0.05. The body is an ellipse with a/b = 10, and $\sigma = 3\pi$.

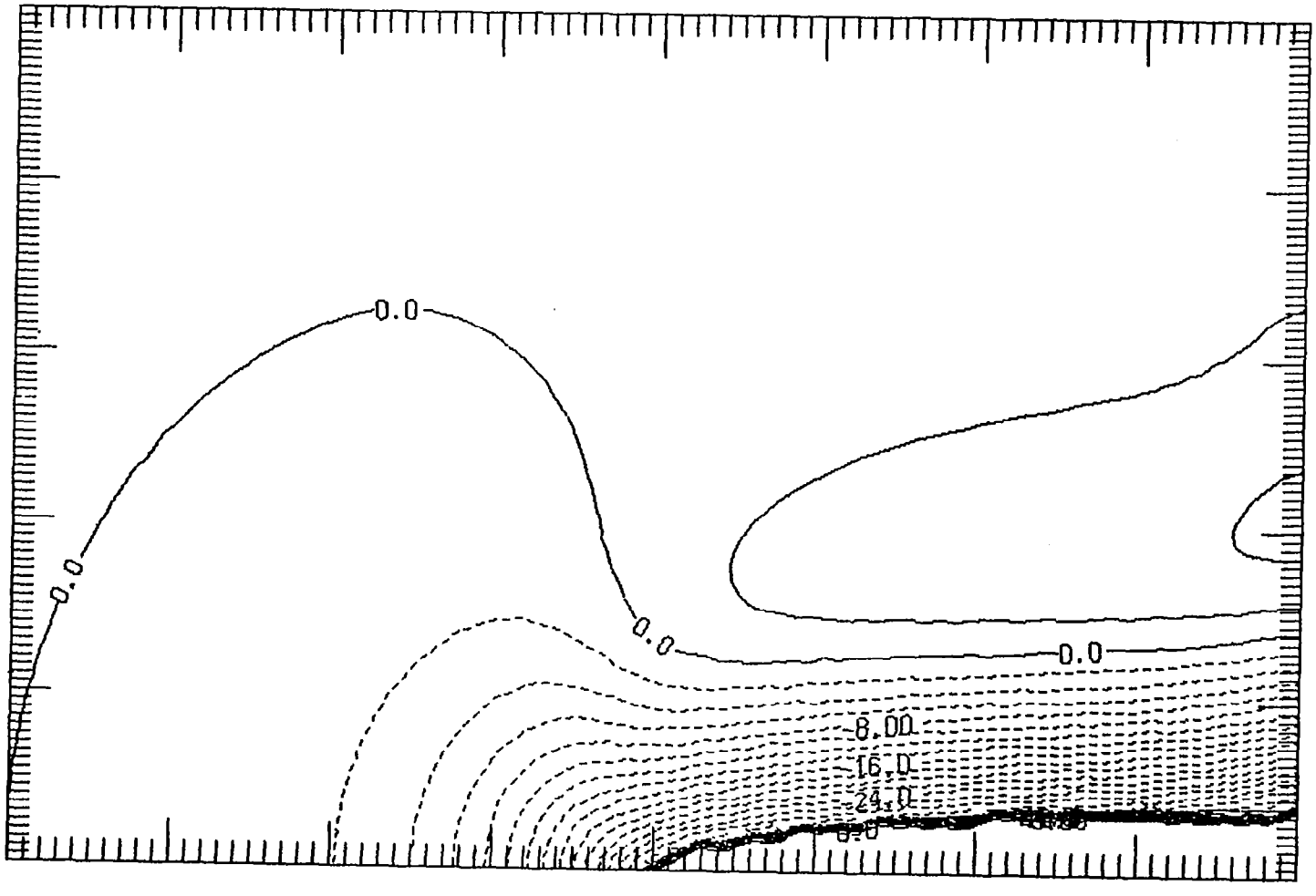

Figure 23b. Contours of the phase, in degrees, $\hat{u}_{o,1}$, the fundamental oscillation. Contours from -36.0° to 4.0° with an interval of 2.0°. The body is an ellipse with a/b = 10, and $\sigma = 3\pi$.

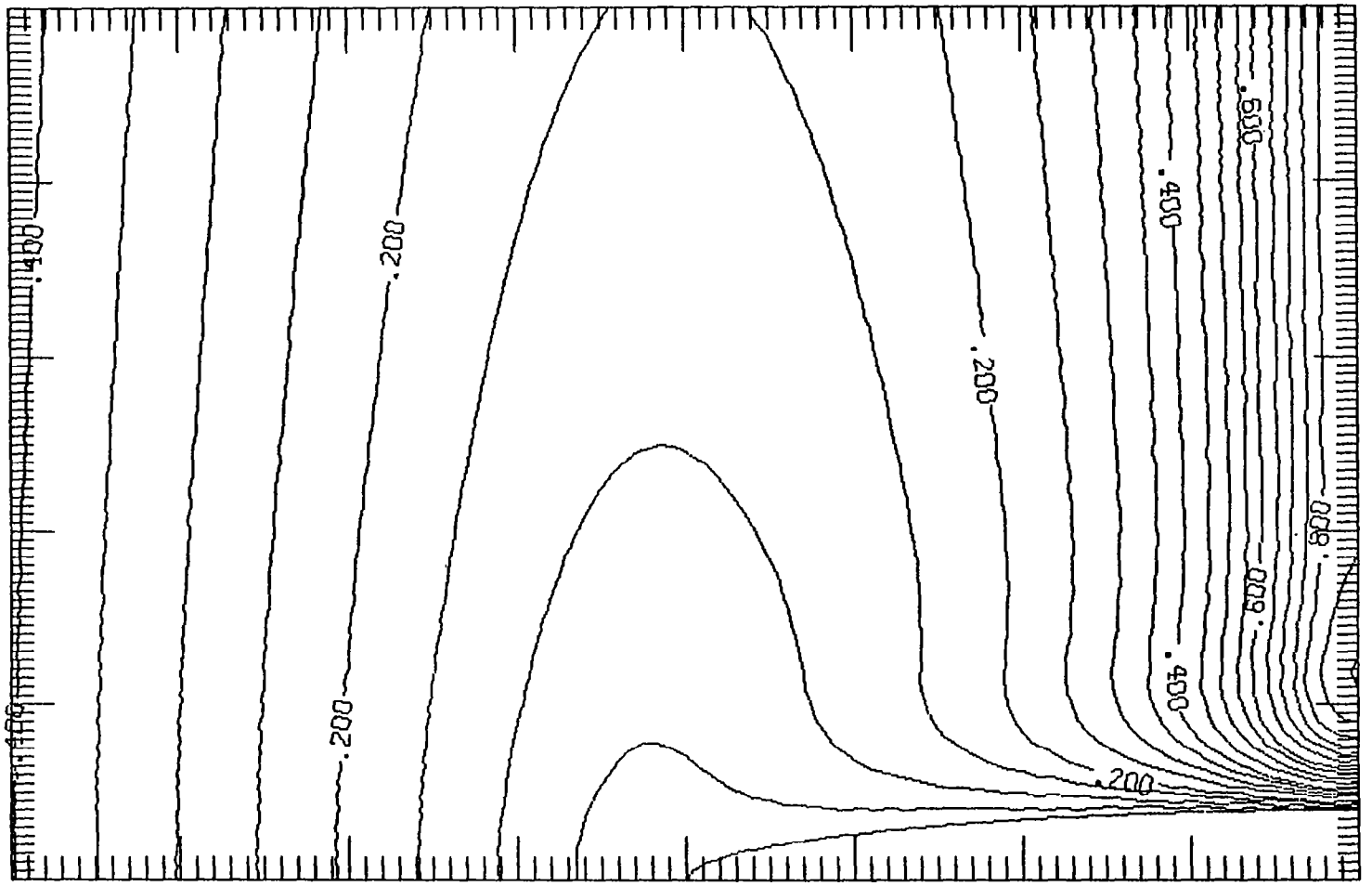

Figure 24a. Contours of the amplitude of $\hat{u}_{o,1}$, the fundamental oscillation. Contours from 0.0 to 0.90 with an interval of 0.05. The body is an ellipse with a/b = 10, and $\sigma = 6\pi$.

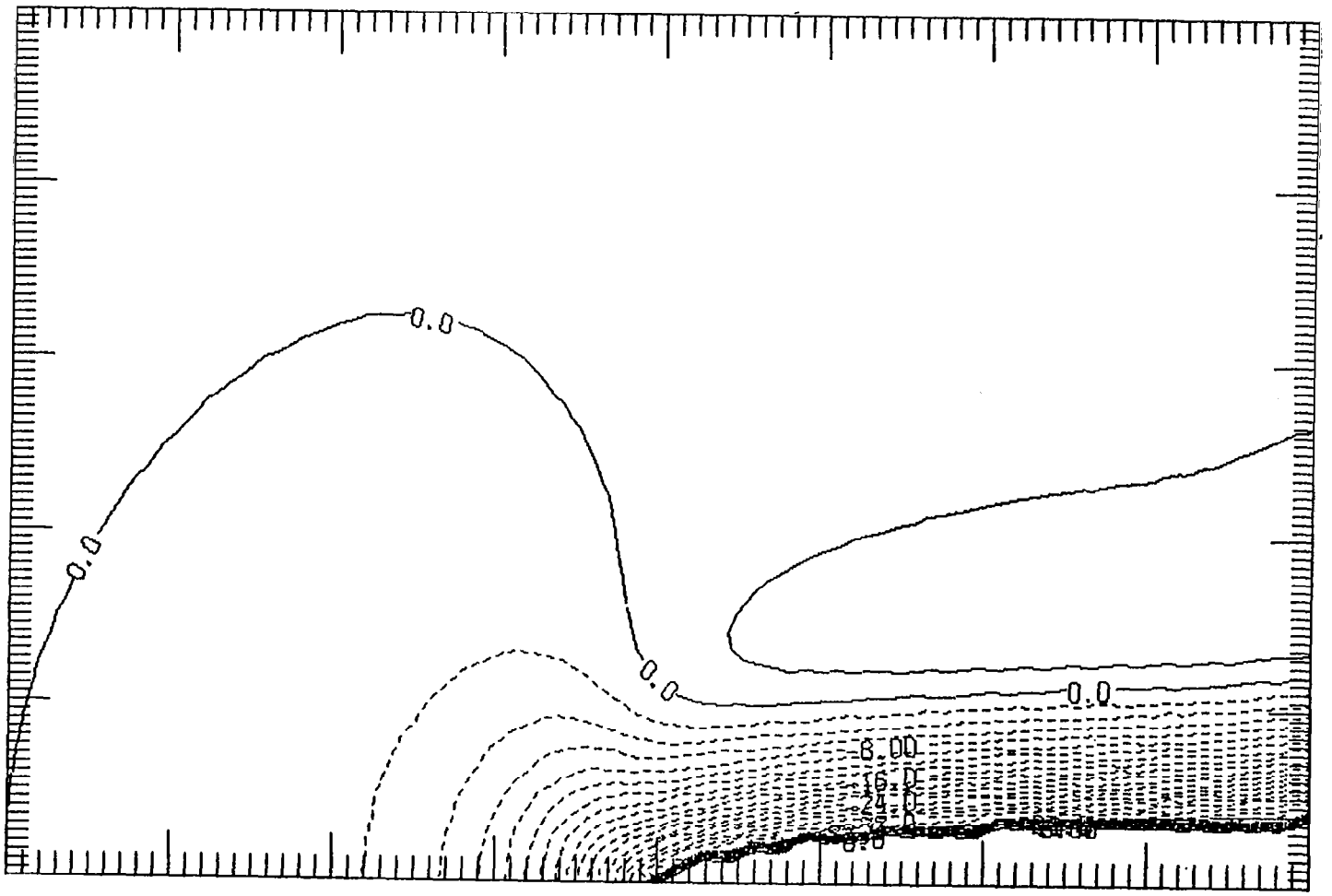

Figure 24b. Contours of the phase, in degrees, of $\hat{u}_{o,1}$, the fundamental oscillation. Contours from -40.0° to 2.0° with an interval of 2.0°. The body is an ellipse with a/b = 10, and $\sigma = 6\pi$.

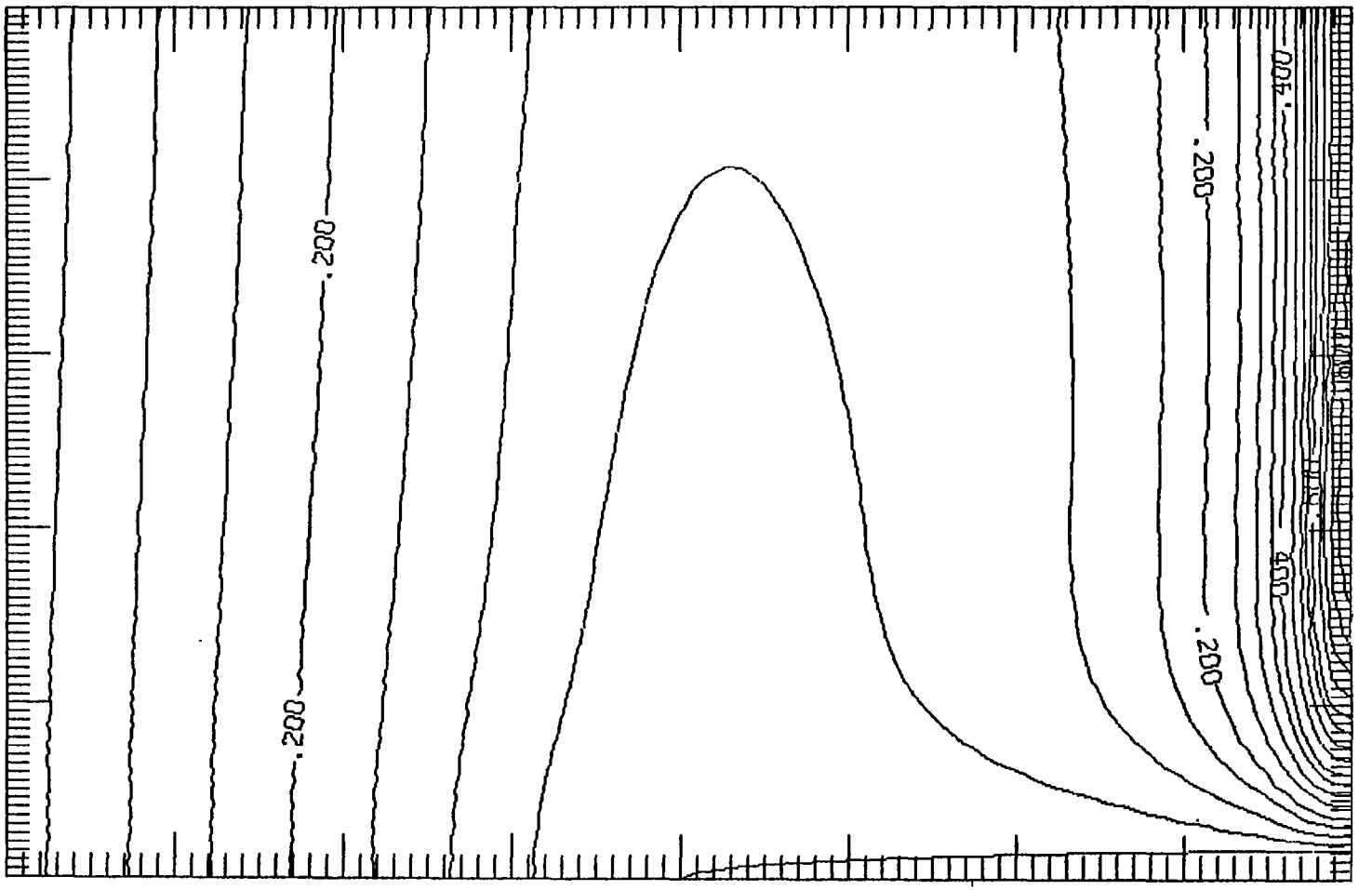

Figure 25a. Contours of the amplitude of $\hat{u}_{o,1}$, the fundamental oscillation. Contours from 0.0 to 0.80 with an interval of 0.05. The body is an ellipse with a/b = 25, and $\sigma = \pi/4$.

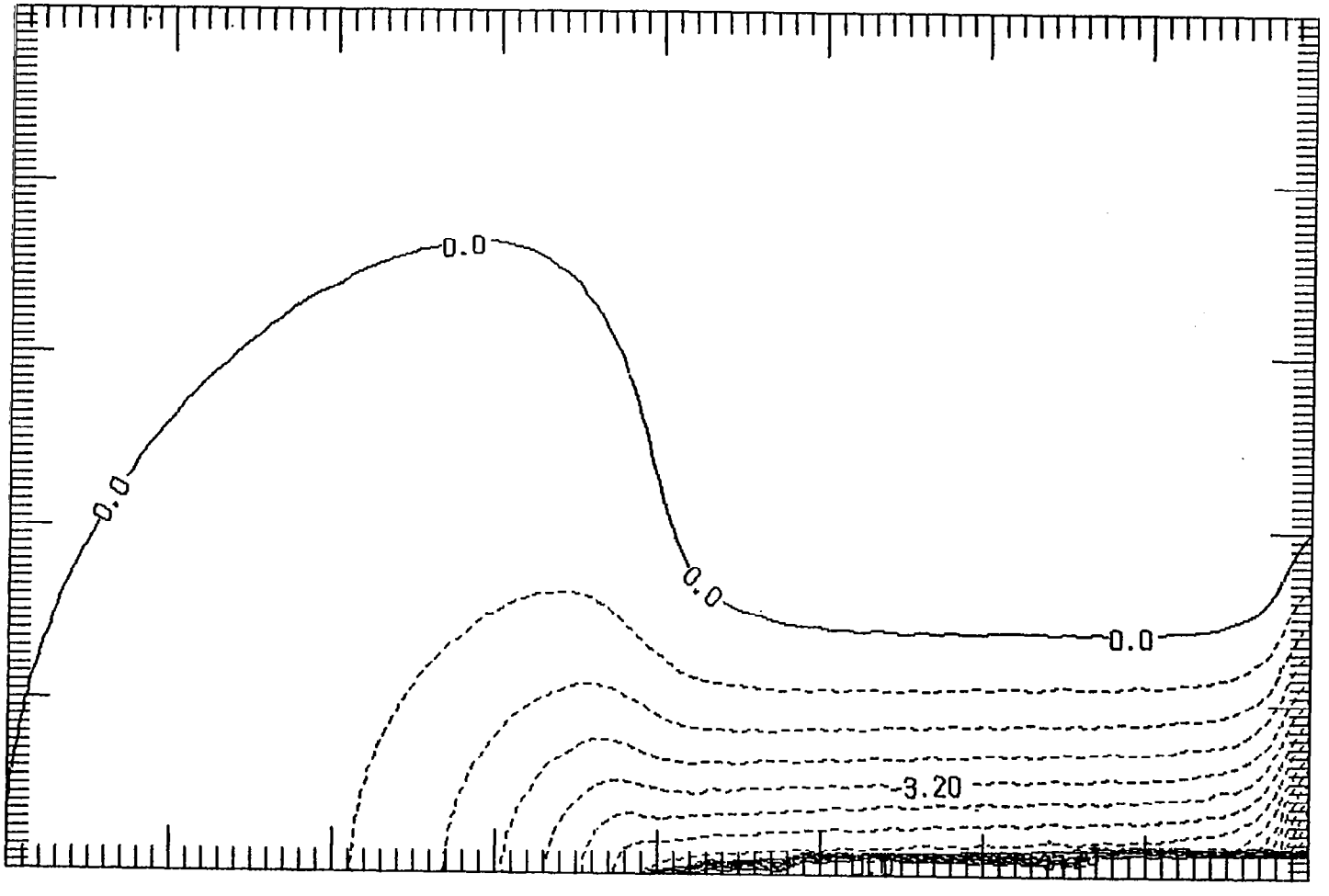

Figure 25b. Contours of the phase, in degrees, of $\hat{u}_{o,1}$, the fundamental oscillation. Contours from -12.0° to 0.0° with an interval of 0.8°. The body is an ellipse with a/b = 25, and $\sigma = \pi/4$.

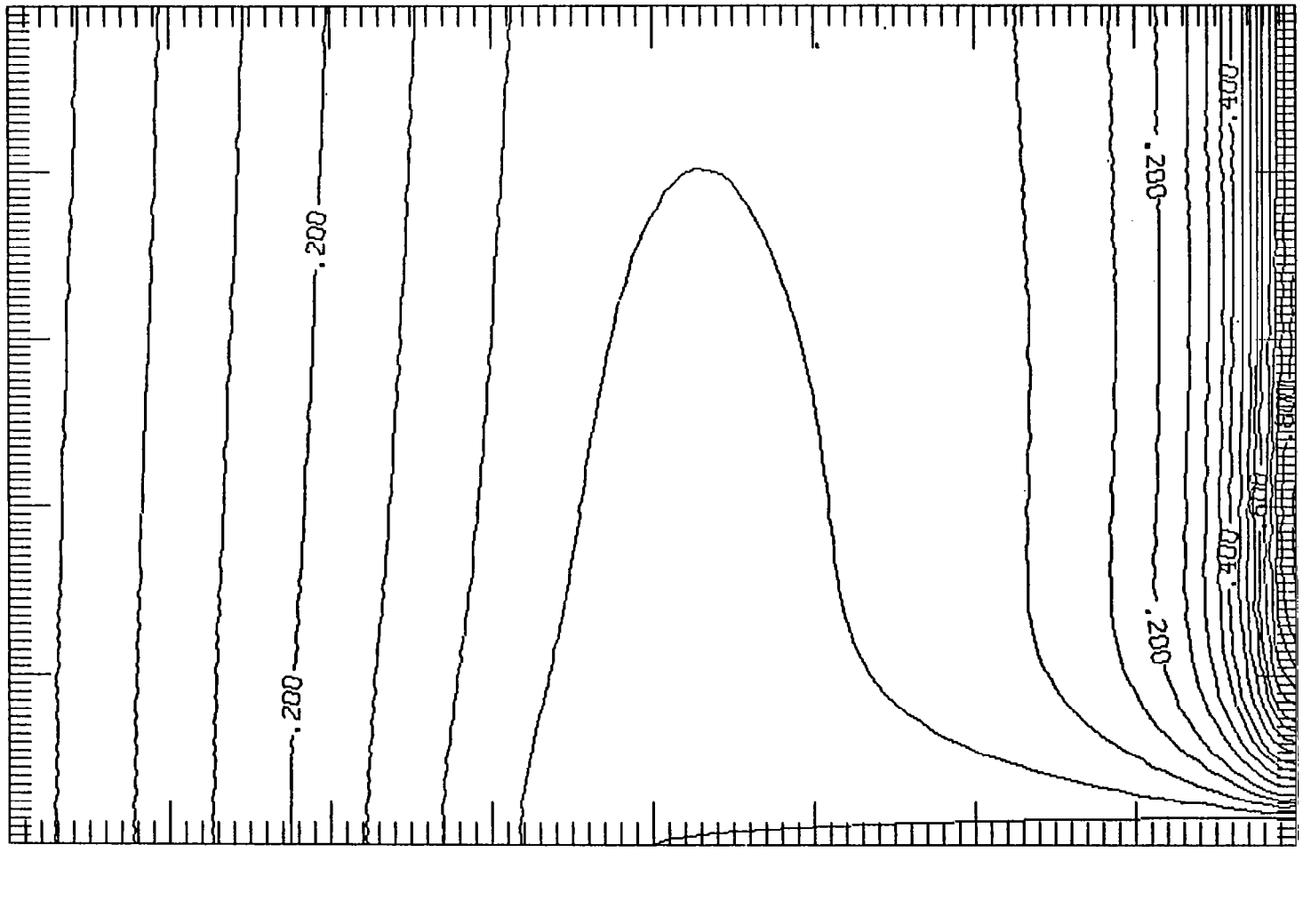

Figure 26a. Contours of the amplitude of $\hat{u}_{0,1}$, the fundamental oscillation. Contours from 0.0 to 0.85 with an interval of 0.05. The body is an ellipse with a/b = 25, and $\sigma = \pi$.

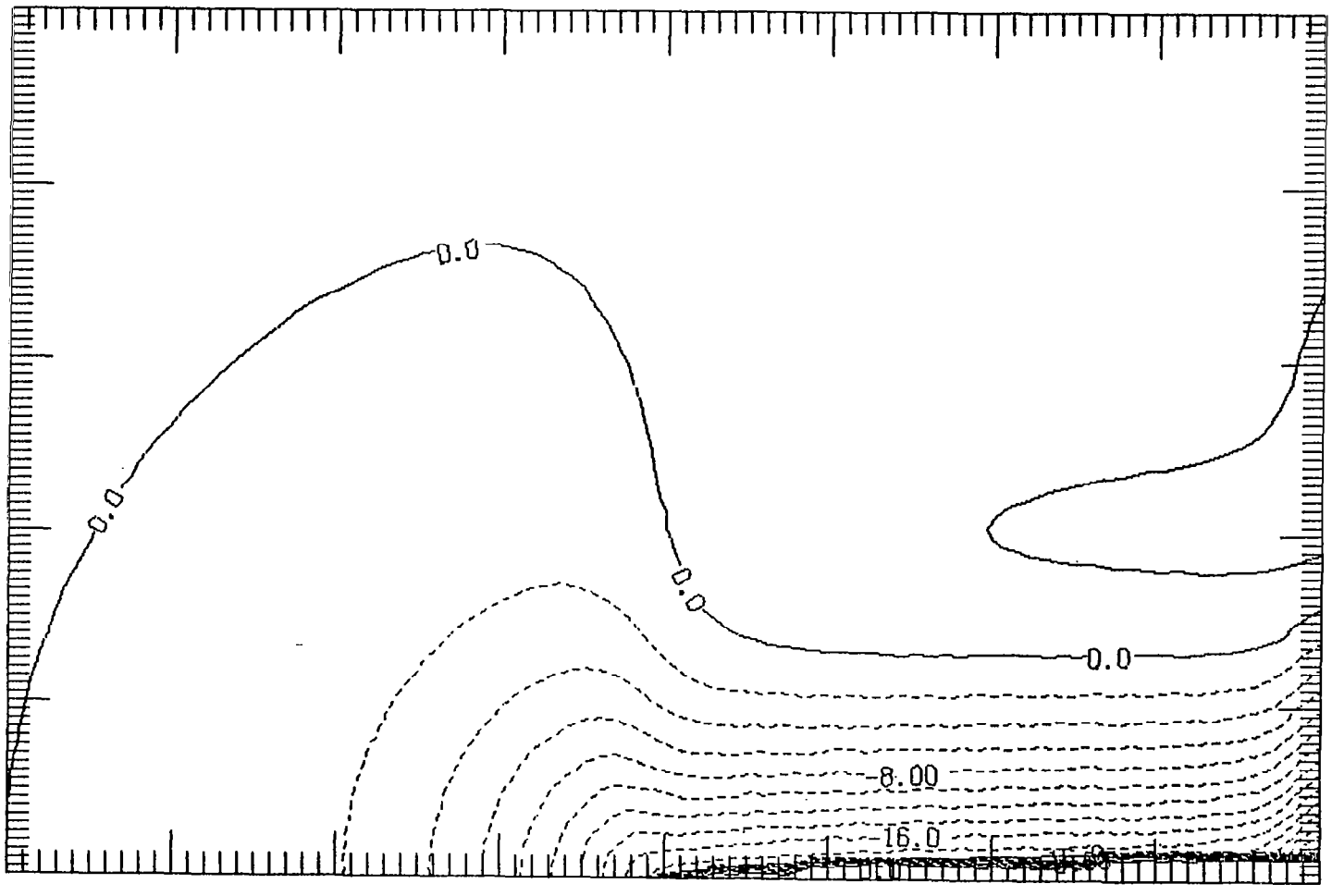

Figure 26b. Contours of the phase, in degrees, of $\hat{u}_{o,1}$, the fundamental oscillation. Contours from -28.0° to 2.0° with an interval of 2.0°. The body is an ellipse with a/b = 25, and $\sigma = \pi$.

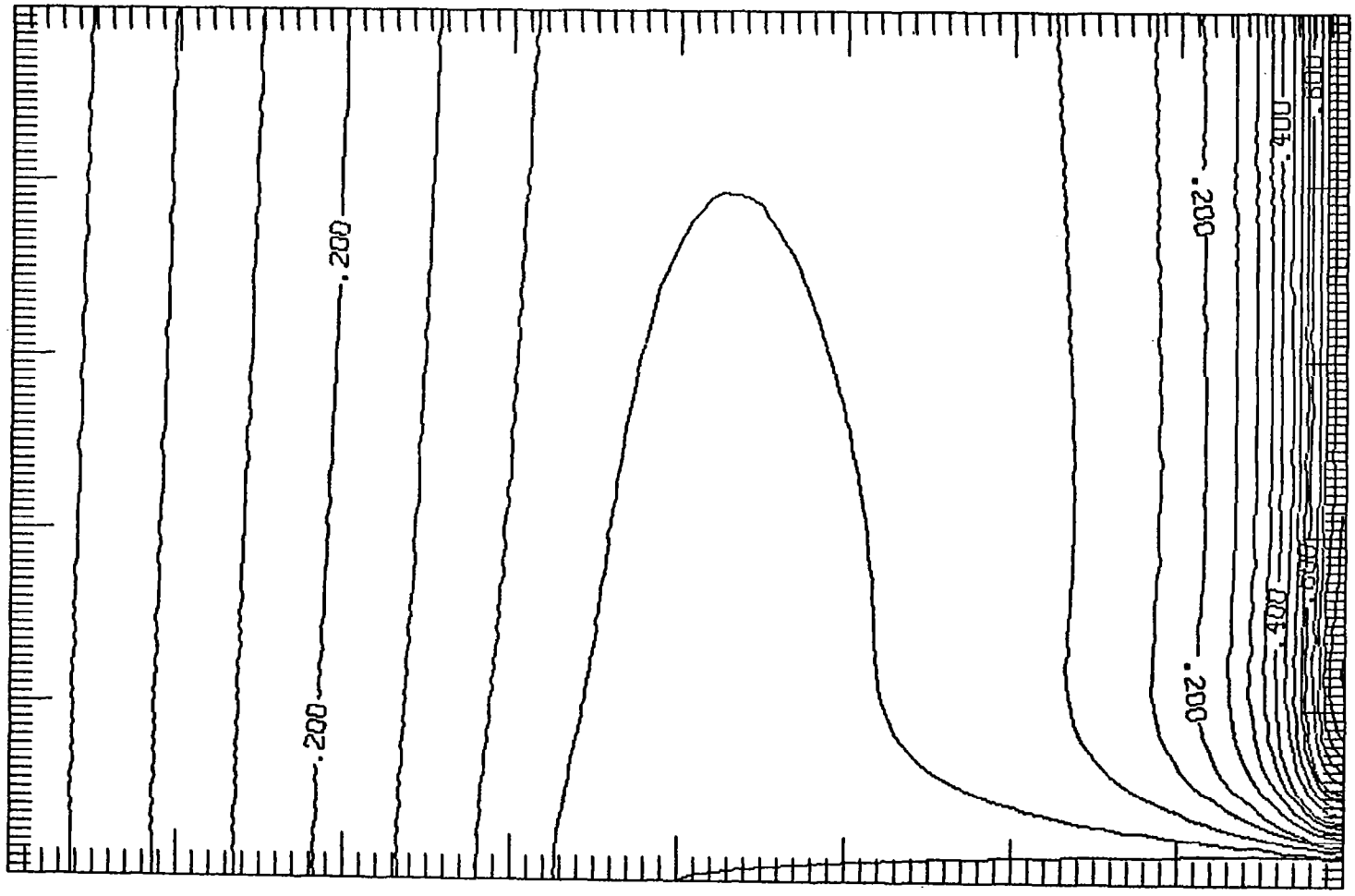

Figure 27a. Contours of the amplitude of $\hat{u}_{o,1}$, the fundamental oscillation. Contours from 0.0 to 0.85 with an interval of 0.05. The body is an ellipse with a/b = 25, and $\sigma = 3\pi$.

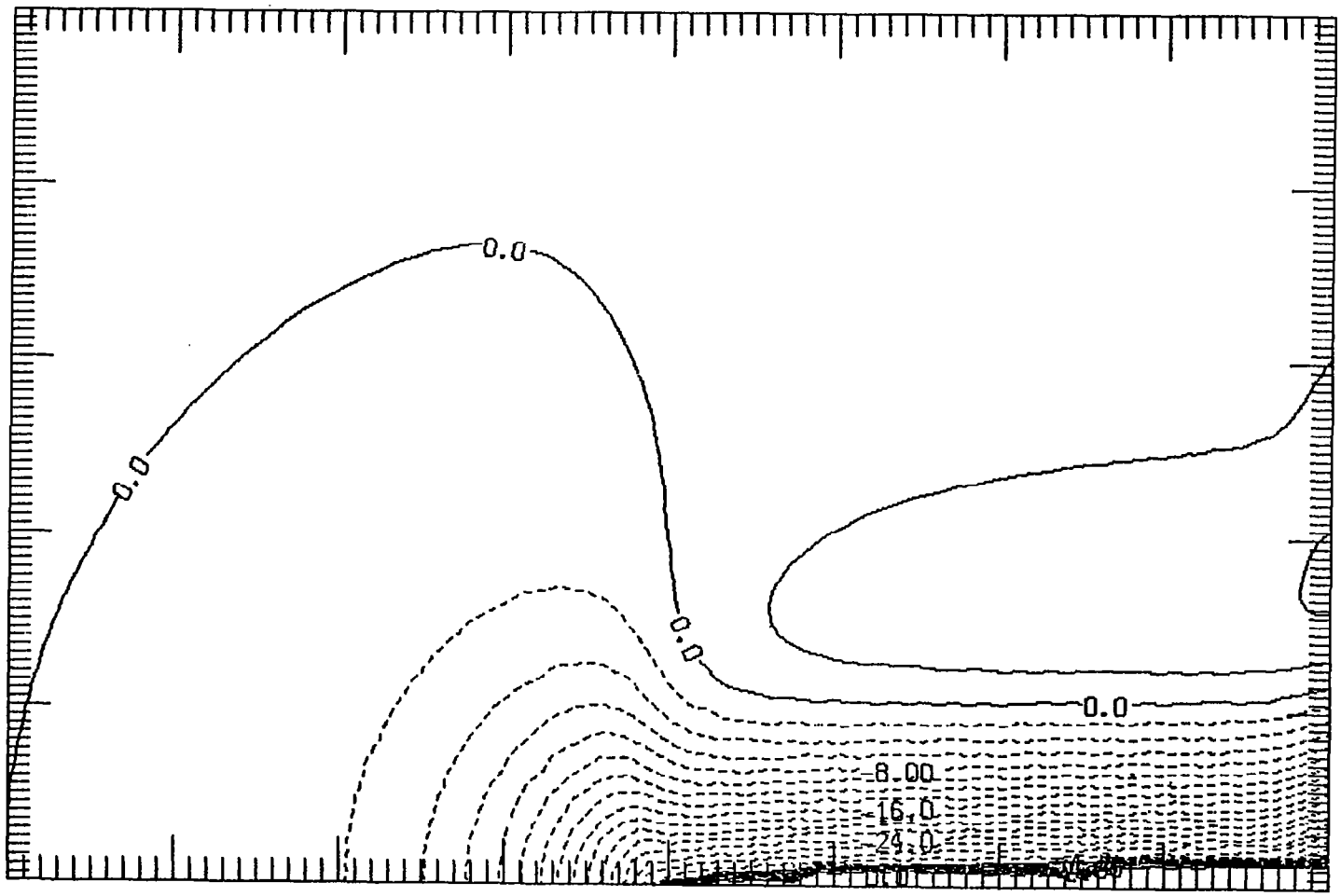

Figure 27b. Contours of the phase, in degrees, of $\hat{u}_{o,1}$, the fundamental oscillation. Contours from -36.0° to 4.0° with an interval of 2.0°. The body is an ellipse with a/b = 25, and $\sigma = 3\pi$.

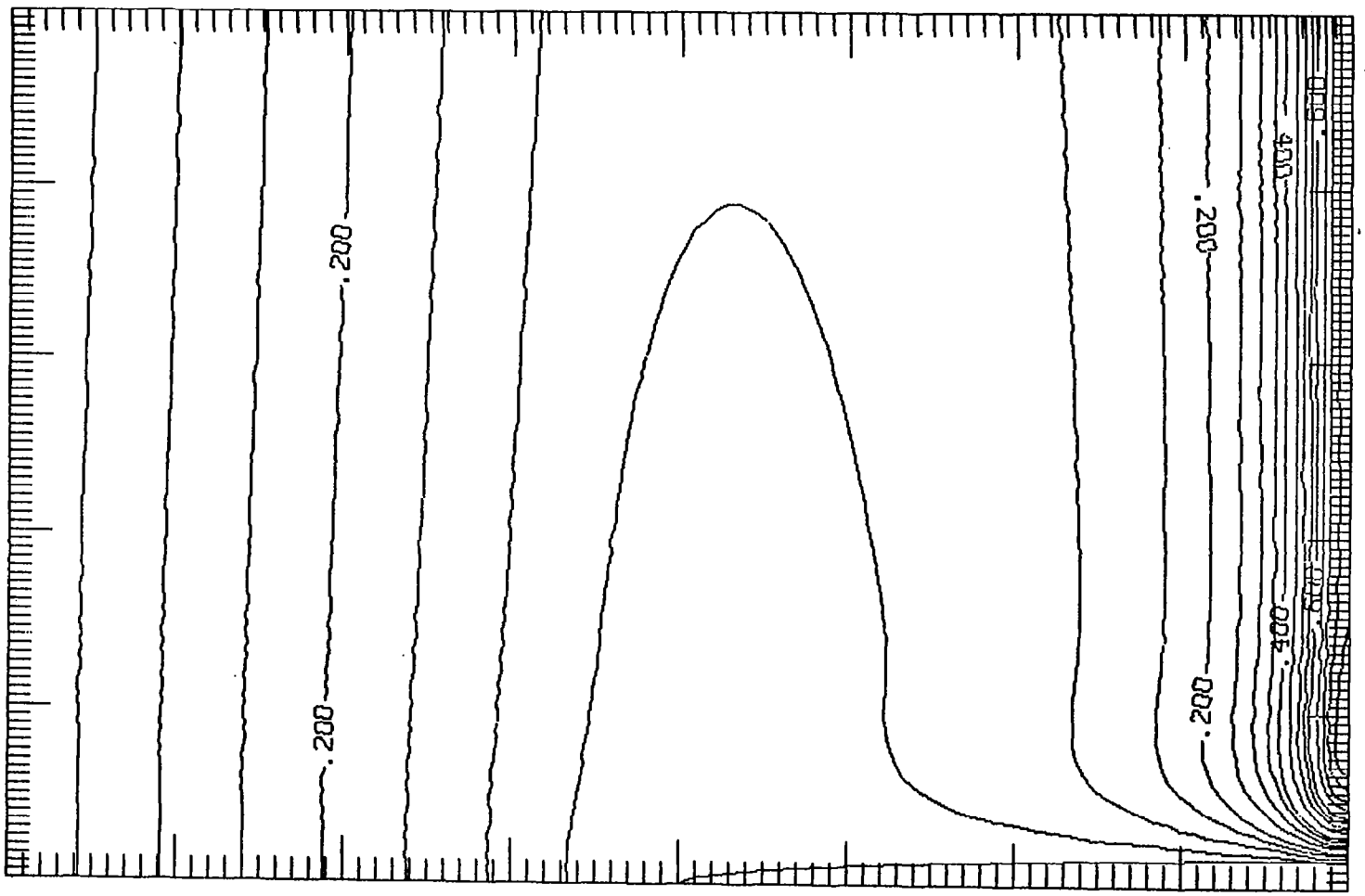

Figure 28a. Contours of the amplitude of $\hat{u}_{o,1}$, the fundamental oscillation. Contours from 0.0 to 0.80 with an interval of 0.05. The body is an ellipse with a/b = 25, and $\sigma = 6\pi$.

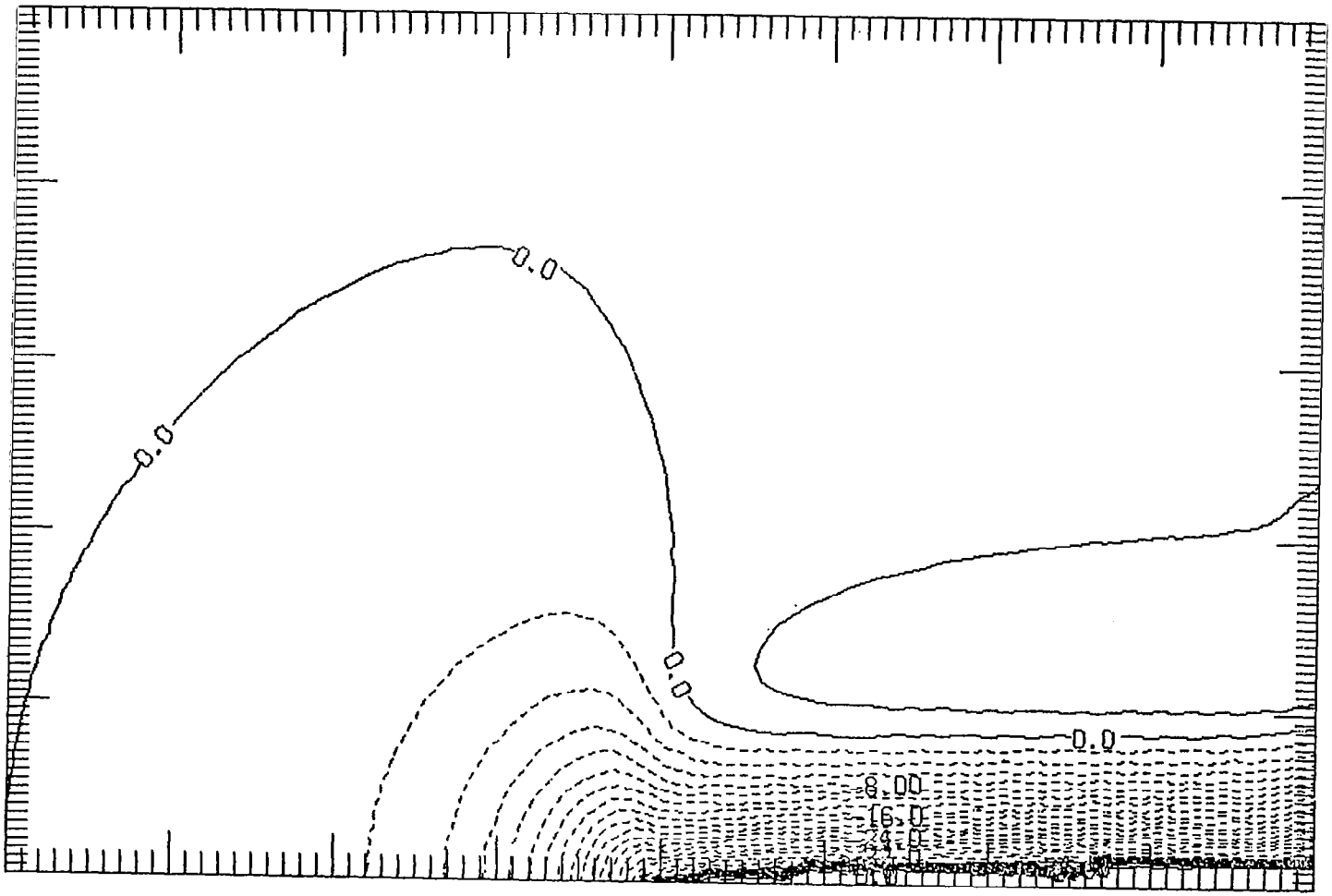

Figure 28b. Contours of the phase, in degrees, of $\hat{u}_{o,1}$, the fundamental oscillation. Contours from -38.0° to 2.0° with an interval of 2.0°. The body is an ellipse with a/b = 25, and $\sigma = 6\pi$.

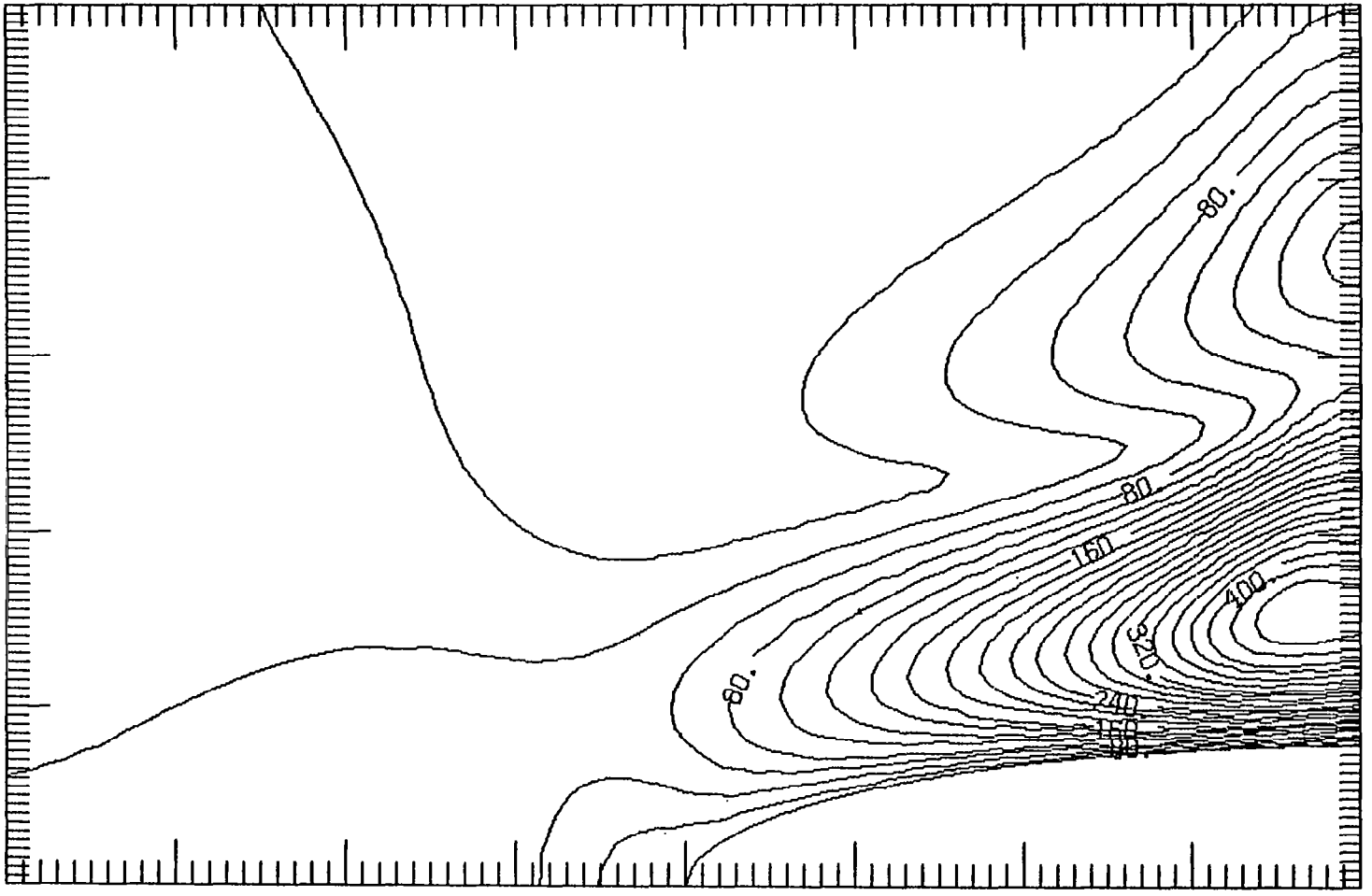

Figure 29a. Contours of the amplitude of $\hat{u}_{o,2}$, the first harmonic of the free stream oscillation. Contours from 0.0 to 4.4×10^{-2} with an interval of 2.0×10^{-3}. The labels are scaled by 10^4. The body is an ellipse with a/b = 5, and $\sigma = \pi/4$.

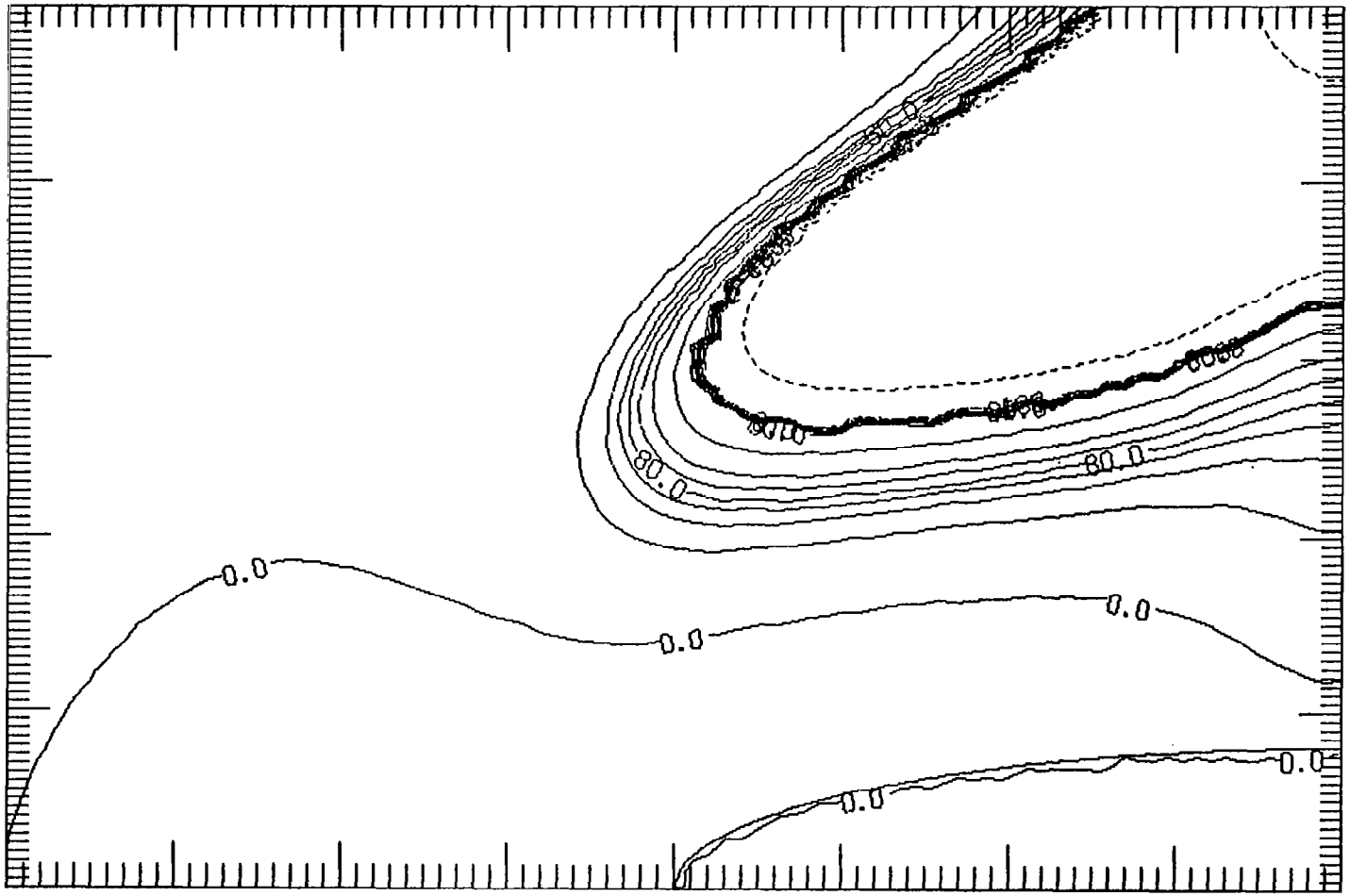

Figure 29b. Contours of the phase, in degrees, of $\hat{u}_{o,2}$, the first harmonic of the free stream oscillation. Contours from -200.0° to 140.0° with an interval of 20.0°. The body is an ellipse with a/b = 5, and $\sigma = \pi/4$.

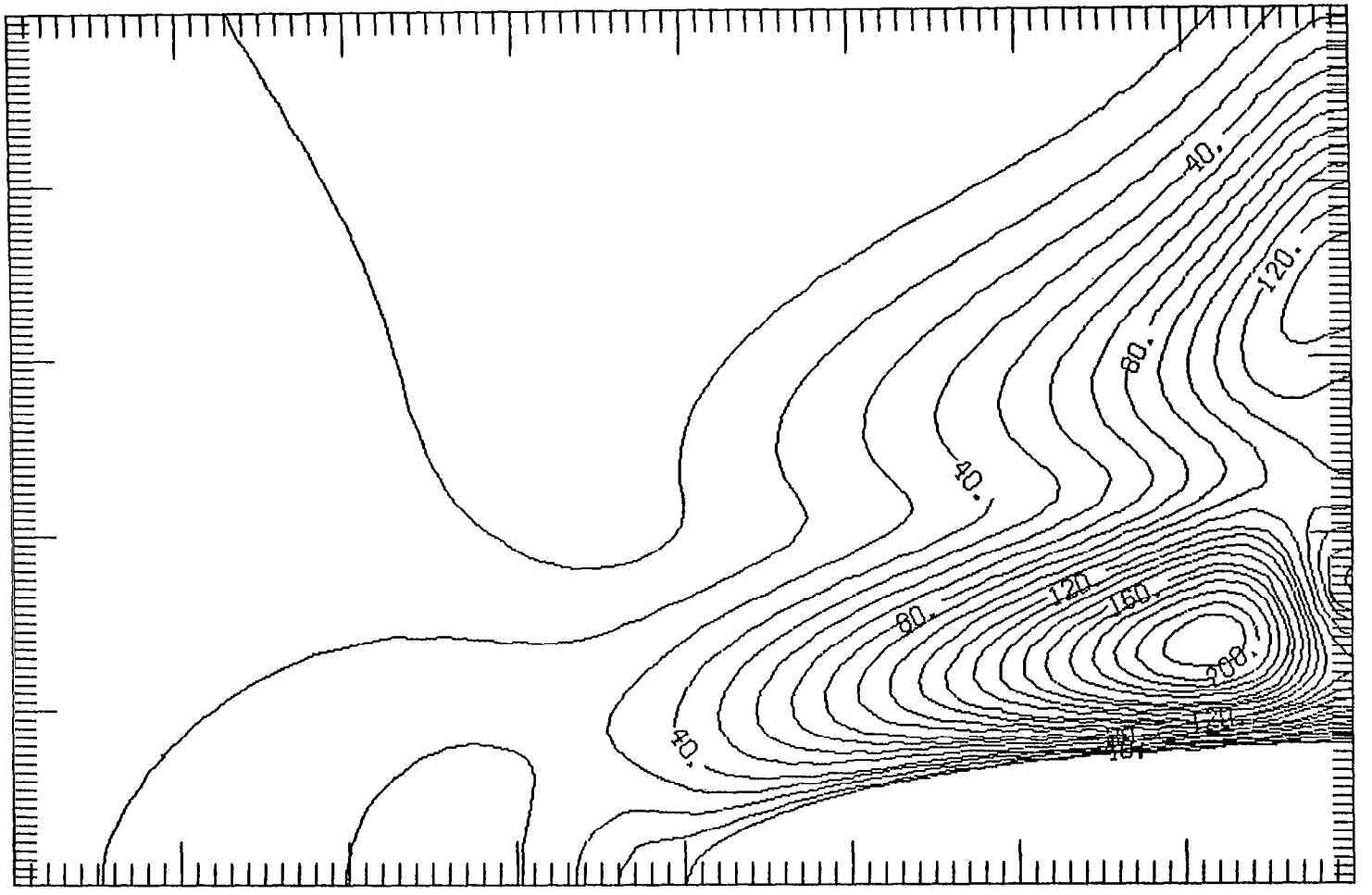

Figure 30a. Contours of the amplitude of $\hat{u}_{0,2}$, the first harmonic of the free stream oscillation. Contours from 0.0 to 2.0×10^{-2} with an interval of 1.0×10^{-3}. The labels are scaled by 10^4. The body is an ellipse with a/b = 5, and $\sigma = \pi$.

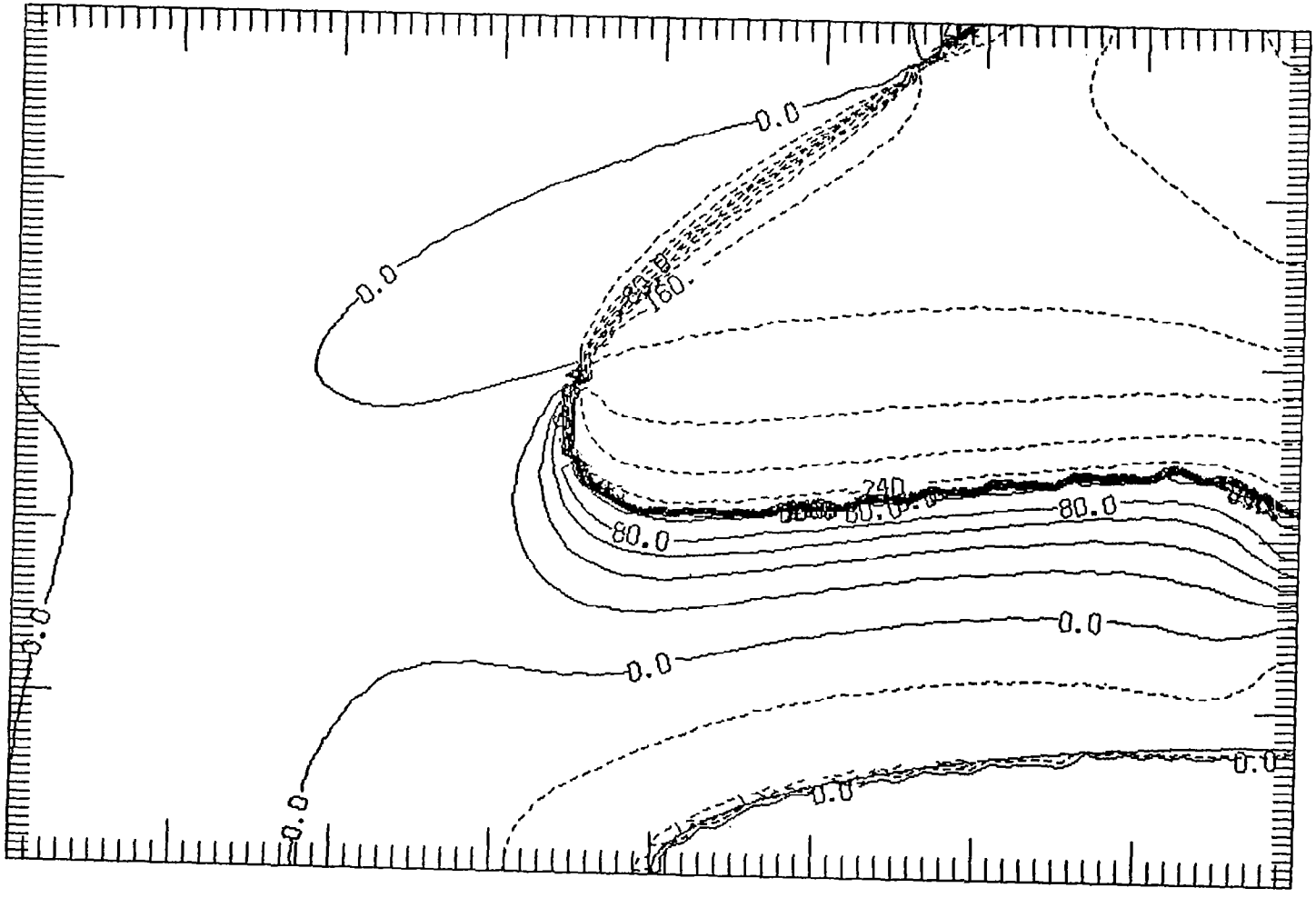

Figure 30b. Contours of the phase, in degrees, of $\hat{u}_{o,2}$, the first harmonic of the free stream oscillation. Contours from $-240.0°$ to $100.0°$ with an interval of $20.0°$. The body is an ellipse with a/b = 5, and $\sigma = \pi$.

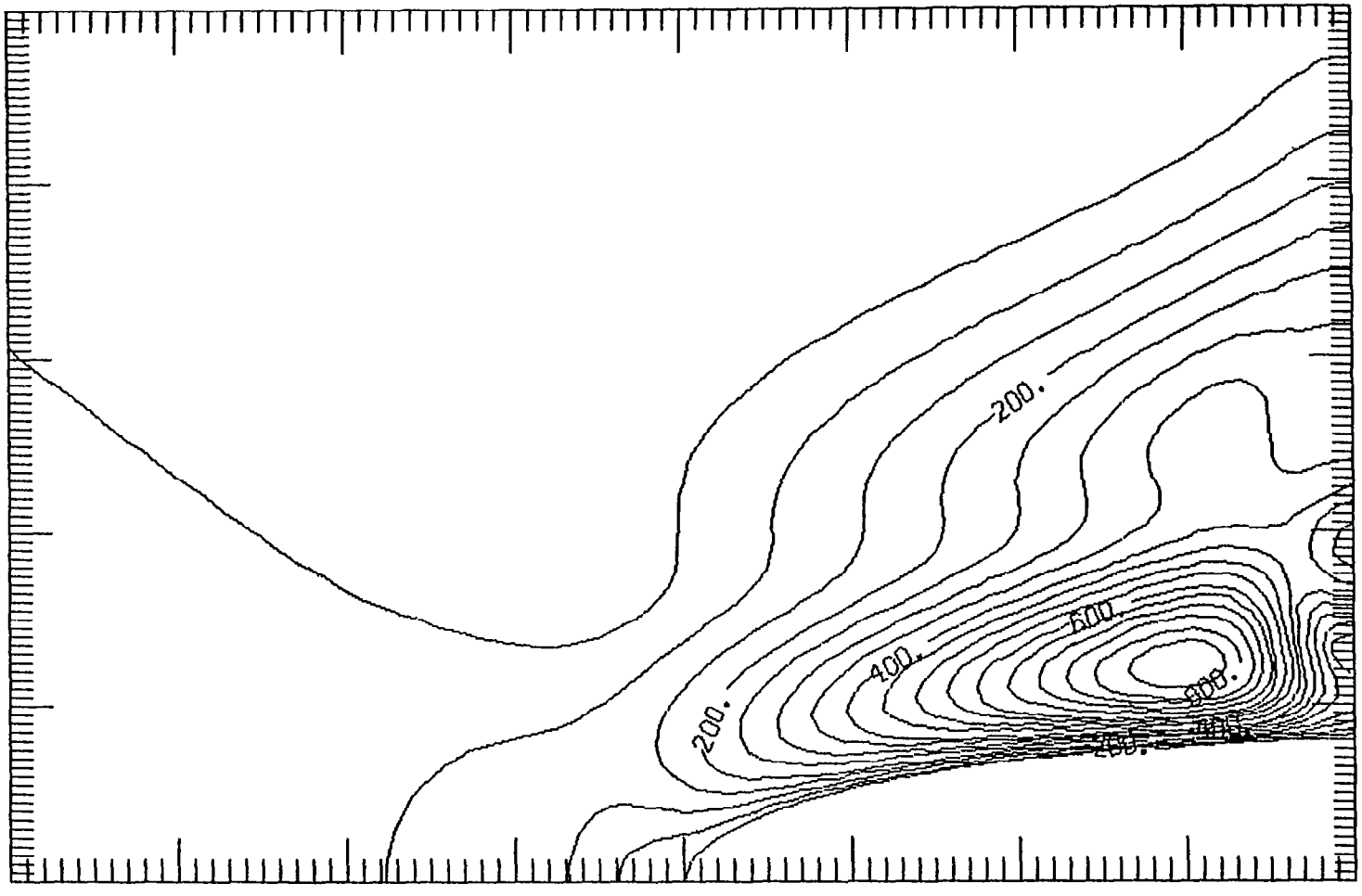

Figure 31a. Contours of the amplitude of $\hat{u}_{o,2}$, the first harmonic of the free stream oscillation. Contours from 0.0 to 4.6×10^{-3} with an interval of 2.0×10^{-4}. The labels are scaled by 10^5. The body is an ellipse with $a/b = 5$, and $\sigma = 6\pi$.

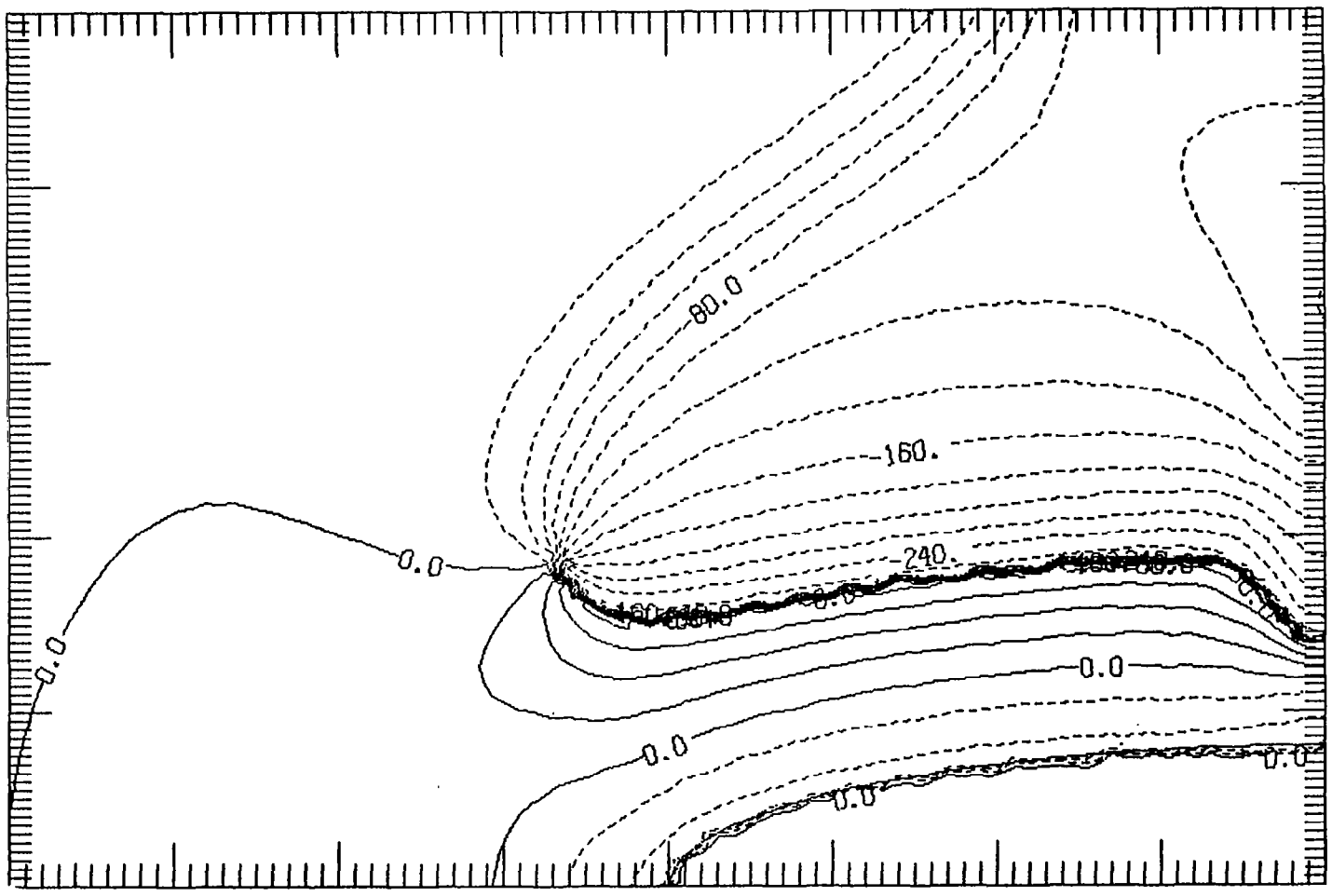

Figure 31b. Contours of the phase, in degrees, of $\hat{u}_{o,2}$, the first harmonic of the free stream oscillation. Contours from -260.0° to 80.0° with an interval of 20.0°. The body is an ellipse with a/b = 5, and $\sigma = 3\pi$.

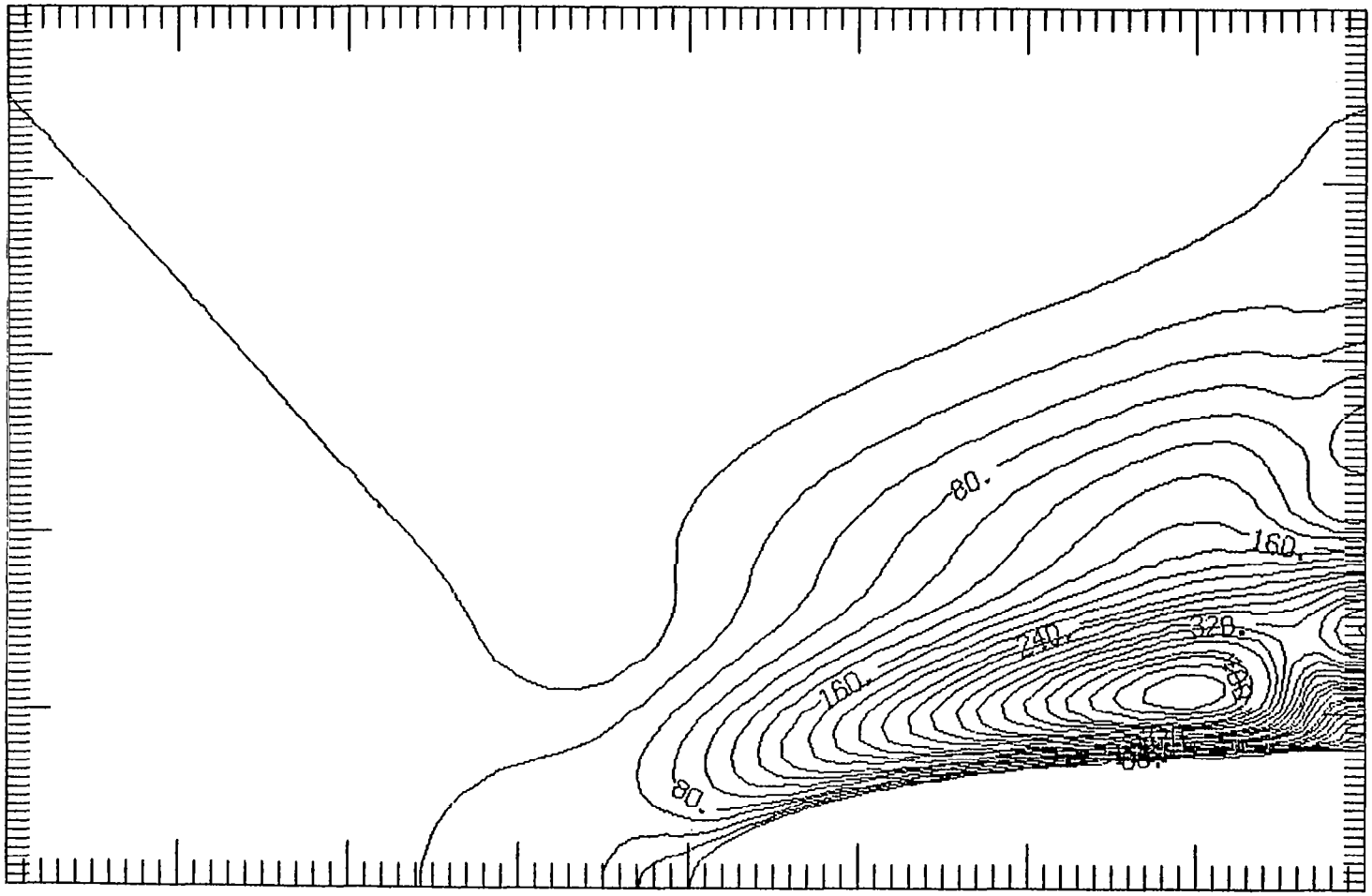

Figure 32a. Contours of the amplitude of $\hat{u}_{o,2}$, the first harmonic of the free stream oscillation. Contours from 0.0 to 4.6×10^{-3} with and interval of 2.0×10^{-4}. The labels are scaled by 10^5. The body is an ellipse with a/b = 5, and $\sigma = 6\pi$.

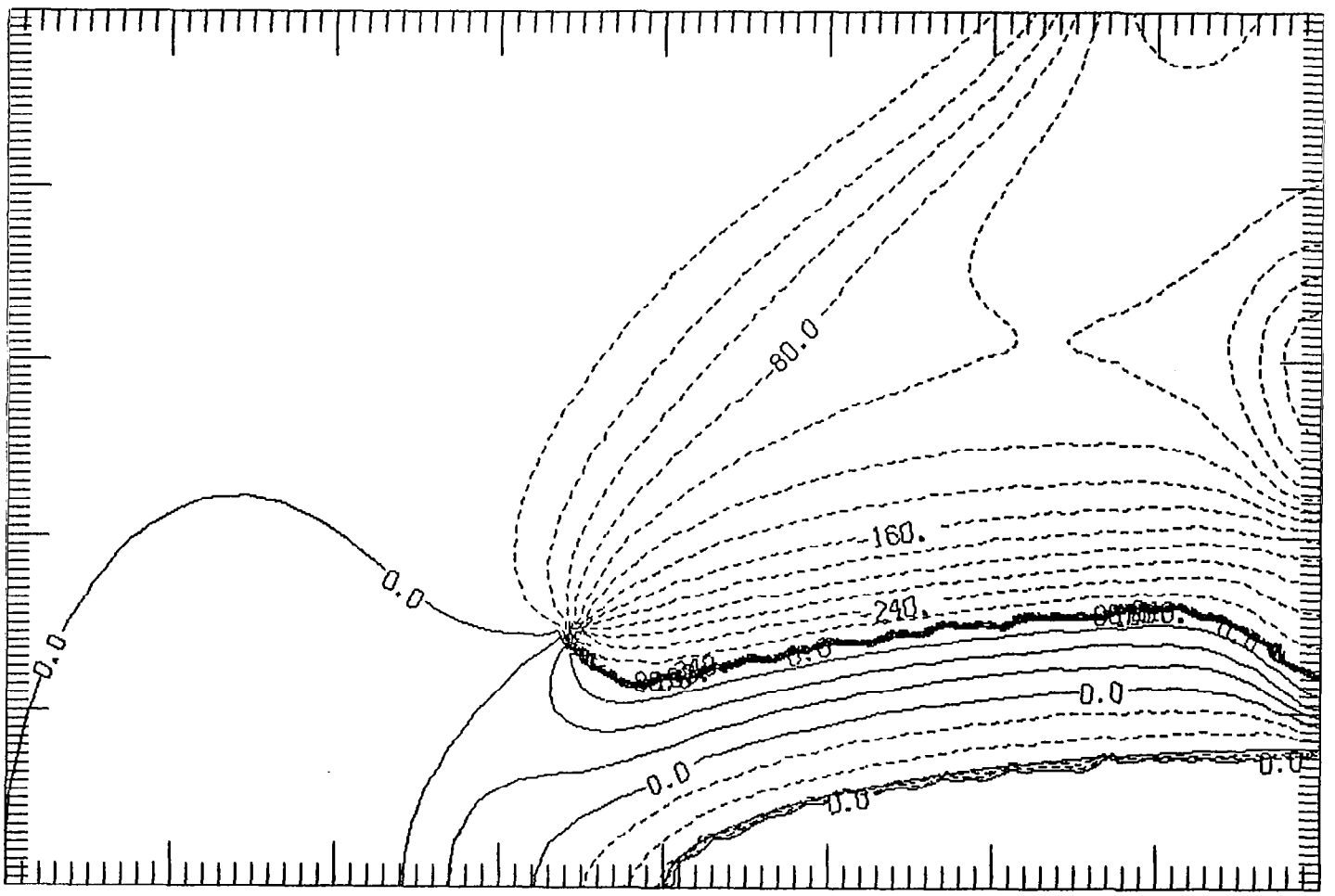

Figure 32b. Contours of the phase, in degrees, of $\hat{u}_{o,2}$, the first harmonic of the free stream oscillation. Contours from -280.0° to 60.0° with an interval of 20.0°. The body is an ellipse with a/b = 5, and $\sigma = 6\pi$.

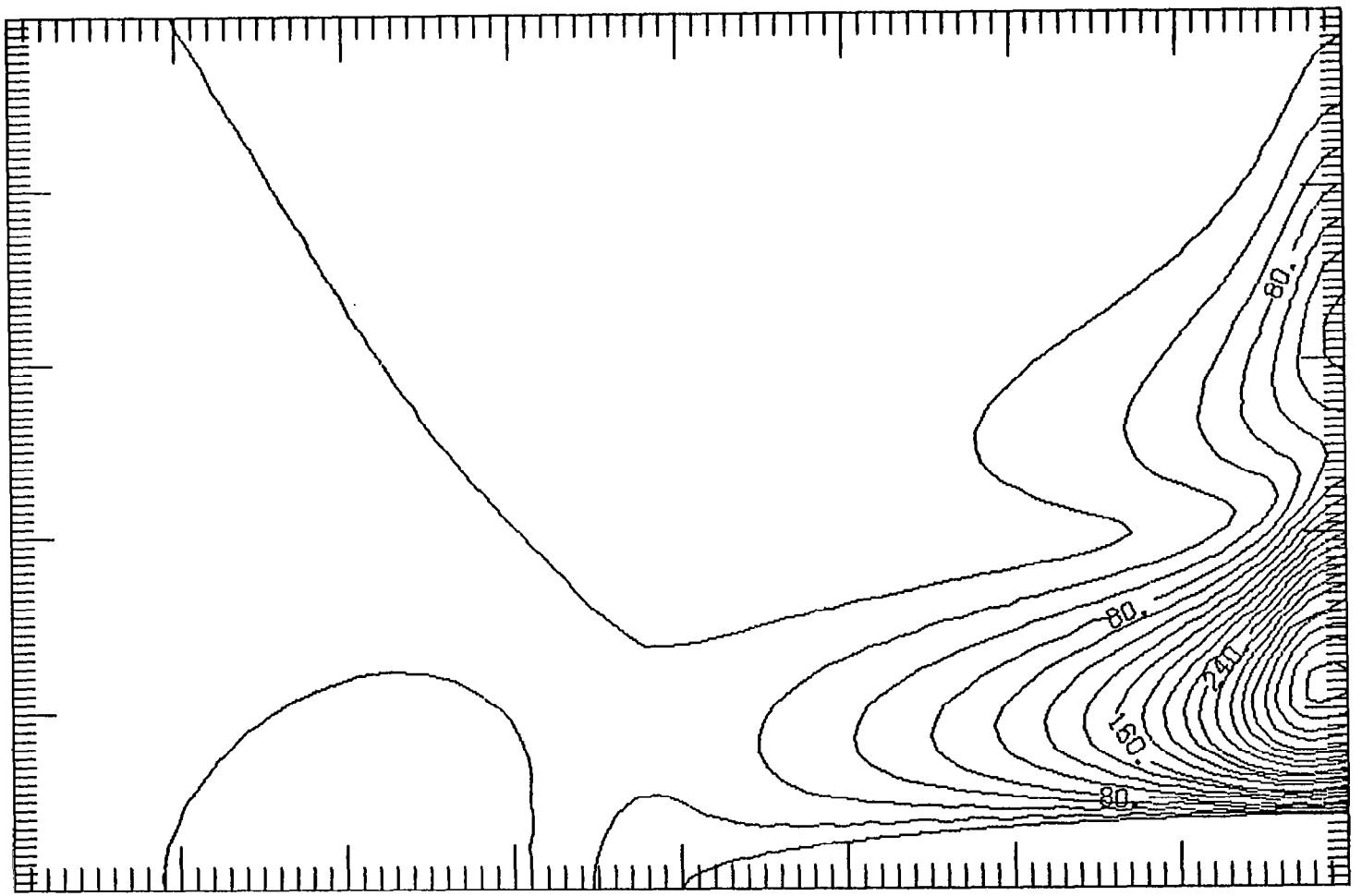

Figure 33a. Contours of the amplitude of $\hat{u}_{o,2}$, the first harmonic of the free stream oscillation. Contours from 0.0 to 4.0×10^{-2} with an interval of 2.0×10^{-3}. The labels are scaled by 10^4. The body is an ellipse with a/b = 10, and $\sigma = \pi/4$.

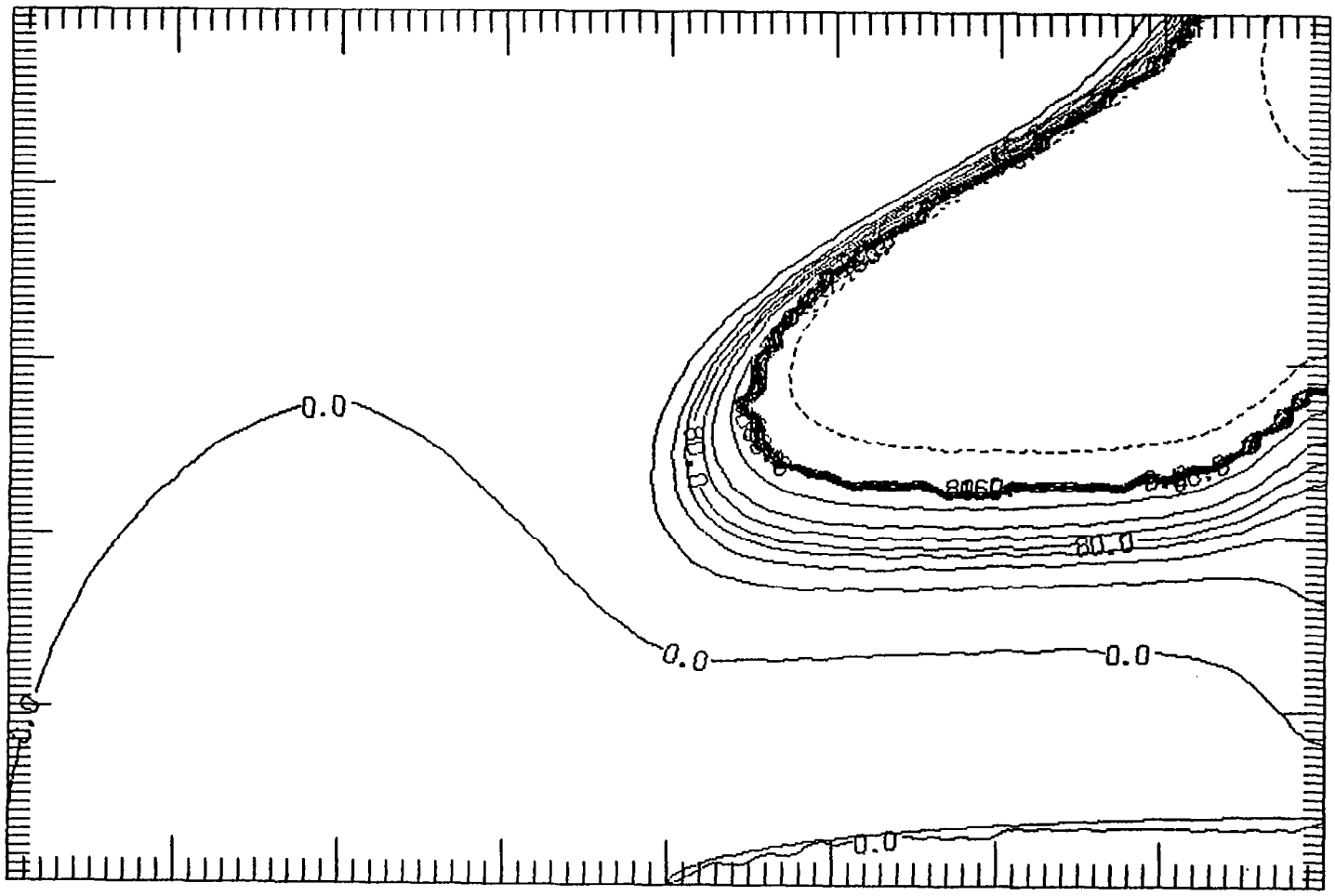

Figure 33b. Contours of the phase, in degrees, of $\hat{u}_{0,2}$, the first harmonic of the free stream oscillation. Contours from -200.0° to 140.0° with an interval of 20.0°. The body is an ellipse with a/b = 10, and $\sigma = \pi/4$.

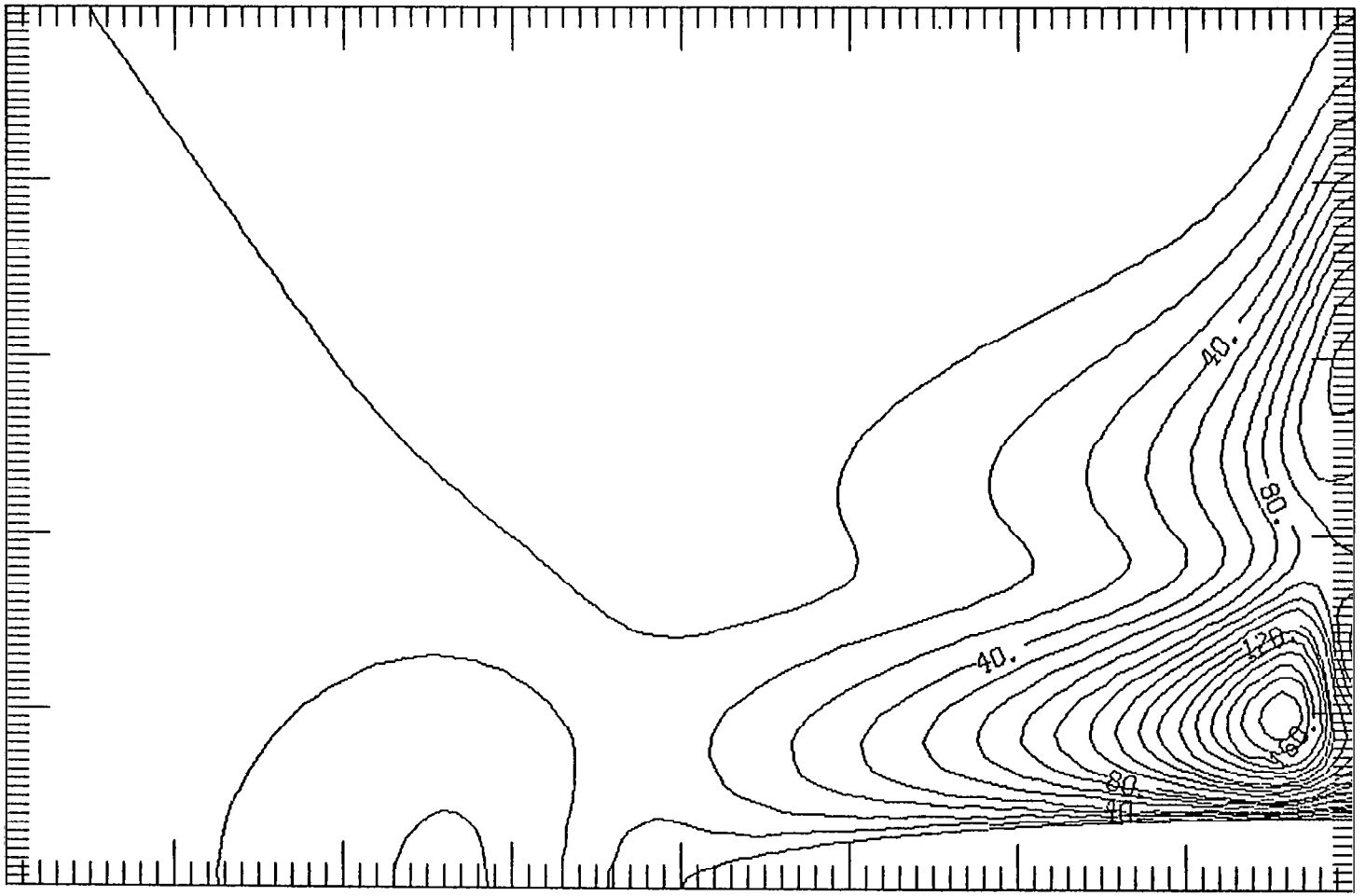

Figure 34a. Contours of the amplitude of $\hat{u}_{o,2}$, the first harmonic of the free stream oscillation. Contours from 0.0 to 1.8×10^{-2} with an interval of 1.0×10^{-3}. The labels are scaled by 10^4. The body is an ellipse with a/b = 10, and $\sigma = \pi$.

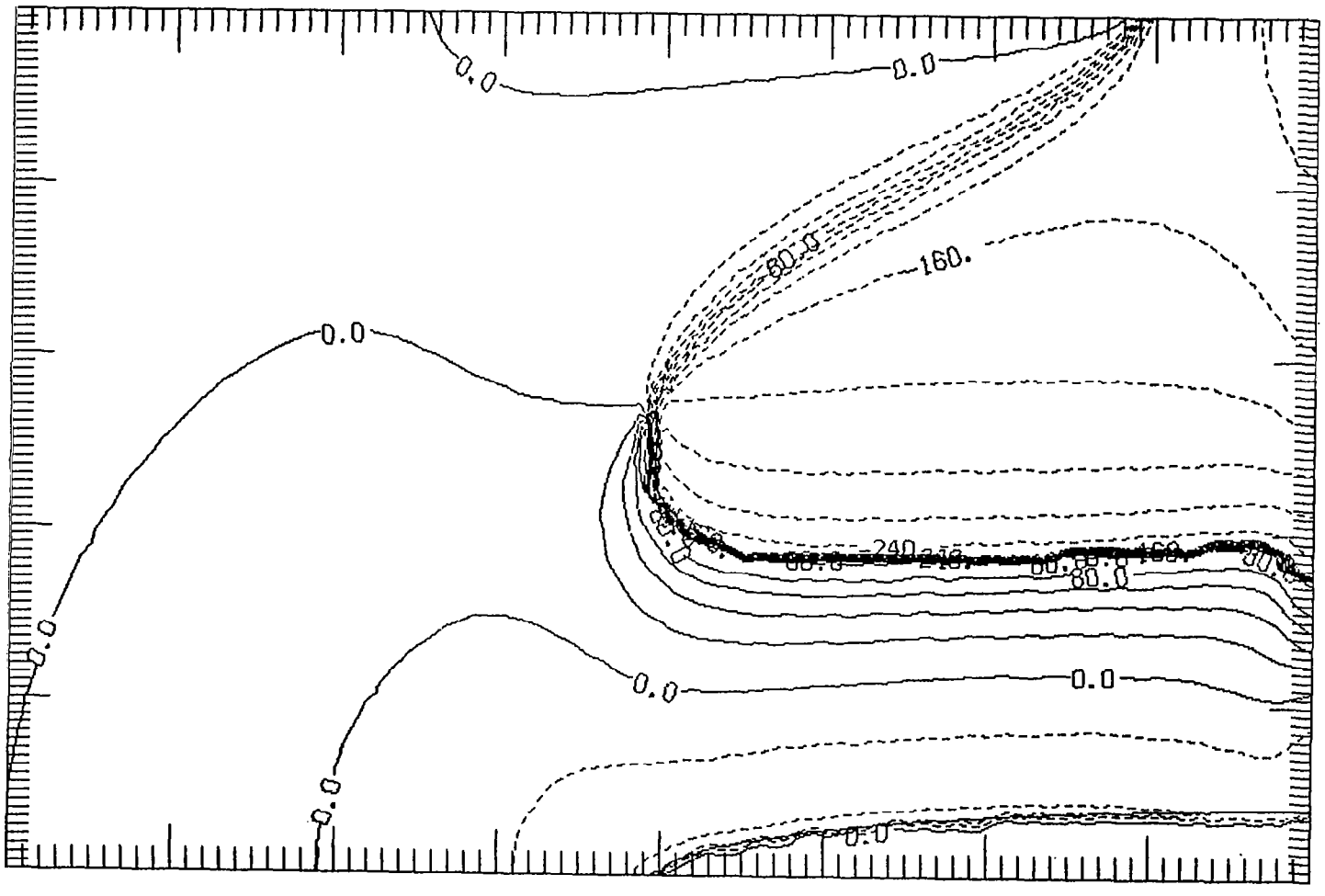

Figure 34b. Contours of the phase, in degrees, of $\hat{u}_{o,2}$, the first harmonic of the free stream oscillation. Contours from -240.0° to 100.0° with an interval of 20.0°. The body is an ellipse with a/b = 10, and $\sigma = \pi$.

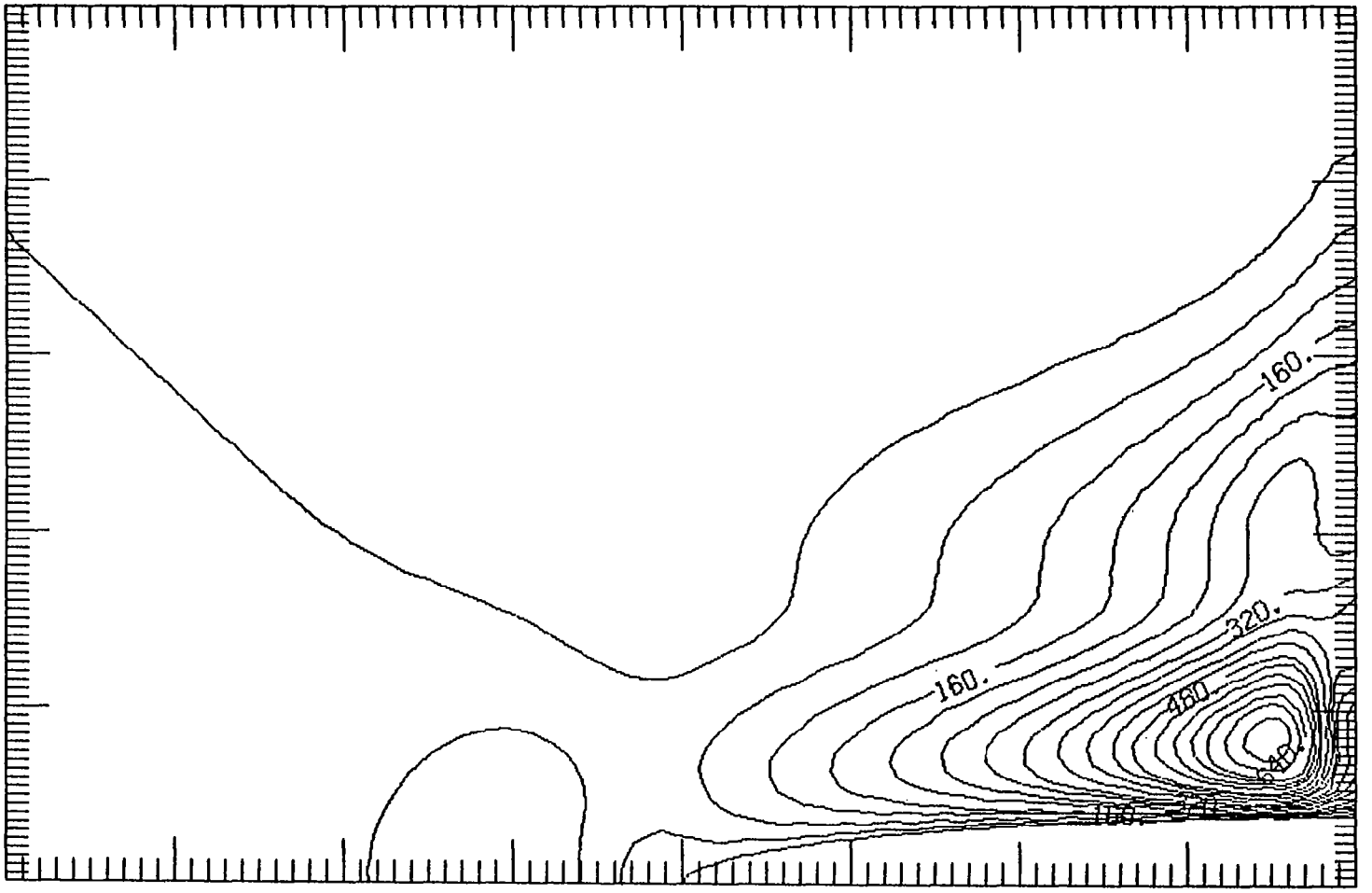

Figure 35a. Contours of the amplitude of $\hat{u}_{0,2}$, the first harmonic of the free stream oscillation. Contours from 0.0 to 7.2×10^{-3} with an interval of 4.0×10^{-4}. The labels are scaled by 10^5. The body is an ellipse with a/b = 10, and $\sigma = 3\pi$.

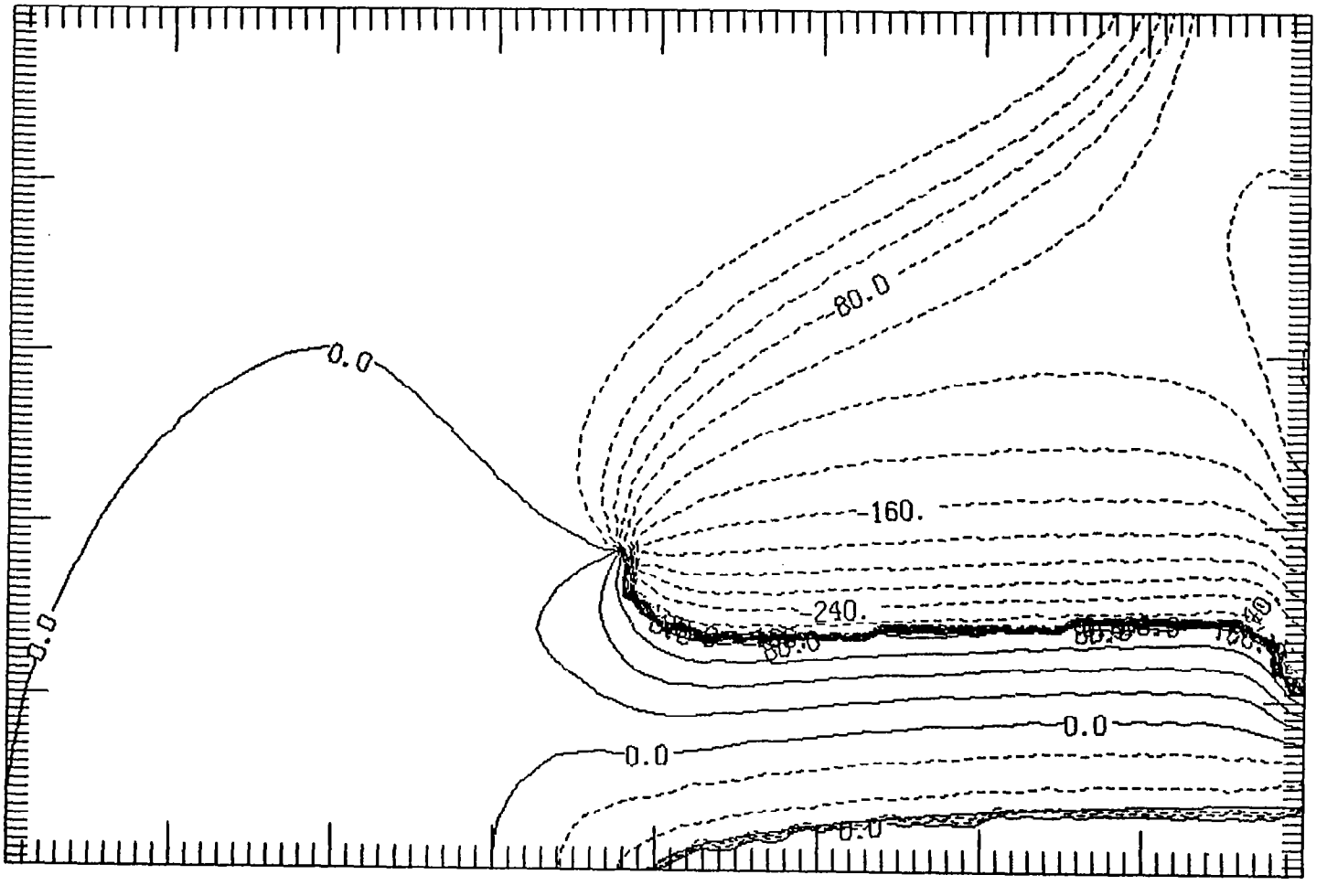

Figure 35b. Contours of the phase, in degrees, of $\hat{u}_{o,2}$, the first harmonic of the free stream oscillation. Contours from -260.0° to 80.0° with an interval of 20.0°. The body is an ellipse with a/b = 10, and $\sigma = 3\pi$.

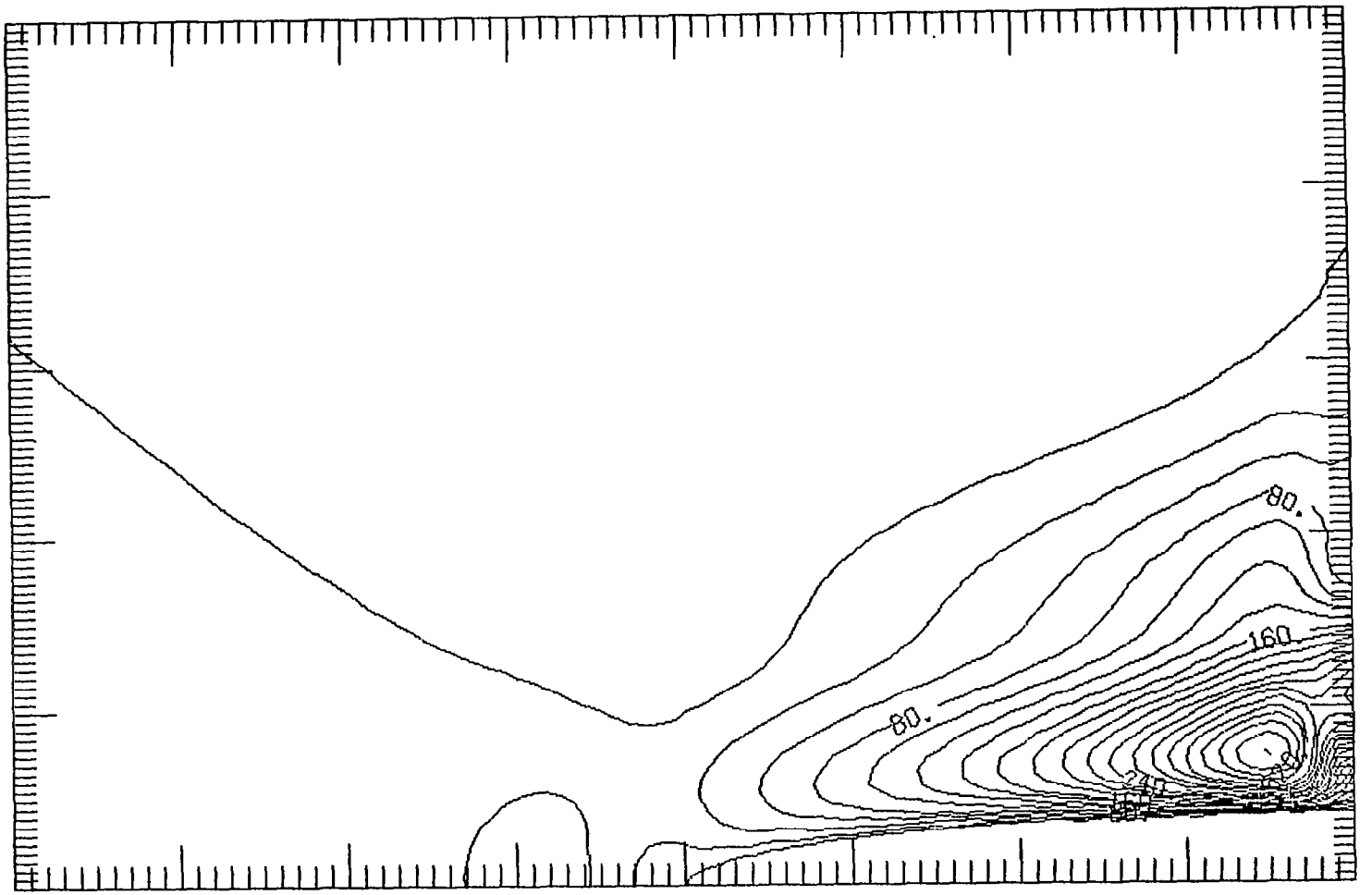

Figure 36a. Contours of the amplitude of $\hat{u}_{o,2}$, the first harmonic of the free stream oscillation. Contours from 0.0 to 4.0×10^{-3} with an interval of 2.0×10^{-4}. The labels are scaled by 10^5. The body is an ellipse with a/b = 10, and $\sigma = 6\pi$.

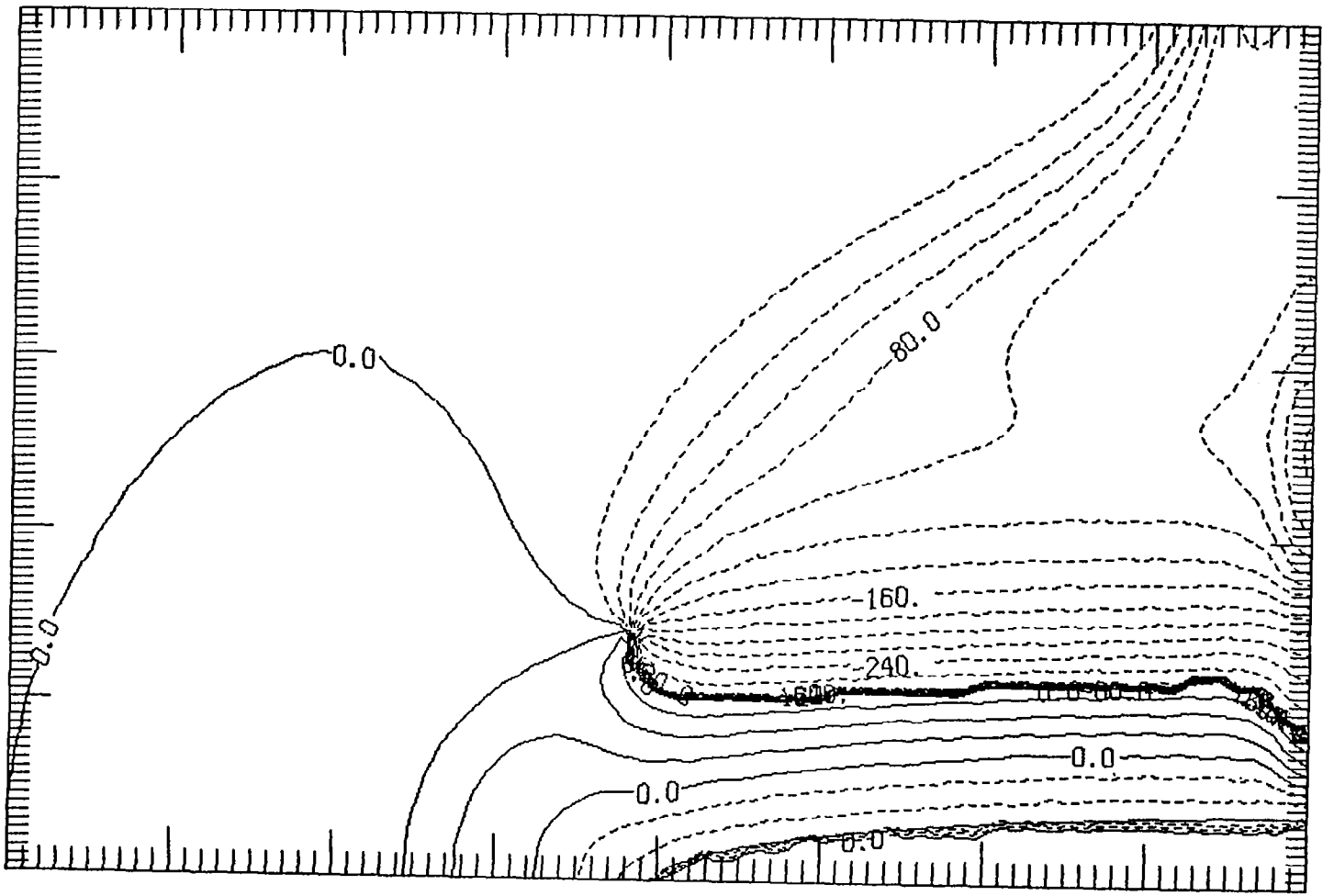

Figure 36b. Contours of the phase, in degrees, of $\hat{u}_{o,2}$, the first harmonic of the free stream oscillation. Contours from -280.0° to 60.0° with an interval of 20.0°. The body is an ellipse with a/b = 10, and $\sigma = 6\pi$.

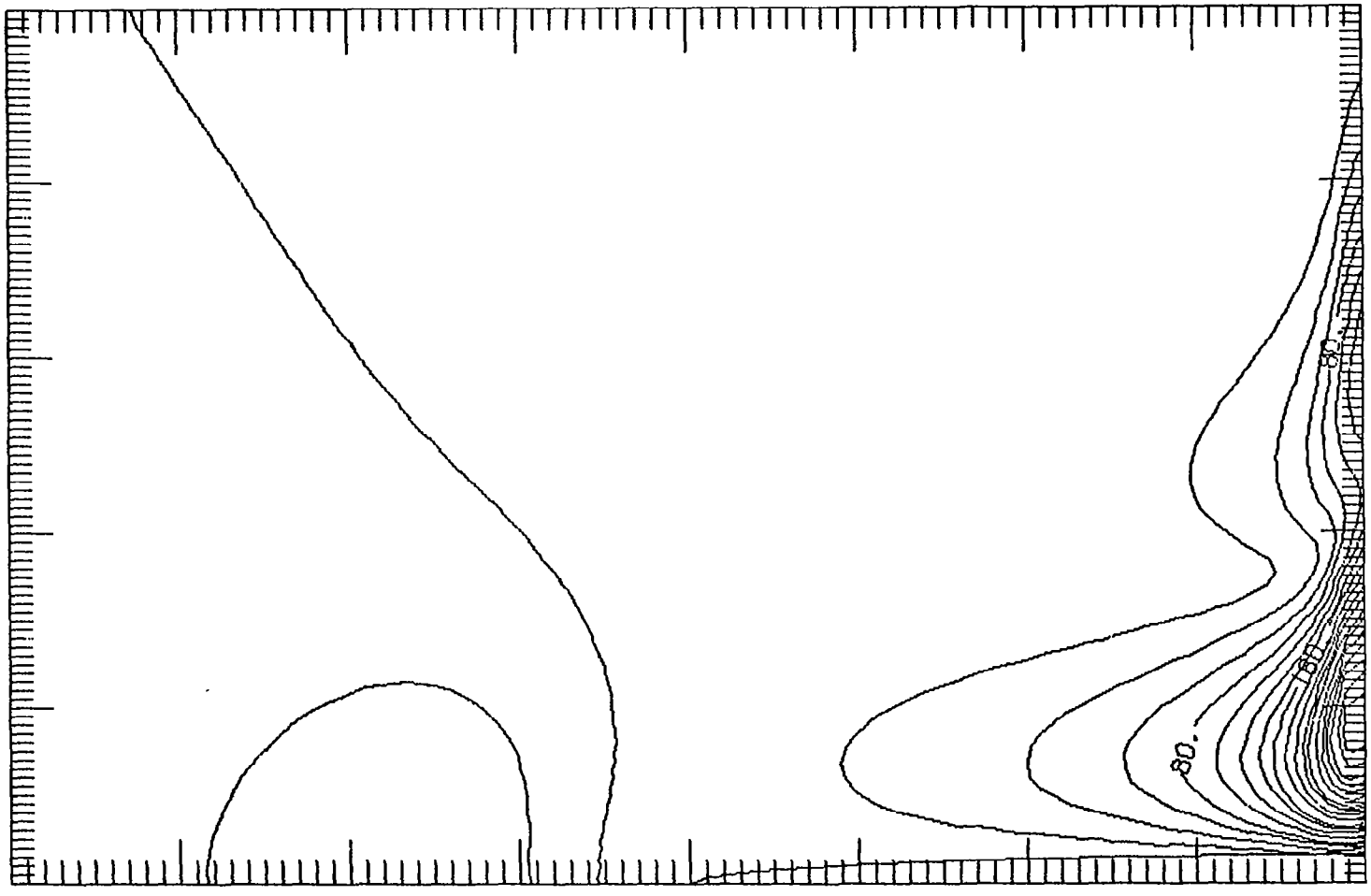

Figure 37a. Contours of the amplitude of $\hat{u}_{o,2}$, the first harmonic of the free stream oscillation. Contours from 0.0 to 3.6×10^{-2} with an interval of 2.0×10^{-3}. The labels are scaled by 10^4. The body is an ellipse with a/b = 25, and $\sigma = \pi/4$.

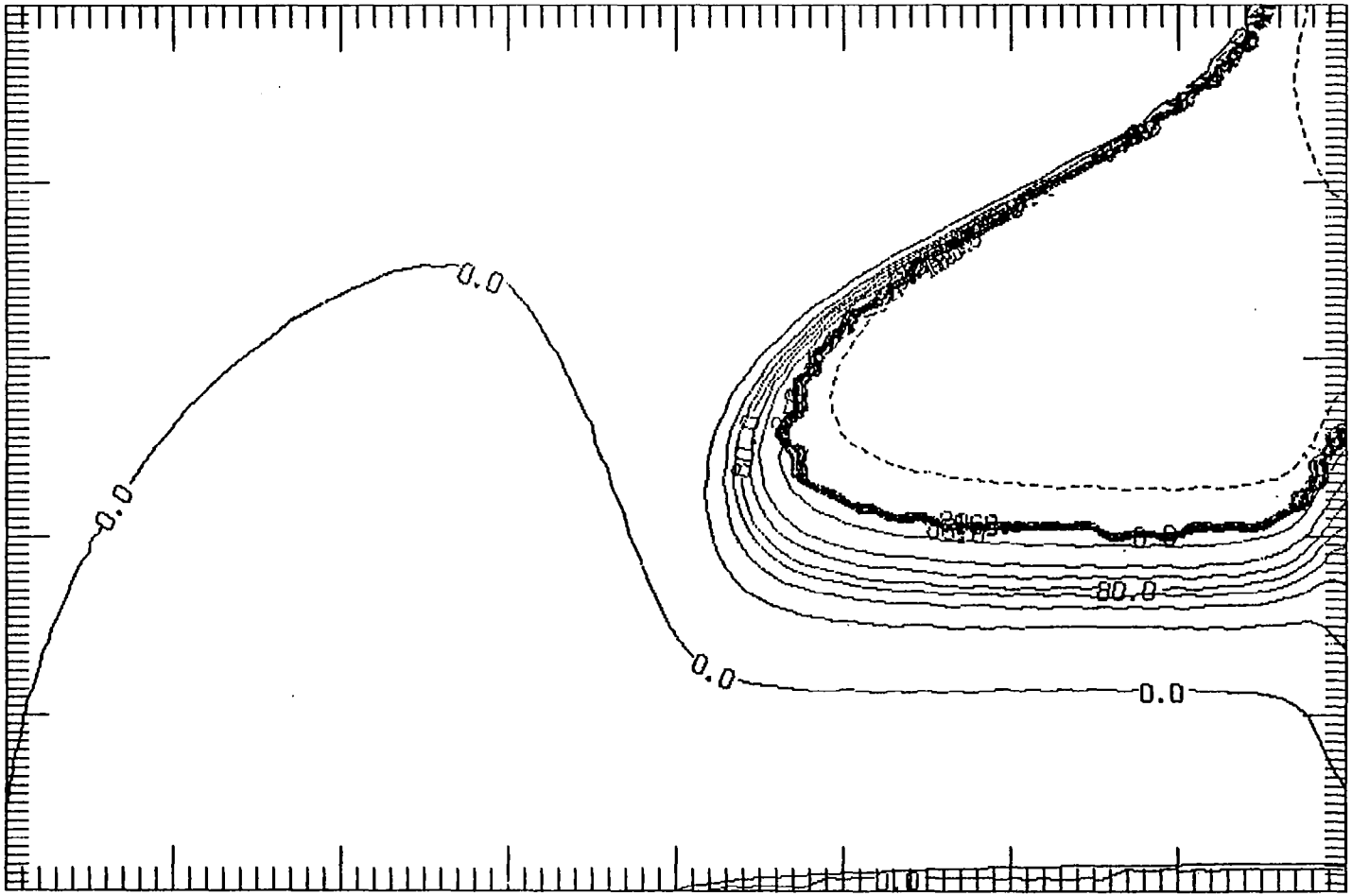

Figure 37b. Contours of the phase, in degrees, of $\hat{u}_{o,2}$, the first harmonic of the free stream oscillation. Contours from -200.0° to 140.0° with an interval of 20.0°. The body is an ellipse with a/b = 25, and $\sigma = \pi/4$.

Figure 38a. Contours of the amplitude of $\hat{u}_{o,2}$, the first harmonic of the free stream oscillation. Contours from 0.0 to 1.6×10^{-2} with an interval of 1.0×10^{-3}. The labels are scaled by 10^4. The body is an ellipse with a/b = 25, and $\sigma = \pi$.

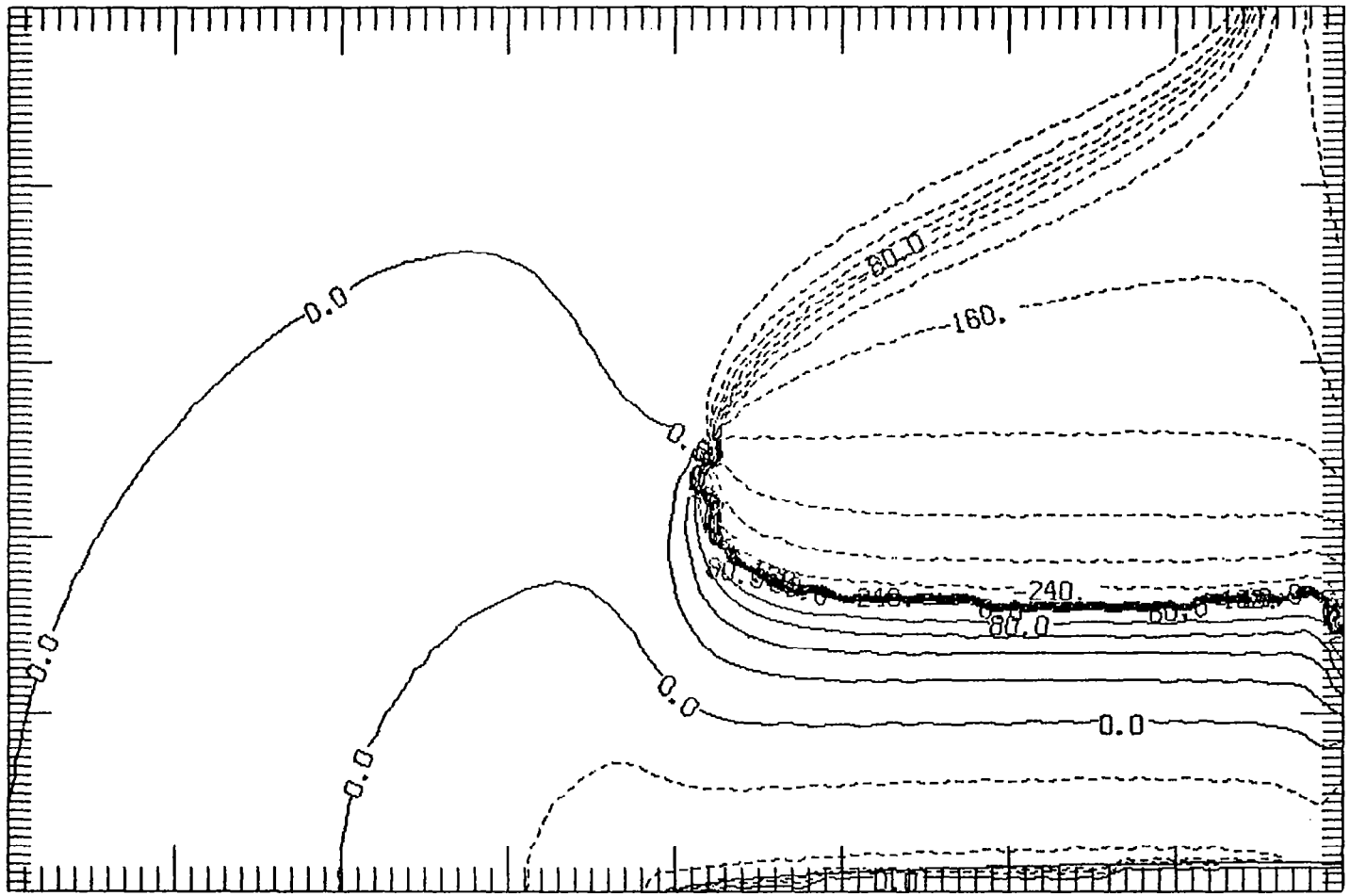

Figure 38b. Contours of the phase, in degrees, of $\hat{u}_{o,2}$, the first harmonic of the free stream oscillation. Contours from -240.0° to 100.0° with an interval of 20.0°. The body is an ellipse with a/b = 25, and $\sigma = .\pi$.

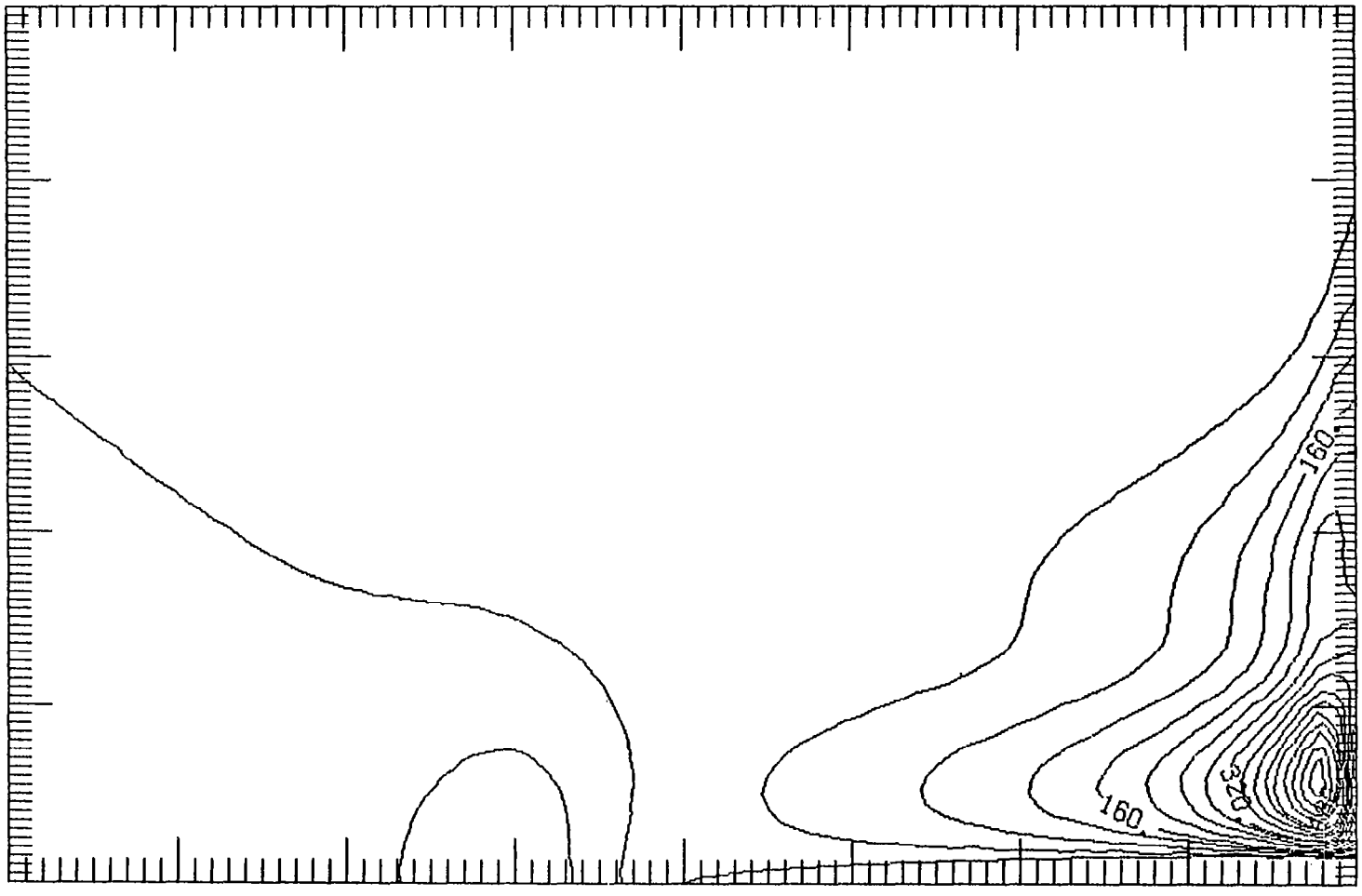

Figure 39a. Contours of the amplitude of $\hat{u}_{o,2}$, the first harmonic of the free stream oscillation. Contours from 0.0 to 6.4×10^{-3} with an interval of 4.0×10^{-4}. The labels are scaled by 10^5. The body is an ellipse with a/b = 25, and $\sigma = 3\pi$.

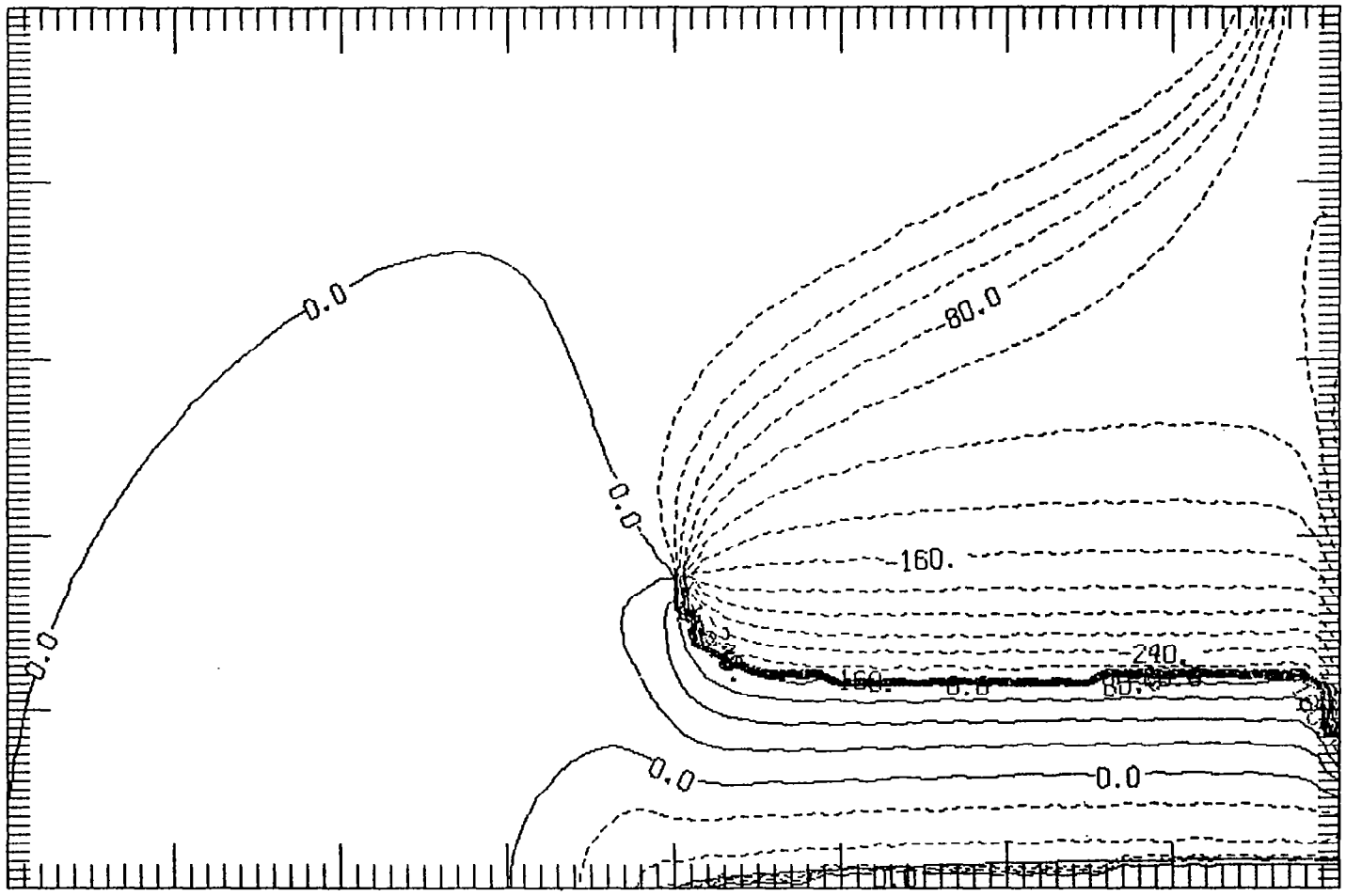

Figure 39b. Contours of the phase of $\hat{u}_{o,2}$, the first harmonic of the free stream oscillation. Contours from -260.0° to 60.0° with an interval of 20.0°. The body is an ellipse with a/b = 25, and $\sigma = 3\pi$.

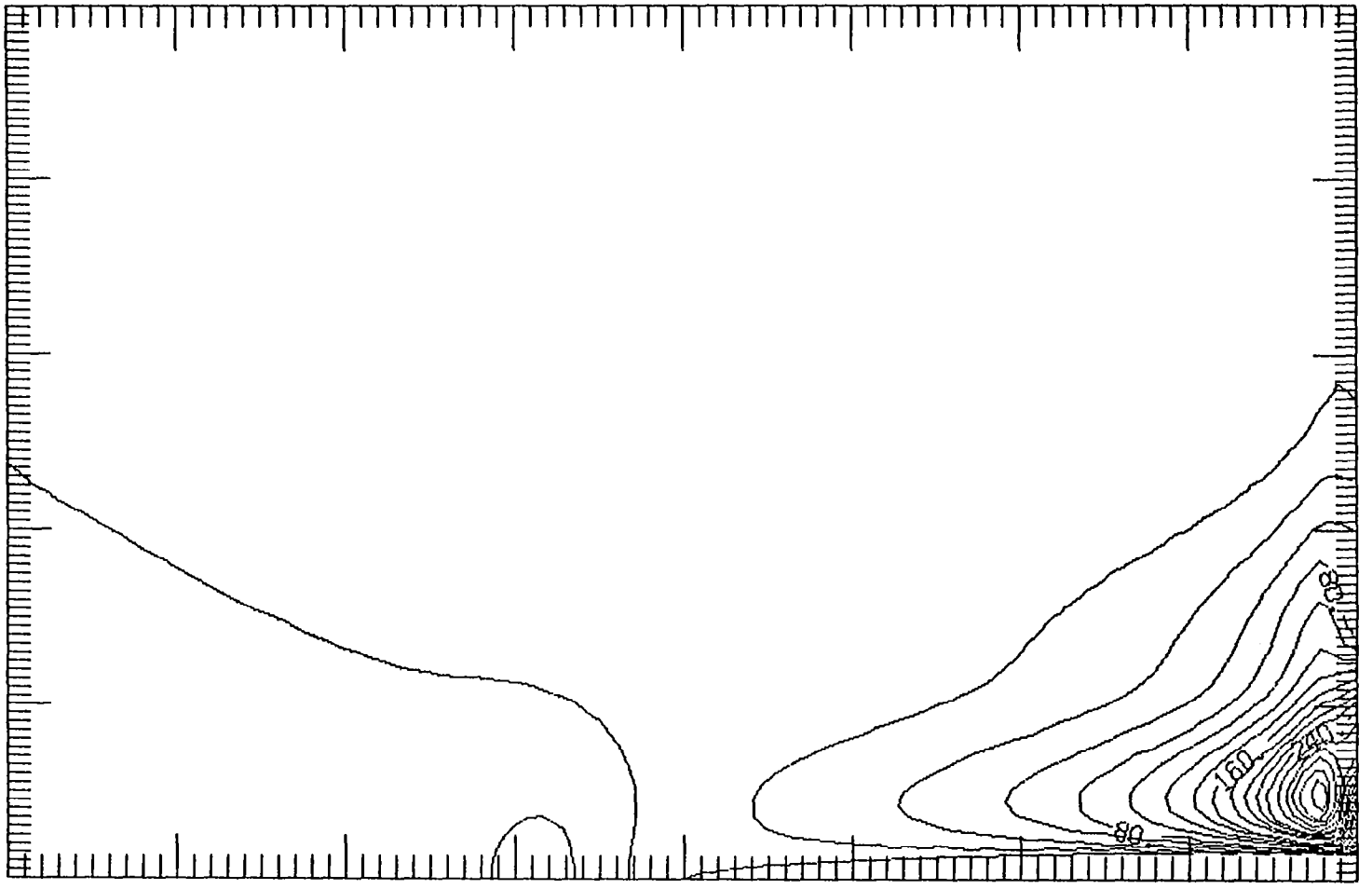

Figure 40a. Contours of the amplitude of $\hat{u}_{o,2}$, the first harmonic of the free stream oscillation. Contours from 0.0 to 3.4×10^{-3} with an interval of 2.0×10^{-4}. The labels are scaled by 10^5. The body is an ellipse with a/b = 25, and $\sigma = 6\pi$.

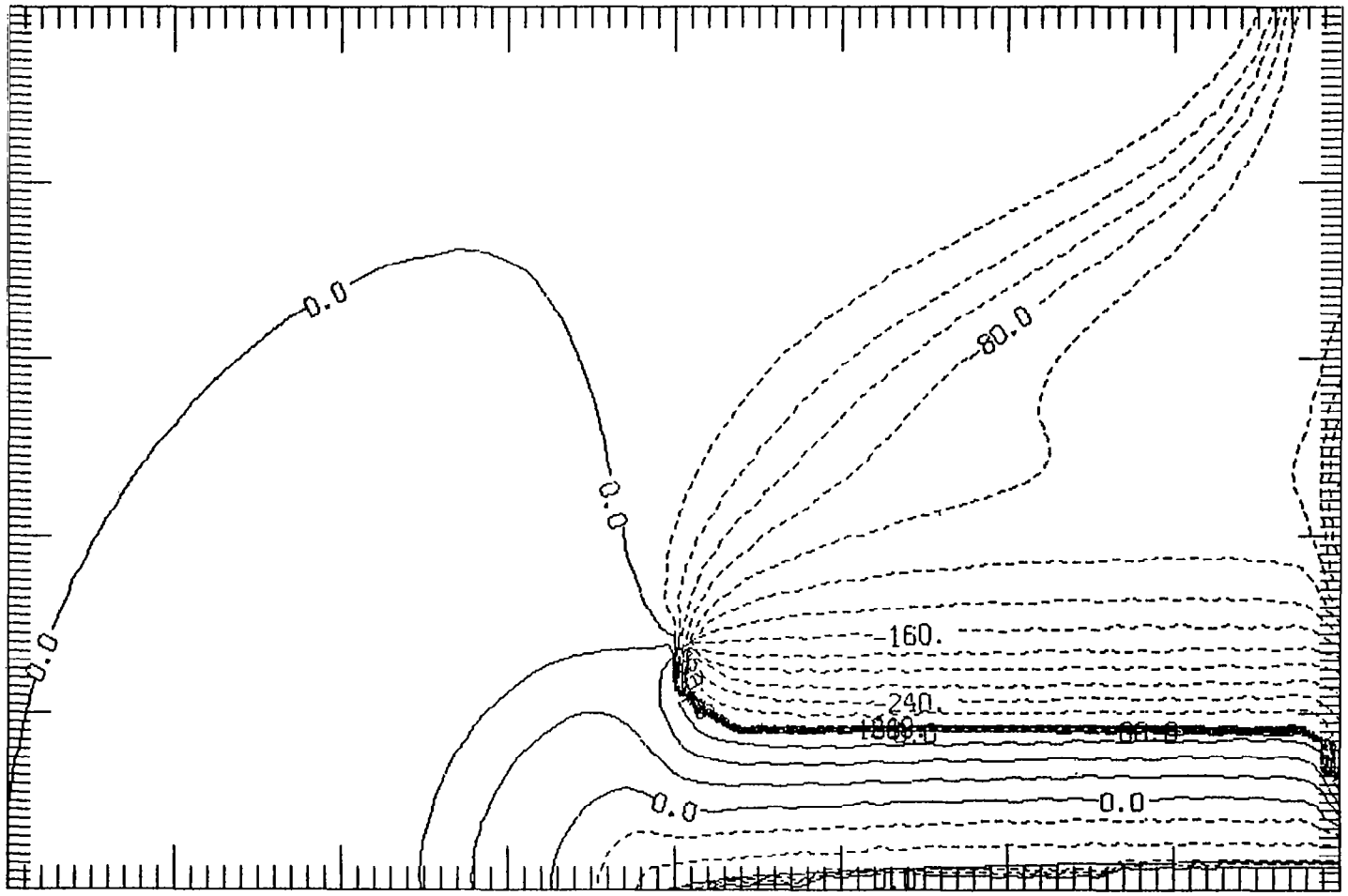

Figure 40b. Contours of the phase, in degrees, of $\hat{u}_{o,2}$, the first harmonic of the free stream oscillation. Contours from -280.0° to 60.0° with an interval of 20.0°. The body is an ellipse with a/b = 25, and $\sigma = 6\pi$.

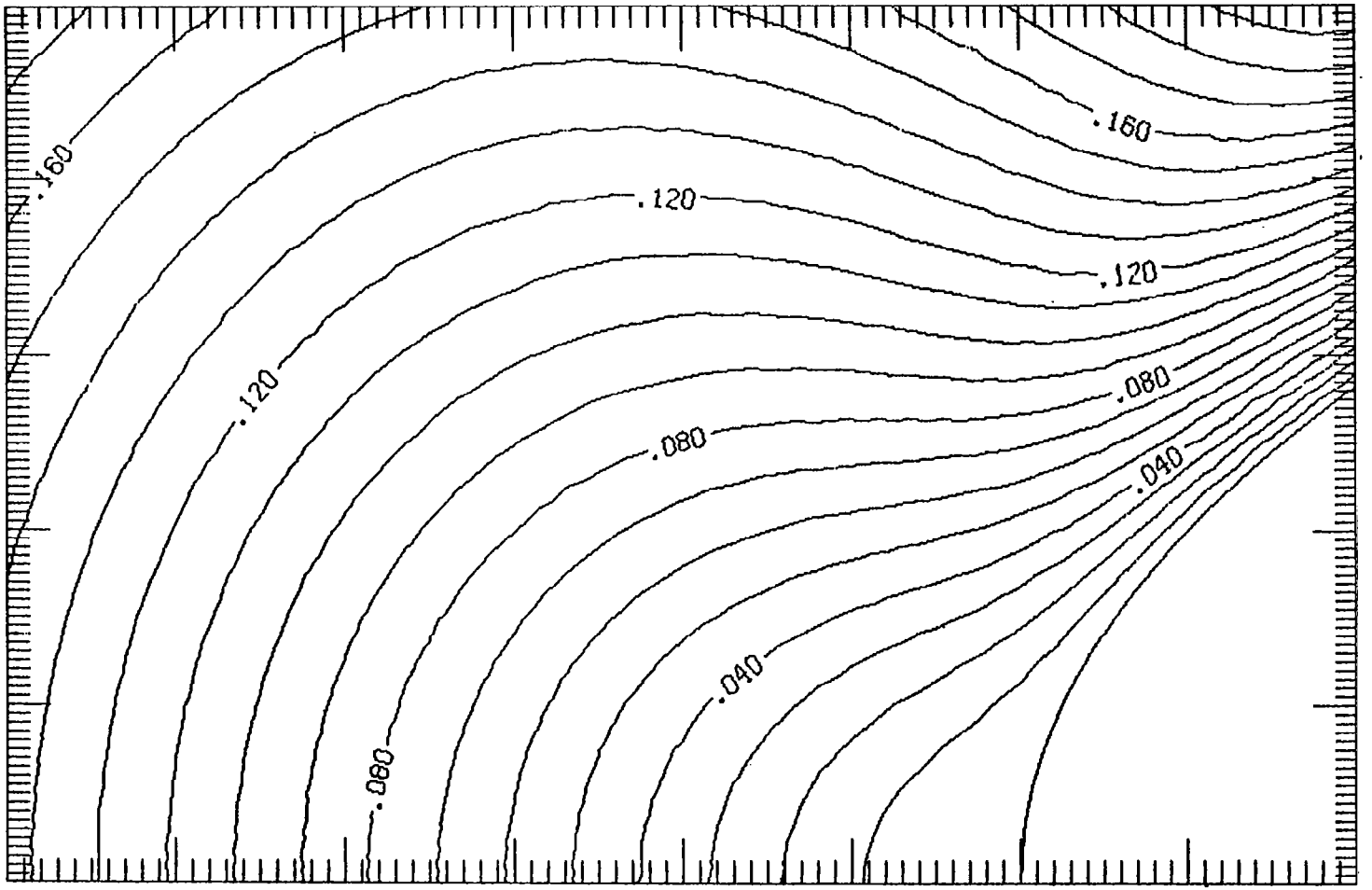

Figure 41. Contours of the amplitude of $\hat{u}_{o,1}$, the fundamental oscillation of the flow past the parabola with $\sigma = \pi/16$. Contours from 0.0 to 0.22 with an interval of 0.01.

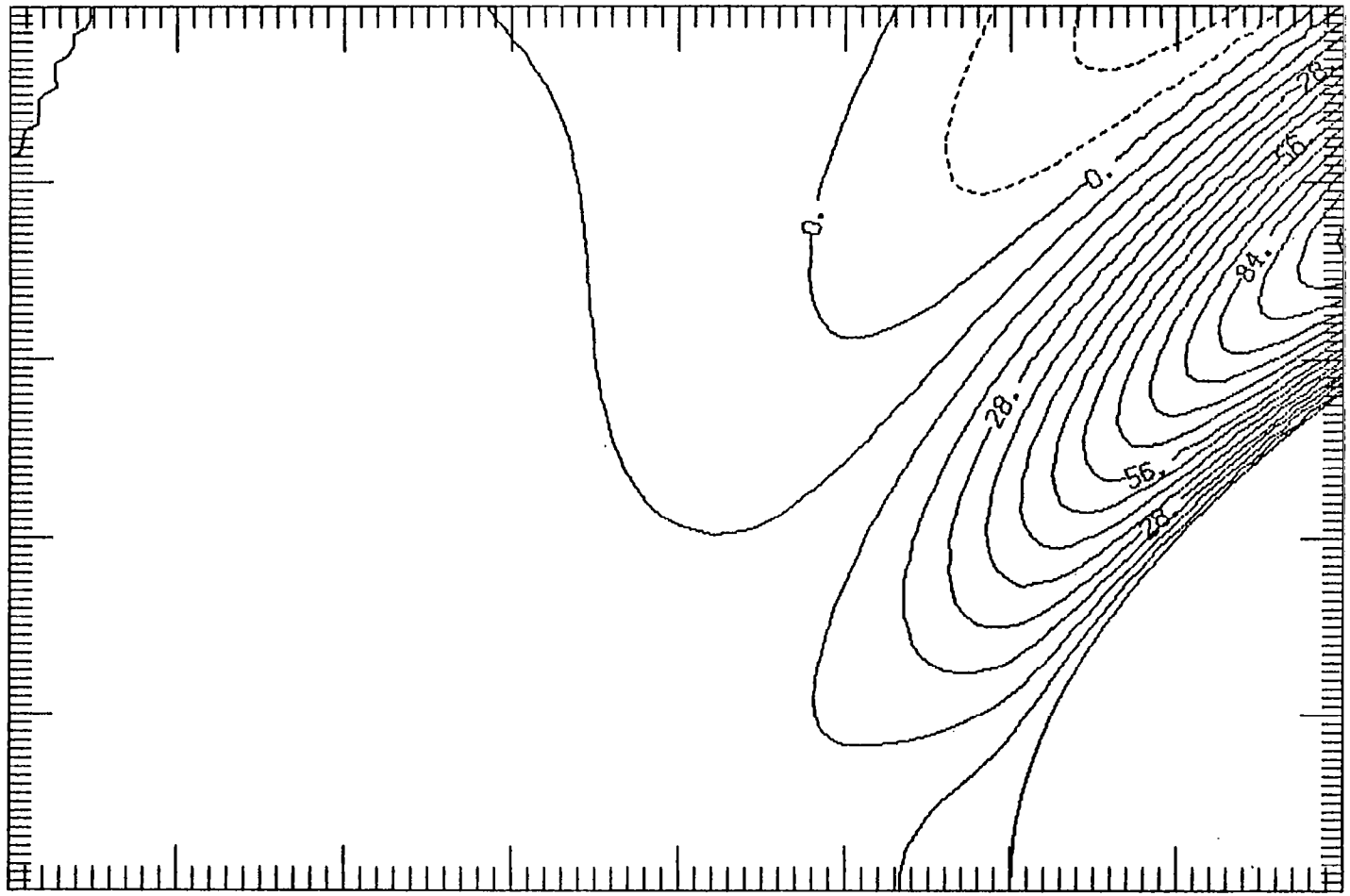

Figure 42. Contours of the second order steady flow, $\hat{u}_{2,o}$, past the parabola with $\sigma = \pi/16$. Contours from -1.4×10^{-3} to 1.05×10^{-2} with an interval of 7.0×10^{-4}. The labels are scaled by 10^4

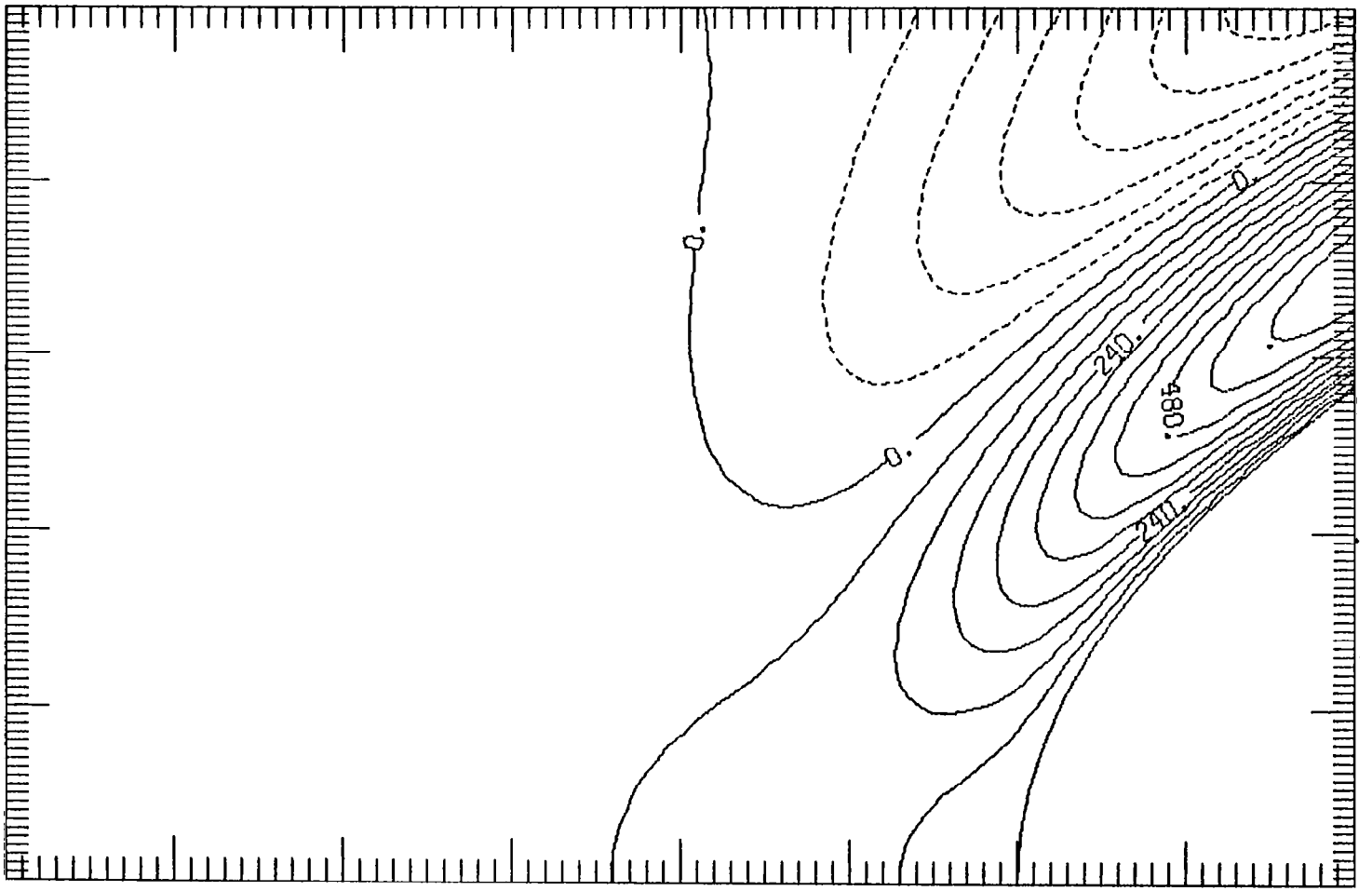

Figure 43. Contours of the second order steady flow, $\hat{u}_{2,o}$, past the parabola with $\sigma = \pi/4$. Contours from -3.6×10^{-3} to 6.6×10^{-3} with an interval of 6.0×10^{-4}. The labels are scaled by 10^5.

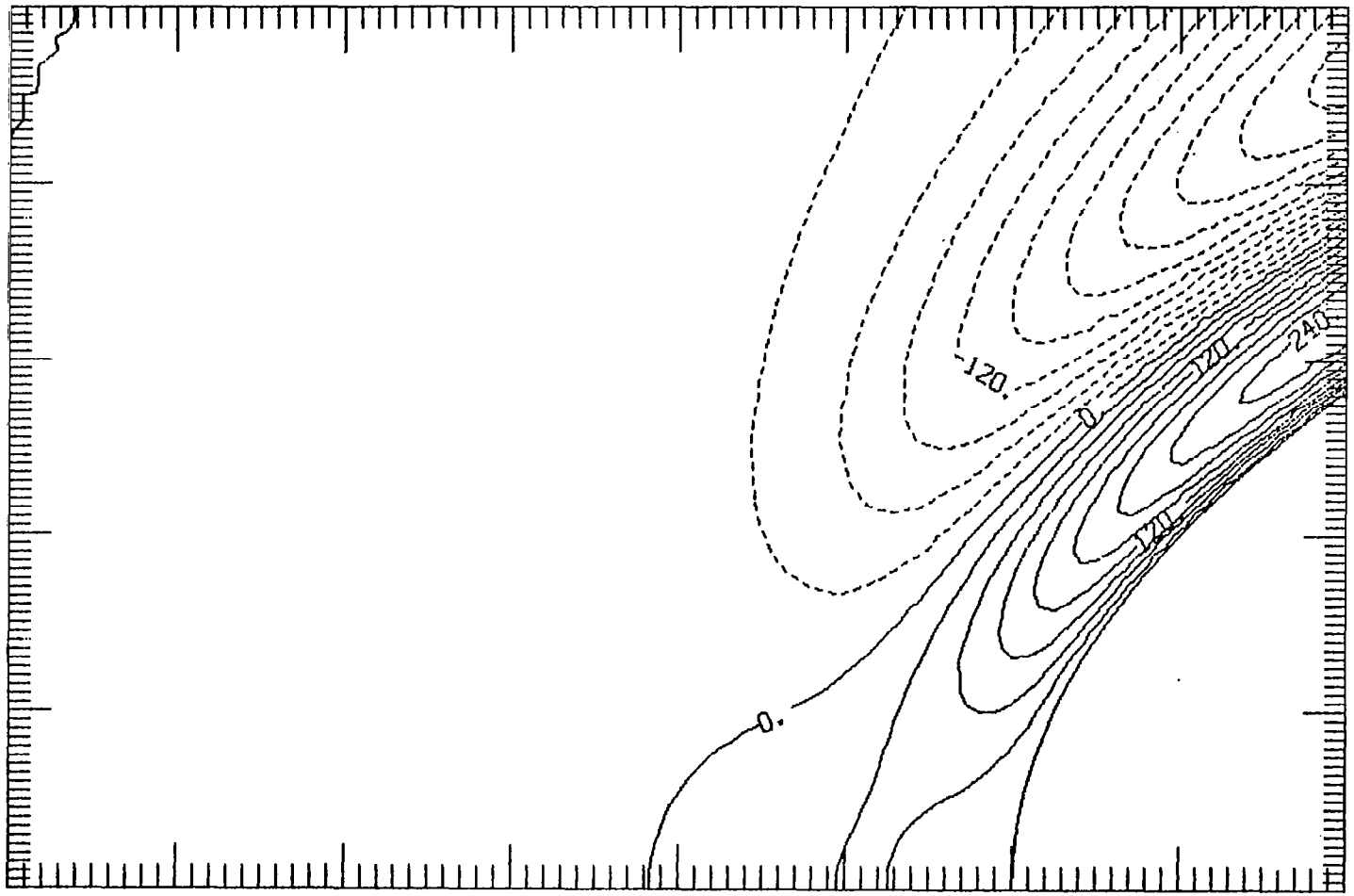

Figure 44. Contours of the second order steady flow, $\hat{u}_{2,o}$, past the parabola with $\sigma = 3\pi/4$. Contours from -3.0×10^{-3} to 2.4×10^{-3} with an interval of 3.0×10^{-4}. The labels are scaled by 10^5.

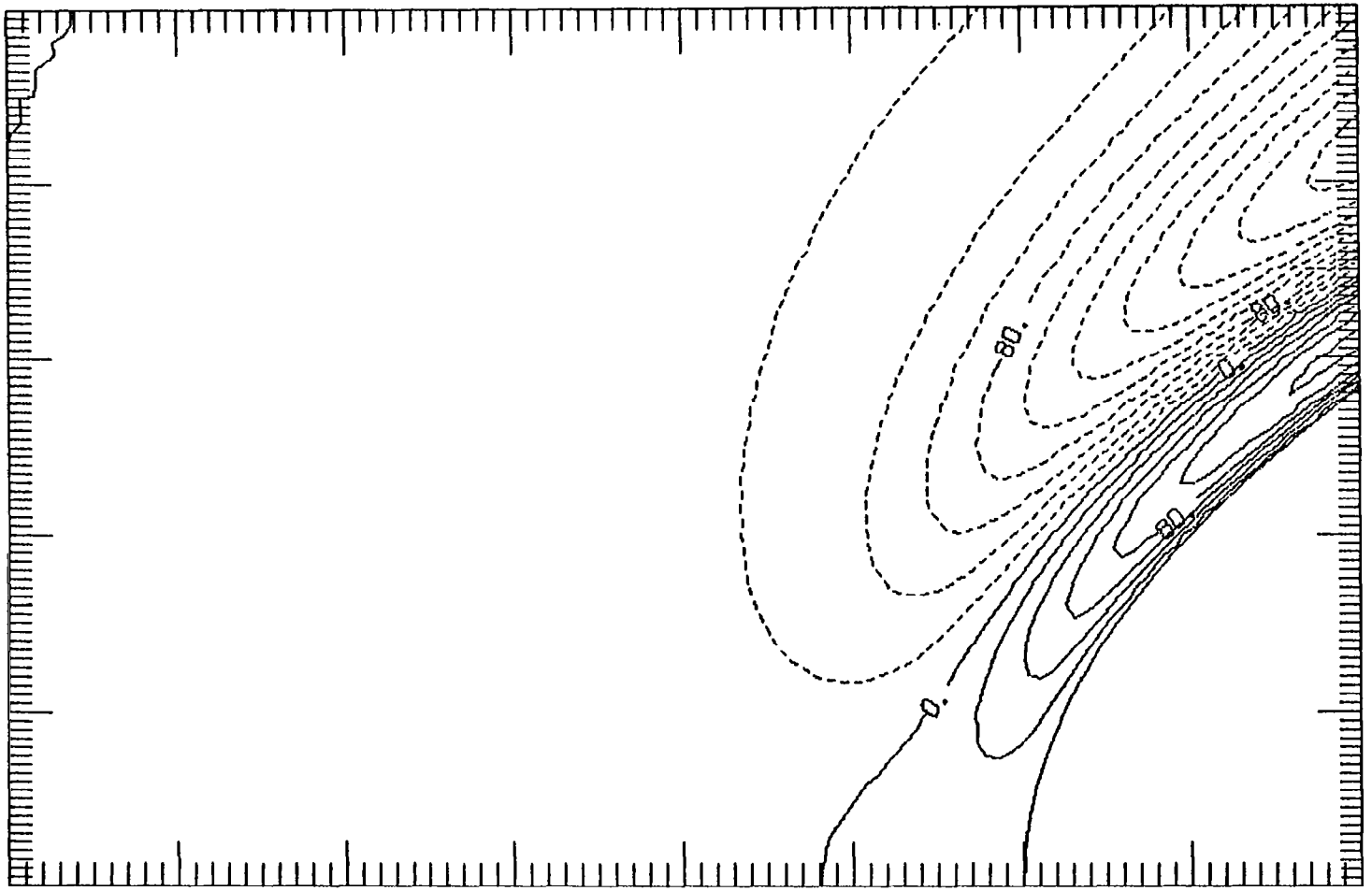

Figure 45. Contours of the second order steady flow, $\hat{u}_{2,o}$, past the parabola with $\sigma = 3\pi/2$. Contours from -2.0×10^{-3} to 1.2×10^{-3} with an interval of 2.0×10^{-4}. The labels are scaled by 10^{5}.

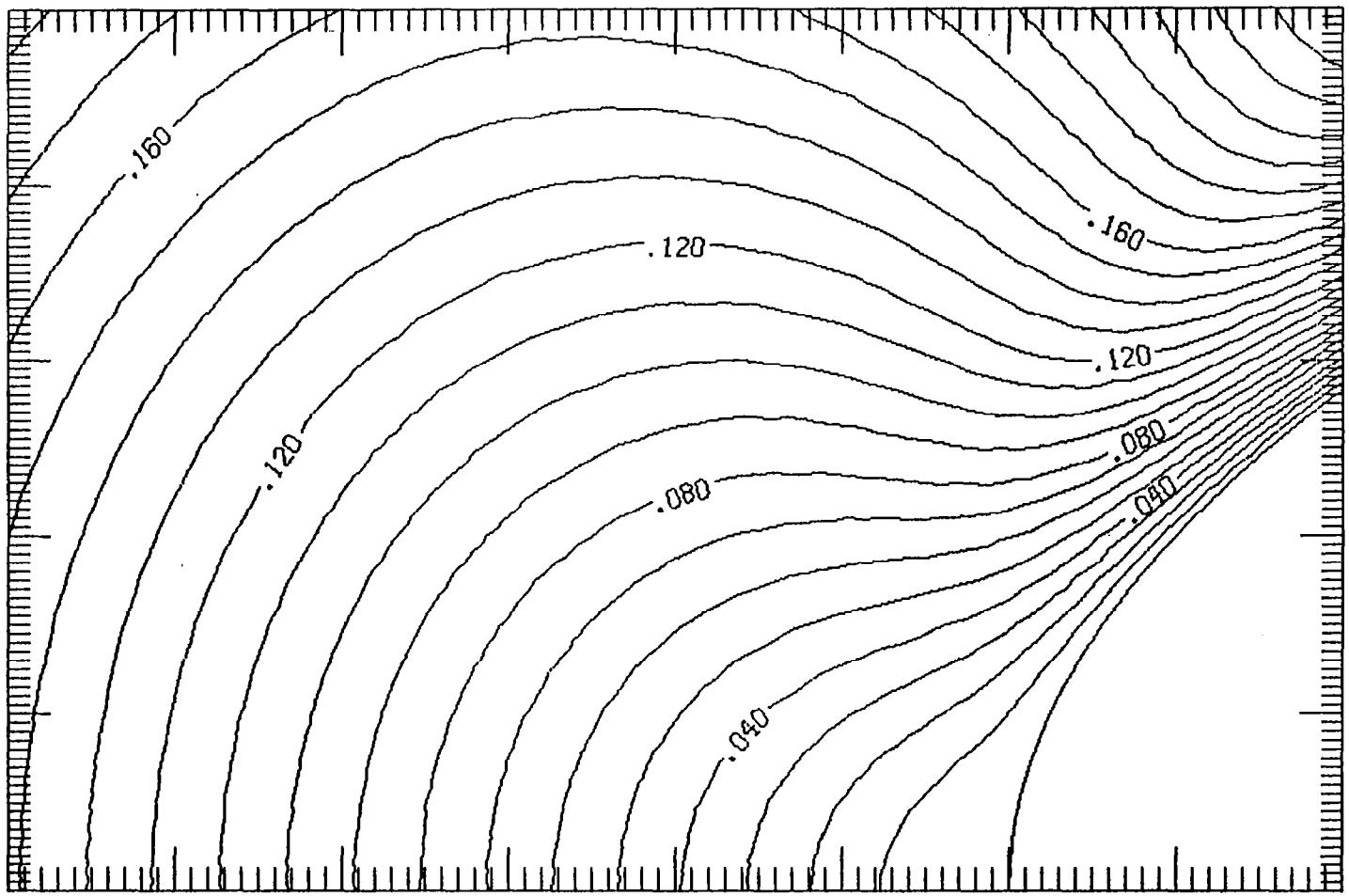

Figure 46a. Contours of the amplitude of $\hat{u}_{o,1}$, the fundamental oscillation of the flow past the parabola with $\sigma = \pi/16$. Contours from 0.0 to 0.22 with an interval of 0.01.

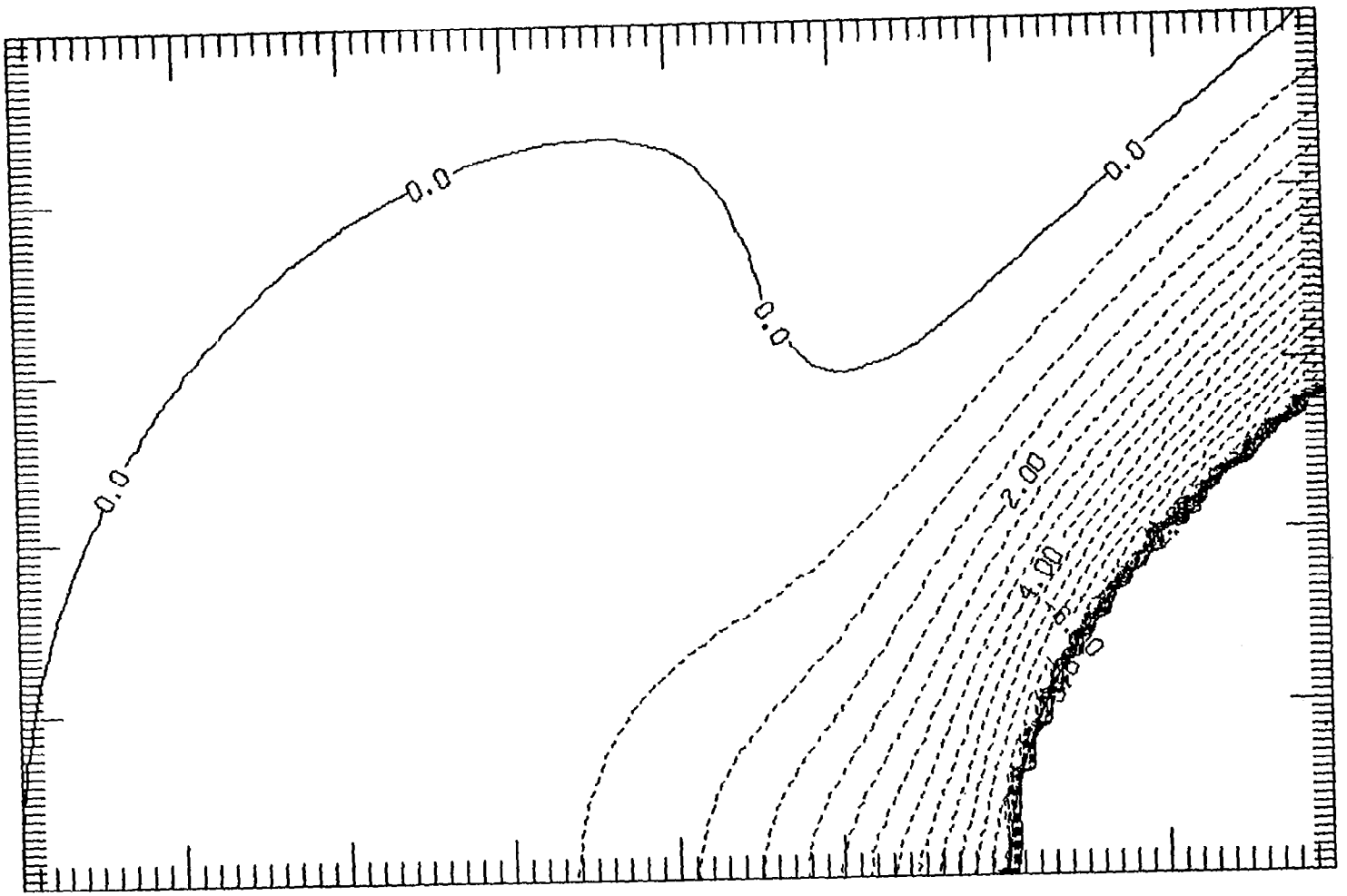

Figure 46b. Contours of the phase, in degrees, of $\hat{u}_{o,1}$, the fundamental oscillation of the flow past the parabola with $\sigma = \pi/16$. Contours from -8.5° to 0.0° with an interval of 0.5°.

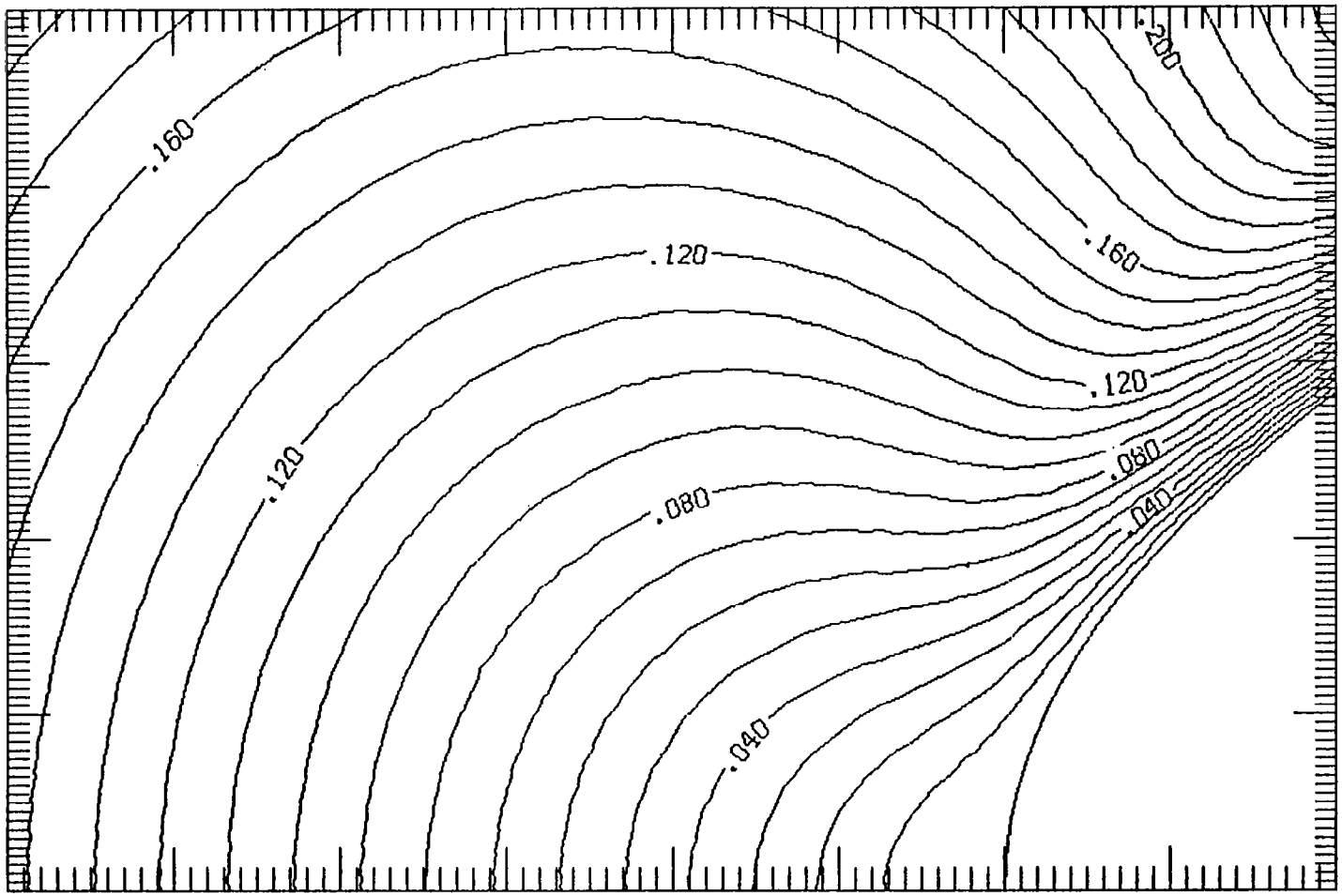

Figure 47a. Contours of the amplitude of $\hat{u}_{o,1}$, the fundamental oscillation of the flow past the parabola with $\sigma = \pi/4$. Contours from 0.0 to 0.23 with an interval of 0.01.

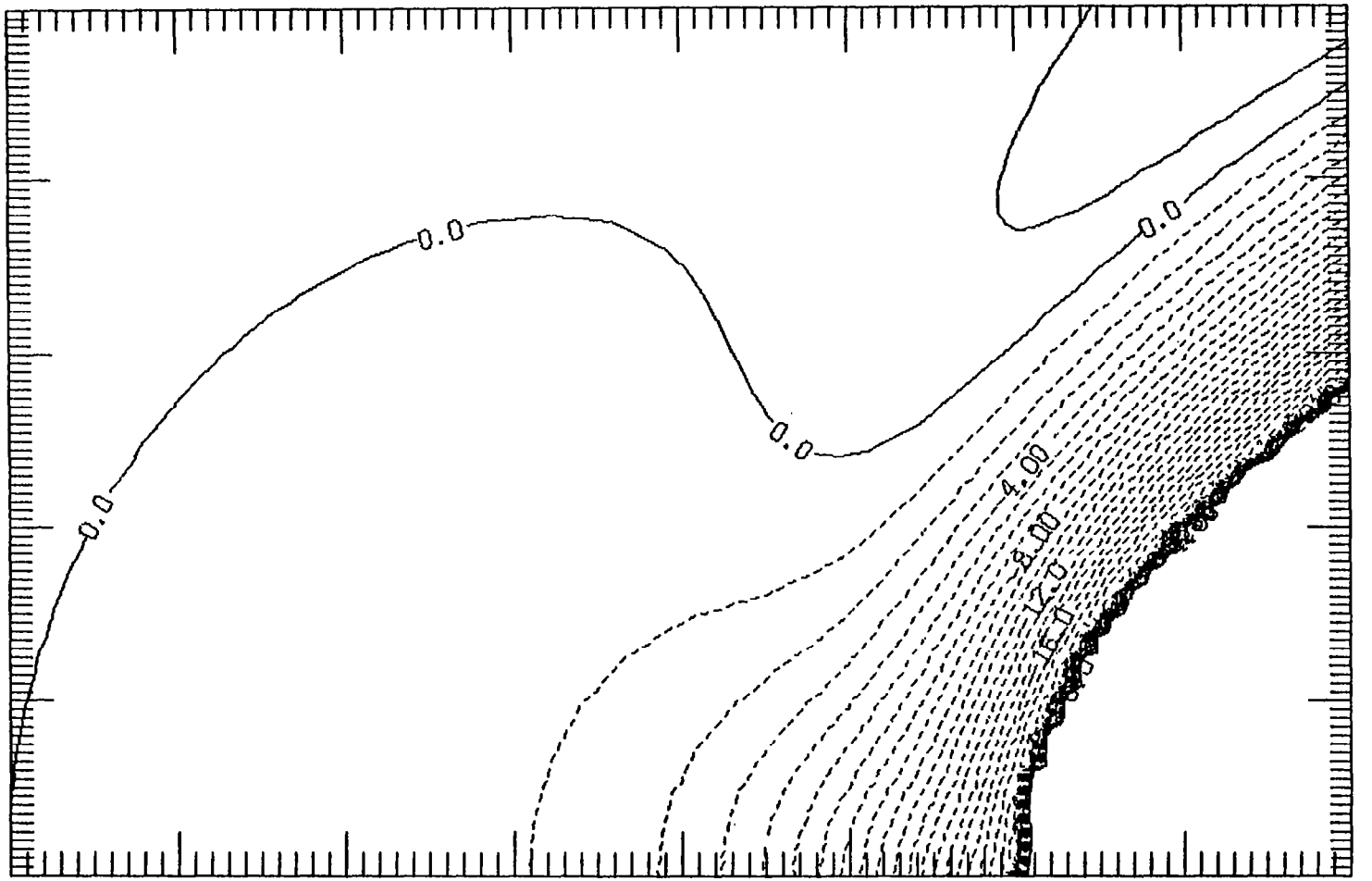

Figure 47b. Contours of the phase, in degrees, of $\hat{u}_{o,1}$, the fundamental oscillation of the flow past the parabola with $\sigma = \pi/4$. Contours from -24.0° to 1.0° with an interval of 1.0°.

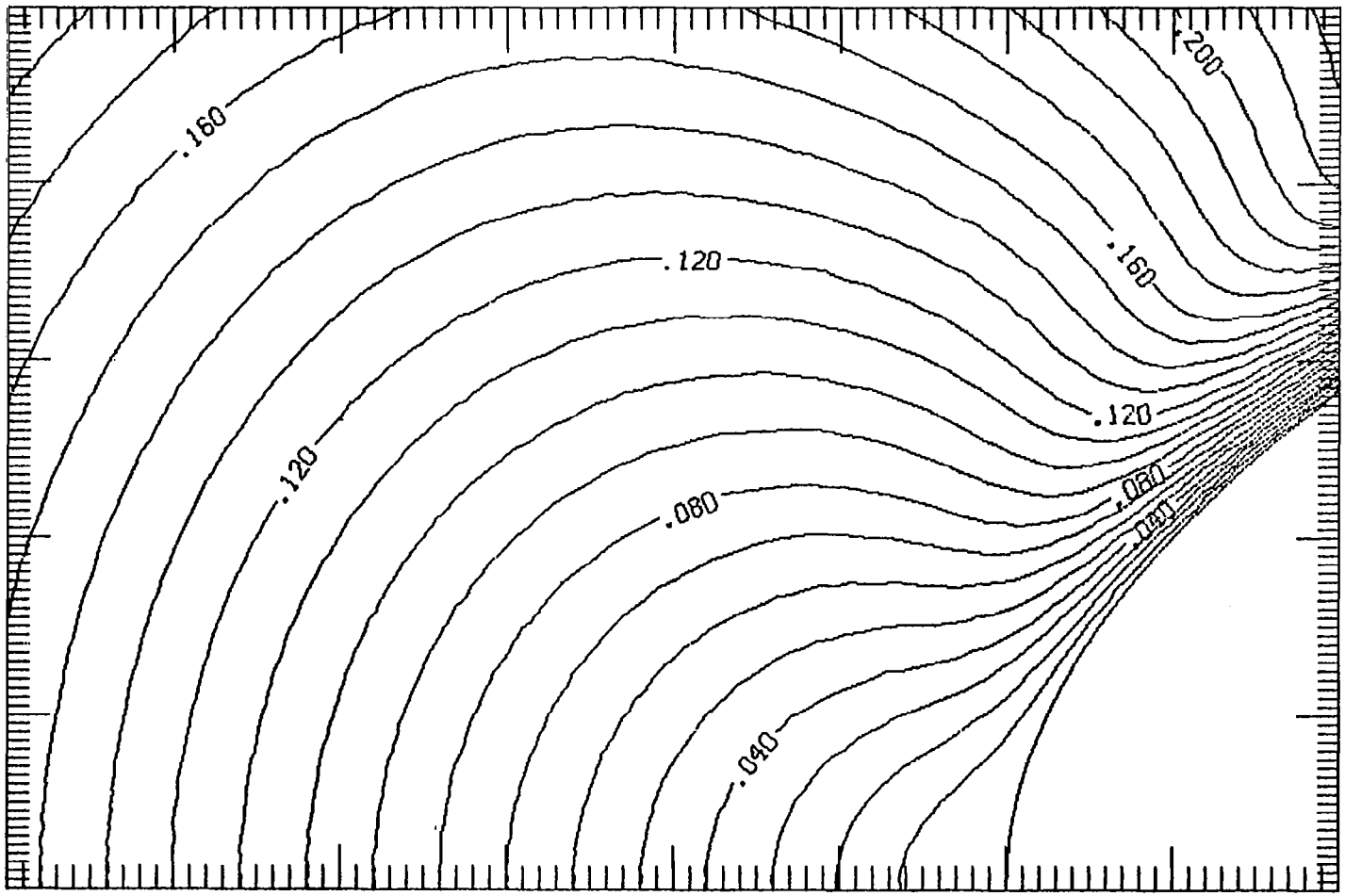

Figure 48a. Contours of the amplitude of $\hat{u}_{o,1}$, the fundamental oscillation of the flow past the parabola with $\sigma = 3\pi/4$. Contours from 0.0 to 0.22 with an interval of 0.01.

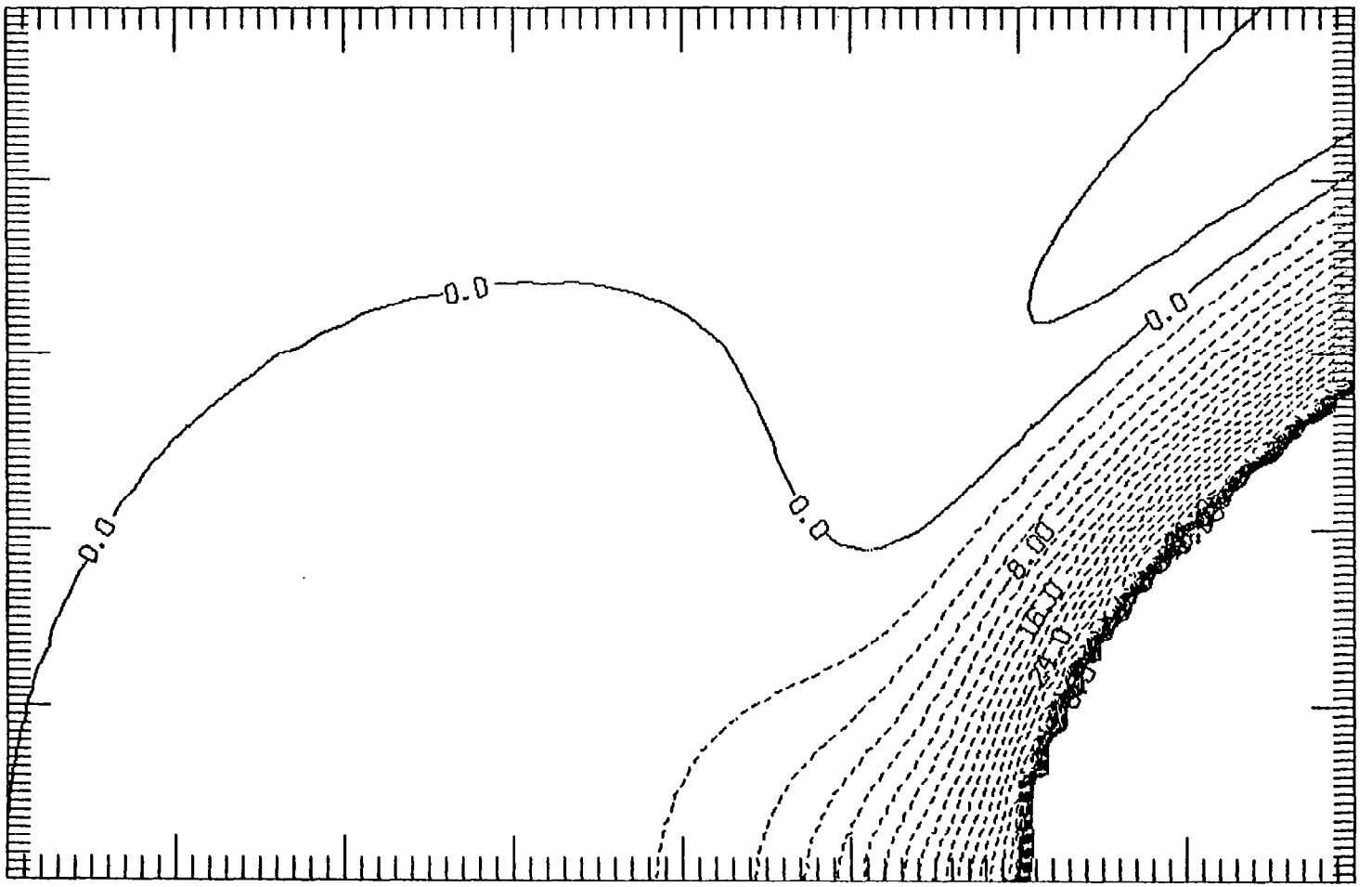

Figure 48b. Contours of the phase, in degrees, of $\hat{u}_{o,1}$, the fundamental oscillation of the flow past the parabola with $\sigma = 3\pi/4$. Contours from -34.0° to 2.0° with an interval of 2.0°.....

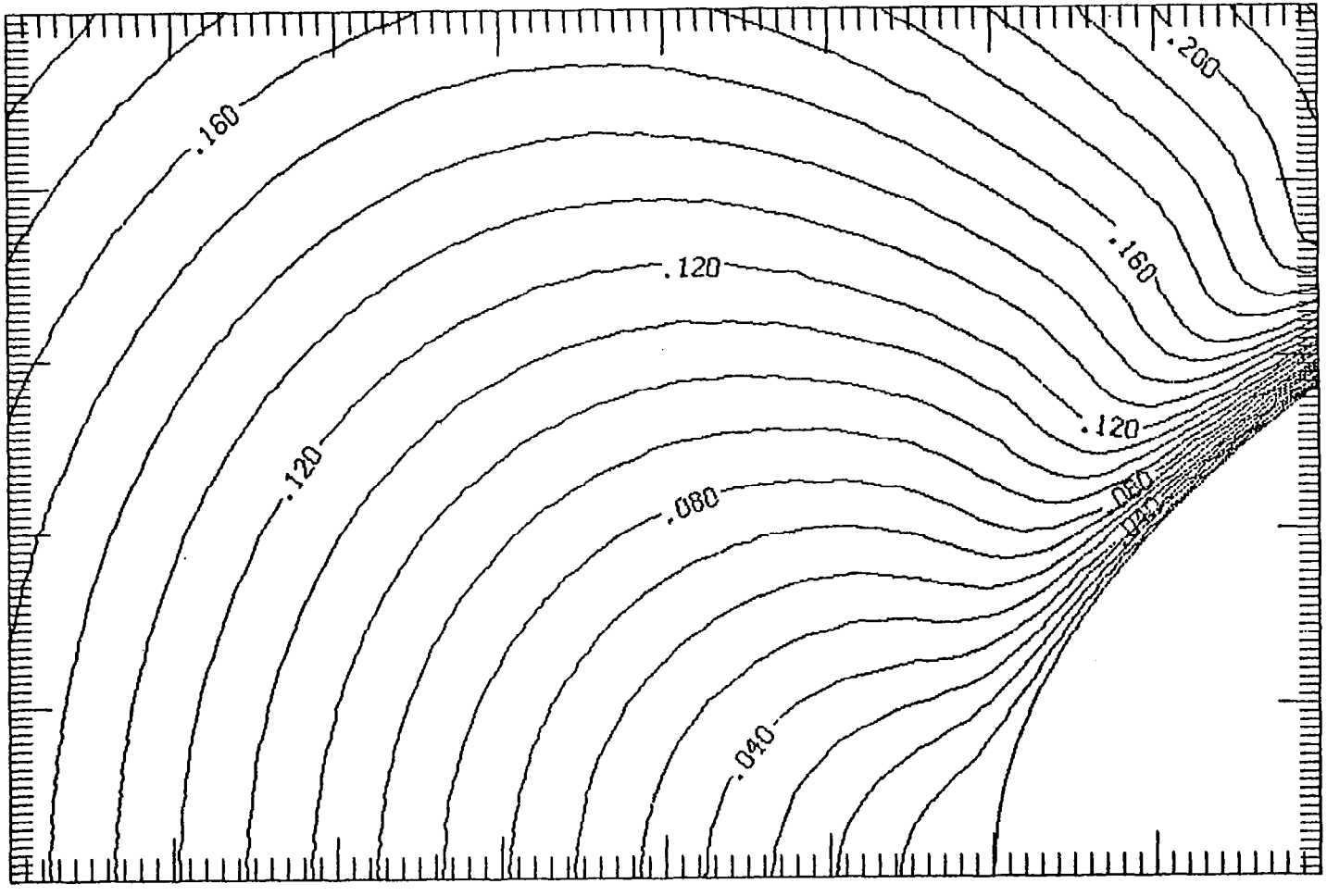

Figure 49a. Contours of the amplitude of $\hat{u}_{0,1}$, the fundamental oscillation of the flow past the parabola with $\sigma = 3\pi/2$. Contours from 0.0 to 0.22 with an interval of 0.01.

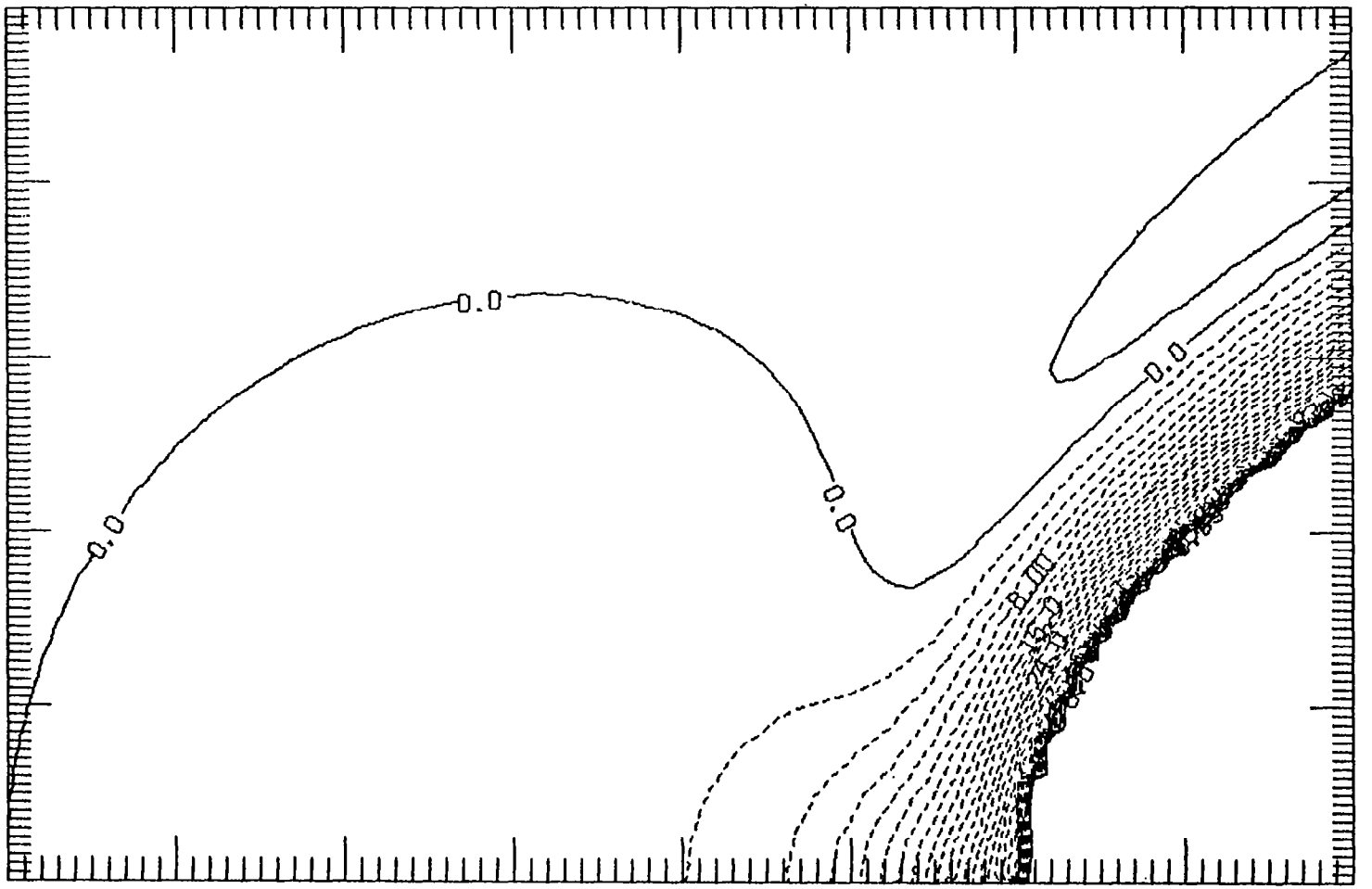

Figure 49b. Contours of the phase, in degrees, of $\hat{u}_{o,1}$, the fundamental oscillation of the flow past the parabola with $\sigma = 3\pi/2$. Contours from -38.0° to 2.0° with an interval of 2.0°.

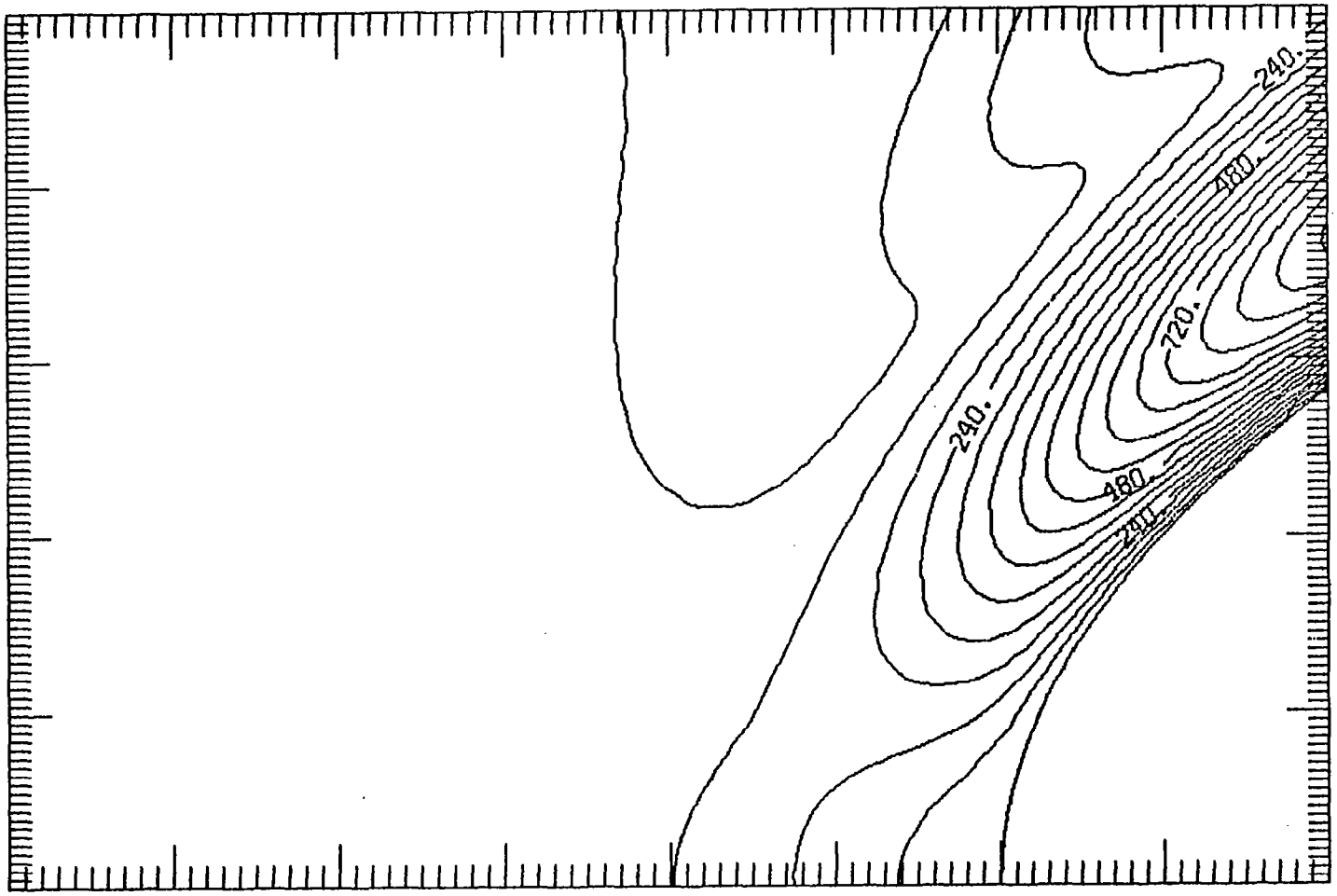

Figure 50a. Contours of the amplitude of $\hat{u}_{o,2}$, the first harmonic of the free stream oscillation of the flow past the parabola with $\sigma = \pi/16$. Contours from 0.0 to 9.6×10^{-3} with an interval of 6.0×10^{-4}. The labels are scaled by 10^5.

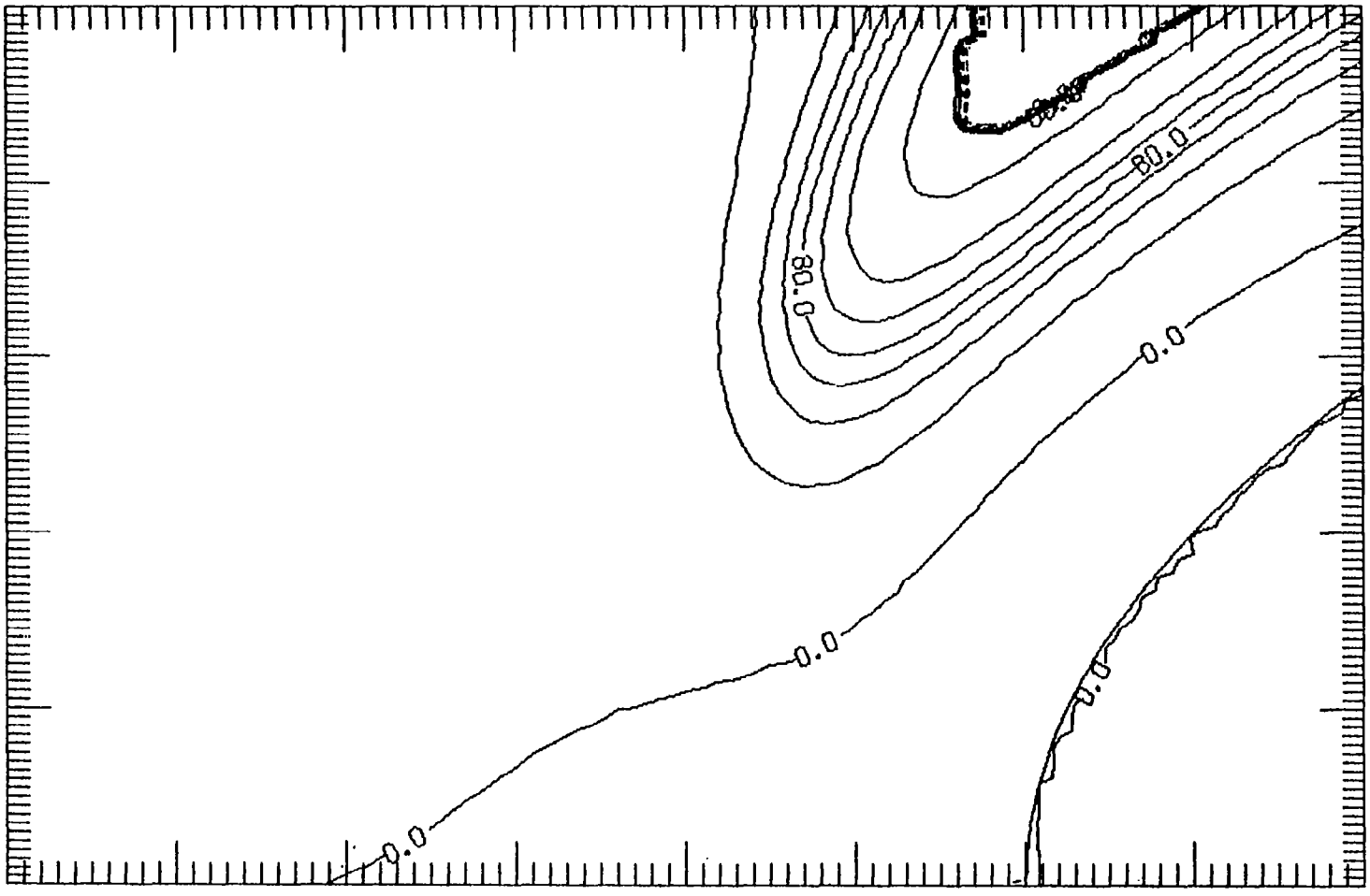

Figure 50b. Contours of the phase, in degrees, of $\hat{u}_{o,2}$, of the first harmonic of the free stream oscillation of the flow past the parabola with $\sigma = \pi/16$, contours from -260.0° to 140.0° with an interval of 20.0°.

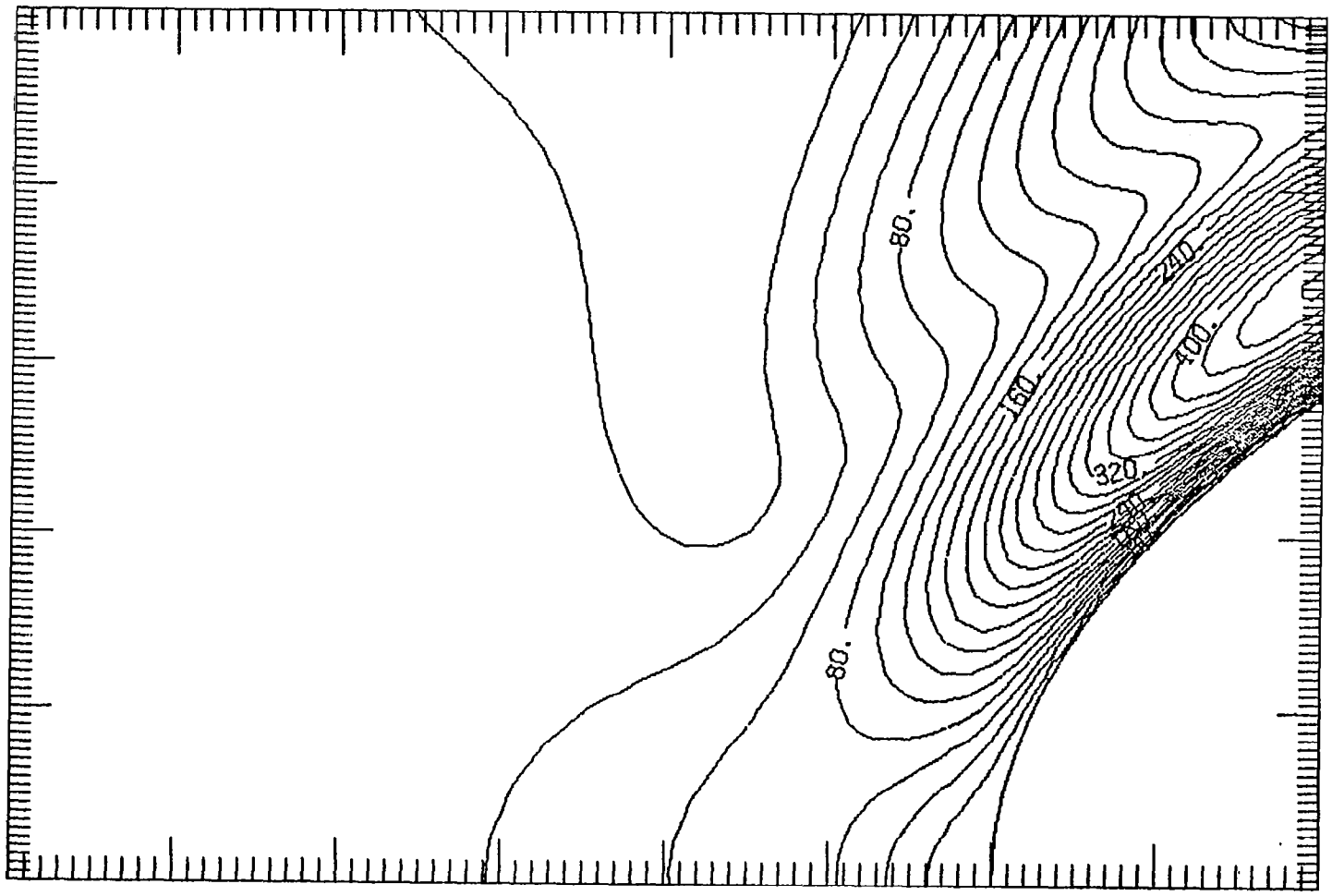

Figure 51a. Contours of the amplitude of $\hat{u}_{o,2}$, the first harmonic of the free stream oscillation of the flow past the parabola with $\sigma = \pi/4$. Contours from 0.0 to 4.6×10^{-3} with an interval of 2.0×10^{-4}. The labels are scaled by 10^5.

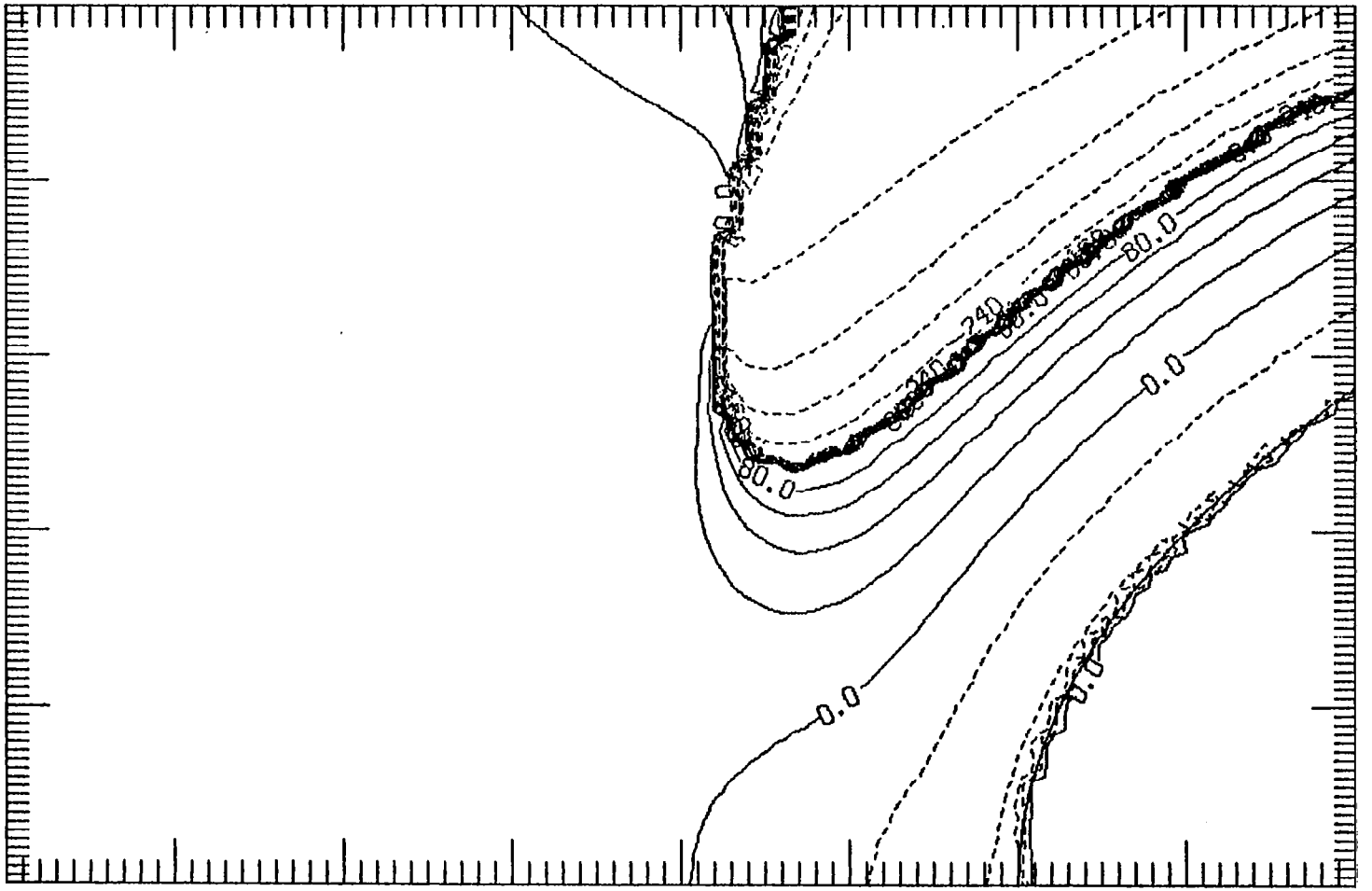

Figure 51b. Contours of the phase, in degrees, of $\hat{u}_{o,2}$, of the first harmonic of the free stream oscillation of the flow past the parabola with $\sigma = \pi/4$, contours from to -240.0° to 100.0° with an interval of 20.0°.

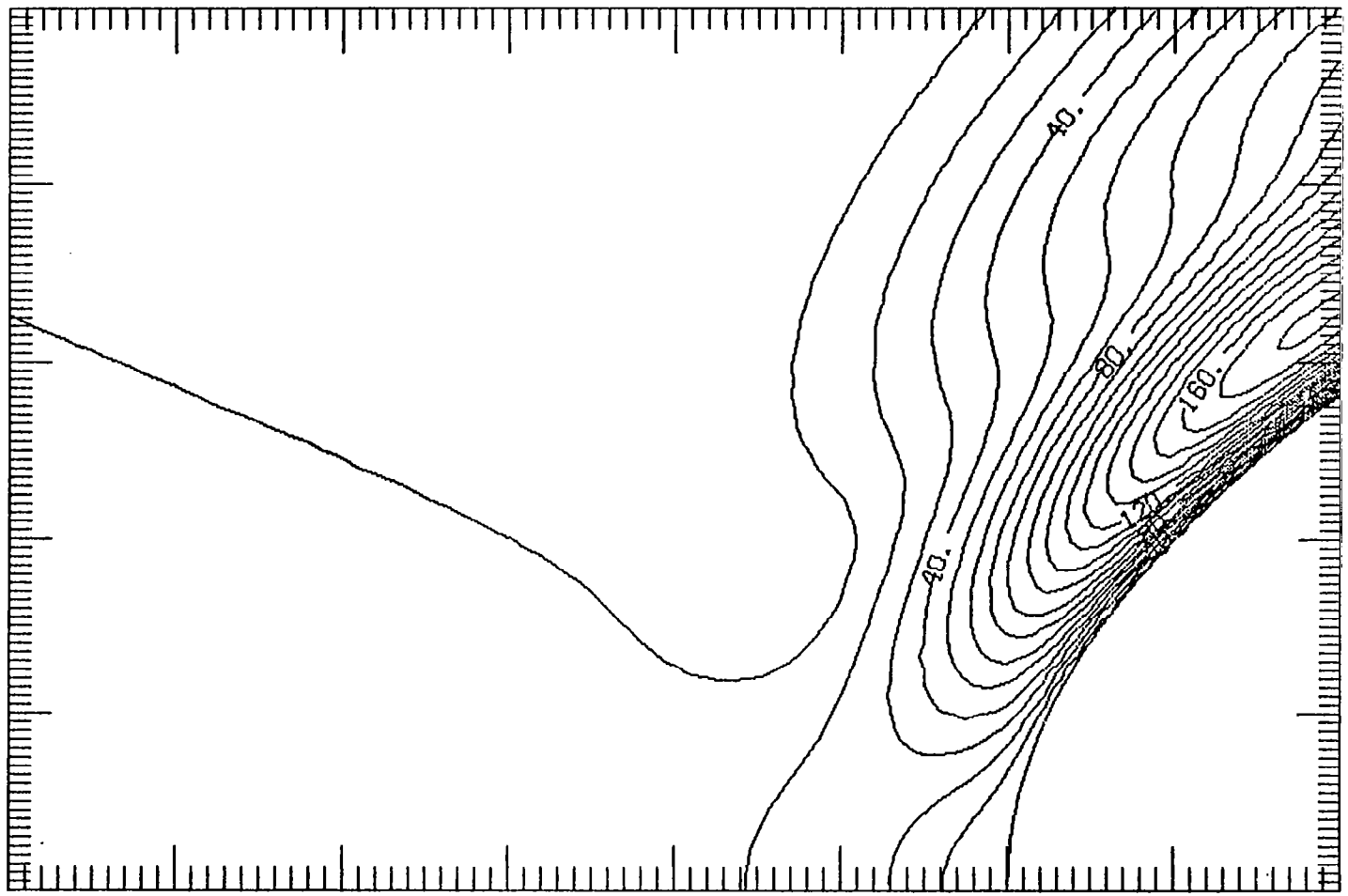

Figure 52a. Contours of the amplitude of $\hat{u}_{o,2}$, the first harmonic of the free stream oscillation of the flow past the parabola with $\sigma = 3\pi/4$. Contours from 0.0 to 1.8×10^{-3} with an interval of 1.0×10^{-4}. The labels are scaled by 10^5.

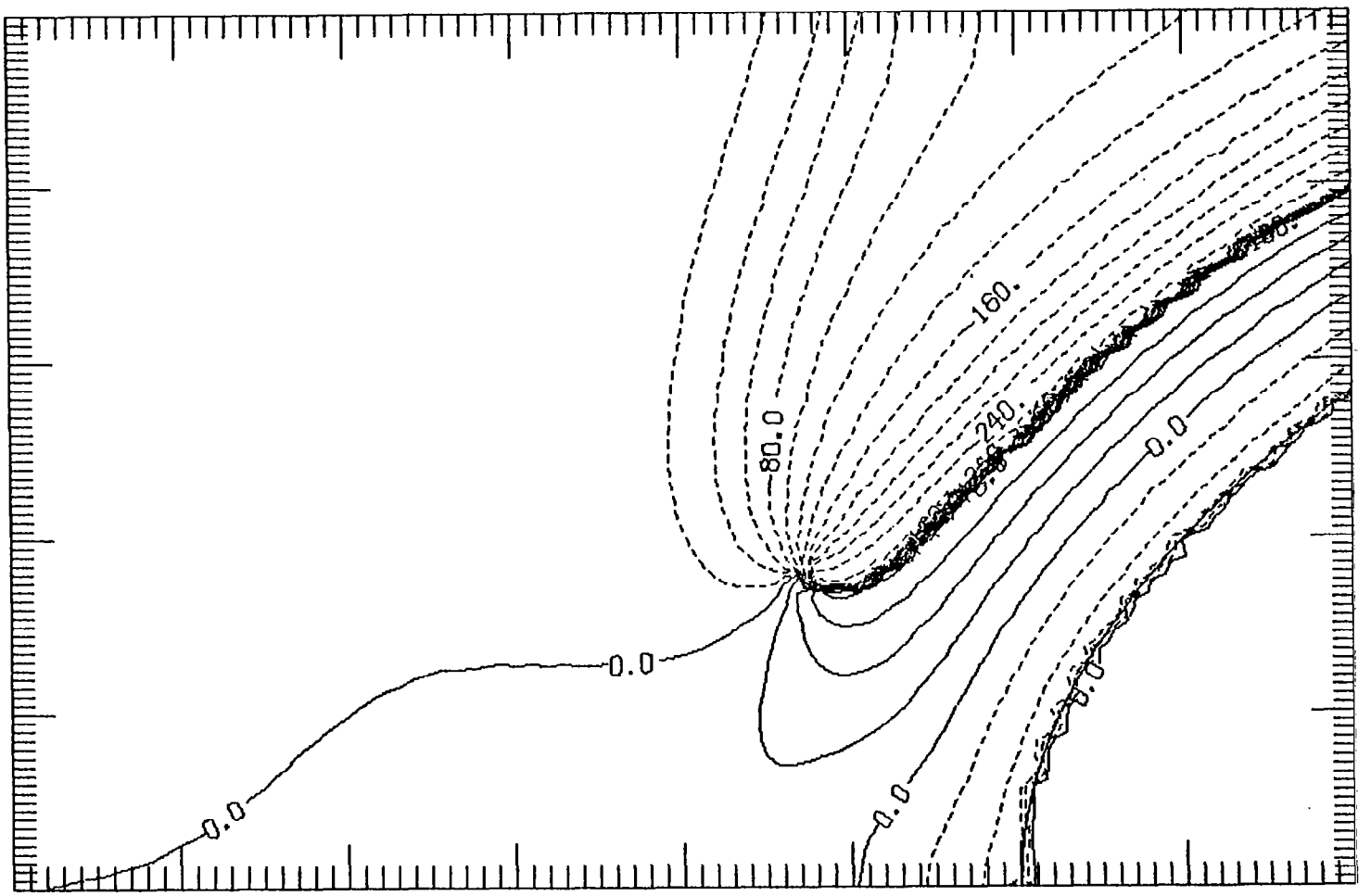

Figure 52b. Contours of the phase, in degrees, of $\hat{u}_{o,2}$, of the first harmonic of the free stream oscillation of the flow past the parabola with $\sigma = 3\pi/4$, contours from -200.0° to 80.0° with an interval of 20.0°.

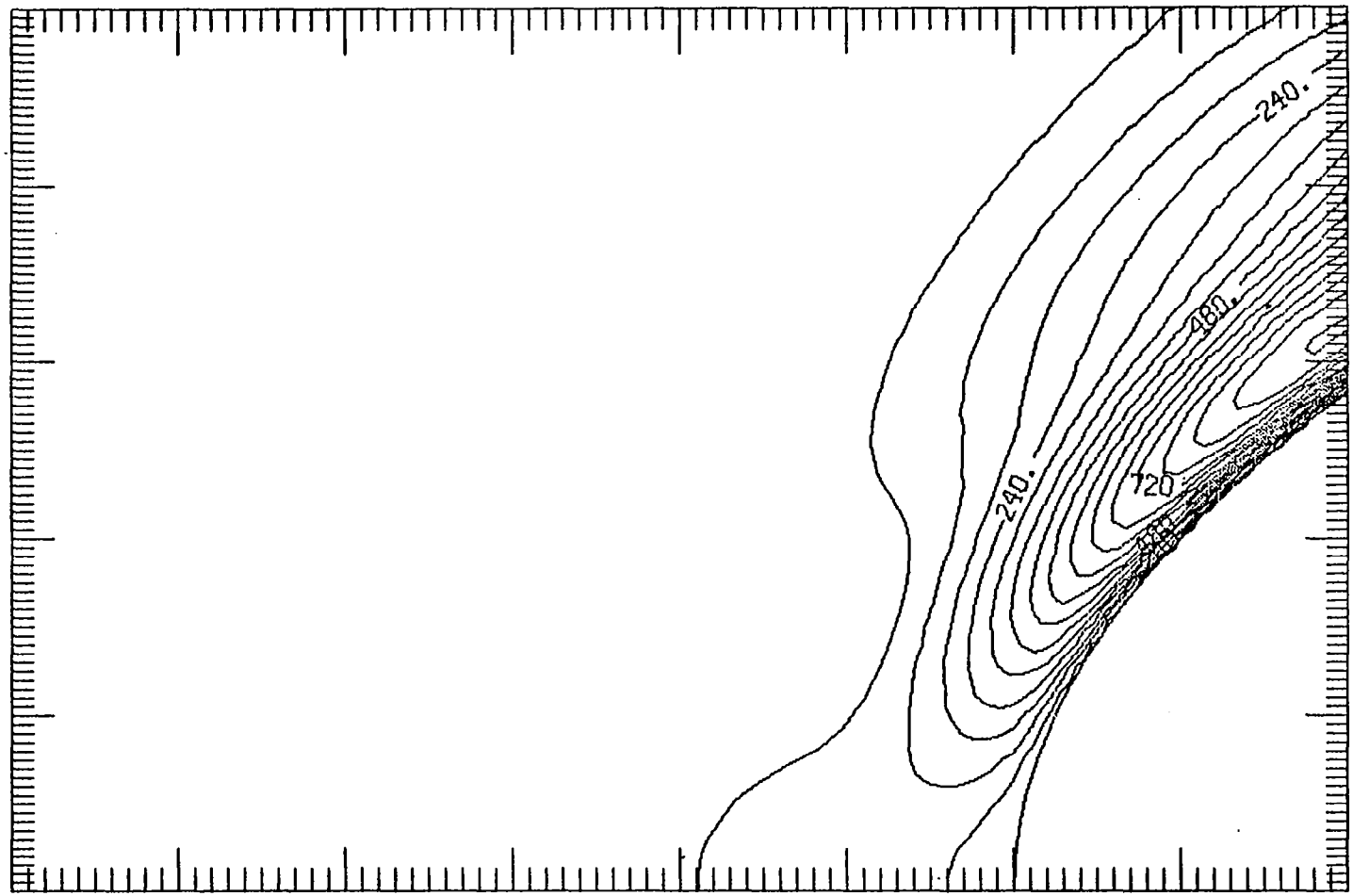

Figure 53a. Contours of the amplitude of $\hat{u}_{o,2}$, the first harmonic of the free stream oscillation of the flow past the parabola with $\sigma = 3\pi/2$. Contours from 0.0 to 9.6×10^{-4} with an interval of 6.0×10^{-5}. The labels are scaled by 10^{6}.

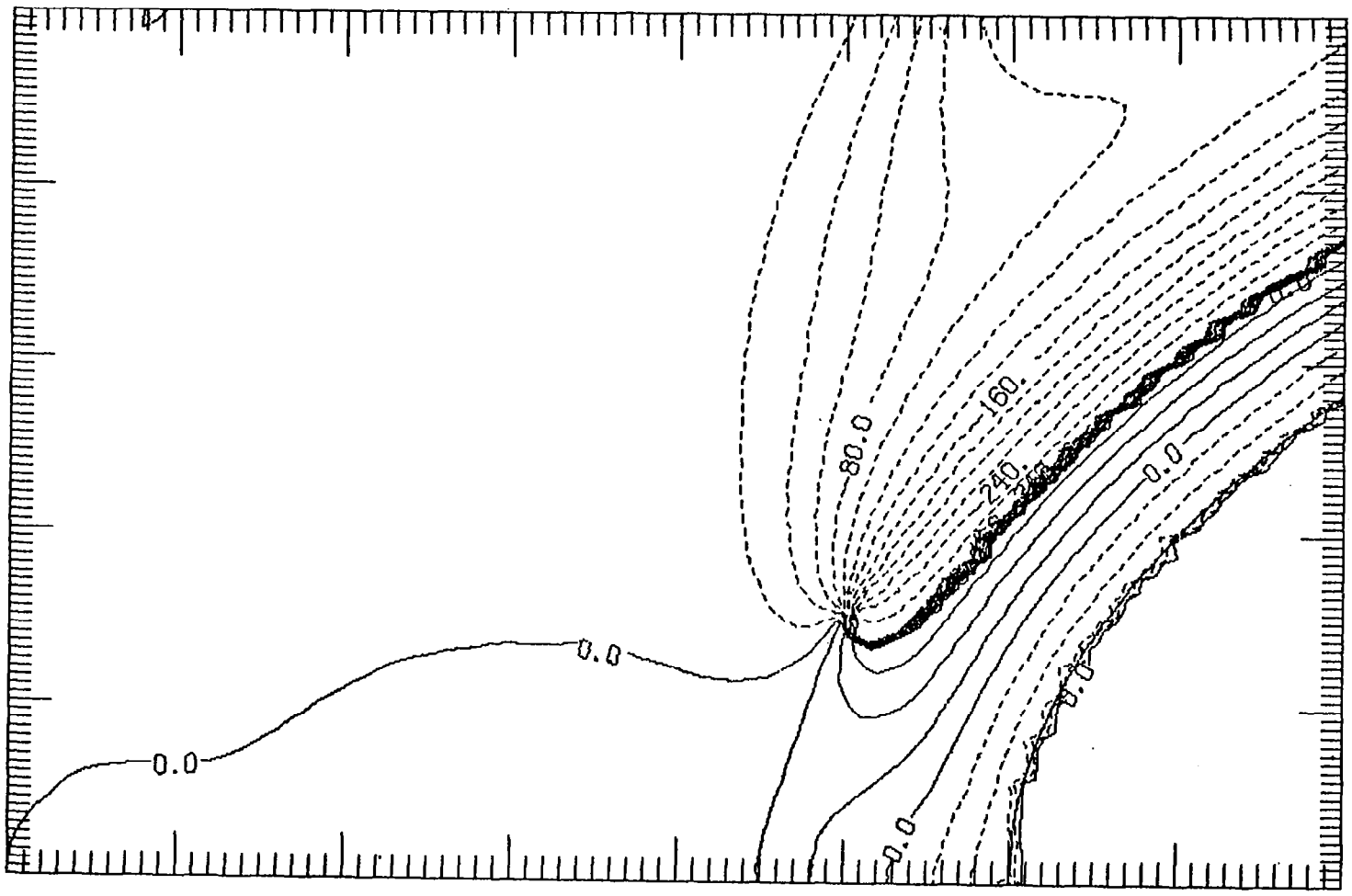

Figure 53b. Contours of the phase, in degrees, of $\hat{u}_{o,2}$, of the first harmonic of the free stream oscillation of the flow past the parabola with $\sigma = 3\pi/2$, contours from $-280.0°$ to $60.0°$ with an interval of $20.0°$.

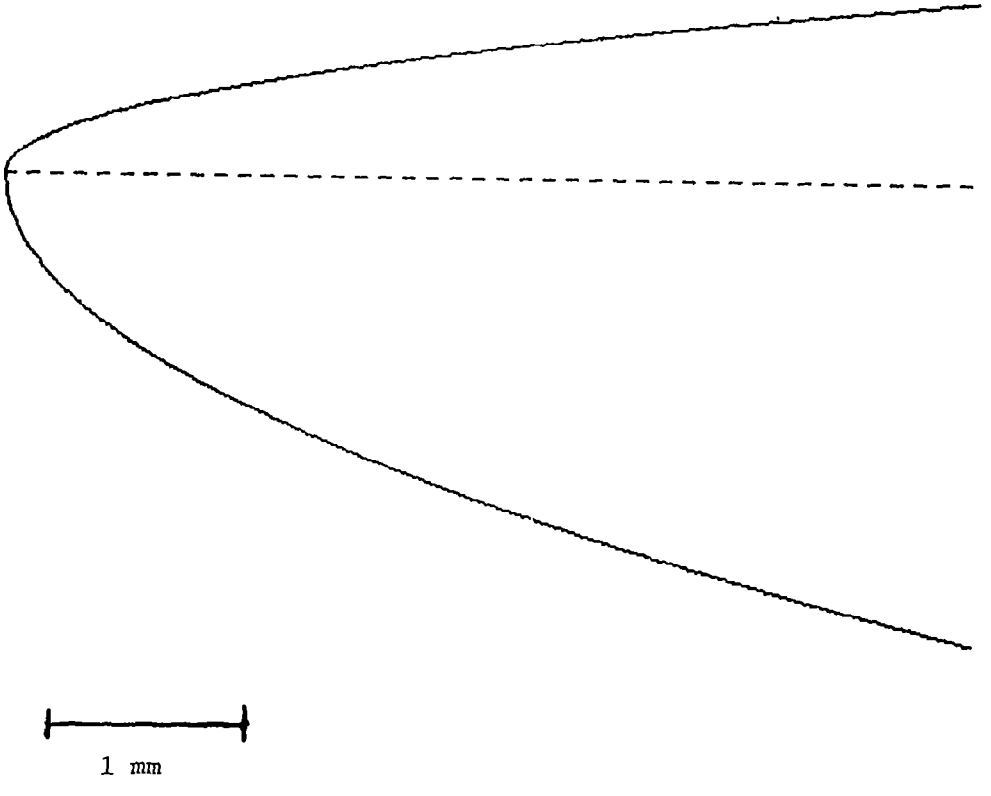

Figure 54. Cross-section of the nose of the body used in the experiment of Kachanov, Kozlov, and Levchenko (1978). One inch on the figure is equal to 1 mm on the body; see the scale on the figure. This figure shows the body from the nose to a distance of 5mm back. The dashed line in the figure is the line y = o for both the upper and lower ellipses. The upper surface in this figure is that above which the measurements were made.

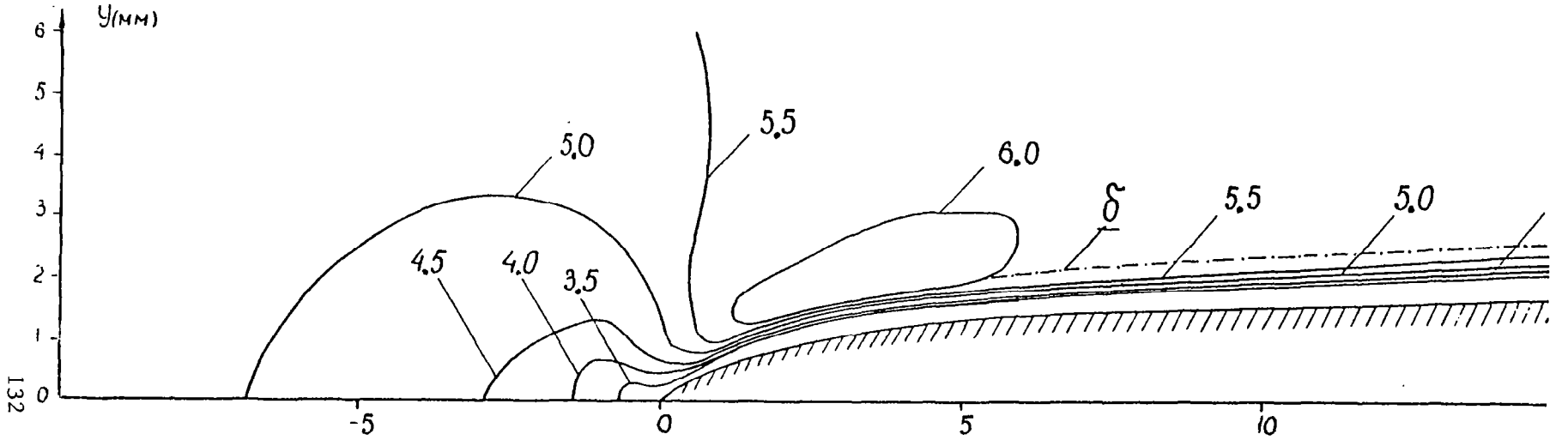

Figure 55. Experimental results of Kachanov, Kozlov, and Levchenko (1978). Contours of $\hat{u}_{o,o}$ (in the notation of this paper) are shown. Contours are labeled with the speed in m /sec and the dashed curve labeled δ is the position of the top of the boundary layer. Distances are in millimeters.

APPENDIX B

OSCILLATING STAGNATION POINT FLOW

Chester E. Grosch

Department of Oceanography

Old Dominion University, Norfolk, Va. 23508

and

Harold Salwen

Department of Physics and Engineering Physics

Stevens Institute of Technology, Hoboken, N.J. 07030

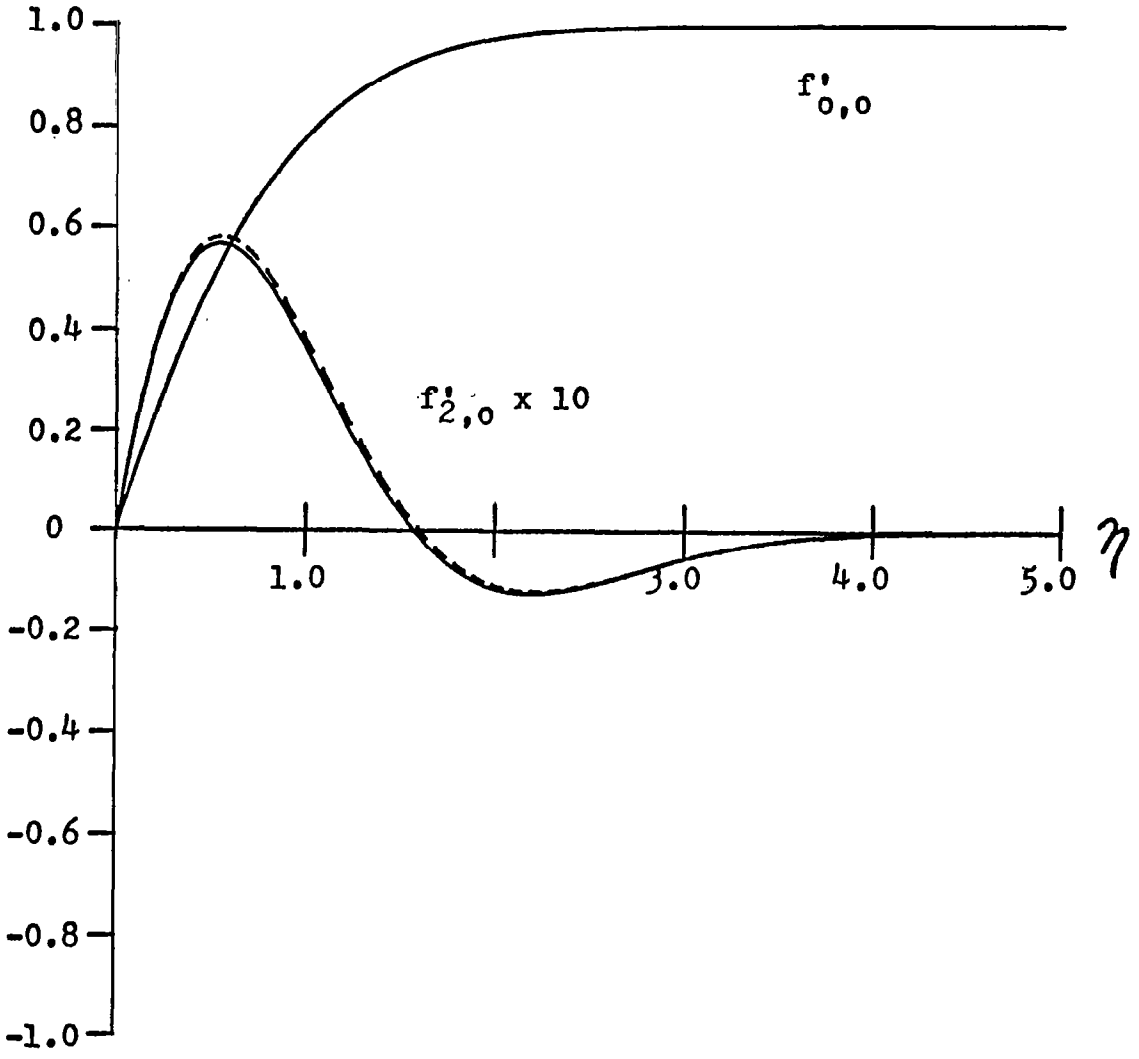

Figure 1. The steady and secondary streaming flow components, $f'_{0,0}$ and $f'_{2,0}$, as a function of η, the dimensionless distance from the boundary. The Strouhal number, $\sigma = \pi/4$. The solid curves are the results of numerical integrations and the dashed curve is the low frequency approximation for $f'_{2,0}$.

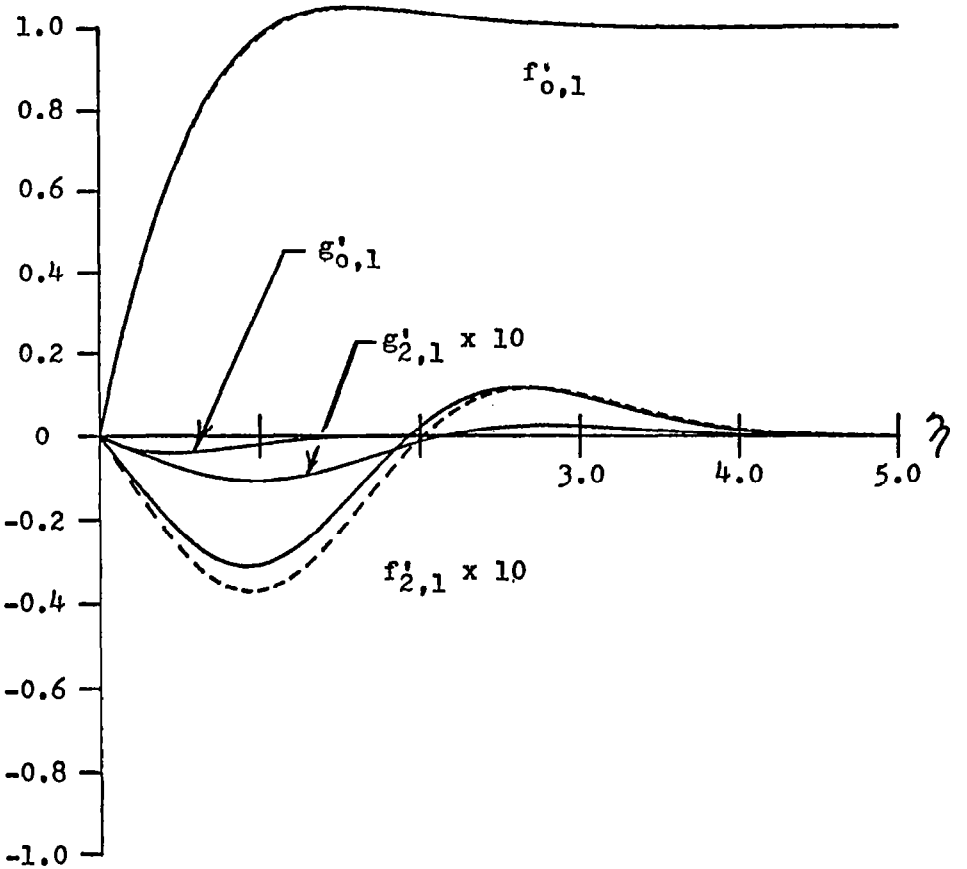

Figure 2. The $O(\varepsilon)$, $f'_{0,1}$, and $g'_{0,1}$, and $O(\varepsilon^3)$, $f'_{2,1}$ and $g'_{2,1}$, amplitudes of the fundamental component of the oscillating flow as functions of η, the dimensionless distance from the boundary. The Strouhal number, $\sigma = \pi/4$. The solid curves are the results of numerical integrations and the dashed curves are the low frequency approximations for $f'_{0,1}$ and $g'_{2,1}$. The low frequency approximation to $f'_{0,1}$, is so close to the result of the numerical integration that the two curves are virtually indistinguishable on this figure.

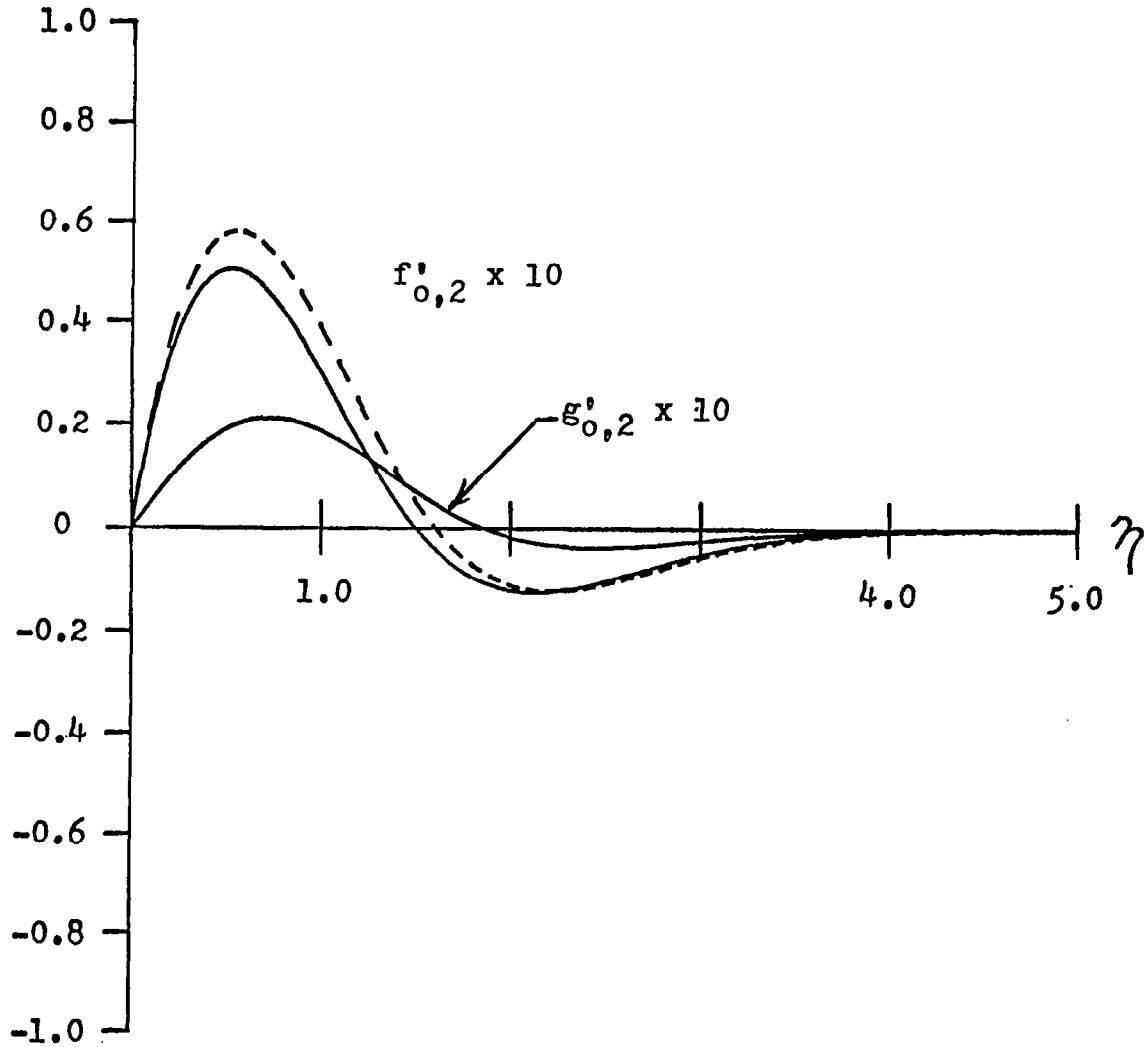

Figure 3. The $O(\varepsilon^2)$ amplitudes of the first harmonic of the oscillating flow as functions of η, the dimensionless distance from the boundary. The Strouhal number, $\sigma = \pi/4$. The solid curves are the results of numerical integrations and the dashed curve is the low frequency approximation to $f'_{0,2}$.

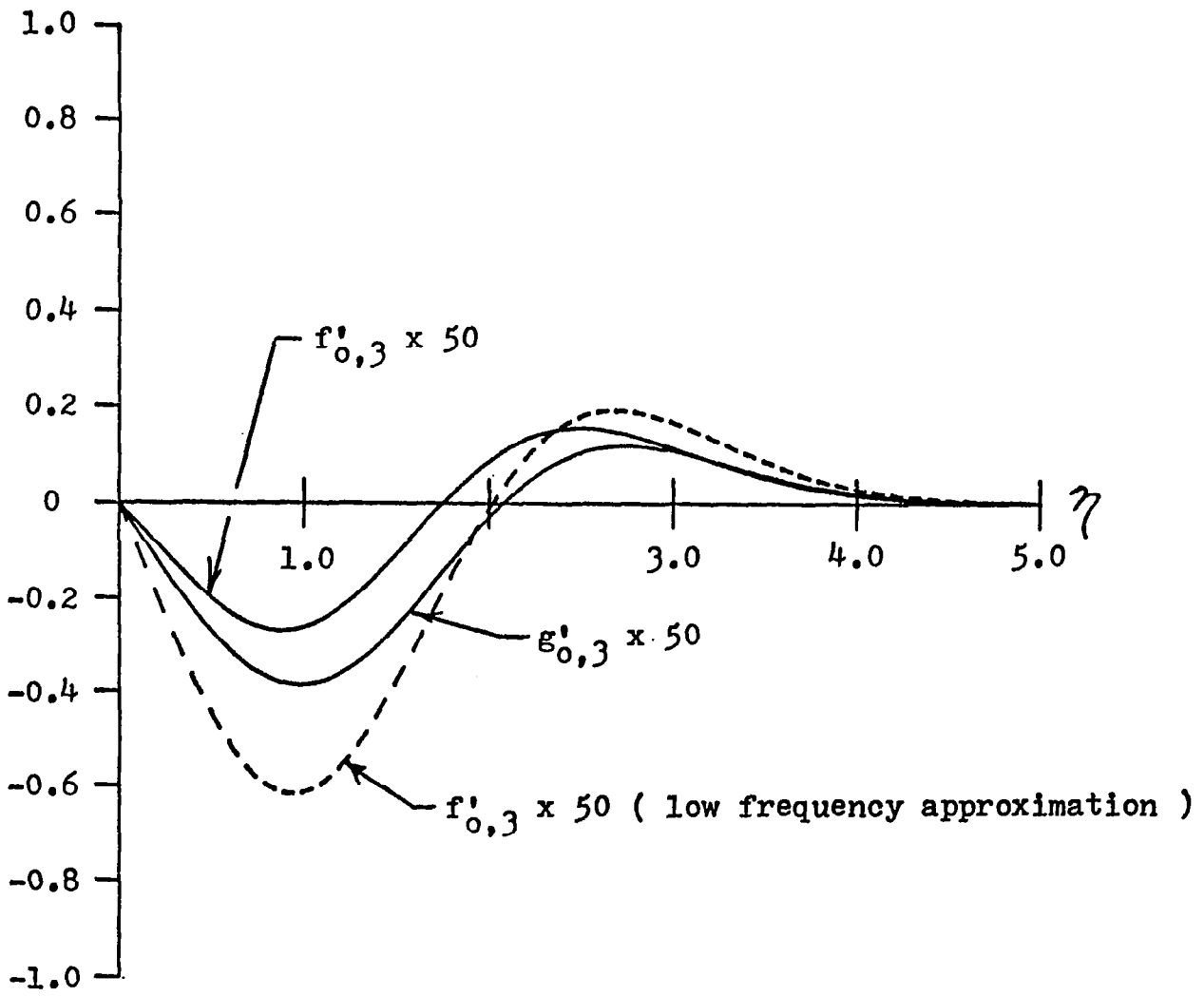

Figure 4. The $O(\varepsilon^3)$ amplitudes of the second harmonic of the oscillating flow as functions of η, the dimensionless distance from the boundary. The Strouhal number, $\sigma = \pi/4$. The solid curves are the results of numerical integrations and the dashed curve is the low frequency approximation to $f'_{o,3}$.

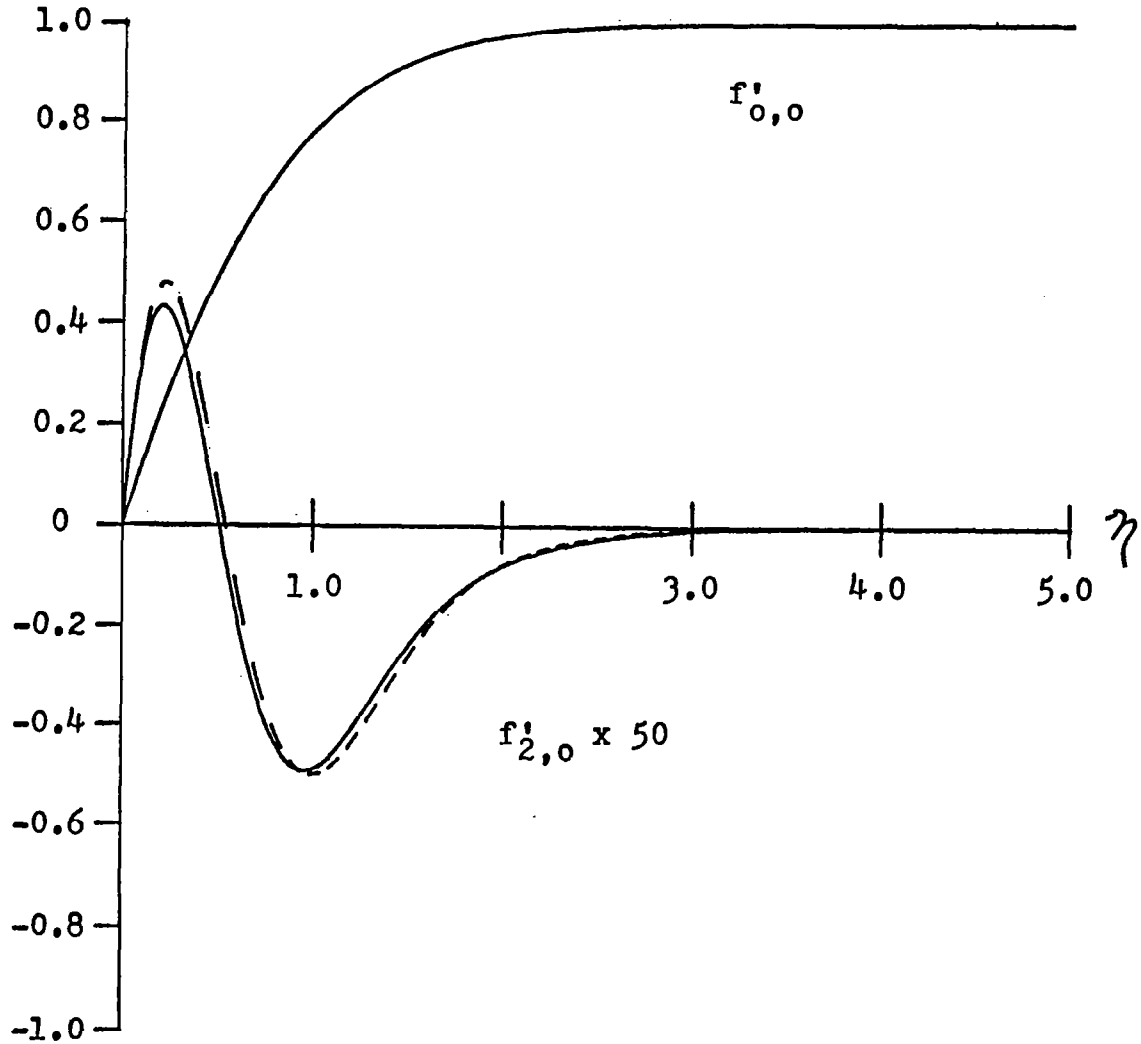

Figure 5. The steady and secondary streaming flow components, $f'_{o,o}$ and $f'_{2,o}$, as a function of η, the dimensionless distance from the boundary. The Strouhal number, $\sigma = 8\pi$. The solid curves are the results of numerical integrations and the dashed curve is the high frequency approximation to $f'_{2,o}$.

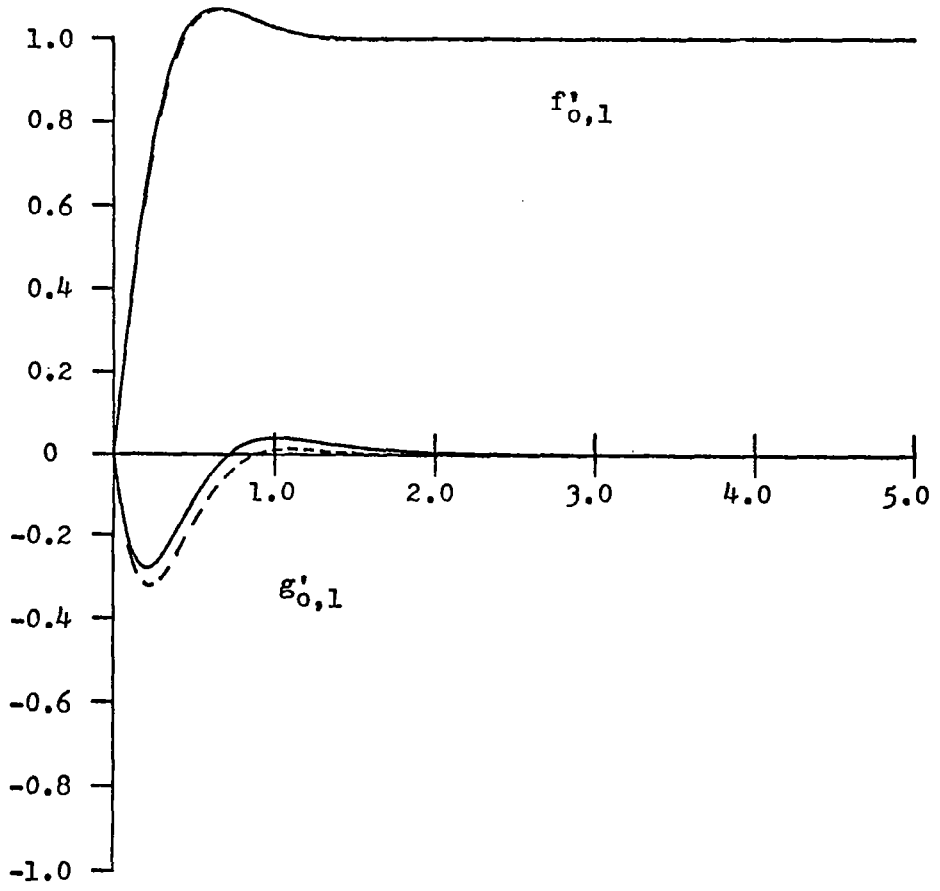

Figure 6. The $O(\varepsilon)$ amplitudes of the fundamental component of the oscillating flow as a function of η, the dimensionless distance from the boundary. The Strouhal number, $\sigma = 8\pi$. The solid curves are the results of numerical integrations and the dashed curves are the high frequency approximations. The high frequency approximation to $f'_{o,1}$ is so close to the result of the numerical integration that the two curves are virtually indistinguishable on this figure.

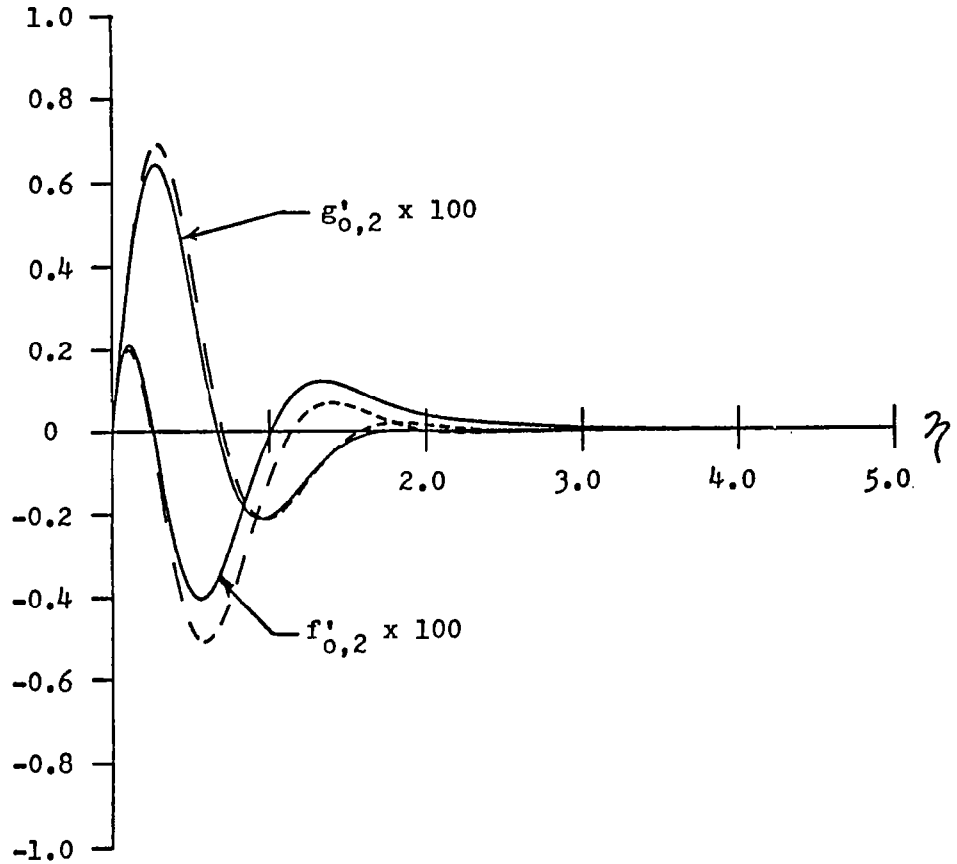

Figure 7. The $0(\varepsilon^2)$ amplitudes of the first harmonic of the oscillating flow as a function of η, the dimensionless distance from the boundary. The Strouhal number, $\sigma = 8\pi$. The solid curves are the results of numerical integration and the dashed curves are the high frequency approximations.

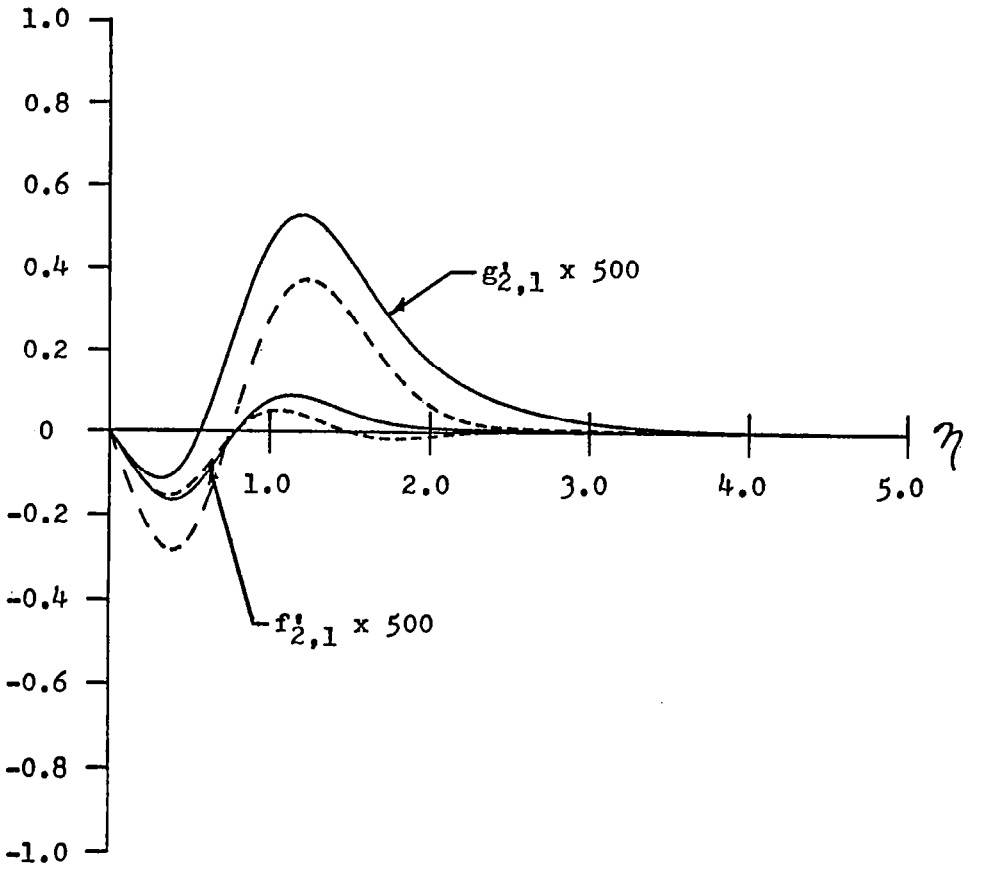

Figure 8. The $O(\varepsilon^3)$ amplitudes of the fundamental component of the oscillating flow as a function of η, the dimensionless distance from the boundary. The Strouhal number, $\sigma = 8\pi$. The solid curves are the results of numerical integrations and the dashed curves are the high frequency approximations.

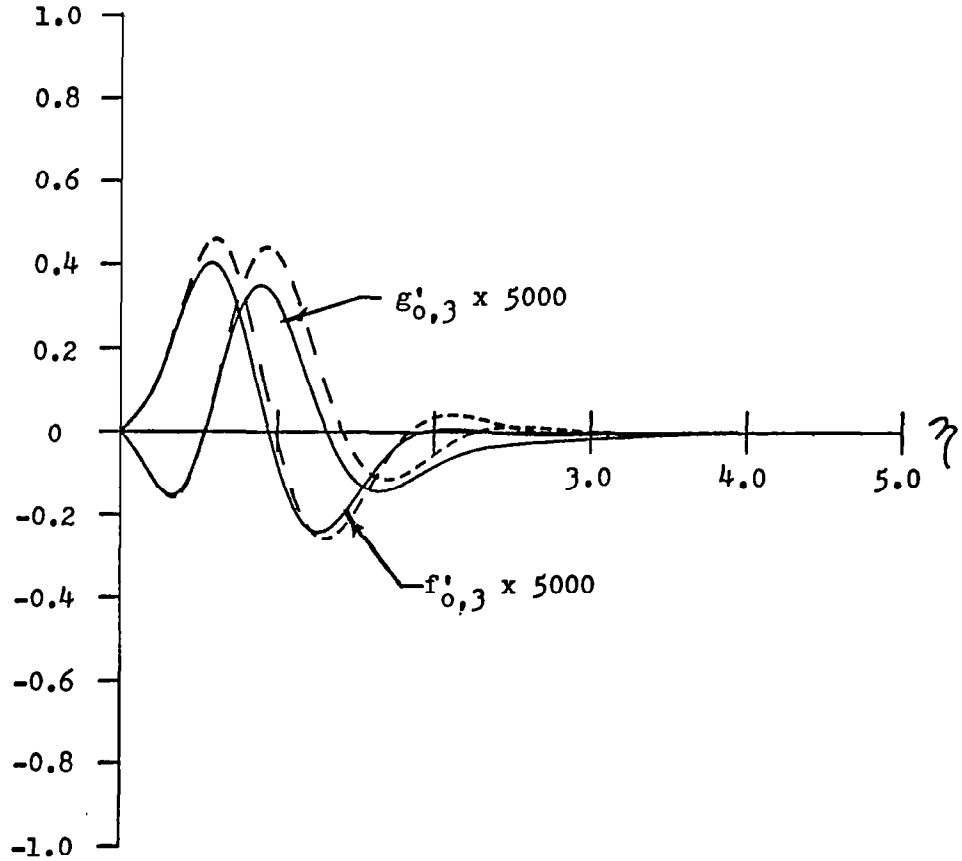

Figure 9. The $O(\varepsilon^3)$ amplitudes of the second harmonic of the oscillating flow as a function of η, the dimensionless distance from the boundary. The Strouhal number, $\sigma = 8\pi$. The solid curves are the results of numerical integrations and the dashed curves are the high frequency approximations.

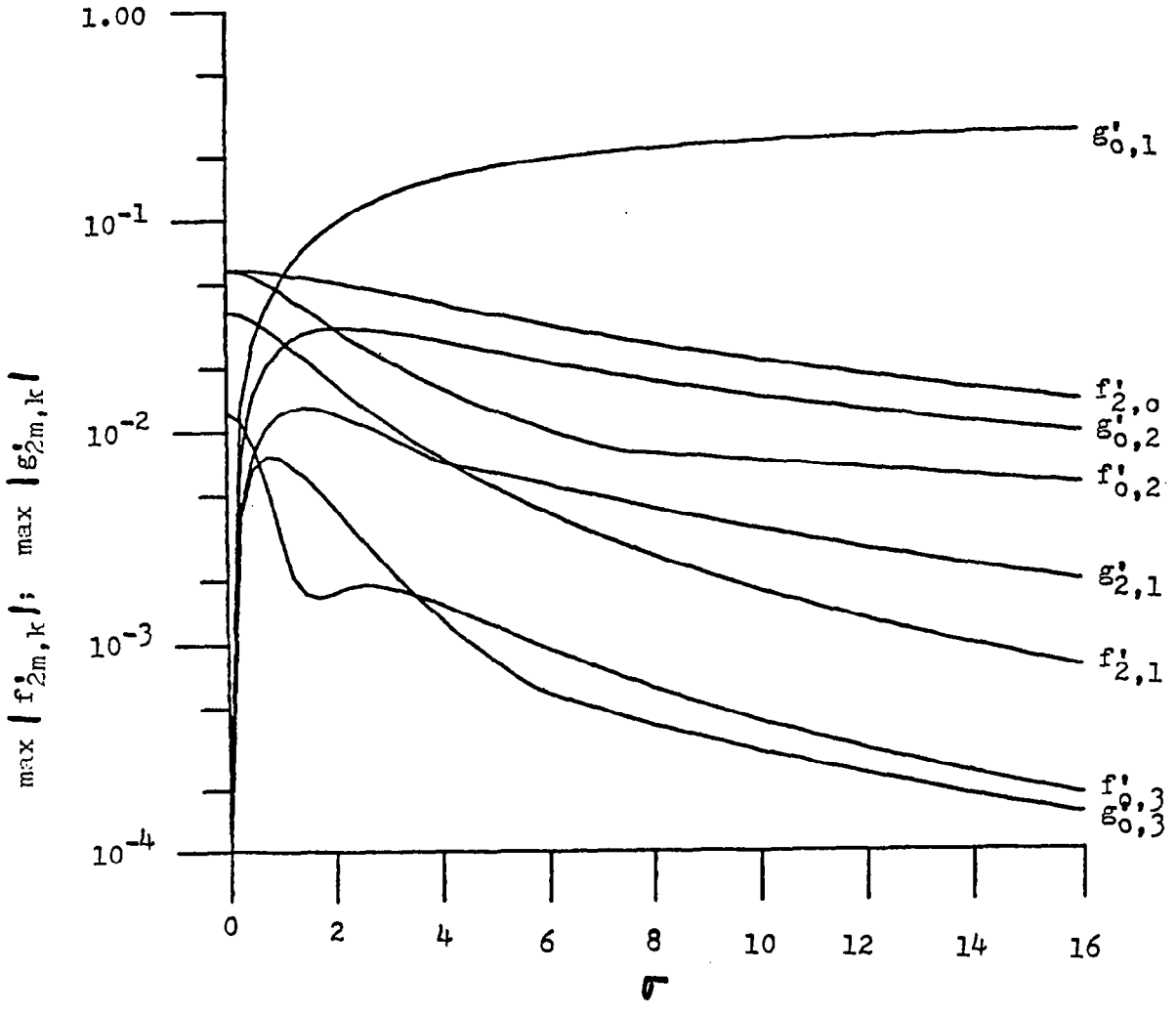

Figure 10a. Variation of $\max|f'_{2m,k}|$ and $\max|g'_{2m,k}|$ with the Strouhal number, σ.

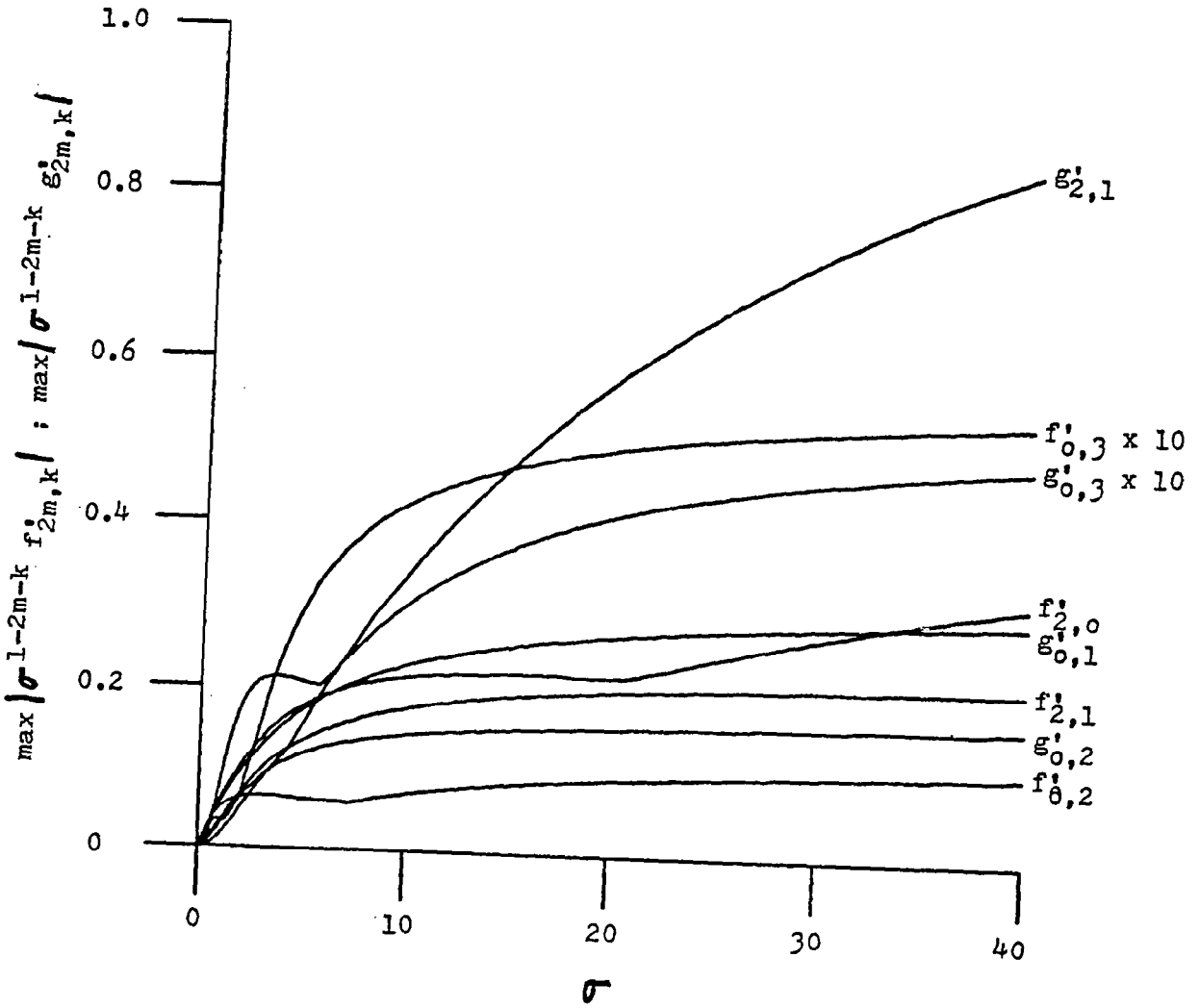

Figure 10b. Variation of $\max|\sigma^{1-2m-k} f'_{2m,k}|$ and $\max|\sigma^{1-2m-k} g'_{2m,k}|$ with the Strouhal number, σ.

ABSTRACT

A solution of the Navier-Stokes equations is given for an incompressible stagnation point flow whose magnitude oscillates in time about a constant, nonzero, value (an unsteady Hiemenz flow). Analytic approximations to the solution in the low and high frequency limits are given and compared to the results of numerical integrations. The application of these results to one aspect of the boundary layer receptivity problem is also discussed.

1. INTRODUCTION

In this appendix we give a solution to the Navier-Stokes equations for an incompressible stagnation point flow whose magnitude oscillates in time about a constant, nonzero, value. Apart from the intrinsic interest of this problem, its solution is the first step in the solution of one aspect of the boundary layer receptivity problem, that is, the determination of the magnitude and form of the disturbance introduced into the boundary layer on a body by a perturbation in the free stream. The solution of this problem would permit the calculation of the initial amplitudes of the Tollmien-Schlichting eigenmodes and continuum eigenfunctions in the boundary layer and give a rational foundation to transition prediction methods.

We have recently given the solution to the boundary layer receptivity problem within the context of incompressible, linear stability theory for a parallel shear flow (Salwen, Kelly, and Grosch, 1980; Grosch & Salwen, 1980; Salwen and Grosch, 1981). There is, however, one aspect of the boundary layer receptivity problem to which our parallel flow solution is clearly not applicable. If we consider the flow near the forward stagnation point of a body, a linearized parallel flow theory cannot be valid because the flow is intrinsically nonlinear and nonparallel. Although we may be able to use the boundary layer equations away from the stagnation point, the full Navier-Stokes equations must be used in the immediate vicinity of the stagnation point. Once a solution of the Navier-Stokes equations for the perturbed stagnation point flow has been found, it is possible to extend this solution away from the stagnation point and around the nose of the body. This is, in fact, what is normally done for the steady flow past an object. The Blasius

series (Schlichting, 1979, pp. 168ff) is the extension around the nose of a blunt body of the Hiemenz solution (Schlichting, 1979, pp. 95ff) to the Navier-Stokes equations near a stagnation point. In section 6, we discuss the analogous extension for our oscillating flow solution.

We were stimulated to do this work by the papers of Glauert (1956) and Stuart (1966). There are a number of other relevant studies in this area including those of Lighthill (1954), Rott (1956), Lin (1956), Carrier and DiPrima (1957), Gibson (1957), Watson (1959), and Sarma (1964). Riley (1975) and Schlichting (1979, chapter 15) give comprehensive reviews of recent work in unsteady boundary layer theory. Lighthill (1978) has recently reviewed the current understanding of the phenomenon of acoustic streaming; i.e., the generation of a steady flow by the Reynold's stress due to an oscillating flow.

2. EQUATIONS AND BOUNDARY CONDITIONS

We consider the flow in the neighborhood of a stagnation point at $(0,0)$ on a plane wall, with x the coordinate along the wall and y the coordinate perpendicular to the wall. We seek the solution $\left(u(x,y,t), v(x,y,t)\right)$ of the two-dimensional Navier-Stokes equations which corresponds to the potential flow

$$U = (U_o x/\ell)(1 + \epsilon \cos \omega t) \tag{1}$$

$$V = - (U_o y/\ell)(1 + \epsilon \cos \omega t) \tag{2}$$

in the far field. Here, U and V are the x- and y-components of velocity of the potential flow, U_o the velocity scale, ℓ the length scale, ε the dimensionless amplitude of the oscillation, and ω the frequency of oscillation. Defining a stream function $\psi(x,y,t)$ by

$$u = \frac{\partial \psi}{\partial y}, \qquad v = -\frac{\partial \psi}{\partial x} \tag{2a,b}$$

and substituting into the incompressible Navier-Stokes equations we find, as usual, that ψ is the solution of

$$\left(\frac{\partial}{\partial t} + \frac{\partial \psi}{\partial y}\frac{\partial}{\partial x} - \frac{\partial \psi}{\partial x}\frac{\partial}{\partial y}\right) \nabla^2 \psi = \nu \nabla^2 (\nabla^2 \psi), \tag{3}$$

with ν the kinematic viscosity and

$$\nabla^2 \equiv \frac{\partial^2}{\partial x^2} + \frac{\partial^2}{\partial y^2} . \tag{4}$$

We define dimensionless variables

$$\xi = x/\ell , \quad \eta = (y/\ell)\sqrt{R_o}, \quad \tau = U_o t/\ell , \tag{5a,b,c}$$

a Reynolds number,

$$R_o = U_o \ell / \nu \tag{6a}$$

and a Strouhal number

$$\sigma = \omega \ell / U_o . \tag{6b}$$

The use of separate velocity and length scales, U_o and ℓ, while correct, is somewhat arbitrary in that they appear only in the combination U_o/ℓ in the potential flow. The scales which are intrinsic to this problem are the time scale of the base flow, $T_o = \ell/U_o$, the frequency, ω, and the kinematic viscosity, ν. We can define velocity and length scales in terms of T_o and ν, thereby setting the Reynolds number equal to unity. In any case, the dimensionless parameters which appear in the equations and boundary conditions are the oscillation amplitude, ε, and the Strouhal number, σ, and the results will be the same. We have chosen to use independent velocity and length scales, U_o and ℓ, because we intend to use the solution presented here as the basis for constructing a solution to the problem of an oscillating flow past a blunt object with length scale ℓ.

If we set, in analogy with the Hiemenz solution (Schlichting, 1979, pp. 95ff),

$$\psi = (U_o \ell / \sqrt{R_o})\, \xi\, F(\eta, \tau), \tag{7}$$

then equation (3) reduces to

$$\frac{\partial}{\partial \eta}\left[\frac{\partial^2 F}{\partial \tau \partial \eta} + \left(\frac{\partial F}{\partial \eta}\right)^2 - F\frac{\partial^2 F}{\partial \eta^2} - \frac{\partial^3 F}{\partial \eta^3}\right] = 0, \tag{8}$$

which may be integrated to yield

$$\frac{\partial^2 F}{\partial \tau \partial \eta} + \left(\frac{\partial F}{\partial \eta}\right)^2 - F\frac{\partial^2 F}{\partial \eta^2} - \frac{\partial^3 F}{\partial \eta^3} = G(\xi,\tau). \tag{9}$$

Because the left-hand side of equation (9) is independent of ξ, it is clear that the "constant of integration", G, only depends on the dimensionless time, τ. In order that the x and t dependence of the pressure in the far field agree with that of the potential flow, we must have

$$(U_o/\ell)^2\ G = \frac{1}{x}\frac{\partial U}{\partial \eta} + \frac{U}{x}\frac{\partial U}{\partial x} = (U_o/\ell)(-\varepsilon\omega \sin \omega\tau) + (U_o/\ell)^2$$

$$\times (1 + \varepsilon \cos \omega t)^2. \tag{10}$$

Therefore, $F(\eta,\tau)$ is the solution of

$$\frac{\partial^2 F}{\partial \tau \partial \eta} + \left(\frac{\partial F}{\partial \eta}\right)^2 - F\frac{\partial^2 F}{\partial \eta^2} - \frac{\partial^3 F}{\partial \eta^3} = 1 + \varepsilon(2 \cos \sigma\tau - \sigma \sin \sigma\tau)$$

$$+ \frac{1}{2}\varepsilon^2(1 + \cos 2\sigma\tau) \tag{11}$$

with the boundary conditions

$$F(0,\tau) = 0, \tag{12a}$$

$$\left(\frac{\partial F}{\partial \eta}\right)_{\eta=0} = 0, \tag{12b}$$

$$\frac{\partial F}{\partial \eta} \to 1 + \cos \sigma\tau \quad \text{as} \quad \eta \to \infty. \tag{12c}$$

3. METHOD OF SOLUTION

To solve equation (11), we will expand $F(\eta,\tau)$ in a Fourier series in the dimensionless time, τ. The coefficients of the expansion are functions of η and the parameter ε and each of these will be expanded in a power series in ε. It is easy to see, from the form of (11), that the τ-independent term in the Fourier series contains only even powers of ε. Therefore, we look for a solution of the form

$$F(\eta,\tau) = \sum_{m=o}^{\infty} \{\varepsilon^{2m} f_{2m,o}(\eta) + \sum_{k=1}^{\infty} \varepsilon^{2m+k} [f_{2m,k}(\eta) \cos k\sigma\tau + g_{2m,k}(\eta) \sin k\sigma\tau]\}. \tag{13}$$

To find the equations obeyed by the $f_{2m,k}$ and $g_{2m,k}$ we substitute (13) into (11), collect the coefficients of like terms in the Fourier series, and set the coefficients of the successive powers of ε equal to zero. We find, first, that $f_{o,o}$ is the solution of

$$\frac{d^3 f_{o,o}}{d\eta^3} + f_{o,o} \frac{d^2 f_{o,o}}{d\eta^2} - \left(\frac{df_{o,o}}{d\eta}\right)^2 + 1 = 0 \tag{14}$$

with

$$f_{o,o}(0) = f'_{o,o}(0) = 0, \quad f'_{o,o} \to 1 \quad \text{as} \quad \eta \to \infty. \tag{15a,b,c}$$

As was expected , $f_{o,o}$, the τ-independent, ε-independent term in the series, is the Hiemenz solution for the steady stagnation point flow.

Next we define the operator L by

$$L \equiv \frac{d^3}{d\eta^3} + f_{o,o} \frac{d^2}{d\eta^2} - 2f'_{o,o} \frac{d}{d\eta} + f''_{o,o}, \tag{16}$$

with primes denoting differentiation with respect to η. Then it can be shown that the equations and boundary conditions for the $\{f_{2m,k}\}$ and $\{g_{2m,k}\}$ are, for $k \geq 1$,

$$Lf_{2m,k} - k\sigma\, g'_{2m,k} = P_{2m,k},$$

$$Lg_{2m,k} + k\sigma\, f'_{2m,k} = Q_{2m,k}, \tag{17b}$$

$$f_{2m,k}(0) = g_{2m,k}(0) = f'_{2m,k}(0) = g'_{2m,k}(0) = 0, \tag{17c}$$

$$f'_{2m,k} \to \delta_{m,o}\,\delta_{k,1}, \quad g'_{2m,k} \to 0 \quad \text{as} \quad \eta \to \infty, \tag{17d}$$

and, for $m > o$ and $k = 0$,

$$L\, f_{2m,o} = R_{2m,o}, \tag{18a}$$

$$f_{2m,o}(0) = f'_{2m,o}(0) = 0, \tag{18b}$$

$$f'_{2m,o} \to 0 \quad \text{as} \quad \eta \to \infty. \tag{18c}$$

The $\{P_{2m,k}\}$, $\{Q_{2m,k}\}$, are linear combinations of products of the $\{f_{2r,s}\}$, $\{g_{2r,s}\}$ and their derivatives, where $s < k$ and $0 \leq r \leq m$ or $s = k$ and $r < m$, and are given in Section 7. Therefore, these equations can be solved sequentially. The equations can be integrated numerically quite easily, although care must be taken to control roundoff errors. The results of these integrations are given and discussed in Section 5.

4. LOW AND HIGH FREQUENCY APPROXIMATIONS

4.1 The Low Frequency Limit

As $\sigma \to 0$, it is expected that the solution will approach a quasi-steady solution. It is straightforward to show that the quasi-steady solution,

$$F(\eta,\tau) = (1 + \varepsilon \cos \sigma\tau)^{1/2} f_{o,o}([1 + \varepsilon \cos \sigma\tau]^{1/2}\eta), \tag{19}$$

satisfies equation (11) and the boundary conditions (12) to $0(\sigma)$.

It is also easy to show that this quasi-steady solution is consistent with the expansion given in equation (13). If F, as given in (19), is expanded in a Taylor series in ε, we find that

$$F = \sum_{n=o}^{\infty} \frac{(\varepsilon \cos \sigma\tau)^n}{2^n n!} S_n(\eta)$$

$$= \sum_{k=o}^{\infty} (2 - \delta_{ko}) \sum_{m=o}^{\infty} (\frac{\varepsilon}{4})^{2m+k} \frac{S_{2m+k}(\eta)}{m!(m+k)!} \cos k\sigma\tau, \tag{20}$$

with

$$S_n(\eta) = f_{o,o}(\eta), \quad n = 0$$

$$= \eta^n f_{o,o}^{(n)}(\eta) + \sum_{r=o}^{n-1} (-1)^{n-r-1} \frac{(2n-5-2)!}{2^{n-r-1} r!(n-r)!} [n - \frac{r(r+1)}{2}] \eta^r f_{o,o}^{(r)}(\eta),$$

$$n \geq 1, \tag{21}$$

and

$$f_{o,o}^{(r)} \equiv \frac{d^r f_{o,o}}{d\eta^r} . \tag{22}$$

Equating the coefficients of ε in (21) to the corresponding coefficients of ε in (13) we find that, to order σ,

$$f_{2m,0} = \frac{1}{2^{4m}(m!)^2} S_{2m}, \tag{23a}$$

$$f_{2m,k} = \frac{1}{2^{4m+2k-1}(m+k)!m!} S_{2m+k}, \tag{23b}$$

$$g_{2m,k} = 0 \tag{23c}$$

Taking the $\sigma \to 0$ limit in the differential equations (17) and (18), for the $\{f_{2m,k}\}$ and $\{g_{2m,k}\}$, and substituting the low frequency approximations (23), it can be shown by induction, after some lengthy but straightforward calculations, that these approximations satisfy the differential equations to $O(\sigma)$. Therefore, the quasi-steady solution is the same as the expansion in the low frequency limit.

4.2 The High Frequency Limit

In the high frequency limit, $\sigma \to \infty$, it would be natural to look for approximate solutions for the $\{f_{2m,k}\}$ and $\{g_{2m,k}\}$ in the form of a power series expansion in σ^{-1}. However, it is clear from the form of the differential equations, that this expansion would be non-uniform because the highest derivatives would be multiplied by the small parameter σ^{-1} and thus would vanish as $\sigma \to \infty$.

We therefore rescale the equations, defining a new independent variable, an inner variable,

$$z = (\sigma/2)^{1/2}\eta = (\omega/2\nu)^{1/2}y, \tag{24}$$

with the length scale $(2\nu/\omega)^{1/2}$, that of Stokes's second problem (Schlichting, 1979; pg. 75 and Chapter 11). In this limit we assume that there is an inner expansion of the form,

$$F = f_{o,o}(\eta) + \sum_{m=1}^{\infty} \varepsilon^{2m} \hat{f}_{2m,o}(z)$$

$$+ \sum_{m=o}^{\infty} \sum_{k=1}^{\infty} \varepsilon^{2m+k}\left[\hat{f}_{2m,k}(z) \cos k\sigma\tau + \hat{g}_{2m,k}(z) \sin k\sigma\tau\right] \tag{25}$$

It is easy to see that the differential equations for the $\{\hat{f}_{2m,k}\}$ and $\{\hat{g}_{2m,k}\}$ are just equations (17) and (18) with a transformation of variables from η to z. It can be inferred from the form of the equations that $f_{2m,k}$ and $g_{2m,k}$ are $O((2/\sigma)^{2m+k-1/2})$ in the high frequency limit. We then solve these equations, retaining only the highest order terms in an expansion in powers of $(2/\sigma)$.

We find

$$\hat{f}_{o,1}(z) = (2/\sigma)^{1/2}\left[z + \frac{1}{2}\, e^{-z}\,(\cos z - \sin z) - \frac{1}{2}\right], \tag{26a}$$

$$\hat{g}_{o,1}(z) = (2/\sigma)^{1/2}\left[\frac{1}{2}\, e^{-z}\,(\cos z + \sin z) - \frac{1}{2}\right], \tag{26b}$$

a Stokes shear layer flow caused by the $O(\varepsilon)$ part of the far flow field. In the high frequency limit it is decoupled from the $O(\varepsilon^o)$ steady outer flow. This is, of course, a familiar result in time dependent boundary layer theory and has been derived and discussed by Carrier and DiPrima (1957), Stuart (1966), and Riley (1975), among others.

If we let $\delta_{o,o}$ and $\delta_{o,1}$ be the boundary layer thickness of the steady flow and the Stokes shear layer flow, respectively, then, for $\sigma \gg 1$,

$$\delta_{o,1}/\delta_{o,o} \approx 2\,(2/\sigma)^{1/2} \ll 1. \tag{27}$$

Next, we solve the equations for the $O(\varepsilon^2)$ oscillatory flow and find that

$$\hat{f}_{o,2}(z) = (2/\sigma)^{3/2}\{\frac{\sqrt{2}}{16}\left[e^{-\sqrt{2}\,z}\,(\sin\sqrt{2}\,z + \cos\sqrt{2}\,z) - 1\right]$$

$$+ \frac{1}{4}\,ze^{-z}\sin z\} \tag{28a}$$

$$\hat{g}_{o,2}(z) = (2/\sigma)^{3/2}\{\frac{\sqrt{2}}{16}\left[e^{-\sqrt{2}\,z}\,(\sin\sqrt{2}\,z + \cos\sqrt{2}\,z) - 1\right]$$

$$- \frac{1}{4}\,ze^{-z}\cos z\} \tag{28b}$$

Again we have a Stokes shear layer, decoupled from the steady flow and, for large σ, confined to a thin layer imbedded within the steady boundary layer.

Proceeding next to the $O(\epsilon^2)$ steady streaming flow component, we find that the most general solution which satisfies the boundary conditions at $z = o$, is

$$\hat{f}_{2,o} = (2/\sigma)^{3/2}(\frac{1}{16})\left[13 - 6z - e^{-2z} - 4e^{-z}\,(3\cos z + 2\sin z)\right.$$

$$\left. - 4ze^{-z}\sin z\right] + Dz^2, \tag{29}$$

where D is an arbitrary constant. This secondary steady streaming flow is identical to that found by Stuart (1966) using the boundary layer equations. Stuart's small parameter, α, is the reciprocal of σ and Stuart's expansion is in powers of α, while ours is in powers of $(2/\sigma)$. Therefore,

$\hat{f}_{2,o}$, with D = 0, is equal to 1/2 of the χ_s given by Stuart (see Stuart, 1966; eq. 2.11). Our solution and Stuart's satisfy the boundary conditions at the wall but do not satisfy the outer boundary condition because

$$\frac{d\hat{f}_{2,o}}{d\eta} \to -\left(\frac{3}{8}\right)(2/\sigma) + \sigma D\eta \quad \text{as} \quad \eta \to \infty \tag{30}$$

and does not vanish, as required by the far field boundary condition, for any value of D. This is explained by the fact (pointed out by Stuart) that there is an outer boundary layer, thick compared to the Stokes layer thickness, $\delta_{o,1}$, but thin compared to the scale of the body, within which this secondary steady streaming flow decays to zero.

Since the $\sigma \to \infty$ limit is non-uniform and z is an inner variable, all of the $\hat{f}$'s and $\hat{g}$'s are inner solutions and could be expected to require matching to appropriate outer solutions. The functions $\hat{f}_{o,1}$, $\hat{g}_{o,1}$, $\hat{f}_{o,2}$, and $\hat{g}_{o,2}$, however, are also outer solutions and, unlike $\hat{f}_{2,o}$, do not require matching.

Outside of the Stokes layer, the interaction between the secondary streaming flow, $\hat{f}'_{2,o}$, and the oscillatory potential flow, $\hat{f}'_{o,1}$, is unimportant. In the case studied by Stuart, the dominant non-linear interaction is that between $\hat{f}'_{2,o}$ and itself. Since the velocity of this flow at the top of the Stokes layer is $O(U_o/\sigma)$, the corresponding Reynolds number is $R_s = (U_o/\sigma)(\ell/\nu) = R_o/\sigma$. From this, Stuart concluded that the thickness of the outer layer is $O(\ell R_s^{-1/2}) = O(\ell R_o^{-1/2}\sigma^{1/2})$, which is larger than that of Stokes layer by a factor of the order of σ.

For the case under consideration here,. the situation is completely changed by the existence of the large steady flow, $f'_{o,o}$ with boundary layer thickness $\delta_{o,o} = O(\sigma^{1/2}\ \delta_{o,1})$. The dominant non-linear interaction of $f_{2,o}$ in the outer layer is with $f'_{o,o}$ and, consequently, it falls off in a distance of the order of $\delta_{o,o}$ (instead of $\sigma^{1/2}\ \delta_{o,o}$). The appropriate outer variable is therefore $\eta = y/\delta_{o,o}$.

If we express $\hat{f}_{o,1}$ and $\hat{g}_{o,1}$ in terms of η, substitute them into the differential equation for $f_{2,o}$, and let $\sigma \to \infty$, it can be seen that the outer solution, $\hat{\hat{f}}_{2,o}$, is the solution of

$$L(\hat{\hat{f}}_{2,o}) = \left(\frac{d^3}{d\eta^3} + f_{o,o}\frac{d^2}{d\eta^2} - 2f'_{o,o}\frac{d}{d\eta} + f''_{o,o}\right) f_{2,o} = 0, \tag{31}$$

with the outer boundary condition

$$f'_{2,o} \to o \quad \text{as} \quad \eta \to \infty. \tag{32}$$

Using the asymptotic expansion for $f_{o,o}$,

$$\hat{\hat{f}}_{o,o} \sim \eta + A, \tag{33}$$

with A a constant, it can be shown that the general solution of (31) is

$$f_{2,o} = C_o\, f'_{o,o}(\eta) + C_1 h_1(\eta) + C_2\, h_2(\eta) \tag{34}$$

where, as $\eta \to \infty$,

$$h'_1 \sim (1 + \beta^2) \int_{\beta}^{\infty} e^{-\gamma^2/2} d\gamma - \beta e^{-\beta^2/2} \tag{35}$$

$$h'_2 \sim \beta + \frac{1}{3}\beta^3, \tag{36}$$

with

$$\beta = \eta + A. \tag{37}$$

The outer boundary condition requires that C_2 be set equal to zero. This leaves three arbitrary constants, C_o, C_1, and D, in the inner and outer solutions so we can match the inner and outer solutions and their first two derivatives. Matching the inner limit of the outer solution and the outer limit of the inner solution shows that

$$C_o = O(\sigma^{-1}), \quad C_1 = O(\sigma^{-3/2}), \quad \text{and} \quad D = O(\sigma^{-2}). \tag{38a,b,c}$$

The inner solution was obtained by expanding in powers of $\sigma^{-1/2}$ and retaining only the lowest order terms. Consistent use of this approximation requires that we set C_1 and D to zero and match the first derivative. We find that

$$C_o = -3/(4B\sigma). \tag{39}$$

where $B = f''_{o,o}(0)$. The composite solution for $\hat{f}_{2,o}$ is

$$\hat{f}_{2,o} = (2/\sigma)^{3/2} \left(\frac{1}{16}\right) \left[13 - e^{-2z} - 4e^{-z} (3 \cos z + \sin z)\right.$$

$$- 4ze^{-z} \sin z] - \frac{3}{4B\sigma} f'_{o,o}(\eta), \tag{40}$$

which satisfies the boundary conditions at z equal to zero as well as $z \to \infty$. The thickness of the inner layer of the steady streaming flow is $\delta_{o,1}$, while that of the outer layer is $\delta_{o,o}$ which is much larger than $\delta_{o,1}$ for $\sigma \to \infty$.

We have also calculated the high frequency approximations for the $O(\varepsilon^3)$ functions, for $f_{o,3}$, $g_{o,3}$, $f_{2,1}$ and $g_{2,1}$. These are given in Section 8. The components of the amplitude of the $O(\varepsilon^3)$ portion of the second harmonic $f_{o,3}$ and $g_{o,3}$ are driven by the interaction of the $O(\varepsilon)$ fundamental $(f_{o,1}, g_{o,1})$ and the $O(\varepsilon^2)$ first harmonic $(f_{o,2}, g_{o,2})$. The inner expansions for $f_{o,3}$ and $g_{o,3}$, given in Section 8, are also outer expansions.

This is not true for $f_{2,1}$ and $g_{2,1}$, the components of the amplitude of the $O(\varepsilon^3)$ part of the fundamental. They are excited by the interaction of $(f_{o,1}, g_{o,1})$ with $(f_{2,o})$ as well as $(f_{o,1}, g_{o,1})$ with $(f_{o,2}, g_{o,2})$. The inner expansion of the in-phase component, $f_{2,1}$, satisfies the outer boundary condition, but inner expansion for the out-of-phase component, $g_{2,1}$, does not. The outer expansion for $g_{2,1}$ is the same as that for $f_{2,o}$. The composite expansion for $g_{2,1}$ is found in the same way as that for $f_{2,o}$ and is given in Section 8.

5. RESULTS

We have numerically integrated the differential equations for the f's and g's with $2m + k \leq 3$ over a wide range of values of σ. Some typical

results at a moderately low frequency, $\sigma = \pi/4$, are shown in Figures 1 - 4, where the solid curves show the results of the numerical integrations and the dashed curves are obtained from low frequency approximations for the f's given in section 4.1. The g's are identically zero in the low frequency approximation.

It can be seen from the results shown in these figures that at low frequencies there is no Stokes layer; the boundary layer thickness of the various components are generally equal to or greater than that of the steady flow component, $f'_{o,o}$. The steady streaming component, $f'_{2,o}$, is quite small compared to the mean flow, even for $\varepsilon = 1$.

At $\sigma = o$ the g's, the out-of-phase components, are identically zero. At small, but non-zero, frequencies the low order (in ε) in-phase components, the f's are larger than the g's. As the order increases, however, the magnitudes of the f's and g's tend to equalize and decrease.

It is also apparent from an examination of Figures 1 - 4 that the low frequency approximations are reasonably accurate even at $\sigma = \pi/4$. In fact, the difference between the numerical solution and the approximation for $f_{o,1}$ is so small that it is not apparent in Figure 2. Taking into account the fact that the higher order terms, which have the largest deviations from the low frequency approximations, have very small magnitudes, it is clear that the low frequency approximations, equation (19), is reasonably accurate, even for Strouhal numbers as large as $\pi/4$.

Figures 5 - 9 show the f's and g's for $2m + k \leq 3$ at a moderately high Strouhal number, $\sigma = 8\pi$, as obtained from the numerical integrations (solid curves) and the asymptotic approximations (dashed curves). The top of the Stokes layer is at $z \approx 4.6$ and this corresponds to $n \approx 6.5\, \sigma^{1/2}$.

Therefore, the top of the Stokes layer is at $n \approx 1.3$ for $\sigma = 8\pi$. The secondary streaming flow (see Fig. 5) extends far beyond the Stokes layer. The variation of the fundamental component (see Fig. 6) is confined to the Stokes layer. The amplitude functions of the higher harmonics tend, like $f'_{2,o}$, to extend beyond the Stokes layer because they are also driven by Reynolds stresses due to $f_{o,o}$.

The secondary steady streaming flow, $f'_{2,o}$, is considerably smaller at high frequencies than at low frequencies. In addition, the nature of the secondary flow changes as σ increases; at a small σ, the net secondary flow is positive while, for large σ, it is negative. As discussed by Stuart (1963), it is known from experiments that this effect occurs in the steady streaming flow generated by a circular cylinder oscillating along a diameter.

The tangential velocity component, u, is proportional to $\frac{\partial F}{\partial \eta}$, that is to the $\{f'_{2m,k};\ g'_{2m,k}\}$. In Figure 10 we present some of the results of the numerical integrations; a plot of the variation of $\max |f'_{2m,k}|$ and $\max |g'_{2m,k}|$ as functions of σ. The maximum of $f'_{o,o}$ is 1.0 for all σ and the absolute maximum of $f'_{o,1}$ is about 1.069 at $\sigma \approx 17$; the maxima of $f'_{o,o}$ and $f'_{o,1}$ are not plotted in Figure 10. We can conclude, from the results shown in Figure 10, that the high frequency estimate, $\{|f'_{2m,k}|, |g'_{2m,k}|\} = O(\sigma^{-2m-k+1})$, is quite good.

6. DISCUSSION

The applied far-field flow consist of a time-independent mean flow and a fundamental with a $\cos\omega t$ time-variation. Non-linear interactions result

in the generation of components at all multiples of the fundamental frequency and modifications of the mean flow and fundamental components, though, at moderate $\varepsilon(\lesssim 1)$, the fundamental and first harmonic tend to dominate.

At low frequencies, our results are well represented by a quasi-steady approximation (19), which has the same form as the steady stagnation-point flow except that the amplitude and scale vary with time. Somewhat surprisingly, this approximation is quite good for a dimensionless frequency, σ, as large as $\pi/4$.

At high frequency, the viscous boundary layer corresponding to the oscillating components is largely, but not completely, confined to a Stokes layer of thickness $(2/\sigma)^{1/2}$ times that of the steady boundary layer. For these large values of σ, the inner asymptotic approximations are solutions of differential equations which are independent of $f_{o,o}$ and are, therefore, decoupled from the mean flow. For a number of components, the inner expansions are also the correct outer expansions; these components are, therefore, totally decoupled from the mean flow to lowest order in σ and are, in fact, identical to the corresponding solutions found by Stuart (1966) for a purely oscillatory flow past a body.

Not all of the components are decoupled from the mean flow in the high frequency limit. The high frequency expansion is a non-uniform asymptotic expansion and thus, for certain components, in particular the steady second order flow, $f'_{2,o}$, an outer expansion, matched to the inner expansion, is needed for a uniformly valid approximation. The results given in Section 4.2 show that such composite expansions can be found for $\sigma \gg 1$; they

satisfy, to lowest order in σ, the differential equations and all of the boundary conditions. We believe, although we have not carried out the calculations, that this is also true for an expansion to any order in σ. The results of the numerical integrations, shown in Figures 5-9 are consistent with this belief. We conclude that, both for this flow and for the oscillatory flow studied by Stuart (1966), there are second, and higher, order steady streaming flow components that do not extend to infinity but are confined to a layer adjacent to the solid boundary. This layer is much thicker than the Stokes layer but much thinner than the length scale of the body.

There are other aspects of Stuart's solution which can be compared with ours. He used three parameters, α, β, and R_s in his solution, which are related to our Strouhal number, σ, and Reynolds number, R_o, by:

$$\alpha = U_o/(\omega \ell) = \sigma^{-1},$$

$$\beta + \nu/(\omega \ell^2) = 1/(\sigma R_o),$$

$$R_s = U_o^2/(\omega \nu) = R_o/\sigma.$$

Stuart used the boundary layer equations and an expansion for $\alpha \to o$; we have used the Navier-Stokes equations and, in addition to the numerical solutions, an expansion for the high frequency limit, $\sigma \to \infty$. It is clear that Stuart's expansion, and ours, are high frequency approximations. Stuart assumed that β was small and R_s large in order to justify the use of the boundary layer equations. In the high frequency limit $\sigma \to \infty$, and, with R_o fixed, α, β, and R_s are all small. We do not need to make any assumptions concerning the magnitude of R_o or R_s because we used the

Navier-Stokes equations. We can determine the f's and g's by numerically integrating the ordinary differential equations; however, the quasi-steady solution for low frequencies and the high frequency expansion are useful analytic approximations.

We have not attempted to determine the radius of convergence, in ε, of the series for $F(\eta,\tau,\varepsilon)$, equation (13). However, some observations can be made. We have found that $f'_{2m,k}$ and $g_{2m,k}$ are $O(\sigma^{-2m-k+1/2})$ for large σ. Therefore, max $\{|f'_{2m,k}|, |g'_{2m,k}|\}$, the amplitude functions for u, are $O(\sigma^{-2m-k+1})$. Thus the series for u is in terms of $(\varepsilon/\sigma)^{2m+k}$, for large σ, and this suggests that it converges for $\varepsilon/\sigma < 1$ and converges rapidly for $\varepsilon \ll 1$. On the basis of the results presented in figure (10) we conclude that the high frequency bound on max $\{|f'_{2m,k}|, |g'_{2m,k}|\}$ is valid at all frequencies and, therefore, that the series converges rapidly for $\varepsilon \ll 1$. Of course the convergence will be slower at low frequencies but we have shown that, for $\sigma \lesssim \pi/4$, the quasi-steady solution is an accurate approximation.

In the introduction we suggested that the solution to the problem of oscillating stagnation point flow was the first step in the solution of one aspect of the boundary layer receptivity problem. A few years ago, Morkovin (1978) reviewed the rather rudimentary state of knowledge of the dynamics of boundary layer receptivity. He identified four general classes of free stream disturbances which might generate Tollmien-Schlichting waves in the boundary layer. These are: vorticity fluctuations, sound, entropy disturbances, and unsteadiness in the mean flow. In the incompressible limit, there can be only vorticity fluctuations and unsteadiness. Morkovin argues, however, that a temporally oscillating incompressible flow is a

reasonably accurate approximation for a sound wave impinging normally on the nose of a body if the wavelength of the sound wave is much greater than the radius of curvature of the nose.

The solution of the Navier-Stokes equations given here is the solution, in the neighborhood of the stagnation point, of the receptivity problem for a simple unsteady flow. In order to interpret this solution in terms of a stability model it is necessary to extend it around the nose of the body into a region where the flow is, at least, quasi-parallel. If we can assume that the tangential component of the potential flow at the edge of the boundary is of the form $U = U_o H(\xi)\ (1 + \varepsilon \cos\sigma t)$, with $H(\xi)$ having a power series expansion in ξ, the distance along the body from the stagnation point, we can use an unsteady variant of the Blasius series to solve this problem. For the first term we use the full two-dimensional Navier-Stokes equations and the solution is that given here. For the subsequent terms, we use the boundary layer equations. We have carried out this calculation procedure up to and including the terms in ξ^{11} and we are now applying it to bodies which are elliptic or parabolic cylinders. We hope to report the results of these calculations at a later date.

This work was supported, in part, by grant NAG-1-96, from the National Aeronautics and Space Administration.

7. DERIVATION OF $P_{2m,k}$ AND $Q_{2m,k}$ MATRICES

The expressions for $P_{2m,k}$, $Q_{2m,k}$, and $R_{2m,o}$ in (17a), (17b), and (18a) are simplified by use of the notation

$$M(f,g) = f''g - 2f'g' + fg''. \tag{7-1}$$

In terms of M,

$$P_{ok} = -\frac{1}{4}\{8\delta_{k1} + 2\delta_{k2} + (1 - \delta_{k1}) \sum_{r=1}^{k-1} [M(f_{o,r}, f_{o,k-r}) - M(g_{o,r}, g_{o,k-r})]\} \quad \text{for } k \geq 1, \tag{7-2}$$

$$P_{2m,k} = -\frac{1}{4}\left\{4 \sum_{s=o}^{m-1} M(f_{2(m-s),o}, f_{2s,o}) + (1 - \delta_{k1}) \sum_{s=o}^{m} \sum_{r=1}^{k-1} \times [M(f_{2s,r}, f_{2(m-s),k-r}) - M(g_{2s,r}, g_{2(m-s),\,k-r}) + 2 \sum_{s=o}^{m-1} \sum_{s'=o}^{m-1-s} [M(f_{2s,k+m-s-s'}, f_{2s',m-s-s'}) + M(g_{2s,k+m-s-s'}, g_{2s,m-s-s'})]\right\} \quad \text{for } m \geq 1, \; k \geq 1, \tag{7-3}$$

$$Q_{ok} = \frac{1}{2}\left\{2\sigma\delta_{k1} - (1 - \delta_{k1}) \sum_{r=1}^{k-1} M(f_{o,r}, g_{o,k-r})\right\} \quad \text{for } k \geq 1, \tag{7-4}$$

$$Q_{2m,k} = -\frac{1}{2}\ 2\sum_{s=o}^{m-1} M(f_{2(m-s)},g_{2s,k}) + (1-\delta_{k1})\sum_{s=o}^{m}\sum_{r=1}^{k-1}$$

$$\times\ [M(f_{2s,r},g_{2(m-s),k-r}) + \sum_{s=o}^{m-1}\sum_{s'=o}^{m-1-s} [M(f_{2s,\ m-s-s'}$$

$$\times\ g_{2s',k+m-s-s''} - M(f_{2s',k+m-s-s''},g_{2s',m-s-s'})]$$

$$\text{for}\quad m \geq 1,\quad k \geq 1, \tag{7-5}$$

and

$$R_{2m,o} = -\frac{1}{4}\ 2\delta_{m1} + 2(1-\delta_{m1})\sum_{s=1}^{m-1} M(f_{2s,o},f_{2(m-s),o})$$

$$+\sum_{s=o}^{m-1}\sum_{s'=o}^{m-1-s} [M(f_{2s,m-s-s'},f_{2s',m-s-s'}) + M(g_{2s,m-s-s'},$$

$$\times\ g_{2s',m-s-s'})] \qquad \text{for}\quad m \geq 1. \tag{7-6}$$

Here, δ_{ij} is the Kronecker δ symbol.

8. HIGH FREQUENCY APPROXIMATIONS TO THE $O(\varepsilon^3)$ FUNCTIONS

The approximations to $\hat{f}_{o,3}$ and $\hat{g}_{o,3}$ for $\sigma \to \infty$ are:

$$\hat{f}_{o,3}(z) = (2/\sigma)^{5/2} \{[9 - 8\sqrt{2} + 3(2 + 1)] + e^{-z}[(\sqrt{2}$$

$$-6 + 4z - 4z^2) \cos z + (6 - \sqrt{2} - 4z^2) \sin z]$$

$$+ e^{-\sqrt{2}z}(4 + 2\sqrt{2} - 8z) \cos \sqrt{2}z - (4 + 2\sqrt{2}) \sin \sqrt{2}z]$$

$$- \sqrt{3}(\sqrt{2} + 1) e^{-\sqrt{3}z}(\cos \sqrt{3}z - \sin \sqrt{3}z) + (5\sqrt{2} - 7)$$

$$\times e^{-(\sqrt{2} + 1)z}[\cos (\sqrt{2} + 1) z - \sin (2 + 1)z]\}/128, \qquad (8\text{-}1)$$

$$_{,3}(z) = (2/\sigma)^{5/2} \{[9 - 8\sqrt{2} + \sqrt{3}(\sqrt{2} + 1)] + e^{-z}[(\sqrt{2}$$

$$-6\ 4z^2) \cos z + (\sqrt{2} - 6 + 4z - 4z^2) \sin z]$$

$$+ e^{-\sqrt{2}z}[(4 + 2\sqrt{2}) \cos \sqrt{2}z + (4 + 2\sqrt{2} - 8z) \sin \sqrt{2}z]$$

$$- \sqrt{3}(\sqrt{2} + 1) e^{-\sqrt{3}z}(\cos \sqrt{3}z + \sin \sqrt{3}z) + (5\sqrt{2} - 7)$$

$$\times e^{-(\sqrt{2} + 1)z}[\cos (\sqrt{2} + 1)z + \sin (\sqrt{2} + 1)z]\}/128. \qquad (8\text{-}2)$$

The approximation to $\hat{f}_{2,1}$ for $\sigma \to \infty$ is:

$$\hat{f}_{2,1}(z) = (2/\sigma)^{5/2}\{(349-335\sqrt{2})/1920 + e^{-z}[(60\sqrt{2}-213)/960$$

$$+ ((5z/64)(z-1)/64)\cos z + ((93 + 15\sqrt{2})/240-10z$$

$$\times (z + 1)/64)\sin z] + e^{-\sqrt{2}z}[(7\sqrt{2} - 2 + 4z)\cos \sqrt{2}z$$

$$- (7\sqrt{2} + 2)\sin \sqrt{2}z]/64 + (13/160)e^{-2z} + e^{-(\sqrt{2}+1)z}$$

$$[(\sqrt{2} -5)\cos(\sqrt{2} - 1)z - (\sqrt{2} + 5)\sin(\sqrt{2} - 1)z]/384$$

$$+ e^{-3z}\cos z/320\}. \qquad (8-3)$$

The composite approximation to $\hat{g}_{2,1}$ for $\sigma \to \infty$ is:

$$\hat{g}_{2,1}(z) = (2/\sigma)^{5/2}\{ - (1513 + 125\sqrt{2})/1920 + e^{-z}[(558- 45\sqrt{2})/960$$

$$+ ((3z(6-z)/64)\cos z + ((177 + 45\sqrt{2})/960 +$$

$$\times z(31 + 9z)/64)\sin z] + e^{-\sqrt{2}z}[(7\sqrt{2} + 2)\cos \sqrt{2}z$$

$$+ (7\sqrt{2} - 2 + 4z)\sin \sqrt{2}z]/64 + e^{-2z}[(13/80 + z/16)]$$

$$+ e^{-(\sqrt{2}+1)z}\left[(5\sqrt{2})\cos(\sqrt{2}-1)z - (5-\sqrt{2})\right.$$

$$\left.\times \sin(\sqrt{2}-1)z\right]/384 + e^{-3z}\sin z/320\Big\}$$

$$+ (2/\sigma)^2 \, 3f'_{o,o}(\eta)/(8B), \tag{8-4}$$

with

$$B = f''_{o,o}(0). \tag{8-5}$$

REFERENCES

Carrier, G. F. & DiPrima, R.C. 1957. On the unsteady motion of a viscous fluid past a semi-infinite flat plate. J. Math. & Phys., 35, 359.

Gibson, W.E. 1957. Unsteady laminar boundary-layer flow, Ph.D. Mathematics Thesis, Mass. Inst. of Tech.

Glauert, M.B. 1956. The laminar boundary layer on oscillating plates and cylinders. J. Fluid Mech., 1, 97.

Grosch, C.E. & Salwen, H. 1980. Eigenfunction expansions and boundary layer receptivity in the theory of hydrodynamic stability. Proc. 15th Int. Cong. Theor. Appl. Mech., 155.

Lighthill, M.J. 1954. The response of laminar skin friction and heat transfer to fluctuations in the stream velocity. Proc. Roy. Soc., A, 224, 1.

Lighthill, M.J. 1978. Acoustic streaming. Journal of Sound and Vibration 61, 391.

Lin, C.C. 1956. Motion in the boundary-layer with a rapidly oscillating external flow. Proc. 9th int. Cong. appl. Mech., Brussels 1, 136.

Morkovin, M.V. 1978. Instability, transition to turbulence and predictability. AGARDograph No. 236.

Riley, N. 1975. Unsteady boundary layers. SIAM Rev., 17, 274.

Rott, N. 1956. Unsteady viscous flow in the neighborhood of a stagnation point. Quart. appl. Math. 13, 444.

Salwen, H., Kelly, K.A. & Grosch, C.E. 1980. Completeness of the spatial eigenfunctions of the boundary layer. Bull. Am. Phys. Soc., 25, 1085.

Salwen H. & Grosch, C.E. 1981. The continuous spectrum of the Orr-Sommerfeld equation. Part 2. Eigenfunction expansions. J. Fluid Mech., 104, 445.

Sarma, G.N. 1964. Solutions of unsteady boundary layer equations. Proc. Camb. Phil. Soc., 60, 137.

Schlichting, H. 1979. Boundary Layer Theory. McGraw-Hill.

Stuart, J.T. 1963. "Unsteady boundary layers." Chapt. VII of Laminar Boundary Layers, ed. by L. Rosenhead. Clarendon Press, Oxford.

Stuart, J.T. 1966. Double boundary layers in oscillatory viscous flow. J. Fluid Mech., 24, 673.

Watson, J. 1959. The two-dimensional laminar flow near the stagnation point of a cylinder which has an arbitrary transverse motion. Quart. J. Mech. Appl. Math., 12, 175.

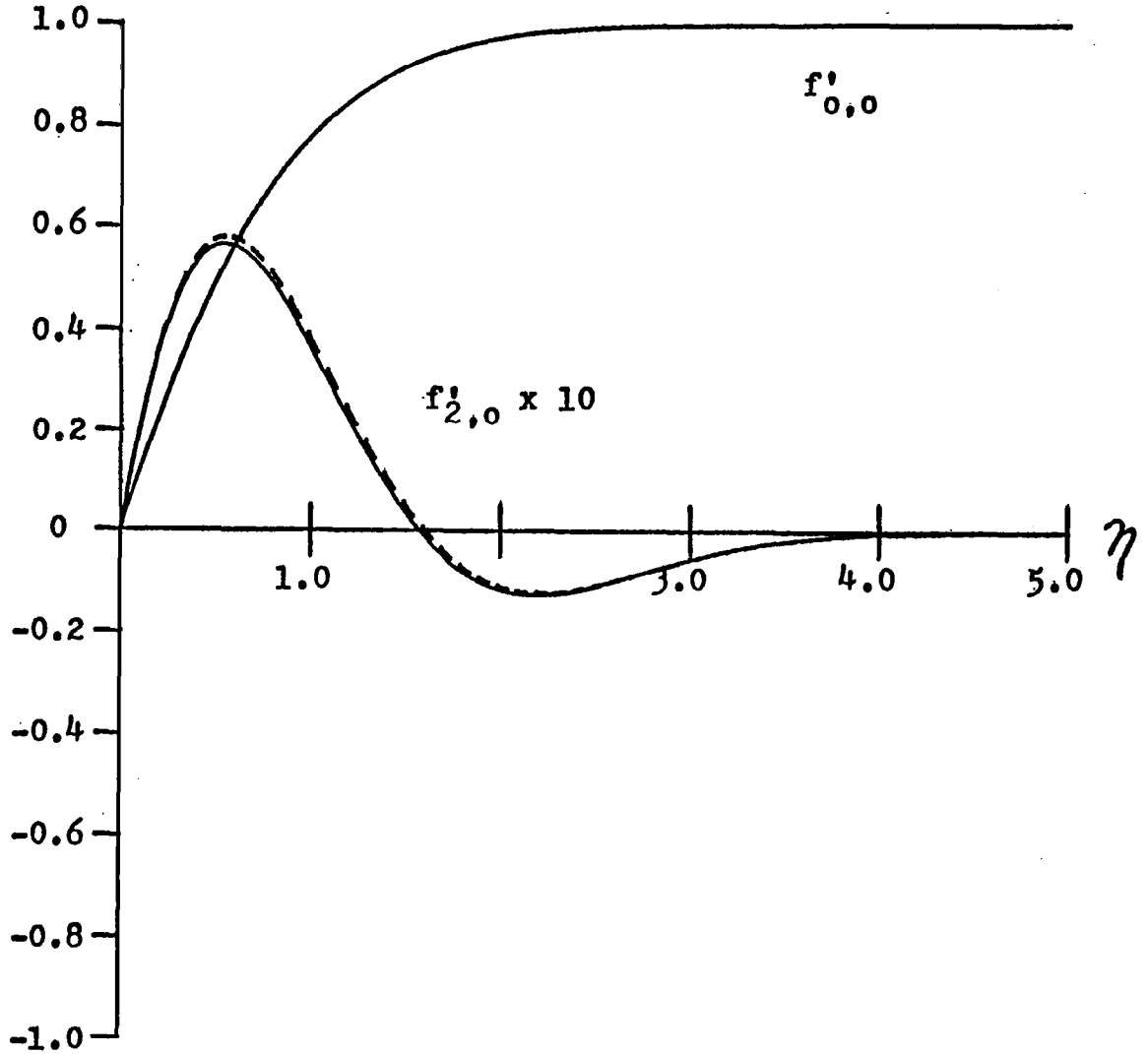

Figure 1. The steady and secondary streaming flow components, $f'_{o,o}$ and $f'_{2,o}$, as a function of η, the dimensionless distance from the boundary. The Strouhal number, $\sigma = \pi/4$. The solid curves are the results of numerical integrations and the dashed curve is the low frequency approximation for $f'_{2,o}$.

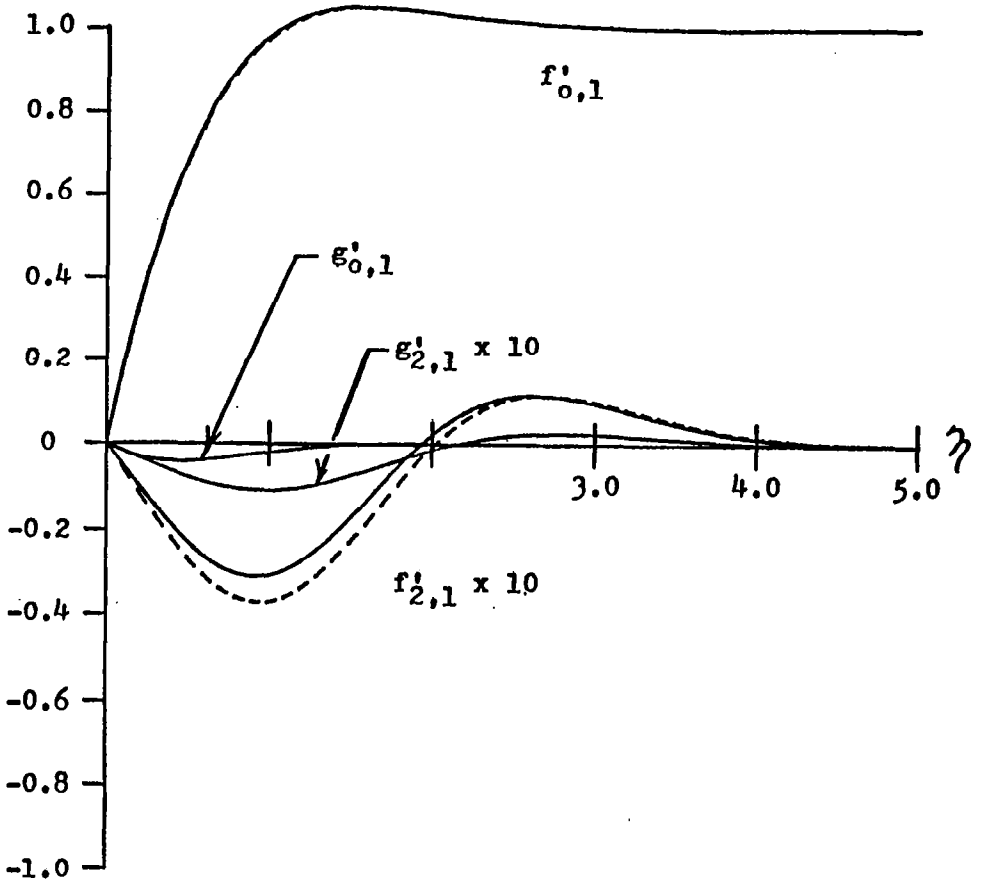

Figure 2. The $O(\varepsilon)$, $f'_{o,1}$, and $g'_{o,1}$, and $O(\varepsilon^3)$, $f'_{2,1}$ and $g'_{2,1}$, amplitudes of the fundamental component of the oscillating flow as functions of η, the dimensionless distance from the boundary. The Strouhal number, $\sigma = \pi/4$. The solid curves are the results of numerical integrations and the dashed curves are the low frequency approximations for $f'_{o,1}$ and $g'_{2,1}$. The low frequency approximation to $f'_{o,1}$, is so close to the result of the numerical integration that the two curves are virtually indistinguishable on this figure.

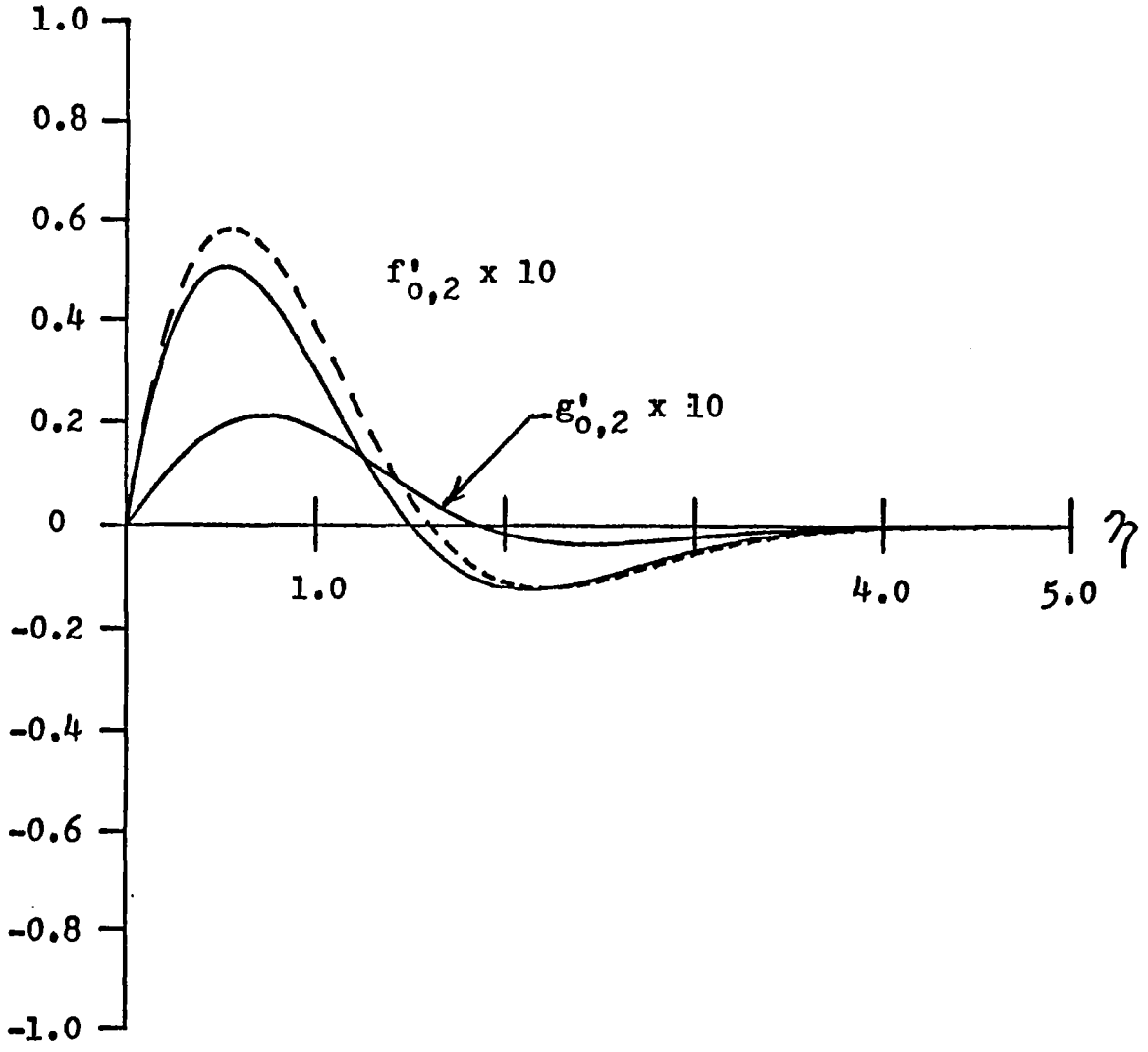

Figure 3. The $O(\varepsilon^2)$ amplitudes of the first harmonic of the oscillating flow as functions of η, the dimensionless distance from the boundary. The Strouhal number, $\sigma = \pi/4$. The solid curves are the results of numerical integrations and the dashed curve is the low frequency approximation to $f'_{o,2}$.

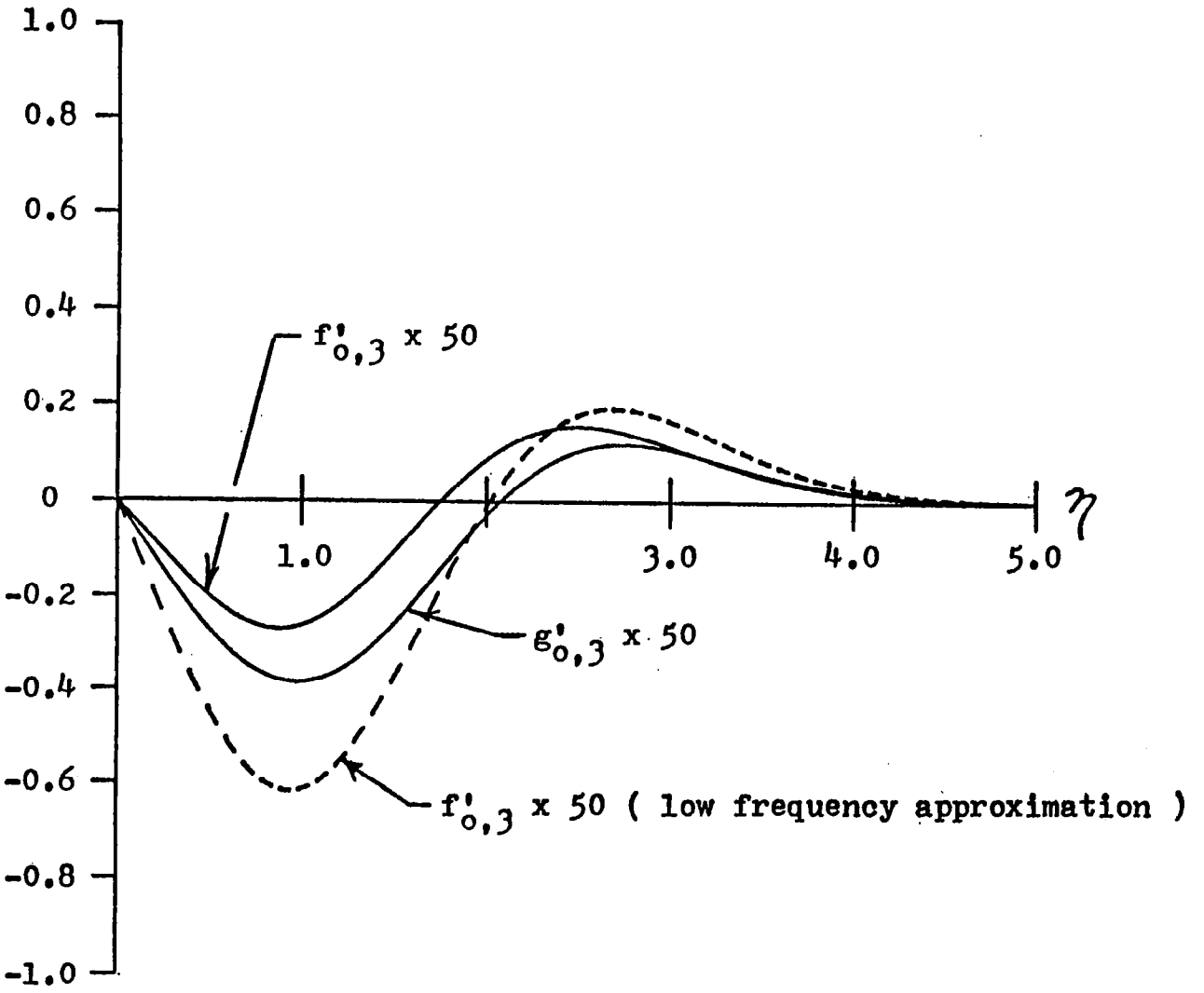

Figure 4. The $O(\varepsilon^3)$ amplitudes of the second harmonic of the oscillating flow as functions of η, the dimensionless distance from the boundary. The Strouhal number, $\sigma = \pi/4$. The solid curves are the results of numerical integrations and the dashed curve is the low frequency approximation to $f'_{o,3}$.

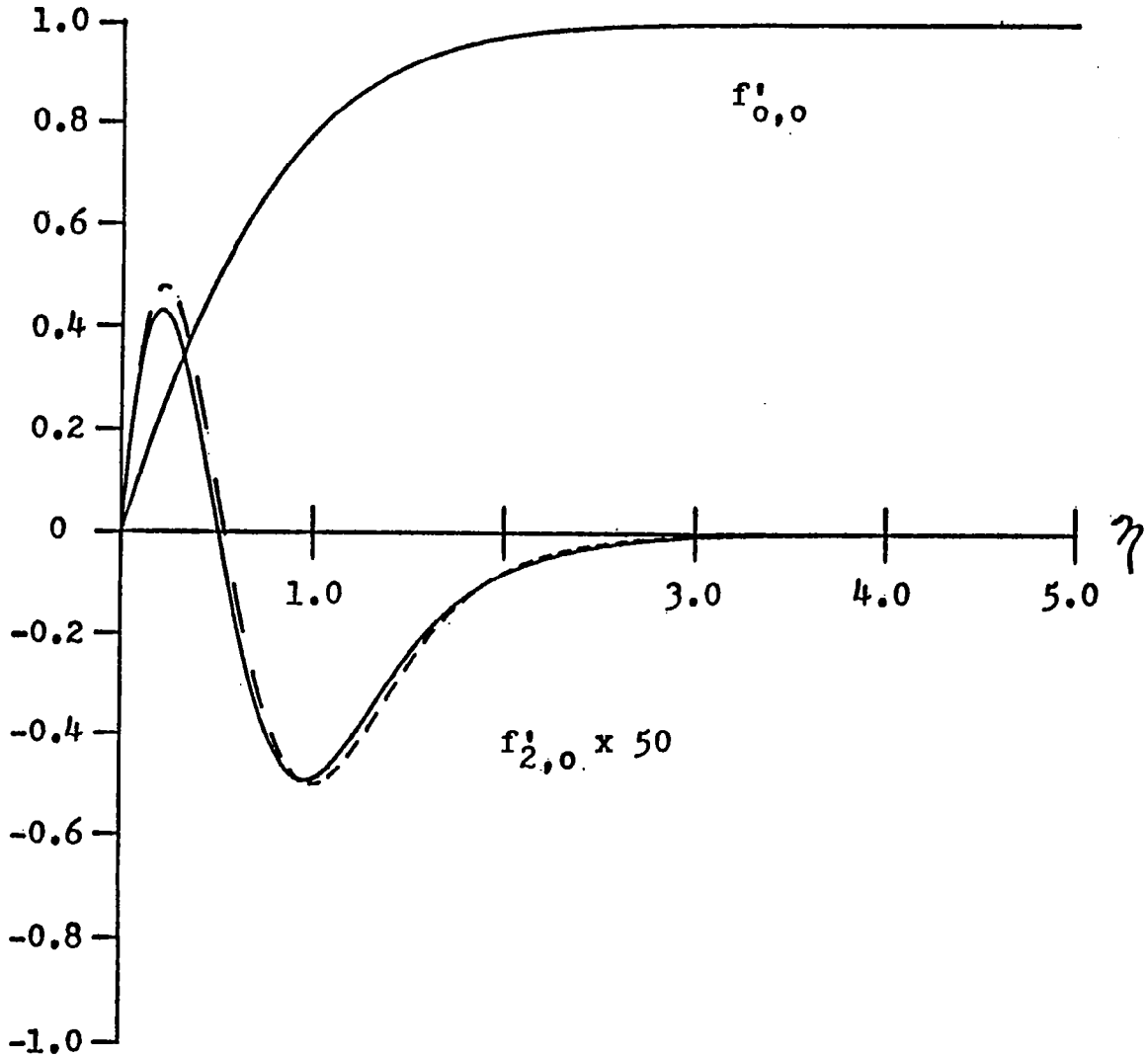

Figure 5. The steady and secondary streaming flow components, $f'_{o,o}$ and $f'_{2,o}$, as a function of η, the dimensionless distance from the boundary. The Strouhal number, $\sigma = 8\pi$. The solid curves are the results of numerical integrations and the dashed curve is the high frequency approximation to $f'_{2,o}$.

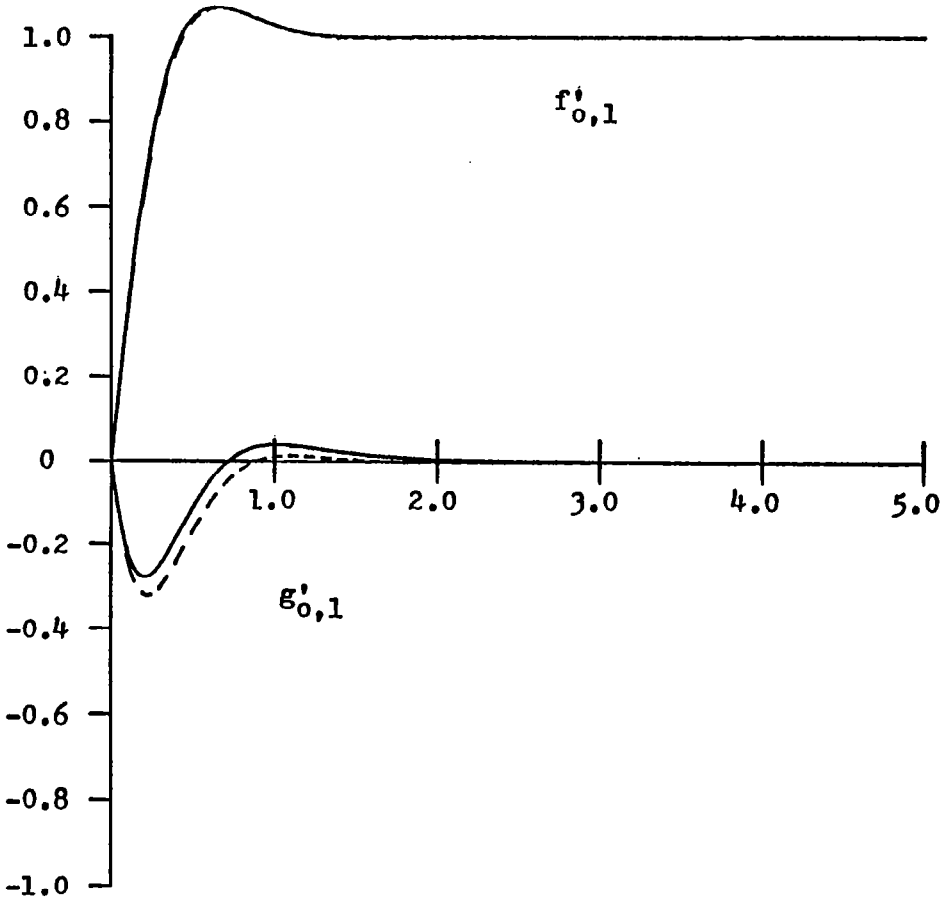

Figure 6. The $O(\varepsilon)$ amplitudes of the fundamental component of the oscillating flow as a function of η, the dimensionless distance from the boundary. The Strouhal number, $\sigma = 8\pi$. The solid curves are the results of numerical integrations and the dashed curves are the high frequency approximations. The high frequency approximation to $f'_{o,1}$ is so close to the result of the numerical integration that the two curves are virtually indistinguishable on this figure.

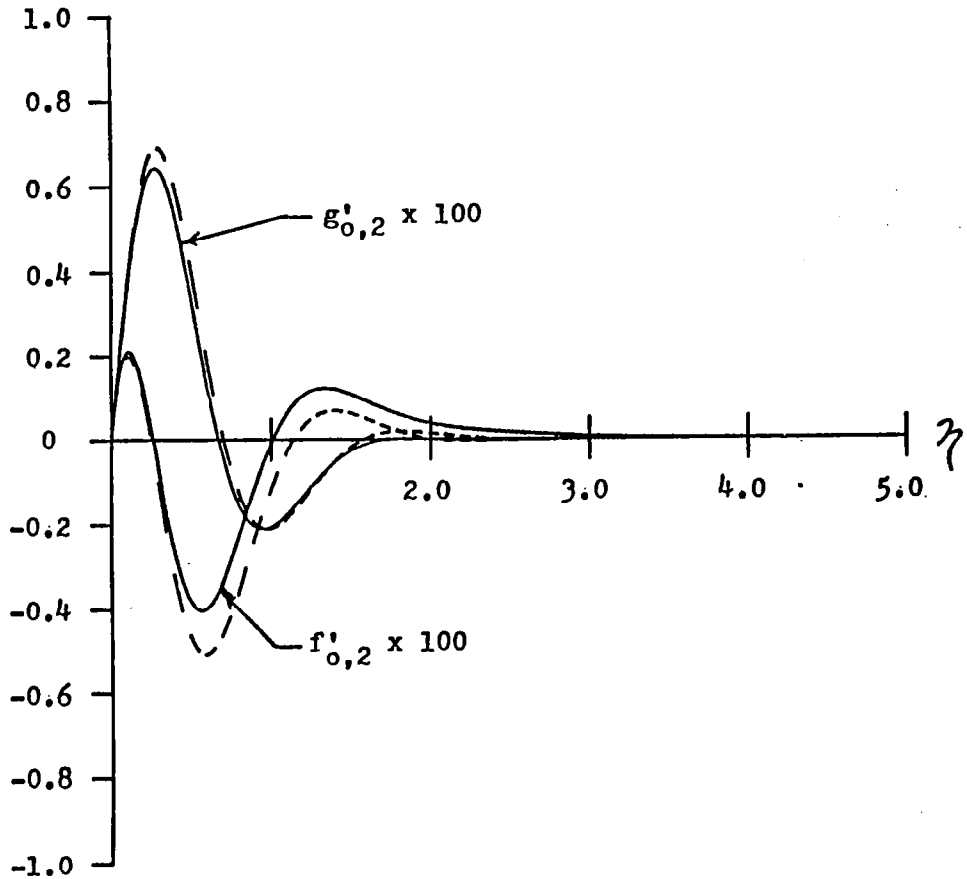

Figure 7. The $O(\varepsilon^2)$ amplitudes of the first harmonic of the oscillating flow as a function of η, the dimensionless distance from the boundary. The Strouhal number, $\sigma = 8\pi$. The solid curves are the results of numerical integration and the dashed curves are the high frequency approximations.

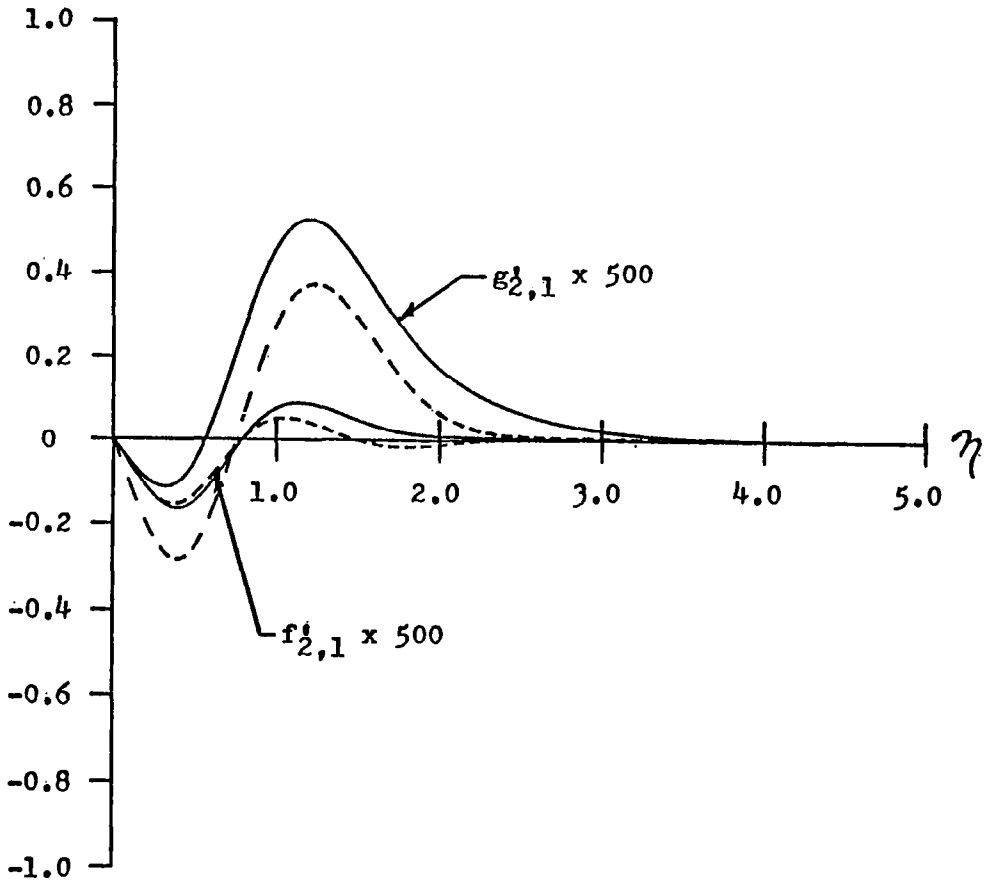

Figure 8. The $O(\varepsilon^3)$ amplitudes of the fundamental component of the oscillating flow as a function of η, the dimensionless distance from the boundary. The Strouhal number, $\sigma = 8\pi$. The solid curves are the results of numerical integrations and the dashed curves are the high frequency approximations.

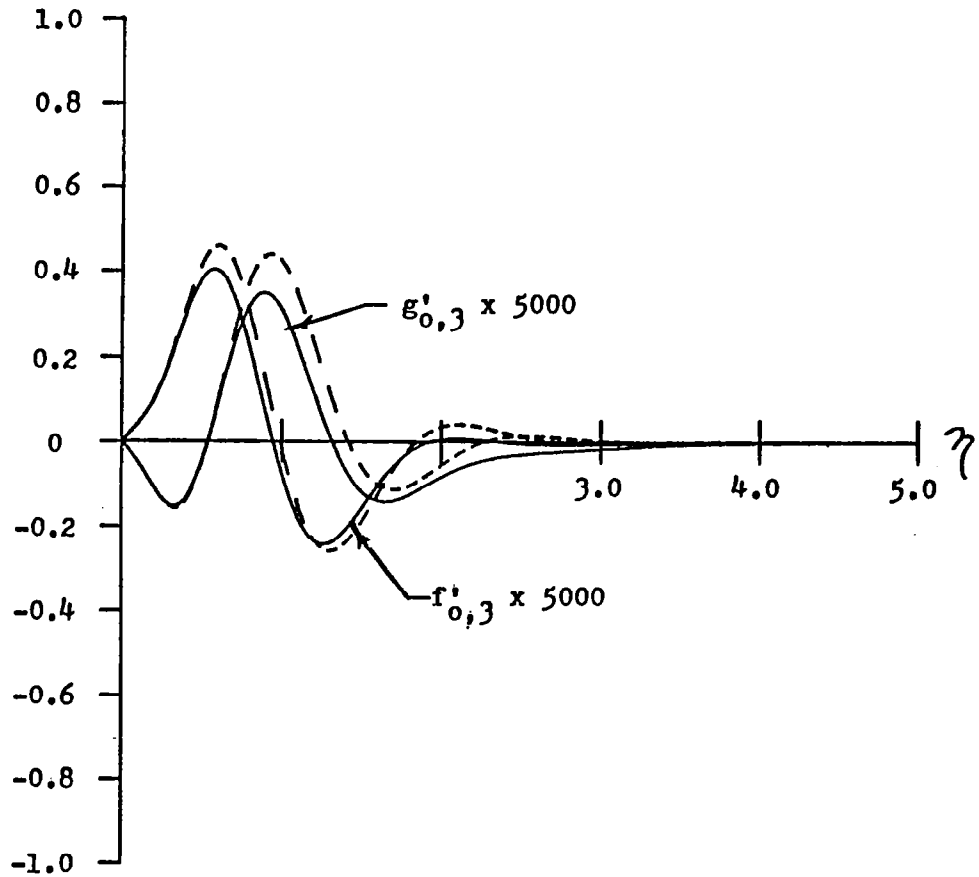

Figure 9. The $O(\varepsilon^3)$ amplitudes of the second harmonic of the oscillating flow as a function of η, the dimensionless distance from the boundary. The Strouhal number, $\sigma = 8\pi$. The solid curves are the results of numerical integrations and the dashed curves are the high frequency approximations.

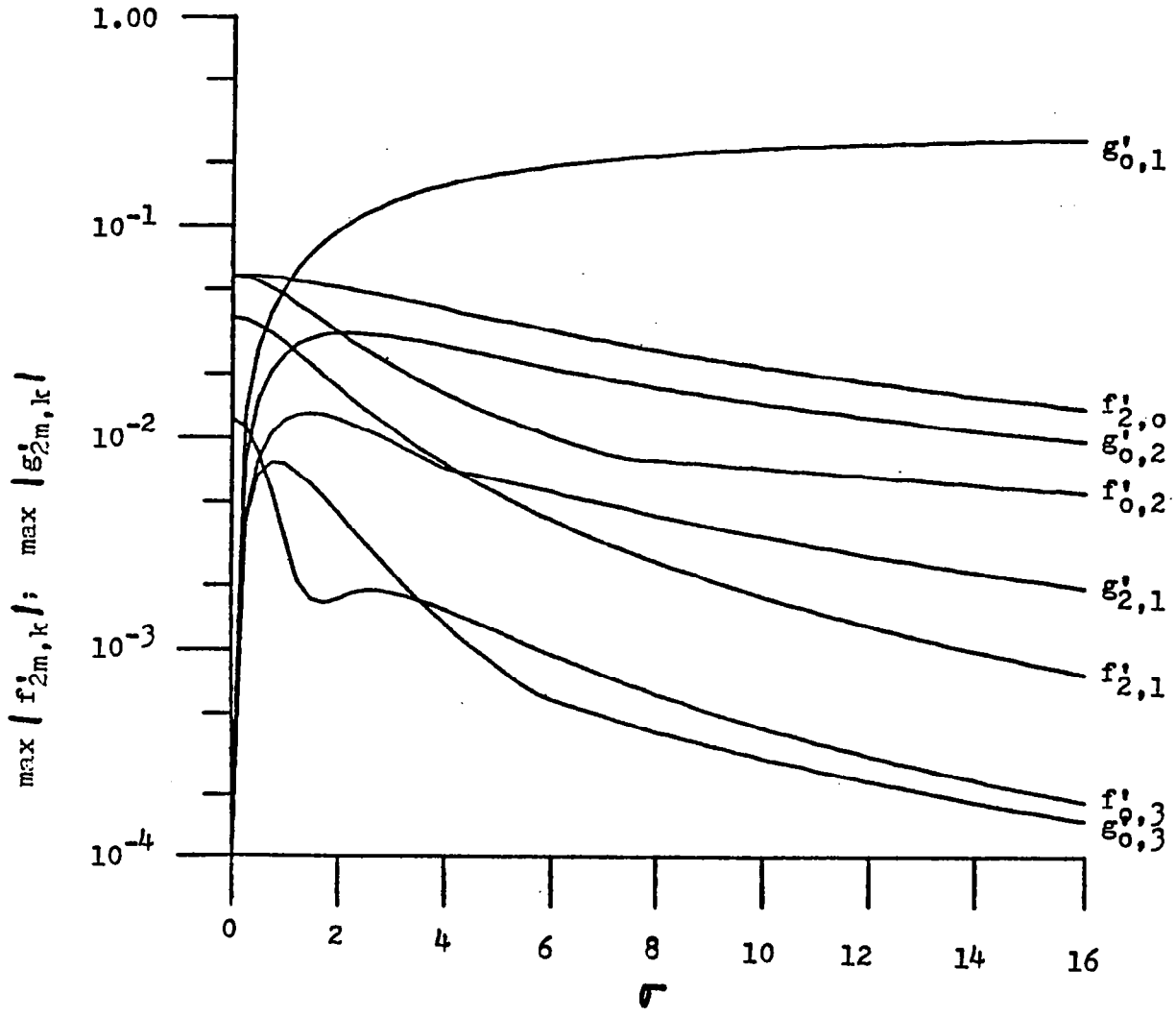

Figure 10a. Variation of $\max|f'_{2m,k}|$ and $\max|g'_{2m,k}|$ with the Strouhal number, σ.

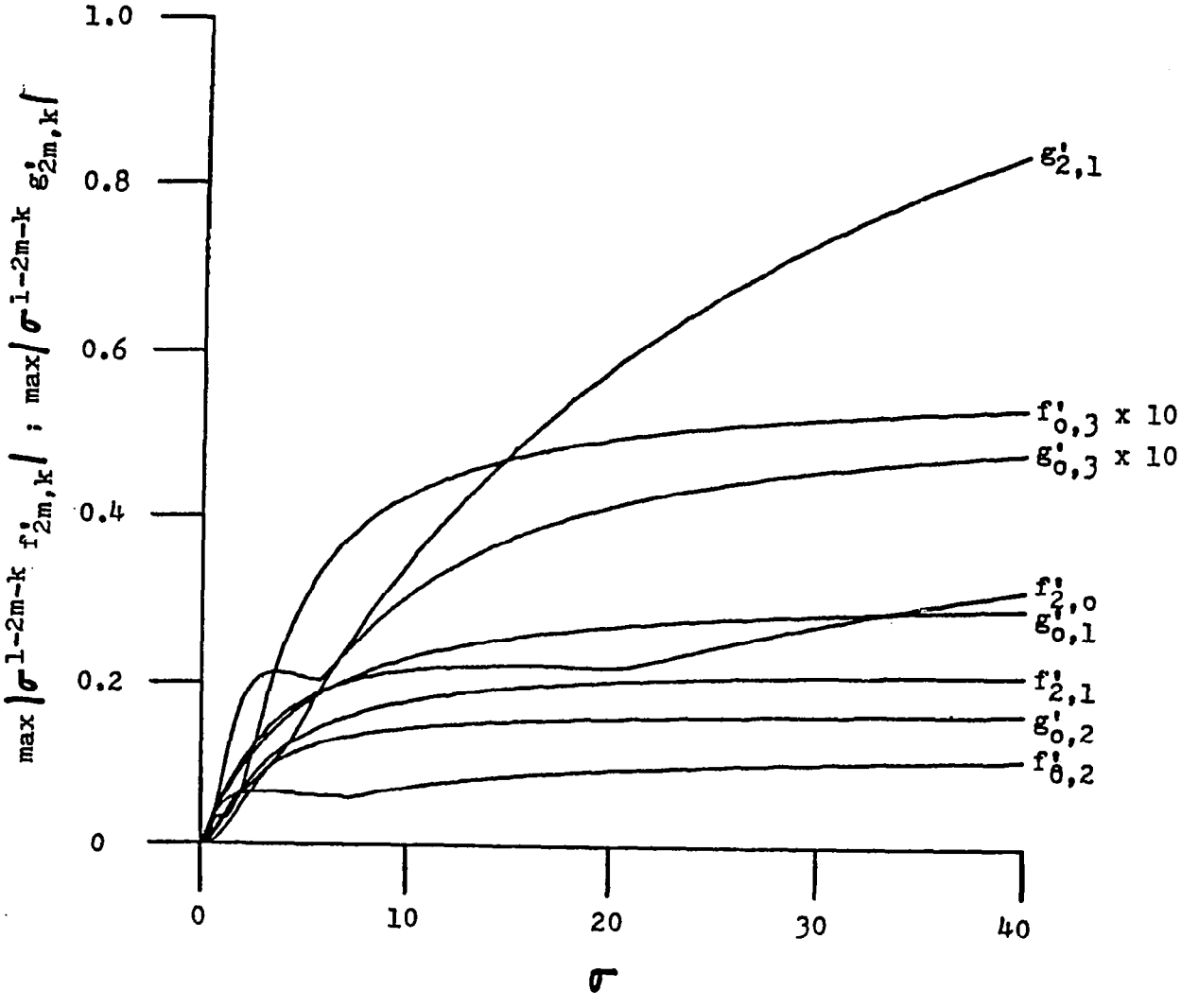

Figure 10b. Variation of $\max|\sigma^{1-2m-k} f'_{2m,k}|$ and $\max|\sigma^{1-2m-k} g'_{2m,k}|$ with the Strouhal number, σ.

1. Report No.	2. Government Accession No.	3. Recipient's Catalog No.
NASA CR-3639		

4. Title and Subtitle	5. Report Date
THE RECEPTIVITY OF BOUNDARY LAYERS ON BLUNT BODIES TO OSCILLATIONS IN THE FREE STREAM	November 1982
	6. Performing Organization Code
7. Author(s)	8. Performing Organization Report No.
C. E. Grosch	
	10. Work Unit No.
9. Performing Organization Name and Address	
Department of Oceanography School of Sciences and Health Professions Old Dominion University Norfolk, VA 23508	11. Contract or Grant No. NAG1-96
	13. Type of Report and Period Covered
12. Sponsoring Agency Name and Address	Contractor report
National Aeronautics and Space Administration Washington, DC 20546	14. Sponsoring Agency Code

15. Supplementary Notes

Appendix B by Chester E. Grosch, Old Dominion University, and Harold Salwen, Stevens Institute of Technology, Hoboken, New Jersey

Langley Technical Monitor: Dennis M. Bushnell FINAL REPORT

16. Abstract

Perhaps the most general conclusion which can be drawn from the results of this study is that in the region of the nose of a symmetric, two-dimensional blunt body at zero angle of attack, the steady plus oscillating flow is very similar for a wide class of body shapes. This conclusion has been shown to be true for elliptic cylinders with $a/b < 25$, and for the parabolic cylinder. Additional calculations, not reported here, were carried out for elliptic cylinders with values of a/b up to 100, with results which are very similar to those reported here. In all cases, the flow field in the nose region of a two-dimensional blunt body is generic to that of the flow in the neighborhood of the stagnation point on a plane wall.

17. Key Words (Suggested by Author(s))	18. Distribution Statement
Boundary layer receptivity Boundary layer transition Stream oscillation Blunt bodies	Unclassified-Unlimited Subject Category 34

19. Security Classif. (of this report)	20. Security Classif. (of this page)	21. No. of Pages	22. Price
Unclassified	Unclassified	190	A09

For sale by the National Technical Information Service, Springfield, Virginia 22161

NASA-Langley, 1982